UNIVERSITÀ DEGLI STUDI DI MILANO

CORSO DI DOTTORATO IN SCIENZE BIOCHIMICHE CICLO XXXII

DIPARTIMENTO DI Biotecnologie Mediche e
Medicina Traslazionale (BioMetra)

TESI DI DOTTORATO DI RICERCA

Proteomic analysis of neuronal cells and tissues

FRANCESCA GRASSI SCALVINI

TUTOR: Prof.ssa Gabriella Tedeschi

COORDINATORE: Prof. Alessandro Prinetti

A.A 2018/2019

Abstract

During my three years of PhD I had the opportunity to work with different biological samples analyzing the content and type of proteins through the proteomic approach.

In the thesis I describe how a proteomic approach could be useful to analyze different aspect connected to central nervous system. Indeed, the present work is divided in three different parts but the *fil rouge* is represented by the same analysis technique, a shotgun label-free proteomic approach, for the identification and quantification of expressed proteins, applied to different neuronal cells and tissues: 1) PC12 cells, a well-studied neuronal cell model due to the ability to easily differentiate into neuron-like cells, 2) Neuro2a cells, another neuronal cellular model very well studied, and 3) the brain of Zebrafish. It is a poikilotherm and eurytherm and therefore it has a wide thermal tolerance, from 6°C to 38°C, temperatures between 24 and 30°C are more suitable for its development, growth and reproduction. Moreover, *Danio rerio* represents a good animal model for different type of research because it has a generation time of 3-4 months, its maintenance is cheaper than that for rats and mice and required little space.

Starting with the first project the proteomic approach is used to dissect at the proteome level similarities and differences between the biochemically and mechanotransductively promoted neuronal differentiation of PC12 cells growth on cluster-assembled zirconia surface with 15nm of roughness, polylysine coated glass in the presence (NGF) or absence (PLL) of NGF.

This work lays a substantial cell biological foundation for the intelligent design of substrates for cell culturing based on nanostructured surfaces produced by cluster assembling that mimic more closely physiological 3D extracellular microenvironmental features. Our data suggest that the nanoscale information provided by these surfaces could have a strong potential in favoring neurogenic processes by mechano-transductive processes.

The results obtained on zirconia nanostructure can be the fundamental starting point to further characterize the neuronal differentiation process in adequate primary and stem cell systems for regenerative medicine approach.

The second part of this work has the aim to understand how the activation of the TrkA pathway is able to trigger biochemical signaling, like ERK1/2, leading to cell differentiation when GM1 oligosaccharide, II3Neu5Ac-Gg4 (OligoGM1), which interacts with NGF receptor TrkA, is administered to cultured murine Neuro2a neuroblastoma cells.

The results of our work confirm and reinforce the idea that the molecular mechanisms underlying the GM1 neurotrophic and neuroprotective effects depend on its oligosaccharide chain, suggesting the activation of a positive signaling starting at plasma membrane level.

The third part of this thesis regards the determination of the effect of ambient temperature on the molecular mechanism and the behavioural responses in *Danio rerio*. This project can be framed in a quite interesting area of research, important because global warming occurring in our planet is, especially nowadays, an urgent problem amplified by the anthropic action, the release of CO_2 and other greenhouse gases. The huge temperature increase causes climate changes that can deeply alter the habitat of the species, leading to substantial environmental changes possibly impairing the prosecution of the species. We applied for the first time a shotgun proteomic approach to analyze the effect of acclimatization on zebrafish brain proteome and to correlate the results at the protein level with the behavioural tests.

As stated above, the shotgun proteomic approach adopted is a powerful analytical method for characterizing the complex proteomes of various types of biological specimens.

To characterize the protein component of our sample, we have adopted a quantitative label free shotgun proteomic approach. In recent years, non-gel-based, shotgun proteomic technique has emerged as powerful tool for studying large scale differential protein expression [1]. This method

allows to examine the impact of different conditions by achieving the simultaneous identification of thousands of proteins and their quantification in each sample. It does not require a previous purification of the sample, but identifies proteins from tandem mass spectra (MS/MS) of their proteolytic peptides, which are separated by liquid chromatography (LC) [2].

In particular, the identification of the proteins from the MS/MS data was achieved using a database search by MaxQuant which compares acquired mass spectra to a database of known sequences to identify the proteins.

BACKGROUND

1. Nervous system

1.1 General organization of nervous system

Nervous system is divided in two parts central nervous system, composed by brain and spinal cord and peripheral nervous system, made up of nerves which branch off from the spinal cord and extend all over the body. The nervous system controls movement, breathing, seeing, thinking and more, through signals transmitted between the brain and the rest of the body. The basic unit of the nervous system is neuron, which are 100 billion in human brain. Neurons have a cell body, which includes the cell nucleus, and two types of extension axons and dendrites. The latter allow neurons to communicate, even across long distances. Different types of stimuli are driven by different types of neurons, for example, motor neurons transmit messages from the brain to the muscles to generate movement, sensory neurons detect light, sound, odor, taste, pressure and heat and send messages about those things to the brain. The remaining parts of the nervous system control involuntary processes.

The messages between neurons are electrical signals that changes, at the end of the axon, to chemical signals. The axon then releases chemical messengers called neurotransmitters into the synapse, the space between the end of an axon and a dendrite from another neuron, allowing signal transmission.

The nervous system also includes other cells called glia, which have important functions that keep the nervous system working properly. They:

- help, support and hold neurons in place;
- protect neurons;

- create myelin;
- remove dead neurons;
- regulate neurotransmitters.

In the next chapters Central Nervous System characteristic will be elucidated with more details.

1.2 The formation of brain structure

Fertilization is the starting point of development of the nervous system, so an ovary's oocyte is sent to the uterine tube to be fertilized. A fertilized ovum is subjected to repeated cell cleavage, the first division results in two blastomeres, and successive produce a spherical ball of cells. The rearrangements of blastomeres give rise to a fluid-filled cavity, the blastocoel. Inside the blastocyst appears a cluster of cells called inner cell mass whose cavity is the embryonic disc.

The three germ layers, endoderm, mesoderm and ectoderm derive from the embryonic disc and form all the tissue and organs of the embryo.

The dorsomedial area of the ectoderm differentiates into neural ectoderm [3], a flat area made of a single cell layer. The tubular primordium of the central nervous system is form through three developmental stages: neural plate, neural fold and neural tube. The neural ectoderm thickens to become the neural plate, which folds into a neural groove and contains the neural progenitors. The latter becomes narrower and the dorsal edges of the fold fuse so the neural fold becomes the neural tube, first well-defined neural structure. Brain originates from the rostral end and the remaining part of the neural tube develops into the spinal cord. While deepening the neural groove, a cluster of cells forms the neural crest which detaches from the ectoderm to become ganglia of the cranial and the spinal nerves.

The neural tube results from fusion of the dorsal edges of the neural fold, its closure starts from the middle of the embryo and proceeds toward the two ends. As a result, three stages of neural development coexist simultaneously in different regions of the embryo.

1.3 Development of brain and nervous system

The brain is the principal organ of nervous system in all vertebrate and most invertebrate animals. The development of it and more in general of all the nervous system is a process that involves molecular events of gene expression and environmental input, both essential for normal brain growth, whose disruption can alter neural outcomes. In humans this process starts at the third gestational week and extends at least through late adolescence [4] but the neurons production begins on embryonic day 42 till midgestation [5, 6]. Once produced neurons migrate to different brain areas where they make connections with other neurons to create rudimentary neural networks.

1.3.1 Neurons

The mature brain is composed of more than 100 billion neurons [7] which are the cell delegated to information processing in the brain.

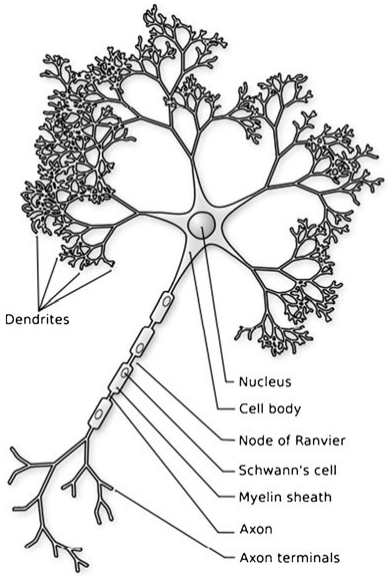

Figure 1: **Schematic drawing of a neuron.** Each neuron a single large axon. At the distal tip of the axon is a growth cone that serves to guide the axon to targeted brain regions. Once the axon reaches the target site, synapses, or

points of connection, form between the axon and the target neuron. The synapse allows electrochemical signals to be transmitted to the target neuron. Each neuron also has a complex arbor of dendrites that receive information from other neurons. Original image from Nicolas Rougier [4].

They differ according to the shape, size and function and they form, through connections with others neurons, the information processing networks being responsible for all our thought, sensation, feelings and actions. According to their function they are divided into three classes: sensory neurons, motor neurons and interneurons, that connect neurons to other neurons within the same region of the brain or spinal cord.

They are composed by a cell body, soma, dendrites and a single axon. The soma contains the nucleus where occurs protein synthesis. Dendrites are sets of short fibers that resemble the branches of a tree, making the dendritic arbors; they extend only a short distance away from the neuron cell body. They are deputies to the reception of the electrochemical input signals from other neurons. Axons, instead, are long connecting fibers that, creating connections with other neurons, are extended over long distances sending electrochemical signals. Another important part is the axon terminal which contains synapses, the space where neurotransmitter chemicals are released to communicate with target neurons. Synapses can be excitatory or inhibitory, which increase or decrease activity in target neuron. When an action potential reaches the axon terminal, voltage-gated calcium channels is open and calcium ions enter in the terminal. Calcium causes the fusion between synaptic vesicles with membrane releasing their contents into the synaptic cleft, here neurotransmitters diffuse and activate receptors on the postsynaptic neuron. The high calcium concentration in the axon terminal activates mitochondrial calcium uptake, leading mitochondrial energy metabolism to produce ATP to guarantee continuous neurotransmission.

Axons are enveloped in myelin, a fatty substance that makes efficient the transmission of electrochemical signals. Myelin has the 40% of water and its dry mass is composed by high proportion of lipid (70 to 85%) and low proportion of protein (15-30%). The most typical lipid of myelin is cerebroside, also known as galactosylceramide, which concentration increase in relation to the

amount of myelin and it has insulating and stability roles. In addition to cerebroside, the major lipids of myelin are cholesterol and ethanolamine-containing plasmalogens. Lecithin is also a major myelin constituent, and sphingomyelin is a relatively minor one [8]. Minor components of myelin are represented by three fatty acid esters of cerebroside and two glycerol-based lipids, collectively called galactosyldiglyceride. Myelin from mammals contains 0.1 to 0.3% gangliosides, which are complex sialic acid-containing glycosphingolipids [8]. It is mainly composed by monosialoganglioside GM1, instead of other brain membranes, enriched in the polysialo species.

The protein composition of CNS myelin is mainly characterized by proteolipid proteins and basic proteins and, to a lesser extent, other proteins and glycoproteins. They aren't easily extractable, since unsoluble in aqueous media, but they could be solubilized in sodium dodecylsulfate (SDS) and, in this condition, separated readily by electrophoresis in polyacrylamide gels. Through this technique two major proteins, myelin basic protein and proteolipid protein, were characterized in human CNS myelin. These proteins are mainly present in all mammalian CNS myelin, and similar proteins are present in myelin of many lower species [4].

The site of most neuron production is the wall of the ventricles which are a series of interconnected cavities filled with cerebral spinal fluid, completely recycled several times per day. It deadens and protect the brain removing waste material and transporting hormones and other substances [4].

1.4 Differentiation of the neural progenitor cells

At embryonic day 13 the embryo is an oval-shaped, simple, two-layered structure. These two layers contain a different, very primitive cell type: epiblast cells, in the upper layer, and in the lower one hypoblast cells. Gastrulation, which set the stage for all subsequent developments, transforms the embryo into a three-layered structure. The epiblast cells will differentiate into primary stem cell lines that will eventually give rise to all of the structures in the developing embryo, while the hypoblast

cells will give rise to the extraembryonic tissues, like the fetal component of the placenta and the connecting stalk. Among the stem cell lines there are the neural stem cells, which are able to produce all the different cells that built the brain and the central nervous system, for this reason they are called neural progenitor cells.

The first step in gastrulation is the formation of the primitive streak, an opening in the upper layer of the embryo; epiblast cells pass, firstly, in this structure, then they migrate toward another structure called primitive node, located at the rostral end of the primitive steak. The primitive node is a molecular signaling center [4] whose cells send a molecular signal to the subset of cells that migrate along the rostral-caudal midline of the embryo and that signal, in turn, triggers gene expression in the migrating cells. In the space between the migrating cells and the cells of the midline region of the upper epiblast layer is secreted a protein which binds to receptors on the surface of the cells in the upper layer of the embryo, inducing the differentiation of the epiblast cells into neural progenitor cells.

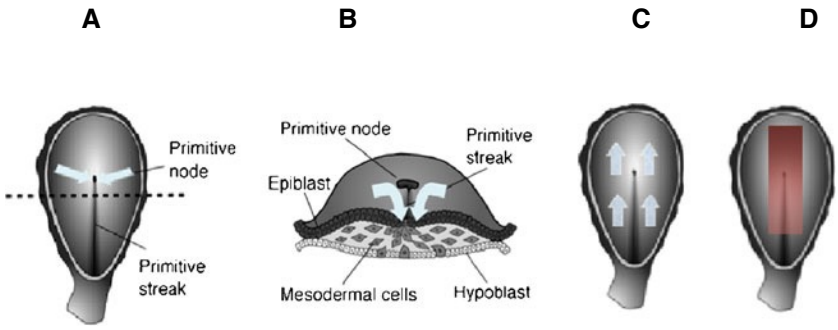

Figure 2: the major events of gastrulation. A The first step is the formation of the primitive streak and the primitive node, which is a critical molecular signaling center. Cells from the epiblast layer begin to migrate toward the primitive node and streak (blue arrows). **B** The migrating cells change direction and move down, under the upper layer (blue arrows). **C** The cells begin migrating rostrally. **D** Cells that migrate along the axial midline send molecular signals that induce cells in the overlying epiblast layer to differentiate into neuroectodermal cells (red band) which are the neural progenitor cells [4].

The differentiation of stem cells into neural progenitors requires a complex molecular signaling, that involves multiple gene products, among at least three cell populations: the cells of the node, the migrating cells and the cells that will become the neural progenitors.

Pax6 and Emx2, transcription factor proteins, are two signaling molecules responsible for the production of neuron from progenitors. They are present in different concentration in the neocortical proliferative zone. The concentration of Emx2 is highest in posterior and medial regions, and lowest in anterior lateral regions; Pax6 has the opposite expression pattern [4]. Two gradients induce progenitors to produce neurons of different species, motor neurons thanks to high concentration of Pax6 combined with low concentration of Emx2, and neurons for visual cortex with the opposite concentration.

1.5 Neuron production

The changes that occur in the gross anatomy of the fetal brain reflect dramatic changes occurring at the cellular level [4]. Neuron production starts at the embryonic period and extends through midgestation. The pool of neural progenitor cells is too small for neuron production, so it has to increase in size, through symmetrical division, before starting this process. Neural progenitors are mitotic population of cells, so they can divide forming new cells. Neurons are post-mitotic cells, once formed they are no longer able of dividing and producing new cells. There are three types of neurogenic progenitors within the developing neocortex: neuroepithelial cells, radial glia and intermediate progenitors. Firstly, a single sheet of pseudostratified neuroepithelial cells undergoes to symmetric cell division, which later begins to shift to asymmetrical one producing two different types of cells, one neural progenitor and one neuron. The first one remains in the proliferative zone and continues to divide, while neuron migrates away from the proliferative regions of the ventricular zone. Once placed in cortex neurons start to differentiate producing neurotransmitters and neurotrophic factors, and extending the dendritic and the axonal processes that form the fiber pathways of the brain neural networks.

1.6 Neuron differentiation

The different layers of cortex contain different types of neurons. Early neural progenitor cells are capable of producing any neuron type, but then with development they become more and more restricted in the types of neurons they can produce. The progenitor cells can receive signals to produce any neural cell line, but with development these cells become useless and so the progenitor loses the ability to produce those cells, exhibiting fate restriction. Shifts in the progenitor population are induced by a particular signaling pathways which is still poorly defined [9]. Once they have reached their target region of the cortex, the newly neurons need to become part of information processing network, and so they need to develop axon and dendrites that allow them to communicate with other neurons. At the tip of each axon is a structure called a growth cone, the site of axon elongation and extension [10]. As the axon extended some guidance cues, attractive or repulsive, direct them toward their targets where they make connections called synapses.

2. Label-free shotgun mass spectrometry

2.1 Neural plasticity

Neural plasticity can be defined as the ability of the central nervous system (CNS) to adapt in response to changes in the environment or lesions [11]. Through modifications the CNS try to cope in the best way with new challenges, it recruits new or different neural networks, or changes in strength of such connections or specific brain areas in charge of carrying out a particular task [12]. At the cellular level many studies have demonstrated membrane excitability, synaptic plasticity and structural changes in dendritic and axonal anatomy both in human and animals [13, 14]. CNS consists in neuronal circuit formed by synaptic connections between axons and dendrites that, extending over the brain, has the potential for a large number of possible interacting combinations allowing for great flexibility. Modification of sensory input may induce rapid changes in cortical representations through various mechanisms including unmasking of connections that are silent in the native state [15]. Synaptic plasticity is the base for learning and memory and cell require de novo protein synthesis to maintain it. Although the requirement for protein synthesis in long-term plasticity is widely recognized, the identities of proteins that are differentially synthesized in response to experience and their functions in neuronal and behavioral plasticity are still largely unknown [16]. In these studies, we performed a shotgun label-free proteomic approach to identify candidates which changed in abundance in response to different stimuli against which CNS has to adapt. In particular in all the three studies presented in this thesis we performed a shotgun proteomic analysis, in order to:

- characterize the effect of the extracellular ambient on neuronal differentiation by comparing the proteome of PC12 cells grown on neuritogenesis-inducing ns-Zr15 substrates with the one of cells grown on PLL in the presence and in absence of NGF (after 24 h cell/substrate interaction) [18];

- understand how the activation of the TrkA pathway is able to trigger key biochemical signaling, in Neuro2a cells treated with 50 μM OligoGM1 for 24 h [19].
- determine the effects of environmental temperature changes on the proteome of zebrafish brain [17];

2.2 Shotgun approach

For many years 2D-PAGE/MS, which is an overall, comparative, quantitative proteomic technique, was the gold standard for analysis of protein expression and biomarker discovery. However, there are several disadvantages associated with gel-based proteomic techniques. For example, any 2D approach is subjected to the restrictions imposed by the gel method, which include limited dynamic range, difficulty in handling hydrophobic proteins, and difficulty in detecting proteins with extreme molecular weights and pI values. Another negative aspect is that spots on a 2D gel often contain more than one protein, making quantification ambiguous. [1]. Moreover, low-abundance proteins may be masked in the gel by high-abundance housekeeping proteins. Therefore, in more recent years, there has been a move towards gel-free MS methods for proteome analysis. The gel-free methods are based on the high-throughput "shotgun" analysis of peptides from a digested complex protein sample using an on-line high-performance liquid chromatography (HPLC) method, prior to identification using MS/MS [20].

In this study we applied a shotgun proteomic protocol, that is a non-gel-based technique, without any previous separation of the proteins before MS/MS analysis [21] and label free for quantitation.

Shotgun proteomics consists of distinct steps. The first step, and perhaps one of the most critical, is the preparation of the sample. The second step is the separation of peptides by HPLC followed by the analysis by mass spectrometry. The final step is the bioinformatic analysis to assess the results.

Shotgun proteomic has provided powerful tools for studying large scale protein expression and characterization in complex biological systems [22, 23]. This proteomic strategy converts a complex protein mixture to an even more complicated peptide mixture. For this reason, to resolve complex peptide mixtures, high-resolution HPLC separations are necessary to maximize peptide separation for acquisition of tandem mass spectra.

2.2.1 Label-free protein quantification

There are two different approaches used for quantitate protein changes in complex samples: labeling-based and label-free quantitative approaches.

In protein-labeling approaches, different protein samples are combined together once labeling is finished and the pooled mixtures are then taken through the sample preparation step before being analyzed by a single LC-MS/MS or LC/LC-MS/MS experiment.

In contrast, with label-free quantification methods, each sample is separately prepared then subjected to individual LC-MS/MS or LC/LC-MS/MS runs [1].

Most labeling-based quantification approaches have potential limitations. These include increased time and complexity of sample preparation, requirement for higher sample concentration, high cost of the reagents, incomplete labeling and the requirement for specific quantification software. In particular, the labeling efficiency of amino acids or proteins varies depending on the rate of protein turnover in cells; MS-based quantification requires detection of chromatographic peaks for both light and heavy peptides. Moreover, substantial changes in protein expression often result in a poor peak correlation between the light and heavy peptides and reduce the number of quantifiable peptide measurements. The implementation of the stable isotopic labeling strategy is further hampered by the cost of stable isotope-labeled amino acids as well as the limited availability of isotope/metabolic labeling media.

Compared with isotope-labeling methods, label-free experiments need to be more carefully controlled, due to possible error caused by run-to-run variations, LC separation and MS analysis. However, the development of highly reproducible nano-HPLC separation, high resolution mass spectrometer, and dedicate computational tools have greatly improved the reliability and accuracy of label-free methods.

Regardless of which label-free quantitative proteomics methods is used, they all include the following fundamental steps: i) sample preparation including protein extraction, reduction, alkylation and digestion; ii) sample separation by liquid chromatography and analysis by MS/MS; iii) data analysis including peptide/protein identification, quantification, and statistical analysis [1].

Protein quantification is generally based on two type of measurements. First the measurement of ion intensity changes such as peptide peak areas or peak heights in chromatography. The second is based on the spectral counting of identified proteins after MS/MS analysis. Peptide peak intensity or spectral count are measured for individual LC-MS/MS or LC/LC-MS/MS runs and changes in protein abundance are calculated via direct comparison between different analyses.

In the spectral counting approach, relative protein quantification is obtained by comparing the number of identified MS/MS spectra from the same protein in each of the multiple LC-MS/MS or LC/LC-MS/MS datasets. This is operable because an increase in protein abundance typically results in an increase in the number of its proteolytic peptides, and vice versa. This increased number of digests then usually results in an increase in protein sequence coverage, the number of identified unique peptides, and the number of identified total MS/MS spectra (spectral count) for each protein [24].

In this study a label-free quantitative proteomic protocol based on peak intensity measurement is applied. In LC-MS, an ion with a particular m/z is detected and recorded with a particular intensity, at a particular time. It has been observed that signal intensity from electrospray ionization correlates with ion concentration [25]. Infact, when chromatographic peak areas were calculated, the peak areas were found to increase with increased concentration of injected peptides and to correlate linearly to the concentration of protein.

Thus, relative quantification of the peptides could be achieved via direct comparison of peak intensity of each peptide ion in multiple LC-MS datasets.

Several similar steps in data processing were carried out in these label-free quantifications. Peptide peaks were first distinguished from background noise and from neighboring peaks (peak detection). LC-MS retention times were carefully adjusted in order to correctly match the corresponding mass peaks between multiple LC-MS runs (peak matching). Chromatographic peak intensity, either peak area or peak height, was calculated and normalized to enable a more accurate matching and quantification. Finally, statistical analysis was performed to determine the significance of changes between multiple samples [26, 27].

Proteomic analysis of neuron-like PC12 cells growth on supports with diverse nanotopographies, and their phosphoproteomic profiles in these settings

1. INTRODUCTION

1.1 Rat pheochromocytoma cell line (PC12)

PC12 is a cell line derived from a pheochromocytoma of the rat adrenal medulla, that has an embryonic origin from the neural crest, a mixture of neuroblastic cells and eosinophilic cells. This cell line was first cultured by Greene and Tischler in 1976. It was developed in parallel to the adrenal chromaffin cell model because of its extreme versatility for pharmacological manipulation, easiness of culture, and the large amount of information available on their proliferation and differentiation. The embryological origin from neuroblastic cells implies that they can easily differentiate into neuron-like cells even though they are not considered adult neurons. Neuron-like means they share properties similar to neurons, in this case it is referring to releasing neurotransmitter by vesicles. PC12 cells stop dividing and terminally differentiate when treated with nerve growth factor (NGF) or dexamethasone. For this reason, this cell line has been widely used as a neuronal model system to study neuronal differentiation and specific growth factor signalling mechanisms [28].

Treatment of PC12 cells with dexamethasone differentiates them into chromaffin-like cells, instead using nerve growth factor these cells assume many of the features of sympathetic neurons including cell cycle arrest, survival in serum-free medium, and neurite extension [29-34]. It has been demonstrated that NGF induces NO production by the induction of all three nitric oxide synthases (NOS) isoforms [35] and that, in the absence of NGF, NO itself has the ability to produce neurite outgrowth by extracellular signal-regulated kinase (ERK) activation through NO-cGMP-PKG pathway [36].

Beside NGF, which is the classical inducer of differentiation, there are other factor that promote growth arrest and neuritogenesis, such as cAMP-elevating agents.

In PC12 cells, the extension of neurite is one hallmark of the neuronal phenotype, along with cessation of proliferation and production of specific neurotransmitters such as nitric oxide (NO) [37].

1.2 The Extracellular Matrix

Cellular behaviour *in vivo* and *in vitro* is heavily influenced by the mechanical, biochemical and topographical properties of the extracellular environment where cells grow [38-40]. In the last two decades a rapidly increasing amount of data suggested that the modulation of topographical and chemical cues at the nanoscale plays a relevant role in determining cell adhesion, proliferation and differentiation [41]. Cells in their natural environment interact with extracellular matrix (ECM) components structured at the nanometer scale [42] and they respond to nanoscale features when grown on synthetic substrates [43-47].

ECM (Extracellular Matrix) is a complex mixture of proteins and proteoglycans that cells secrete and organise [48].

It is composed of three major classes of biomolecules (Figure 3):

1. Structural proteins: collagen, fibrillin, and elastin;
2. Specialized proteins: fibronectin, laminins, and integrins;
3. Proteoglycans**:** these are composed of a protein core to which long chains of repeating disaccharide units termed of glycosaminoglycans (GAGs) are attached forming extremely complex high molecular weight components of the ECM;

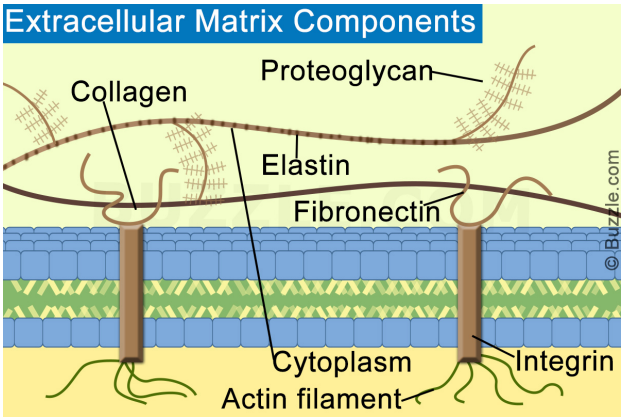

Figure 3: Components of the ECM [from 538]

These components are secreted locally and assembled into the organized meshwork that is the ECM. Connective tissue refers to the matrix composed of the ECM, cells (primarily fibroblasts), and ground substance that is tasked with holding other tissues and cells together forming the organs. Ground substance is a complex mixture of GAGs, proteoglycans, and glycoproteins (primarily laminin and fibronectin) but generally does not include the collagens. In most connective tissues, the matrix constituents are secreted principally by fibroblasts but in certain specialized types of connective tissues, such as cartilage and bone, these components are secreted by chondroblasts and osteoblasts, respectively. The ECM is not only critical for connecting cells together to form the tissues, but is also a substrate upon which cell migration is guided during the process of embryonic development and importantly, during wound healing. In addition, the ECM is responsible for the relay of environmental signals to the surfaces of individual cells.

1.2.1 Extracellular Matrix of the Brain

The low elastic modulus of the adult brain and spinal cord coincides with the near absence of the kind of ECM that forms scaffolds in most other soft tissues [49, 50]. Neurons and astrocytes are well gifted with integrins and other transmembrane proteins typically associated with the adhesion of cells to a fibrous ECM or basement membrane, but normal brain is conspicuously unprovided of fibrillar collagens or fibronectin fibrils except in the meninges, the vasculature, and the blood-brain

barrier [51]. Rather than a 3D protein scaffold consisting of a mesh-like basement membrane and long stiff fibrils that permeate the space of most tissues, even some such as adipose that also have very low elastic moduli [52], the ECM of the adult brain consists largely of much softer elements, such as the anionic carbohydrate polymers hyaluronan (HA) and other glycosaminoglycans, the integrin ligand tenascin C, and a large set of proteoglycans, many of which bind to HA and other elements of the ECM [50, 53]. In the brain, the ECM appears to be less a structural support providing elasticity to the tissue than a trophic and topographical guidance cue during development and remodelling [49].

Despite containing relatively scarce amounts of ECM proteins common in other tissues, most CNS cells express integrins and possibly other receptors that allow them to adhere to collagen-, fibrin-, fibronectin-, and laminin-coated surfaces and to exhibit mechanosensing properties in these materials [54, 55, 56-59]. *In vivo*, however, their function might be more strongly regulated by glycosaminoglycans [60] and proteoglycans, which generally are much more flexible than gels made from stiffer biopolymers such as collagen or fibrin. *In vitro* networks of such polymers can be formulated to have low elastic moduli similar to those of normal brain, and biomaterials formed from collagen, fibrin, HA, alginate, and other synthetic soft hydrogels have been extensively studied as carriers of stem cells, neurotrophic factors, or other active agents or as neutral scaffolds to facilitate wound healing. Decellularized brain scaffolds have also been prepared and have potential as soft scaffolds that most nearly mimic the native biochemical and topographical cues encountered by neurons *in vivo* [61].

1.3 Cells culture substrates

It's very important to evaluate a cell in the context of the ECM and not as a solitary entity defined by its genome; in order to do this, different substrates for cell growth, that mimic the extracellular matrix, have been developed.

1.3.1 The first and the second generation of substrates: from 2D to 3D

It's possible to divide the process of development of these substrates into three generation; the first generation is represented by two-dimensional (2D) substrates, such as tissue culture polystyrene (TCPS) or the surface of tissue analogues.

Polystyrene was chosen because it has excellent optical clarity, it is easy to mold and can be sterilized by irradiation. However, it also has one significant drawback, it is a very hydrophobic (non wettable) polymer to which cells have difficulty attaching. For good cell attachment the hydrophobic polystyrene surface must be modified to a more hydrophilic surface, process showed in figure 4. This allows cell attachment proteins (vitronectin and fibronectin) found in the serum containing culture medium to adhere and spread on the vessel bottom providing a better surface for cells to attach.

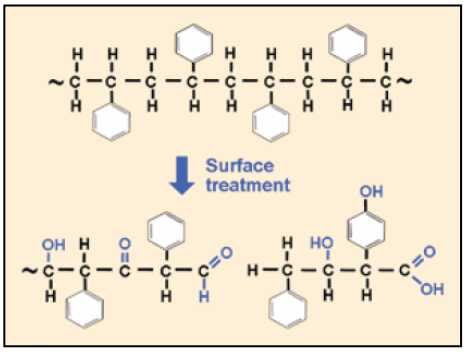

Figure 4: polystyrene can be surface modified by the addition of a variety of different chemical groups, breaking the carbon chain backbone or opening the benzene ring. These processes both generate highly energetic oxygen ions which oxidize and graft onto the surface polystyrene chains so that the surface becomes hydrophilic and negatively charged once medium is added. **[Figure from 62]**

By the end of the 1970s researchers were finding that polystyrene had its limitations, especially for growing cells in serum-free media and for maintaining differentiated cell functions in primary

cultures and cell lines. At the same time researchers were experimenting with basement membrane extracts and purified attachment proteins to better understand their roles in cell attachment, migration and function. As a result of this work, some cell researchers began coating culture vessel surfaces to improve both cell attachment and performance. They used a variety of biological materials including extracellular matrix, attachment and adhesion proteins, such as collagen, laminin and fibronectin, and mucopolysaccharides, such as heparin sulphate, hyaluronidase and chondroitin sulphate, both individually and as mixtures. Use of basic synthetic polymers, such as poly-D-lysine (PDL), as coatings have also been used to create a positive charge on polystyrene which, for some cell types, can enhance cell attachment, growth and differentiation, especially in serum-free and low serum conditions. PDL coatings often improve attachment and growth of primary neurons, glial cells, neuroblastomas, and a variety of transfected cell lines.

Experiments with these 2D cell constructs have provided the base for our nascent interpretation of complex biological phenomena, including molecular biology, stem cell differentiation [63], and tissue morphogenesis [64]. Furthermore, 2D experiments have given rise to seminal findings in the dynamic relationship between cell function and interactions with the cellular microenvironment. Discher and co-workers demonstrated that the differentiation of human mesenchymal stem cells (hMSCs) is dependent on the mechanical stiffness of the 2D culture platform [65]. Further, Ingber and co-workers have shown that the degree to which a cell is mechanically distended on a 2D scaffold dictates relative growth and apoptotic rates [66].

The 2D studies have provided many important information. However, the cells growing in 2D are not in physiological condition. They are too far from the real growth condition in animals' tissues. For instance, 2D culture polarizes cells such that only a segment of the cell's membrane can interact with the ECM and neighbouring cells, while the rest of the cell is exposed to the bulk culture media [67]. This leads to unnatural, polarized integrin binding and mechanotransduction, which both affect intracellular signalling and phenotypic fate [68]. The inherent polarity also leads to unnatural

interactions with soluble factors. In 2D culture, cells experience the homogenous concentration of nutrients, growth factors, and cytokines present in the bulk media with the section of the membrane that contacts the surrounding media. In contrast, the concentrations of soluble factors that influence cell migration, cell–cell communication, and differentiation possess dynamic spatial gradients *in vivo* [69]. Morphology alone has been shown to influence subtle cellular processes such as global histone acetylation [70] as well as proliferation, apoptosis [66], differentiation, and gene expression [71]. 2D culture confines cells to a planar environment and restricts the more complex morphologies observed *in vivo*. Furthermore, differences in migration exist between a 2D surface and a 3D environment. Not only is a cell confined to a plane in 2D, but also encounters little to no resistance to migration from a surrounding ECM.

Thus, to properly study cell physiology, mechanotransduction, and tissue morphogenesis *in vitro*, cells should be cultured in 3D model microenvironments, which represent the second generation of substrates. Indeed, many physiological and pathological (e.g., in tumour growth) cellular processes have been demonstrated to occur exclusively when cells are organized in a 3-D fashion. These range from multicomponent matrices derived from cells or tissues (e.g., Matrigel, commercially available from BD Biosciences (San Jose, CA, USA), which is solubilized basement membrane preparations extracted from mouse tumours that contains several components of basement membranes enriched with laminin), to matrices composed of individual purified or recombinantly produced ECM proteins, and modified versions of these ECM components, as well as proteolytic or recombinant fragments [40].

Natural ECM-derived biomaterials can be used as carriers for transplanted cells that are subsequently grafted into tissue defects [72, 73], and also as cell infiltration matrices to induce regeneration and remodelling *in vivo* [74, 75]; they represent valuable models from which one can derive engineering principles to create artificial materials with similar biological function [76, 77].

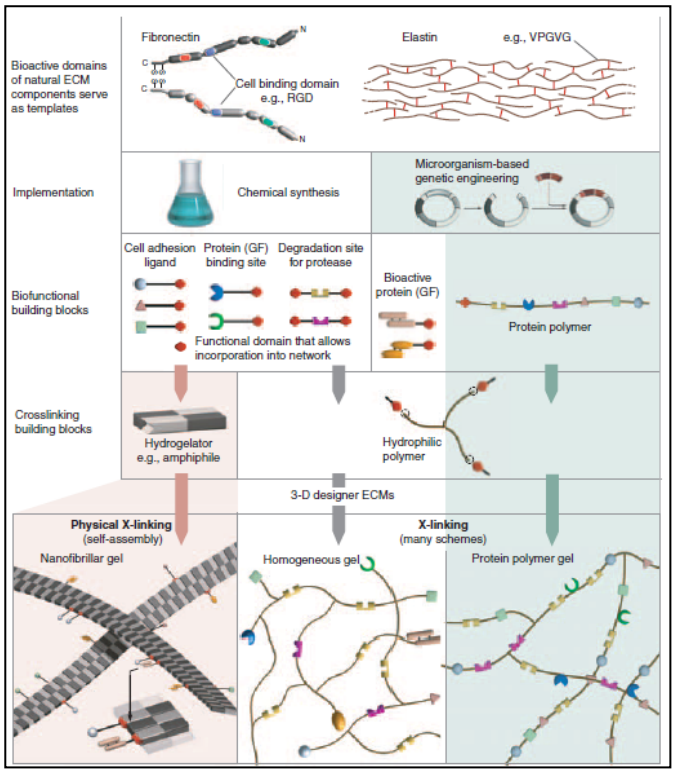

Figure 5: design strategies for the creation of synthetic biomolecular materials that mimic the complexity of natural ECMs. Bioactive domains of naturally occurring proteins are identified as building blocks (top) and synthesized by either chemical strategies or by protein engineering (recombinant technology). The most important components include cell-adhesive ligands (such as integrin-binding peptides of the prototypical RGD family), binding sites for growth factor (GF) proteins, domains with susceptibility to degradation by cell-secreted or cell-activated proteases to facilitate bidirectional cell-matrix interactions, but also domains with structural function (such as the elastin-derived peptide sequence VPGVG). Synthetic networks can then be obtained by crosslinking of these biofunctional components (from an entire array of building blocks) by distinct crosslinking schemes, involving physical (self-assembly to produce nanofibrillar gels) or chemical mechanisms. The use of such synthetic approaches in ECM design may allow matrices to be tailor-made for a specific cell or tissue. **[Figure from 77]**

These artificial materials are:

- Natural ECMs: gels composed of various protein fibrils and fibers interwoven within a hydrated network of glycosaminoglycan chains.

- Micro- and nanofibrillar synthetic biomaterials: the intricate fibrillar architecture of natural ECM components has inspired several researchers to produce materials with similar structure. Under appropriate culture conditions, these matrices have been demonstrated to maintain the functions of differentiated neural cells [78] and chondrocytes [79], and to promote the differentiation of liver progenitor cells [80]. Although not equipped with any specific biofunctional ligands, these gels are scaffolds that biomechanically organize cells in a 3-D fashion.

- Nonfibrillar synthetic polymer hydrogels: several distinctive features make synthetic hydrogels excellent physicochemical mimetics of natural ECMs. The molecular architecture of crosslinked, hydrophilic polymers can result in tissue-like viscoelastic, diffusive transport, and interstitial flow characteristics. They could be natural or non-natural. Natural gels for cell culture are typically formed of proteins and ECM components such as collagen [81], fibrin [82], hyaluronic acid [83], or Matrigel, as well as materials derived from other biological sources such as chitosan [84], alginate [85], or silk fibrils. Since they are derived from natural sources, these gels are inherently biocompatible and bioactive [86]. They also promote many cellular functions due to the myriad of endogenous factors present, which can be advantageous for the viability, proliferation, and development of many cell types. However, such scaffolds are complex and often ill-defined, making it difficult to determine exactly which signals are promoting cellular function [87]. Furthermore, tuning their material properties such as mechanics and biochemical presentation can be difficult, there is risk of contamination, they can be degraded or contracted too quickly, and possess an inherent batch-to-batch variability that confounds the effect of the scaffold on cell proliferation, differentiation, and migration. On the other hand, hydrogels can be formed of purely non-natural molecules such as poly(ethylene glycol) (PEG); [88], poly(vinyl alcohol) [89], and poly(2-hydroxy

ethyl methacrylate) [90]. PEG hydrogels have been shown to maintain the viability of encapsulated cells and allow for ECM deposition as they degrade [91], demonstrating that synthetic gels can function as 3D cell culture platforms even without integrin-binding ligands. Such inert gels are highly reproducible, allow for facile tuning of mechanical properties, and are simply processed and manufactured. However, they lack the endogenous factors that promote cell behaviour and act mainly as a template to permit cell function [87].

- Materials that present insoluble ligands: The creation of such highly defined synthetic ECM analogues, in which ligand type, concentration and spatial distribution can be modulated upon a passive background, may help in deciphering the complexity of signalling in cell-ECM interactions. Relevant studies include work on the quantitative information on the ligand density required for a particular cellular response [92]; the influence of adhesion ligand density on cell migration (that is, the discovery of intermediate adhesion strength for optimal cell migration) in 2-D [93] and also in 3-D, in modified biopolymer matrices [94-96] and synthetic gels [97, 99]; the finding that cells respond to the nanoscale spatial organization of adhesion ligands [98, 99]; the relevance of ligand gradients [100] and finally studies on the coregulation of signals [101, 102].

- Materials that enable binding and release of soluble effectors: a growth factor is bound to the matrix and released upon cellular demand through cell-mediated localized proteolytic cleavage from the matrix [103, 104]; this approach substantially mimics the mechanism by which these factors are released *in vivo* from stores in the natural ECM by invading cells in tissue repair.

- Stimulus-sensitive materials: the macromolecular components of natural ECMs are degraded by cell-secreted and cell-activated proteases, mainly by matrix metalloproteinases (MMP) and serine proteases. This creates a dynamic reciprocal response, with the ECM stimulating the cells within it and cellular proteases remodelling the ECM and releasing bioactive components from it.

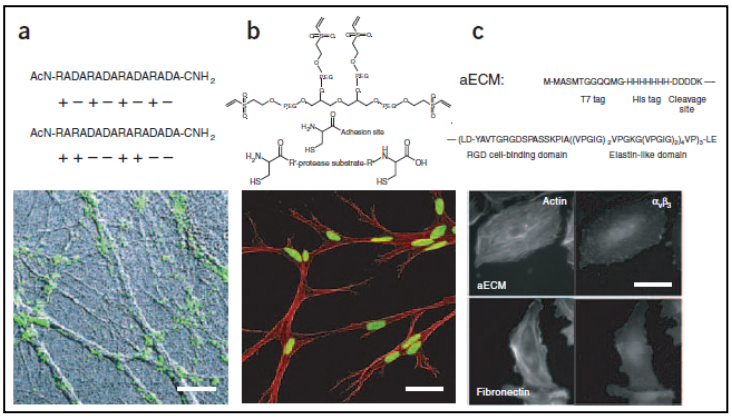

Figure 6: examples of complex synthetic ECM mimetics proposed in Figure 3. (a) Nanofibrillar hydrogels formed under physiological conditions from ionic self-assembling peptides (top). These networks support neuronal cell differentiation and extensive neurite outgrowth (bottom). Scale bar, 10 µM. Adapted and reprinted with permission from T.C. Holmes et al31. © 2003 National Academy of Sciences, USA. **(b)** Hybrid gels formed from cysteine-bearing cell-adhesive and proteolytically degradable peptide building blocks and vinylsulfone-functionalized PEG macromers (top). These gels enable extensive 3-D migration of primary fibroblasts by matrix metalloproteinase- and integrin-dependent mechanisms and, because of localized matrix proteolysis, the morphogenesis of single cells into multicellular structures (bottom). Scale bar, 40 µM. Adapted and reprinted with permission from M.P. Lutolf et al80. © 2004 Wiley-VCH. **(c)** Creation of synthetic ECMs from artificial protein polymers (aECMs, represented here by one example of a broader family) containing bioactive domains derived from elastin and fibronectin (top). Sequence-specific adhesion of human umbilical vein endothelial cells to bioactive proteins can be achieved by this approach. A similar adhesion behavior of the aECM compared to fibronectin can be observed (bottom). Responses to an artificial ECM (aECM, upper panels) are remarkably similar to responses to a natural extracellular matrix molecule, fibronectin (lower panels). This is true at both the level of the cytoskeleton (left panels) and at the level of the adhesion receptors (right panels). Scale bar, 25 µM. Adapted and reprinted with permission from Liu J.C. et al85. © 2004 American Chemical Society.

Mimicking natural ECMs that regulate complex morphogenetic processes in tissue formation and regeneration necessitates novel design strategies for synthetic biomaterials (Figure 5). These synthetic materials should be biologically multifunctional hydrogel networks, synthesized under physiological conditions, that both biochemically and biophysically mimic natural ECMs. Their functionality should be adjustable to a particular biological environment to obtain cell- and tissue-specificity. Ideally, one would create them from an array of biologically functional building blocks, in some form of a modular design.

The precursor building blocks could be crosslinked into solid networks by several means (Figure 5 and Figure 6):

- Small organic gel-formers, such as peptides or peptide-amphiphiles, containing binding sites for biologically functional ligands [40], can be designed to self-assemble into supramolecular

structures, allowing the creation of heterogeneous nanofibrillar ECM mimetics [105] (Figure 5, bottom left; Figure 6, left).

- Hybrid gels can be formed from bioactive building blocks bearing chemically reactive functional groups (such as amines or thiols) [106] or physically interactive groups and end-functionalized hydrophilic polymers such as N-(2-hydroxypropyl)- methacrylamide (HPMA) or PEG that act as chemical or physical crosslinkers (Figure 5, bottom middle; Figure 6, middle).

- Recombinant DNA technology can be used to create artificial protein polymers with desired bioactive domains de novo [107-110] (Figure 5, bottom right; Figure 6, right). Genes corresponding to structural and functional elements found in natural ECMs can be synthesized, cloned and expressed in a convenient production host. Such protein polymers can be covalently crosslinked into a network, for example, by reaction with functionalized hydrophilic polymers [111] or other chemical crosslinkers [112] targeting amines or thiols on the protein polymer, by radiation crosslinking [113] or through self-assembly by protein-protein interactions [114].

In conclusion, a comparison of 2D and 3D substrates shows that:

Table 1. Comparison of 2D and 3D substrates, advantages and disadvantages.

2D	3D
ADVANTAGES	**ADVANTAGES**
• Simple • Economic • Help to preserve a good survival rate of cultured cells	• Assume a real cell architecture • Have a gene expression profile that reflects a differentiation phenotype • Morphology and signalling more physiological cell • Allow a more rapid evaluation of a hypothesis to be tested • The images in microscopy are obtained more easily than from animal tissue • Keep of polarity in epithelial cells in 3D systems
DISADVANTAGES	**DISADVANTAGES**
• Not able to reconstruct the tissue microenvironment, due to the lack of the stroma that provides structural support to the architecture cell • Loss of specific cell characteristics, such as the polarity, because it is directly influenced by the chemical and physical properties of the media.	• The ability to mimic the conditions for growth of tissue vary according to cell line and the chosen media • Usable for short-term experiments • Transport systems are compromised (vascularity) • Possible alteration of cell motility

1.4 The third generation of substrates: nanomaterials

Nanomaterials can be generally defined as materials with at least one dimension in the size range of 1-100 nm. Operating at a length scale of one-billionth of a meter, the properties of nanomaterials are significantly different from the bulk due to the high surface-to-volume ratio [115]. Over the last fifteen years, efforts have focused on the use of nanotechnology to develop nanostructured materials (e.g. graphene and ZnO nanowires, mesoporous silica-based materials, nanotubes, nanowalls and nanorods, nanoparticles) as biomolecule immobilizing matrices/supports to improve biosensing performance [116, 117].

1.4.1 Nanoparticles and nanotubes

Nanoparticle-based biosensors are particularly attractive because they can be easily synthesized in bulk using standard chemical techniques, and do not require advanced fabrication approaches [118]. They also offer particularly high surface areas due to their extremely small size and are typically used as suspensions in solutions (during the time when they interact with the analyse). Most biological molecules can be labelled with metal nanoparticles without compromising their biological activities [119]. One example is the use of gold nanoparticles [120] due to their biocompatibility, their optical and electronic properties, and their relatively simple production and modification [121]. In fact these metal nanoparticles are extensively used in surface plasmon resonance biosensor (SPR): this method is usually based on the change of the dielectric constant of propagating surface plasmons' environment of gold films where the detection of the analyte can be recorded in different ways like the changes of the angle, intensity, or phase of the reflected light [122, 123]. This phenomenon is strongly dependent on the size, shape of the nanoparticle and the dielectric constant of its environment [124]. The environmental dependency represents a great advantage for (bio)-analytics since the recognition event can result in a change of the oscillation frequency and therefore to a colour change of the gold nanoparticles observable with the naked eye. Taking advantage of these properties a wide series of efficient colorimetric biosensors were developed for DNA or oligonucleotide detection, or immunosensors [125-128].

Magnetic nanoparticles are frequently used as alternatives to fluorescent labels in biosensor devices. A relevant advantage of using magnetic nanoparticles is the possibility to concentrate the analyte before the detection event. Magnetic nanoparticles functionalized with a bioreceptor can simply be mixed with the analyte solution and interacts specifically with the target. After applying an external magnetic field, the nanoparticles agglomerate and can be separated from the solution. Efficient isolation of DNA strands in complex media was achieved in a fast and efficient manner using silica or gold coated core/shell nanoparticles [129-131]. The use of magnetic nanoparticles for

labelling is particular interesting for biosensing applications since biological entities do not show any magnetic behaviour or susceptibility and, therefore, no interferences or noise is to be expected during signal capturing [132]. An ultra-high sensitive magnetoresistant biosensor was developed for *Escherichia coli* [133] detection or *Salmonella* identified in skimmed-milk samples with a limit of detection (LOD) of 1 colony forming-unit (cfu)/mL using a magneto-genosensing setup [134].

Another example of nanomaterials devoted to biosensing are carbon nanotubes (CNTs). In particular, carbon nanotubes possess the outstanding combination of nanowire morphology, biocompatibility and electronic properties [135]. Therefore, carbon nanotube interfaces present enhanced capacities, e.g. to approach the active sites of a redox enzyme and to wire it to the bulk electrode. Furthermore, their ease and well documented organic functionalization [136] brings new properties to nanostructured electrodes such as specific docking sites for biomolecules or redox mediation of bioelectrochemical reactions. Moreover, CNT films exhibit high electroactive surface areas due to the natural formation of highly porous three-dimensional networks, suitable for the anchoring of a large amount of bioreceptor units, leading consequently to high sensitivities [137, 138].

1.4.2 Nanostructured metal oxides (NMOs)

Among the various types of nanomaterials that have been developed (polymers, metal nanoparticles, self-assembled monolayers (SAMs)) for biological applications, nanostructured metal oxides (NMOs) have recently aroused much interest as immobilizing matrices for biosensor development [139-142]. Nanostructured oxides of metals such as zinc, iron, cerium, tin, zirconium and titanium have been found to exhibit interesting nanomorphological, functional biocompatible and non-toxic properties. These materials exhibit enhanced electron-transfer kinetics and strong adsorption capability, providing suitable microenvironments for the immobilization of biomolecules [143].

1.4.3 Nanostructured titanium substrates

Pure titanium and titanium alloys are frequently used as dental and orthopaedic implants because of their excellent mechanical strength, chemical stability, and biocompatibility [144, 145], which ultimately arise from the thin oxide layer that spontaneously forms on the titanium surfaces [146]. The fabrication strategies employed to create synthetic substrates with tailored topography at the nano- and microscale are essentially top-down and in particular based on hard and soft lithography for the fabrication of ordered structures [147, 148]. These approaches, when not based on natural matrix-related proteins, despite the great improvements in miniaturization and accuracy, are not able to reproduce the morphology and the hierarchical organization typical of the ECMs [149].

1.4.4 Nanostructured zirconia substrates

As titanium, also zirconia is a biocompatible material used in various clinical applications (i.e. for dental and orthopaedic prostheses), especially due to its favourable chemical and structural properties [150].

In this work the approach for the production of nanostructured ZrO_2 substrates is based on the assembling of zirconia nanoparticles, produced in the gas phase and accelerated in a supersonic expansion, on a flat substrate (Supersonic Cluster Beam Deposition, SCBD) [151]. This procedure allows to obtain a disordered yet controlled topographical features more similar to the ECM, if compared to the ordered structures normally obtained with other methods.

The fundamental tool for the synthesis of thin films with controlled nanoscale morphology by cluster-assembling is an SCBD apparatus equipped with a Pulsed Micro-plasma Cluster Source (PMCS) [153, 152]. The SCBD apparatus is shown schematically in Figure 7.

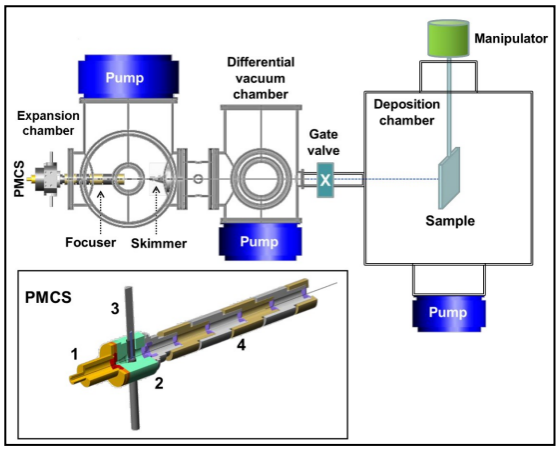

Figure 7: the SCBD apparatus. The mixture of gas and clusters is accelerated by a difference of pressure between the interior of the cluster source (higher pressure) and the expansion chamber (lower pressure, high vacuum), and collimated through the aerodynamic focuser. A skimmer selects the central portion of the beam. Eventually, nanoparticles enter the deposition chamber and are deposited on a substrate to form a film with thickness in the 1-1000 nm range. The details of the PMCS are shown in the inset: the pulsed valve (1) injects the carrier gas into the ceramic body (2) of the source, hosting the Zr rod (3); the focuser (4) containing the aerodynamic lenses concentrates the nanoparticles along the beam axis. **[Figure from 154]**

The apparatus consists of three differentially pumped vacuum chambers. The first stage is an expansion chamber where the supersonic molecular beam is formed; it can be connected to a second chamber by an electroformed skimmer. The cluster deposition takes place in a third chamber connected to the rest of the apparatus through a gate valve. A PMCS is mounted outside the expansion chamber on the axis of the apparatus. A remotely controlled manipulator allows for rastering of the sample to guarantee a uniform deposition over a large area. The structure of a PMCS is shown in the inset of Figure 7: it schematically consists of a ceramic body [155] with a channel drilled to perpendicularly intersect a larger cylindrical cavity. The channel hosts a zirconium target rod [48] acting as a cathode in order to produce the cluster precursors. A solenoid pulsed valve [156] faces one side of the cavity and a removable nozzle closes the other side of it. The valve, backed with a high inert gas pressure (20-50 bars), injects in the source cavity pulses with duration of few hundreds of microseconds at a repetition rate of 3-10 Hz. The nozzle is connected with a series of aerodynamic lenses [157] used to focus neutral nanoparticles on the beam axis. The pulsed injection of the inert carrier gas in the cavity of the PMCS causes the formation of a supersonic jet directed against the

target rod. Synchronous with the gas injection, a pulsed voltage (50-100 μs of duration, 700-1000 V) is applied to the target cathode and the grounded anode (pulsed valve front) in order to ionize the gas and sputter the target. Due to the plasma confinement obtained by the aerodynamic effects of supersonic expansions, the sputtering process is very efficient and reproducible [158]. The species ablated from the target thermalize with the inert gas and condense to form clusters. The carrier gas-cluster mixture expands out of the nozzle forming a seeded supersonic expansion, [159] which impinges on the substrate holder in the deposition chamber. Clusters are not monodispersed in size; instead, they possess a rather broad size distribution when they exit from the PMCS, which depends on the carrier gas and on the operational parameters of the source [152]. Aerodynamic focusing based on inertial effects of clusters, obtained by using special nozzle configurations, filters off the largest clusters and aggregates, and concentrate particles along the beam axis. By controlling the working parameters of the PMCS, the aerodynamic filters, and the portion of the beam intercepting the substrate, the nanoparticles distribution can be precisely tuned and reproduced. Consequently, once the SCBD parameters are set, the deposition time controls the surface morphology of the films, which evolves regularly according to simple and reproducible scaling laws. Ns-ZrO_x clusters have been produced in the PMCS using Ar or He as carrier gas, then deposited on suitable substrates intercepting the beam in the deposition chamber. This bottom-up assembling technique produces nanostructured films obtained by randomly distributed clusters, thus creating a nanoscale topography whose roughness can be accurately controlled and varied in a reproducible manner [160]. This very precise and reproducible control over nanoscale topography can be easily obtained over macroscopic areas which is a necessary requirement for the large number of experiments performed in this study.

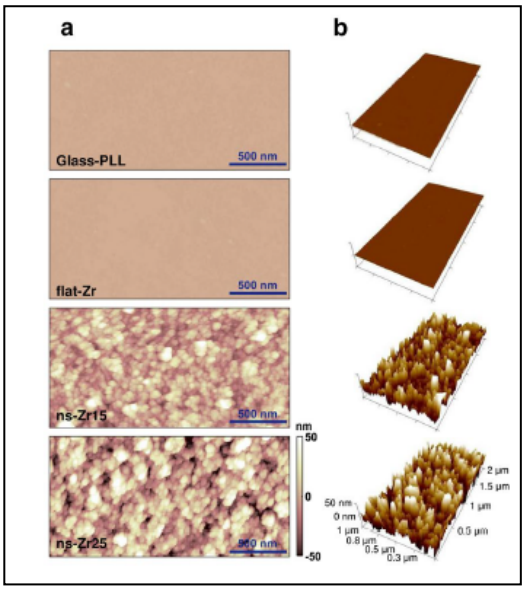

Figure 8: AFM morphological analysis of control and nanostructured surfaces produced by SCBD. The images show representative **(a)** top views and **(b)** 3-dimensional views of the surfaces morphology of glass coated with poly-l-lysine (PLL), flat zirconia (flat-Zr) produced by e-beam evaporation, and nanostructured zirconia (ns-Zr) produced by SCBD with roughness Rq = 15 (ns-Zr15), or 25 nm (ns-Zr25), respectively. **[Figure from 153]**

1.5 Principles of mechanotransduction

Cells are capable of sensing, in a surprisingly precise manner, nanoscale topographical features and mechanical characteristics of the microenvironment they interact with, mainly via integrin-mediated adhesion sites which serve as mechanoreceptors [155-157]. The conversion of these physical signals (structural and mechanical cues) into a modulation of the cellular (biochemical) responses is defined as mechanotransduction [154, 161]. In general, mechanosensitivity requires the conversion of mechanical forces applied to cells from the outside or of an active measurement of stiffness of the surroundings by the cells themselves into intracellular biochemical signals [162]. When the mechanical cue has been received, the signal is amplified and propagated through a series of force-dependent biochemical reactions, whereby intracellular signalling pathways become sequentially activated through mechanotransduction [163]. For example, in response to elevated tension within focal contacts, increases in integrin clustering and in the phosphorylation of focal adhesion kinase (FAK) ensue, and these molecular changes initiate a cascade of signalling events. This cascade includes the activation of Rho-family GTPases, such as RhoA, which stimulates actin remodelling, induces protein phosphorylation to promote cell survival, and alters the levels and activity of transcription factors to regulate gene expression.

Another integrin-dependent signalling pathway that is activated in response to mechanical force is the mitogen-activated protein kinase–extracellular signal-regulated kinase (MAPK–ERK) pathway, which has been implicated in a number of cancers and regulates cell proliferation and differentiation to influence tissue development [164].

All the machanotransduction machinery is summarized in figure 9.

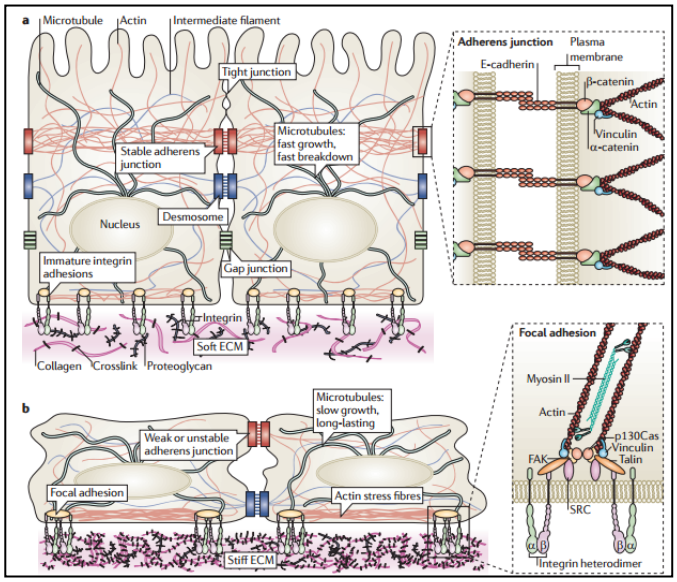

Figure 9: The mechanical network. (a) Tissues are mechanically integrated structures, the physical behaviour of which is defined by interconnected networks of cell–cell junctions, cell–matrix adhesions, intracellular filament networks (of actin, microtubules and intermediate filaments) and the extracellular matrix (ECM). Embedded throughout the network are mechanotransducing machines that convert mechanical stimuli into biochemical signals. This process, termed mechanotransduction, enables cells and tissues to sense and respond to their physical surroundings. The ECM controls network connectivity and tension on the network, thereby regulating sites of mechanotransduction. **(b)** Cell–matrix adhesion complexes containing integrins can also directly sense the physical properties of the ECM. These complexes contain specialized protein sensors, including talin, p130Cas (also known as BCAR1), and integrins themselves, that undergo force-dependent conformational changes to elicit downstream signalling responses. The physical properties of the ECM are determined by its composition, the organization of its components, and their degree of intramolecular and intermolecular crosslinking. Interactions between the cell and ECM are dynamic, interwoven and reciprocal. Transcellular tension transmitted across adherent junctions affects ECM remodeling, which in turn regulates cell–matrix and cell–cell adhesions. Increased ECM stiffness owing to remodeling can result in changes in cell and nuclear shape, chromatin organization, assembly of cell–matrix adhesions (called focal adhesions), formation of actin stress fibers, destabilization of cell–cell adhesions, and changes in microtubule dynamics. FAK, focal adhesion kinase **[Figure from 165]**

Classical experimental approaches do not permit spatially- or temporally-resolved analyses of adhesion receptor function, or the systematic global analysis of adhesion signalling networks. Thanks to recent technological innovation, based on proteomics and advanced imaging techniques, it's possible to reveal the complexity, structure, and dynamics of adhesion complexes, leading to a more comprehensive understanding of adhesion function. These analyses have identified a previously unanticipated level of complexity and regulation (Figure 10).

The core functional adhesion complex has been defined using complementary information from unbiased global proteomic and targeted microscopy approaches. Analysis by mass spectrometry

revealed tension-dependent and integrin heterodimer/extracellular matrix (ECM)-dependent components of adhesions. Proteomic analyses also suggest the existence of a large number of non-canonical adhesome components. By contrast, candidate-based microscopy studies have focused on the architecture, interactions, and dynamics of adhesion complex assembly and disassembly. Together these studies have contributed to our understanding of integrin signalling, force generation, and actin regulation and their impact on numerous downstream cellular processes.

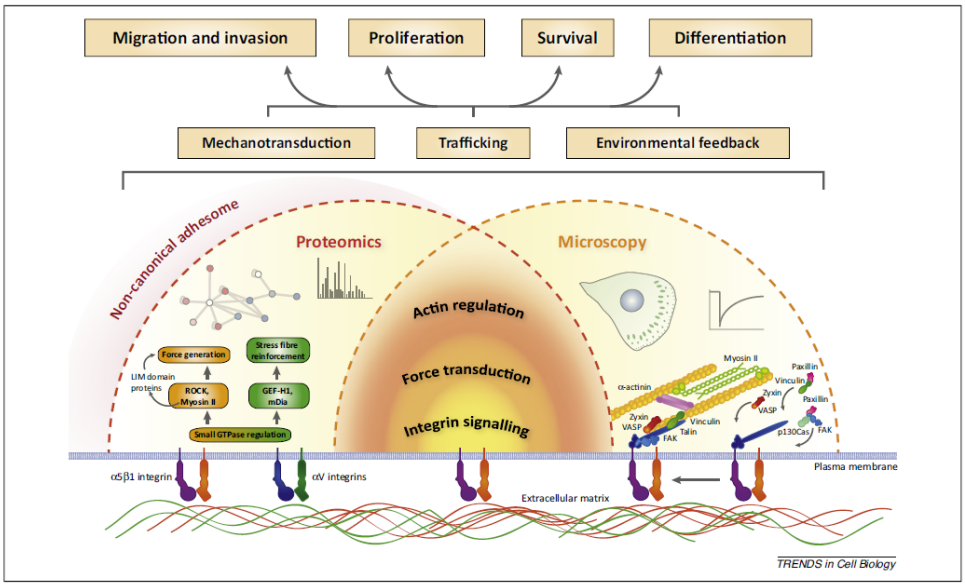

Figure 10: the adhesome complex landscape: integrating recent advances from proteomics and imaging studies. **[Figure from 48]**

1.5.1 Components of mechanotransduction

Mechanotransduction involves different molecules and/or cellular components, i.e. the ECM, channels, focal complexes/ adhesions (FC or FA), the actomyosin network, transcription factors and the nucleus.

1.5.1.1 Extracellular Matrix: role in mechanotransduction

The extracellular matrix has already been discussed in a previous chapter from the structural point of view; in the present chapter we focus on its role in mechanotransduction.

As a structural material, the ECM controls spatial organization in the tissue across broad length scales, ranging from the nanoscale to the microscale and larger. On the nanoscale level, the ECM affects the organization of receptors on the cell surface and the sequestering of soluble factors. The nanoscale organization of the ECM can affect how growth factors are presented to their receptors (some can be tethered to the matrix) and how morphogens diffuse through tissue. On a more specific level, the spatial presentation of ECM ligands, such as fibronectin, vitronectin, laminin and collagen, and the nanotopography of the ECM, control integrin organization, adhesion assembly, and signal transduction to direct cell behaviour [166-168]. As shown through the use of functionalized gold dots on nanopatterned surfaces, differences in average ligand spacing of as little as ~10 nm seem to be capable of dictating whether integrins are able to assemble into focal adhesions [43]. This indicates that there is a critical threshold of ligand density that is required for integrin clustering and focal adhesion assembly. Cells are also capable of sensing and responding to gradual changes in the spacing of ECM ligands of as little as 1nm over the entire length of a cell body. Additionally, such relatively small gradients are able to direct migration and the alignment of cells and their cytoskeleton [169]. Because the cellular response to the spatial organization of matrix components also depends on the material properties of the matrix, this raises the important distinction that chemistry is not independent of mechanics. Matrix stiffness ultimately controls the cellular response to ligand

presentation and matrix organization. Thus, when cells are cultured on ECM substrates of varying stiffness, focal adhesions fail to assemble below a critical stiffness even when matrix ligands are presented to the cell at saturated levels [170]. At the microscale level and larger, the ECM controls cell shape and tissue boundaries. Matrix dimensionality is a dramatic example of how cell behaviour can be controlled at the microscale [171]. For instance, cells cultured in 2D and 3D show pronounced differences in their motility [172, 173], morphology and cytoskeletal organization [174, 175], as well as in the composition and function of their adhesions, their viability, and their response to soluble factors [176, 177]. In summary, nanotopological features and larger-scale organization of the ECM control the motility and positioning of cells, their geometry, and their mechanical connectivity within the surrounding cellular and non-cellular microenvironment. Such physical rearrangements would be expected to occur on the order of hours and days, and are likely to persist at steady-states dictated by the ECM for considerably longer time durations of months and perhaps years. Such ECM topological reorganizing thereby provides for long-term patterning within the tissue that could elicit profound physiological changes through modifications of tissue-level mechanical forces and cellular mechanotransduction.

1.5.1.2 Stress-sensitive ion channel

Probably the best-studied potential transducer of force into biochemistry is the stress-sensitive ion channel [178]. Tension in the membrane alters the probability of channel opening and leads to an immediate influx of ions, often calcium [179-181]. This influx can then lead to the regulation of cell movement [182] or growth cone retraction [180] and is involved in axon pathfinding [183] and even in signalling cascades [181]. Also related to tension in the membrane is the clustering of membrane receptors and cytoskeletal elements, which can serve as biochemical signalling events [184].

1.5.1.3 Adhesion receptor

Other important components involved in mechanotransduction are adhesion receptors, including integrins and syndecans. Integrins are transmembrane proteins, they are α/β heterodimers that mediate cell adhesion to the extracellular matrix (ECM) and to receptors on other cells [185], thereby regulating numerous biological processes that are essential for development, postnatal homeostasis and pathology [185-188]. The mammalian genome encodes 18 α and 8 β integrin genes, which form 24 heterodimers. Mammalian cells usually co-express several integrins, which recognize ECM components by binding specific amino-acid stretches such as the Arg-Gly-Asp (RGD) motif [185, 189]. RGD motifs are found in many matrix proteins including fibronectin, in which RGD mediates binding to $\alpha_5\beta_1$ and all α_v-class integrins. *In vivo* and *in vitro* studies indicated that $\alpha_5\beta_1$ and α_v-class integrins (for example, $\alpha_v\beta_3$) exert both specific and redundant functions [190-198]; however, how these distinct integrins accomplish their individual functions and whether these cooperate remains unclear. The signaling properties and functions of integrins are executed by specialized adhesive structures with distinct morphology, subcellular localization, lifespan and molecular composition. Nascent adhesions are short-lived adhesive structures in membrane protrusions [199] that promote the activity of Rho_GTPases such as Rac1. Some nascent adhesions develop into large focal adhesions (FAs) that initiate multiple signalling pathways, which activate effectors including myosin II.

Myosin II exerts contractile forces resulting in adhesion reinforcement and recruitment of more proteins to focal adhesions, which induces a further increase in myosin II activity [157]. This feedback signaling to myosin II critically depends on biophysical parameters such as ECM stiffness. The identity of mechanosensor(s) in focal adhesions, whether it is an integrin, a focal adhesion protein or a combination of both, is unknown [200]. Receptor trafficking and cell adhesion are shown in figure 11.

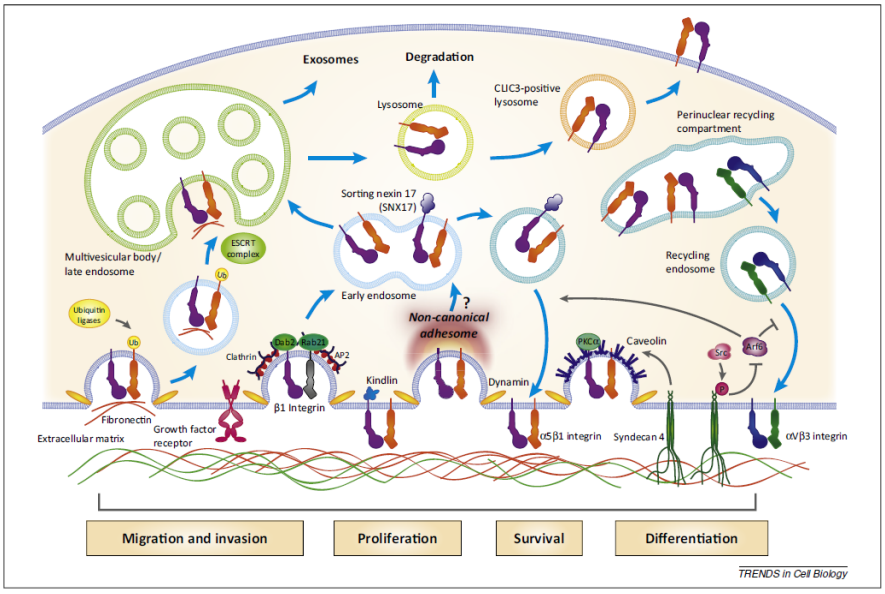

Figure 11: receptor trafficking and cell adhesion. Following internalization, integrins follow multiple trafficking routes (blue arrows) whereby they are recycled back to the cell surface or targeted for degradation in lysosomes. Upon fibronectin binding, integrins can be ubiquitinated and undergo ESCRT (endosomal sorting complexes required for transport)-dependent trafficking to the multivesicular body/late endosome prior to degradation [207, 208]. Conversely, sorting nexin 17 (SNX17) can be recruited to the kindlin binding site of b-integrins and promotes integrin recycling back to the cell surface [209, 210]. Co-receptors of integrins can also coordinate trafficking and therefore cell migration [211, 212]. Src-mediated phosphorylation of syndecan-4 suppresses the activity of the adhesome component Arf6, leading to increased recycling of $\alpha_V\beta_3$ integrin to the cell surface, suppressed $\alpha_5\beta_1$ integrin recycling, and stabilization of adhesion complexes [211]. Dynamic regulation of integrin availability at the cell surface through receptor trafficking pathways is essential for microenvironmental sensing during cell migration and invasion, differentiation, and progression through the cell cycle. **[Figure from 48]**

These receptors have evolved to control information flow across the plasma membrane and integrate the ECM with the contractile machinery of the cell bi-directionally [207, 208]. Ligand binding to the extracellular domain of integrins stabilises activated conformations and leads to recruitment of adaptor and catalytic proteins to the integrin cytoplasmic domains. Conversely, recruitment of specific cytoplasmic proteins to the intracellular face of integrins induces receptor priming and drives ligand engagement [209-211]. Stable association of ligands and effectors with integrins can therefore be regulated from both sides of the plasma membrane. Proteins recruited to integrin-mediated adhesion complexes perform both membrane-proximal and membrane-distal signalling functions that coordinate processes including migration, proliferation, differentiation, and ECM remodelling [207, 222, 213]. Adhesion complex has an emerging role in mechanotransduction and modulation by receptor trafficking; indeed, integrins and adhesion complex components work as mechanotransductive signalling effectors and sensor of environmental stiffness and cell generated

force [213, 214]. Cell–matrix adhesion complexes are dynamic structures that form at the periphery of cells as nascent adhesions and undergo myosin II-dependent maturation into focal adhesions anchored to load-bearing bundled actin stress fibres [215].

Focal adhesion assembly

After binding to matrix-coated surfaces, clusters of activated integrins are formed at the cell edge. Integrin cluster formation leads to the recruitment of talin as well as the activation of SRC family kinases (SFKs) (see the figure 12, part **a**), which then recruit the formin family protein FH1/ FH2 domain-containing protein 1 (FHOD1) to integrin clusters, leading to actin assembly (see the figure 12, part **b**; indicated by the dashed arrow). The resulting actin polymerization enables clusters to be pulled together by myosin (see the figure 12, part **c**).

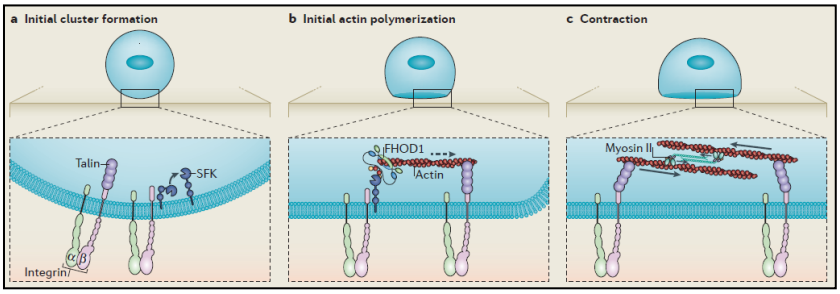

Figure 12: focal adhesion assembly (a, b, c). [Figure from 162]

When nanofabricated barriers (not shown) in the membrane bilayers limit lateral movements, forces are developed on the clusters at the barriers that trigger rapid cell spreading. This presumably involves focal adhesion kinase (FAK), which enhances the activation of the small GTPase RAC1 and targets it to focal adhesions. RAC1 activates actin assembly through actin-related protein 2/3 (ARP2/3), or formins (see the figure 13, parts **d** and **e**). Without barriers, cells will round up and often undergo apoptosis. Analysis of membrane dynamics during cell spreading has indicated that rapid isotropic spreading flattens the initially round cell, drawing membrane from the reservoir of folded surface membrane. Upon the depletion of the folded membrane, tension increases momentarily and

signals the activation of exocytosis to increase the membrane surface area by 40% (see the figure 13, part **f**).

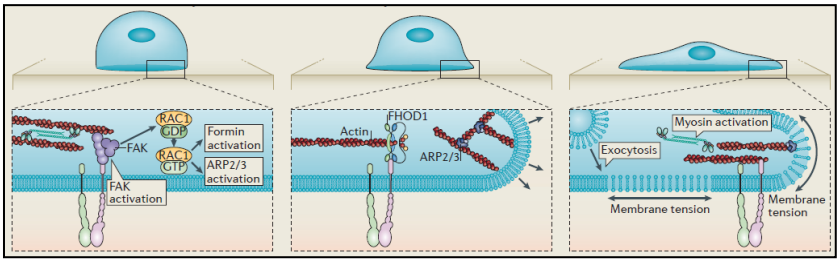

Figure 13: focal adhesion assembly (d, e, f). [Figure from 162]

Then it activates periodic contractions to test substrate rigidity through the local contraction units (see the figure 14, part **g**). Rigidity signalling recruits additional proteins (such as vinculin) and causes adhesion complex reinforcement (see the figure 14, part **h**) or disassembly (if the matrix is too soft; not shown), followed by adhesion maturation (see the figure 14, part **i**). Following adhesion maturation, stress fibres grow from adhesions and will contract to sense matrix rigidity at the whole-cell level.

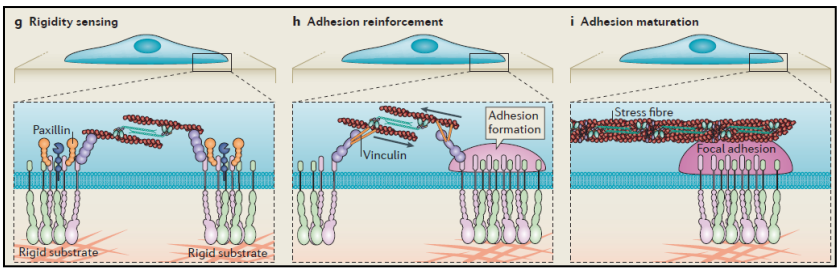

Figure 14: focal adhesion assembly (g, h, i). [Figure from 162]

1.5.1.4 Transcription factors

While these mechanisms can impact cell response rather immediately (on a timescale of seconds to minutes), there is a distinct group of mechanisms that work via transcriptional regulation and on much longer timescales [216]. One class of mechanisms act through transcription factors such as armadillo/β-catenin, serum response factor (SRF), yes-associated protein (YAP), and nuclear factor kappa B (NF-κB). SRF, for example, is a major transcription factor that regulates activity-

driven gene expression in neurons. Activation of SRF-driven transcription occurs through the factor's interaction with cofactors, which in turn are controlled by the amount of G-actin available in the cytoplasm [217]. When the cell interacts with a stiff substrate, it generally has more actin filaments and less G-actin, which frees the cofactors to redistribute from the cytoplasm to the nucleus and activate SRF-dependent transcription, for example in the mouse brain [218]. Inactivation of these cofactors can cause ineffective neuronal migration, aberrant neurite outgrowth during development, and a decreased number of dendritic processes and dendritic length. Overall, the cofactors appear to regulate plasticity-related structural changes in neurons [218]. Other transcriptional coactivators such as YAP and TAZ localize in the nucleus and are transcriptionally active in cells cultured on a stiff ECM; by contrast, YAP and TAZ are excluded from the nucleus and functionally inhibited in cells cultured on a soft ECM [219].

1.5.1.5 Nucleus

Even the nucleus itself could serve as a mechanosensor. The nucleus is mechanically continuously connected to the plasma membrane of cells via the cytoskeleton. As reported in figure 14 cytoskeletal filaments bridge the nucleus to the plasma membrane, which in turn is anchored at sub-cellular sites to extracellular substrates via a plethora of proteins that form focal adhesions. FAs are points of cross-talk between transmembrane integrin receptors and the cytoplasmic filaments and thus are key sites for both biochemical and mechanotransduction pathways. Linkage can be direct or via various adaptor proteins, providing structural support to both cellular and nuclear structures.

Actin filaments and microtubules constantly undergo remodelling by a contractile mechanism and dynamic instability respectively, while domain proteins and the microtubule associated motor protein, dynein, provide structural integrity to the nucleus. From inside, the nuclear lamins and chromatin are anchored to the inner nuclear membrane through adaptor transmembrane SUN (Sad1p, UNC-84) proteins, which in turn are connected to KASH proteins. Hence, though physically separated by the nuclear membrane, the cytoplasm and nucleoplasm are linked by these evolutionarily conserved proteins, that mediate force transmission. Together these proteins are known as the Linker of Nucleoskeleton and Cytoskeleton (LINC) complex. The localization of KASH domain proteins like nesprin at outer nuclear envelope is affected by depletion of SUNs, which in turn depend on nuclear lamins. These links are emerging to be pivotal in various physiological processes including cell migration and cytoskeletal integrity. Together, this network, reported in figure 15, helps the cell cope with mechanical stress.

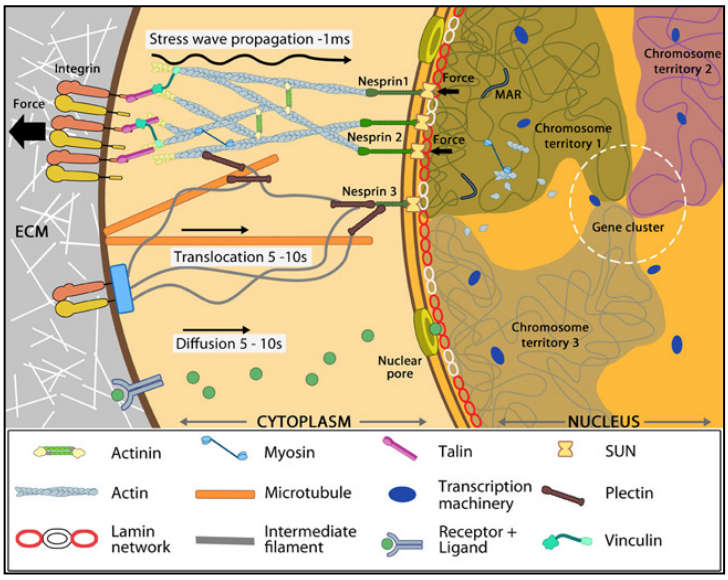

Figure 15: nuclear connectivity and mechanotransduction: Force experienced by integrins at the cell surface via mechanosensing structures like focal adhesions (integrin cluster linked to actin network), hemidesmosomes (blue rectangle) or cell-cell contact (not shown) is accumulated, channeled through SUN1/SUN2 form the LINC (linker of nucleoskeleton and cytoskeleton) complexes connecting further to the nuclear lamina (red and white lamin network) and hence the attached nuclear scaffold proteins (actin and myosin). Chromatin attaches directly to the lamina and to other scaffolding proteins through the matrix attachment regions (MARs). Upon sensing the force, the nuclear scaffold help repositioning the chromatin thus affecting nuclear prestress and activating genes within milliseconds. Spatial segregation of chromosomes with defined territories is represented as colored compartments inside the nucleus. The dotted circle highlights looping of genes from different chromosomes to form a cluster in 3D space and share transcription apparatus (navy ovals). On the contrary, chemical signaling mediated by motor-based translocation along cytoskeletal filaments or diffusion of activated regulatory factors takes few seconds. **[Figure from 540]**

Work by Mazumder et al. ascertained the active involvement of cytoskeletal forces in determining nuclear morphology. Change in nuclear size upon perturbation of actomyosin and microtubules affirmed their roles in exerting tensile and compressive forces respectively on the nucleus, correlating with their functions in the cellular context.

Furthermore, the 'perinuclear cap', which is composed of contractile actin bundles that bridge focal adhesions on either side of the nucleus, has been shown to tightly regulate the nuclear geometry. These bundles pass apically to form a dome covering the top of nucleus and are connected to the nucleus through the LINC complexes. They are completely absent in pluripotent cells whereas during differentiation, their formation accompanies expression and assembly of lamin A/C as well as the LINC complexes on the nuclear envelope. As a result, the nuclear height and shape are under their control, suggesting a role in mediating mechanosensitive processes such as motility and polarization.

Besides nuclear morphology, cytoplasmic forces also govern nuclear positioning in the cell by regulating the translational and rotational dynamics. Positioning is accomplished by the physical connection by nuclear envelope proteins SUN-KASH-lma1 between centromeric heterochromatin regions and the microtubule network. With the centromere providing tensional force on the microtubules that undergo dynamic instability, dynein motors mediate the rotation. Actin links via SUN-nesprin are implicated in force transduction for nuclear movement during cell migration. Regulation of nuclear position and orientation is critical in many cellular processes such as migration, cell division, polarization, fertilization and differentiation. Microtubules with their large persistence length and ability to bear considerable compressive loads can put the nucleus under pressure, and actin in concert with myosin can exert forces on the nuclear membrane (lamins) and the internal nuclear scaffolding. These opposite forces, together with the condensation forces of the chromatin inside the nucleus, are generally balanced and overall put the nucleus under tension. Any deformations of the outer cell surface will thus also be transmitted directly to the nucleus and lead to local or even global nuclear shape changes.

How are these nuclear shape changes then turned into altered cellular function? Although the one dimensional (1D) location of genes and their promoters along DNA has been determined, their resulting 3D position when folded into chromatin inside the nucleus is not (yet) known. However, there is emerging evidence that this positioning is non-random and that changing spatial organization has an impact on nuclear function and gene transcriptional regulation. Relative proximity of gene loci, for example encoding for a gene and that of its controlling transcription factor, or the distance to the transcription machinery could be altered by a deformation of the 3D chromatin distribution inside the nucleus. In that sense, the nucleus could be a mechanosensor influencing gene expression regulation.

1.5 Aim of the project

The aim of this project is to challenge mechanosensing/-transduction and differentiative behaviour of neuron-like PC12 cells with diverse nanotopographies and/or changes of their biomechanical status, and analyse their phosphoproteomic profiles in these settings.

Our previous work [153] revealed that in the latter condition, complex mechanotransductive events were at the basis of cellular processes that lead to the onset of neuritogenesis and neuronal differentiation. However, at the proteome level we only compared the nanostructured surface with a roughness parameter Rq of 15 nm root mean square (RMS) against a flat zirconia surface. Besides these two conditions (ns-Zr15 and flat-Zr), the proteomic analyses in this study comprise instead PC12 in more versatile experimental conditions including a surface nanotopography with higher roughness, the biochemically NGF induced canonical neuronal differentiation and manipulations that affect the biomechanical status of the PC12 cell. This approach allowed us to obtain a deeper understanding of cellular nanotopography sensing and mechanotransductive signal integration.

2. MATERIALS AND METHODS

2.1 Substrate fabrication

As a basis for all substrates standard microscope glass slides with the dimensions of 76×26 mm (surface area∼20 cm^2) were used. On this carrier, the cluster-assembled nanostructured film is produced by supersonic cluster beam deposition (SCBD) of zirconia clusters obtained through a pulsed microplasma cluster source by our collaborators at the CIMAINA Institute-Milano University. In the PMCS an argon plasma jet ignited by a pulsed electric discharge ablates a zirconium rod. Zr atoms and ions sputtered from the target thermalize with the argon and traces of oxygen present in the condensation chamber and aggregate to form ZrO_x clusters. The mixture of clusters and inert gas then expands into a vacuum, through a nozzle, to form a seeded supersonic beam. The clusters carried by the seeded supersonic beam are collected on a substrate intersecting the beam trajectory (deposition rate of about 0.5–2.5 nm/min) and placed in a second vacuum chamber, thus forming a cluster-assembled film. Further oxidation of ZrO_x clusters takes place upon exposure to ambient atmosphere thus forming a ZrO_2 film. These cluster-assembled zirconia surfaces are given the abbreviation ns-Zr throughout the thesis. The number after Zr indicates the roughness parameter Rq. Two different batches of cluster-assembled ZrO_2 films (called ns-Zr, hereafter) with roughness Rq of 15 nm (ns- Zr15) and 25 nm (ns-Zr25) were produced on round glass coverslips (Ø13 mm), microscope glass slides (76 × 26 mm area), glass-bottomed cell culture dishes (Ø40 mm) or Aclar® films.

The roughness and the morphological parameters have been systematically characterized by atomic force microscopy (AFM) [154, 220]. The capacity of SCBD to reliably cover large macroscopic areas with nanostructured films of a predefined roughness allowed us to perform the experiments on microscope glass slides with the dimensions of 76 × 26mm (∼20 cm^2 surface area).

This allowed obtaining a cellular material sufficient for all the proteomic analysis including the phosphorylation status of the proteins.

The flat zirconia surfaces (flat-Zr) with a roughness of ~0.4 nm RMS were obtained with electron beam evaporation. For the canonical reference, the microscope glass slides were coated with poly-L-lysine (PLL) (Sigma-Aldrich, St. Louis, USA, Missouri) for 30 min at room temperature (RT), after cleaning with 70% ethanol and washing twice with PBS. This coating was done directly before plating the cells.

All substrates were sterilized with UV light for 10 minutes before seeding the cells.

2.2 Cell culture and analysis

2.2.1 Cell culture

PC12 (PC-12 Adh ATCC Catalog no.CRL-1721.1^{TM}) were cultured in RPMI-1640 Medium (Sigma-Aldrich) supplemented with 10 % horse serum (HS; Sigma- Aldrich), 5 % fetal bovine serum (FBS; Sigma-Aldrich), 2 mM L-glutamine, 100 units/ml penicillin, 100 µg/ml streptomycin, 1 mM pyruvic acid (sodium salt) and 10 mM HEPES. The culture conditions in the incubator (Galaxy S, RS Biotech, Irvine, UK) were 37◦C and 5% CO_2 (98% air-humified). For subculturing (routinely performed every 2nd–3rd day) the cells were detached from culture dishes using a 1 mM EDTA solution in HBSS (Sigma-Aldrich) or a trypsin solution (Sigma- Aldrich), centrifuged at 1000×g for 5 min, and re-suspended in culture medium.

For the experiments the PC12 cells were detached with 1 mM EDTA in HBSS and centrifuged at 1,000× g (5min), washed with low serum medium (RPMI-1640 with all the supplements, but only 1% HS and without FBS), and centrifuged again at 1,000× g (5 min). Before plating the cells on the different substrate conditions, the cells were counted with an improved Neubauer chamber and then seeded with the concentration of ~4,000 cells/cm^2 (after resuspension in RPMI low serum medium)

onto the microscope slides that were placed into non-treated 4 well dishes with the dimensions 127.8 × 85.5 mm (Thermo Fisher).

For the NGF condition, the NGF stimulus (human NGF-b, Sigma-Aldrich) was added to the medium right after plating the cells making a final concentration of 50 ng/ml. For the ns-Zr15 hypo condition, the cells were re-suspended in RPMI low serum medium diluted 7.5/2.5 with deionised water (supplements were kept at the aforementioned concentrations) and pre-incubated in the hypoosmotic medium for 15 min before plating the cells eventually into the well, always in the hypoosmotic medium. For the PLL hyper condition, after the adhesion of the cells (1 h after plating) a hyperosmotic shock was applied to the cells (150 mM sucrose final concentration in the RPMI low serum medium) for 15min, and washed once with RPMI low serum medium. The cells were left in RPMI low serum medium for the rest of the experiment. The cells were left in the incubator for 24 h in all conditions. After washing twice with PBS, the cellular material was yielded for the proteomic analysis by scratching the cells from the microscope slides with cell scrapers (TPP, Trasadingen, Switzerland) in the presence of icecold PBS supplemented with protease (Roche, Basel, Switzerland) and phosphatase inhibitors (phosphatase inhibitor cocktail (Cell Signalling Technology), calyculine A (serine/threonine phosphatase inhibitor) 10 nM (Cell Signalling Technology), microcystin-LR 10 nM (Enzo Life Sciences).

For the inhibition experiments with SKF96365 (Sigma-Aldrich) and GsMTx4 (Alomone Labs, Israel), the resuspended cells were preincubated with the inhibitors (SKF96365 15µM; GsMTx4 10µM) in RPMI low serum medium (supplemented with 50 ng/ml NGF in the PLL +NGF condition) for 15 min in suspension before plating. The inhibitor treatment was maintained for 1 h, and then the medium was discarded and exchanged with new RPMI low serum medium (plus 50 ng/ml NGF in the PLL +NGF condition). For the rapamycin inhibition (Sigma-Aldrich), the cells were treated with the indicated rapamycin concentrations for the whole duration of the experiment. After 24 h, respectively 48 h for the rapamycin experiments, the morphology of the PC12 cells was recorded

with an inverted Axiovert 40 CFL microscope (Zeiss, Oberkochen, Germany) equipped with LD A-Plan 20x/0.3 Ph1 or CP-ACHROMAT 10x/0.25 Ph1 objectives (both Zeiss) and the analysis was performed with ImageJ (NIH, New York, USA). The neurite length and differentiation rate were evaluated according to the following definition: the length was the straight-line distance from the tip of the neurite to the junction between the cell body and neurite base. In the case of branched neurites, the length of the longest branch was measured. For each cover glass, 20 and 40× images were acquired randomly by scanning the wells, measuring in each image: N, as total number of cells; n, as number of cells with the neurite longer than 20 μM (cells considered positive for neurite extension); l, as neurite length in μM; R, as differentiation rate determined by the equation R = 100 * n / N. Cells with neurites >10μm were counted as differentiated and only neurites with a length >10μm were considered for neurite length quantification. If cells have multiple neurites only the longest two were taken into the quantification, and in case of neurite branching the longest branch was measured. The neurite morphology was comparable between the canonical biochemically (NGF-)induced and the nanotopography-triggered neuritogenesis with 1.82 ± 0.42 neurites per cell for the first and 1.66 ± 0.21 for the latter (in total 160 differentiated cells for each condition were quantified from 8 independent experiments) (Figure 16). In both cases the median was 2 neurites per cell and the vast majority of cells bore 1 or 2 neurites (together 82%, respectively 90%).

All the inhibition experiments were performed on coverslips with a diameter of 13 mm. The substrate preparation itself was the same as in the precedent section.

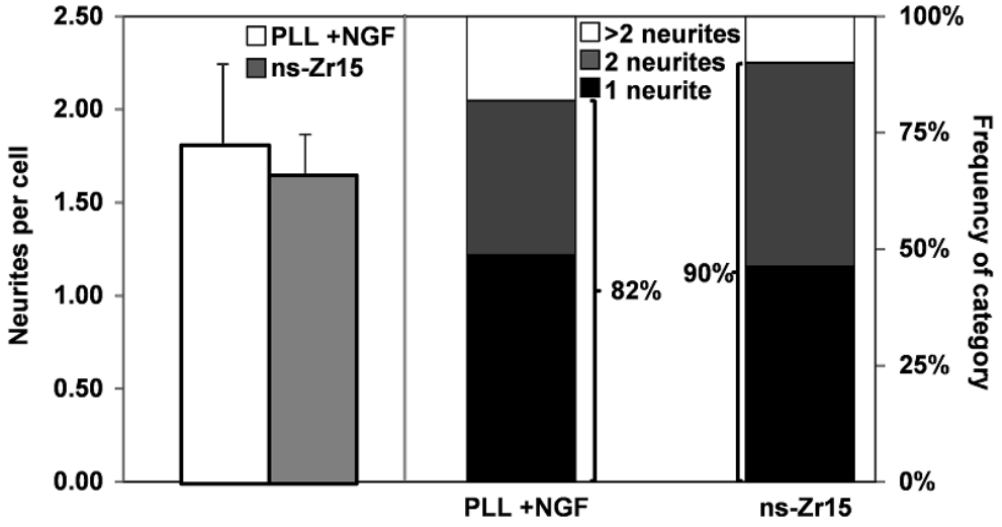

Figure 16: comparison of the neurite morphology of PC12 cells in the between NGF and ns-Zr15 condition. The graph shows on the left the average number neurites per differentiated PC12 cell grown on PLL and stimulated with NGF (white bar) or interacting with ns-Zr15 (gray bar). The bars are flanked by the standard deviation (s.d.). On the right, the bars demonstrate the frequency of the different categories indicating the number of neurites per differentiated cells in the two conditions. In total 160 cells from 8 independent experiments were quantified.

2.3 Bradford assay

The concentration of each sample was determined using the Bradford method. The Bradford assay is based on Coomassie Brilliant Blue G-250 (CBBG) that specifically binds to protein at arginine, tryptophan, tyrosine, histidine and phenylalanine residues. CBBG binds to these residues in the anionic form, which has an absorbance maximum at 595 nm. The assay is monitored at 595 nm in a Du® 730 Life Science Uv/vis Spectrophotometer (Beckman Coulter), and determines the CBBG-protein complex. Bovine plasma immunoglobulin was used as standard protein.

2.4 Protein identification by mass spectrometry

Prior to proteolysis, proteins were subjected to reduction with 1 mM DTE (30 min at 55°C) and alkylation with 20 mM iodoacetamide (IAA; 30 min. at RT). Peptide digestion was conducted using sequence-grade trypsin (Roche) for 16 hours at 37°C using a protein:tripsin ratio of 1:20. The reaction was stopped by acidification with 98% formic acid (FA) at 37°C for 30 minutes. The pellet was desalted using Zip-Tip C18 (Millipore) before mass spectrometric (MS) analysis.

2.4.1 Zip-Tip C18

Each sample was desalted (Zip-Tip C_{18}, Millipore) before mass spectrometric (MS) analysis.

The following protocol was applied:

- Equilibrate the Zip Tip for Sample Binding: **1)** pre-wet the tips with 50% CH_3CN 3 times (3 x 100 µl); **2)** wash the tips with TFA 0.1% 3 times (3 x 100 µl).

- Bind and Wash the Peptides: **1)** bind the sample to Zip Tip pipette tip. Aspirate and dispense the material 10-13 cycles for maximum binding of complex mixtures; **2)** wash the tips with 5% CH_3CN 0.1% TFA at least once.

- Elute the Peptides: elute the sample with 50% CH_3CN in HCOOH 1%, 3 times (3 x 100 µl), into a clean vial, for mass spectrometry analysis.

2.5 Mass Spectrometry

Mass spectrometry is an analytical tool useful for measuring the mass-to-charge ratio (m/z) of one or more molecules present in a sample. These measurements can often be used to calculate the exact molecular weight of the sample components. Typically, mass spectrometers can be exploited to identify unknown compounds via molecular weight determination, to quantify known compounds, and to determine structure and chemical properties of molecules. Basically, a mass spectrometer is composed of an ion source, of a system to separate the ions according to their m/z, and of an ion detector. The sample has to be introduced into the ionization source of the instrument. Once inside the ionization source, the sample molecules are ionized, because ions are easier to manipulate than neutral molecules. These ions are extracted into the analyzer region of the mass spectrometer where they are separated according to their mass (m) to-charge (z) ratios (m/z). The separated ions are detected and this signal sent to a data system where the m/z ratios are stored together with their relative abundance for presentation in the format of a m/z spectrum. The analyzer and detector of the

mass spectrometer, and often the ionization source too, are maintained under high vacuum to give the ions a reasonable chance of travelling from one end of the instrument to the other without any hindrance from air molecules. The entire operation of the mass spectrometer, and often the sample introduction process also, is under complete data system control on modern mass spectrometers.

2.5.1 Ionization tecniques

Ionization techniques are also known as interfaces because they allow the passage of the analytes from samples to the mass analyzer. These techniques are crucial to determine what types of samples can be analyzed by MS (liquid, solid, etc.) and to know which kind of ionizing charged will have the molecules measured. Two techniques often used with liquid and solid biological samples: matrix-assisted laser desorption/ionization (MALDI) [221, 222] and electrospray ionization (ESI) [223].

Electrospray ionization

Electrospray ionization (ESI) produces gaseous ionized molecules directly from a liquid solution creating a fine spray of highly charged droplets in the presence of an electric field. The sample solution is sprayed from a region of the strong electric field at the tip of a metal nozzle maintained at a potential of anywhere from 700 V to 5000 V. The needle to which the potential is applied serves to disperse the solution into a fine spray of charged droplets. Either dry gas, heat, or both are applied to the droplets at atmospheric pressure thus causing the solvent to evaporate from each droplet. As the size of the charged droplet decreases, the charge density on its surface increases. The mutual Coulombic repulsion between like charges on this surface becomes so great that it exceeds the forces of surface tension, and ions are ejected from the droplet through a “Taylor cone”. Another possibility is that the droplet explodes releasing the ions. In either case the emerging ions are directed into an orifice through electrostatic lenses leading to the vacuum of the mass analyzer. These charged

analyte molecules can be singly or multiply charged. This is a very soft method of ionization as very little residual energy is retained by the analyte upon ionization.

Several variations on the electrospray process have been developed such as nanospray ionization. Nanospray is a form of ESI that employs low flow rate from 10 to 1000 nL/min. As the flow rate is lowered, a lower volume of mobile phase passes through the emitter producing smaller aerosol droplets. This makes nanospray ionization more effective than conventional ESI at concentrating the analyte at the emitter tip, producing significant increases in sensitivity demonstrated by the signal response of the mass spectrometry.

2.5.2 Liquid chromatography electrospray-tandem MS/MS analysis

An important enhancement to the mass resolving and mass determining capabilities of MS is obtained by coupling it with chromatographic separation techniques. Common combinations are gas chromatography-mass spectrometry (GC/MS) or liquid chromatography-mass spectrometry (LC/MS).

In this work, samples were separated by liquid chromatography using an UltiMate 3000 HPLC (Dionex, now Thermo Fisher Scientific). Buffer A was 0.1% v/v HCOOH, 2% CH_3CN; buffer B was 0.1% HCOOH in CH_3CN.

Chromatography was performed with a PicoFrit ProteoPrep C18 column (200 mm, internal diameter of 75 μM, Dionex). The gradient was as follows: 1% CH_3CN in 0.1% HCOOH for 10 min, 1-4% CH_3CN in 0.1% HCOOH for 6 min, 4-30% CH_3CN in 0.1% HCCOH for 147 min and 30-50% CH_3CN in 0.1% HCOOH for 3 min at a flow rate of 0.3 μl/min.

Mass spectrometry was performed using an LTQ-Orbitrap Velos (Thermo Fisher Scientific) equipped with a nanospray source (Proxeon Biosystems, now Thermo Fisher Scientific). Eluted peptides were directly electrosprayed into the mass spectrometer through a standard non-coated silica tip (New Objective, Woburn, MA, USA) using a spray voltage of 2.8 kV.

2.5.3 LTQ ORBITRAP VELOS

LTQ Orbitrap Velos is a hybrid mass spectrometer incorporating the LTQ Velos™ dual cell linear trap and the Orbitrap™ analyzer [224, 225]. The ion storage and the injection into the Orbitrap allows high resolving power, mass accuracy, and transmission over a wide dynamic range and forms the basis for a hybrid mass spectrometer combining these analytical parameters with the MS^n capability of the linear ion trap mass spectrometer.

Briefly, the LTQ Orbitrap Velos (Figure 17) consists of four main components: i) a dual cell linear ion trap for sample ionization, selection, fragmentation, and AGC™; ii) an intermediate storage device (curved linear trap) that is required for short pulse injection; iii) an Orbitrap analyzer for Fourier transformation-based analysis and iv) a collision cell for performing higher energy CID experiments.

The LTQ Orbitrap Velos ETD has also an additional reagent ion source for enabling post-translational modification analyses of peptides by Electron Transfer Dissociation (ETD).

As its name suggests, Orbitrap is a device that is able to store and trap ions [226]. It is not conventional ion trap as a linear ion trap [227], because there is neither RF nor a magnet to hold ions inside, but an electrostatic field that trap ions [228]. The electrostatic attraction towards the central electrode is compensated by a centrifugal force that arises from the initial velocity of ions, which makes ion moving like a satellite on orbit. The electrostatic field forces the ions to move in complex spiral patterns. The axial component of these oscillations can be detected as an image current on the two halves of an electrode encapsulating the Orbitrap. A Fourier transform is employed to obtain oscillation frequencies for ions with different m/z values, which can be determined from these values. Since ions can be trapped for long times, the frequency of their image current can be registered with high accuracy, allowing to obtain high resolution mass spectrum.

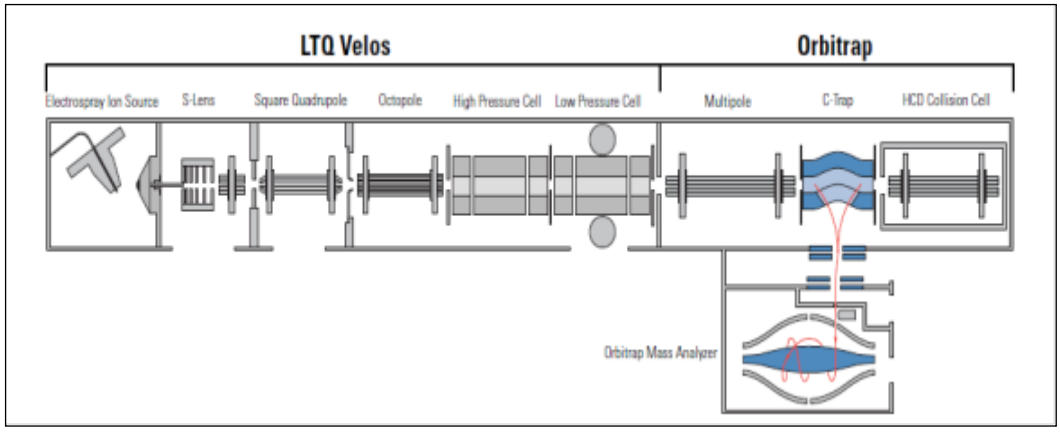

Figure 17: LTQ ORBITRAP VELOS

2.5.4 Tandem Mass Spectrometry

An important application of mass spectrometry is the possibility to fragment molecules to study the different fragments and to better understand the structure and possible mutations of the molecules. These fragmentation studies can be done by Tandem Mass Spectrometry technique or MS/MS analysis. This technique involves the activation of a known precursor ion, formed in the ion source, and the mass analysis of its fragmentation products. MS/MS analysis can be done using different ion activation techniques: CID (Collision-induced dissociation), HCD (Higher energy collision dissociation), and ETD (Electron-transfer dissociation).

In this work, the LTQ-Orbitrap was operated in positive mode in data-dependent acquisition mode to automatically alternate between a full scan (m/z 350-2000) in the Orbitrap (at resolution 60000, AGC target 1000000) and subsequent collision-induced dissociation (CID) MS/MS in the linear ion trap of the 20 most intense peaks from full scan (normalized collision energy of 35%, 10 ms activation). Isolation window: 3 Da, unassigned charge states: rejected, charge state 1: rejected, charge states 2+, 3+, 4+: not rejected; dynamic exclusion enabled (60 s, exclusion list size: 200). Three technical replicate analyses of each sample were performed. Data acquisition was controlled by Xcalibur 2.0 and Tune 2.4 software (Thermo Fisher Scientific).

2.6 Data processing and analysis

Mass spectra were analyzed using MaxQuant software (version 1.3.0.5). the initial maximum allowed mass deviation was set to 6 ppm for monoisotopic precursor ions and 0.5 Da for MS/MS peaks. Enzyme specificity was set to trypsin, defined as C-terminal to arginine and lysine excluding proline, and a maximum of two missed cleavages were allowed. Carbamidomethyl cysteine was set as a fixed modification, while N-terminal acetylation, methionine oxidation and Ser/Thr/Tyr phosphorylation were set as variable modifications. The spectra were searched by Andromeda search engine against the rat Uniprot sequence database (release 29.05.2013). Protein identification required at least one unique or razor peptide per protein group.

Quantification in MaxQuant was performed using the built in XIC-based label free quantification (LFQ) algorithm [228] using fast LFQ. The required false positive rate was set to 1% at the peptide and 1% at the protein level against a concatenated target decoy database, and the minimum required peptide length was set to six amino acids. Statistical analyses were performed using the Perseus software (version 1.4.0.6, www.biochem.mpg.de/mann/tool/).

Only proteins/phosphopeptides present and quantified in at least 3 out of 4 technical repeats were considered as positively identified in a sample and used for statistical analyses. An Anova test (Permutation based FDR 0.05) was carried out to identify proteins/phosphopeptides differentially expressed among the different conditions. To tackle specific biological issues, we then compared subsets of three proteomic data related to specific conditions, namely: [ns-Zr15, NGF, PLL], [ns-Zr15, NGF, flat-Zr], [ns-Zr15, NGF, ns-Zr25]. Therefore, proteins/phosphopeptides were considered differentially expressed if they were present only in one condition or showed a Post-hoc Bonferroni test $p < 0.0167$. Regarding the proteomic data of ns-Zr15 hypo and PLL hyper which refer to peculiar cell conditions, the following comparisons were performed: [ns-Zr15, ns-Zr15 hypo], [PLL hyper and PLL], and [ns-Zr15 hypo, PLL hyper]. Proteins/phosphopeptides were considered differentially

expressed if they were present only in one condition or showed a significant Welch t-test difference (cut-off at 5% permutation-based FDR).

Bioinformatic analyses were carried out by DAVID software (release 6.7) [229], Panther software [230], ClueGO application of Cytoskape software (release 3.2.0) (http://www.cytoscape.org/), and Ingenuity Pathway Analysis (IPAR) (QIAGEN Redwood City, www.qiagen.com/ingenuity) to cluster enriched annotation groups of Molecular Function, Biological Processes, Pathways, and Networks within the set of identified proteins/phosphopeptides. The compared data sets are indicated in the relative figures. Functional grouping was based on a Fisher Exact test $p \leq 0.05$ and at least two counts.

3. RESULTS AND DISCUSSION

3.1 Similarities and differences at the protein level between biochemically and mechanotransductively promoted neuronal differentiation at the protein level

To dissect similarities and differences at the proteome level between the biochemically and mechanotransductively promoted neuronal differentiation we compared the data sets of ns-Zr15 (neuritogenesis-triggering cluster-assembled zirconia surface), PLL and NGF [canonical condition on PLL-coated glass, in the presence (NGF) or absence (PLL) of NGF]. Venn diagram, workflow and volcano plot are showed in figure 18.

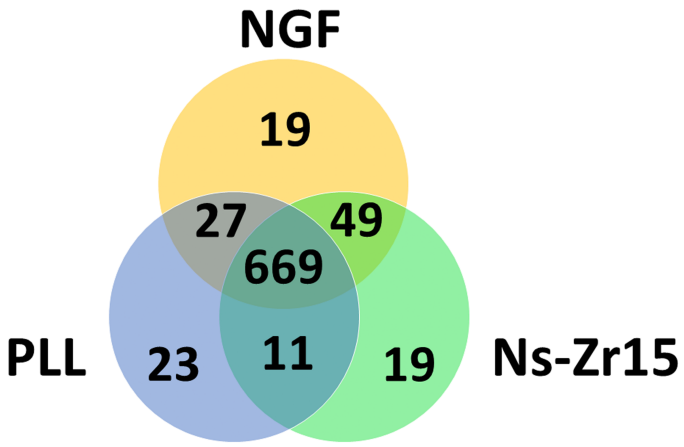

Figure 18: Veen Diagram of the proteins identified in PC12 cells grown on poly-L-lysine-coated glass in absence (PLL) or in presence of NGF (NGF) and nanostructured zirconia 15 nm (nsZr15). An Anova test (FDR 0.05) was carried out to identify proteins differentially expressed among the different conditions: 19, 23 and 19 proteins are exclusively expressed in nsZr15n, PLL and NGF respectively, while 231 out of 669 common proteins differ with statistical significance.

The analysis allowed to identify 669 common proteins among the three conditions as resumed in Figure 18. An ANOVA test (false discovery rate 0.05) was carried out to identify proteins differentially expressed among the three conditions: 231 out of 669 common proteins differ with statistical significance and were selected for further analyses. In particular, to better understand the effect of the surface nanotopography, specific analyses were carried out by comparing specific data sets: the proteome of cells interacting with the nanostructured cluster-assembled zirconia surfaces that trigger neuritogenesis (ns-Zr15) was compared to the proteome of cells grown in the canonical condition on PLL-coated glass, in the presence (NGF) or absence (PLL) of NGF. NGF vs PLL was used as positive control of differentiation induce by NGF.

The analysis provides information on protein expression and also on post translational modification (phosphorylation). Proteins were considered differentially expressed if they were present only in in one condition or showed significant t-test difference (Post hoc Bonferroni test p value = 0.0167) (figure 19).

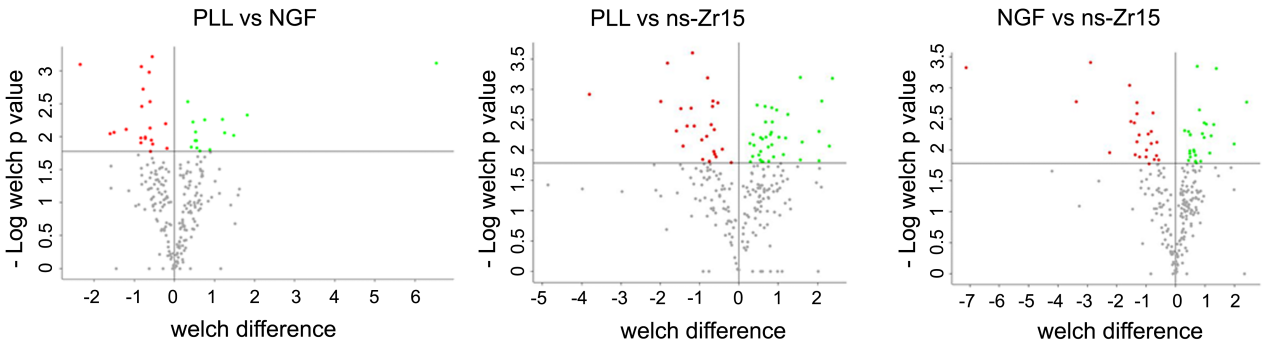

Figure 19: Volcano Plot. The colored data points in the volcano plot that are located above the p value line (t test value cut off is 0.0167) correspond to the proteins that were differentially expressed in two conditions considered upon treatment with large magnitude fold changes and high statistical significance. In green are indicated proteins that are up regulated, in red are the down regulated. The proteins having a fold-change less than 1.5 are shown in gray.

The experimental steps performed in the proteomics approach are summarized in Figure 20.

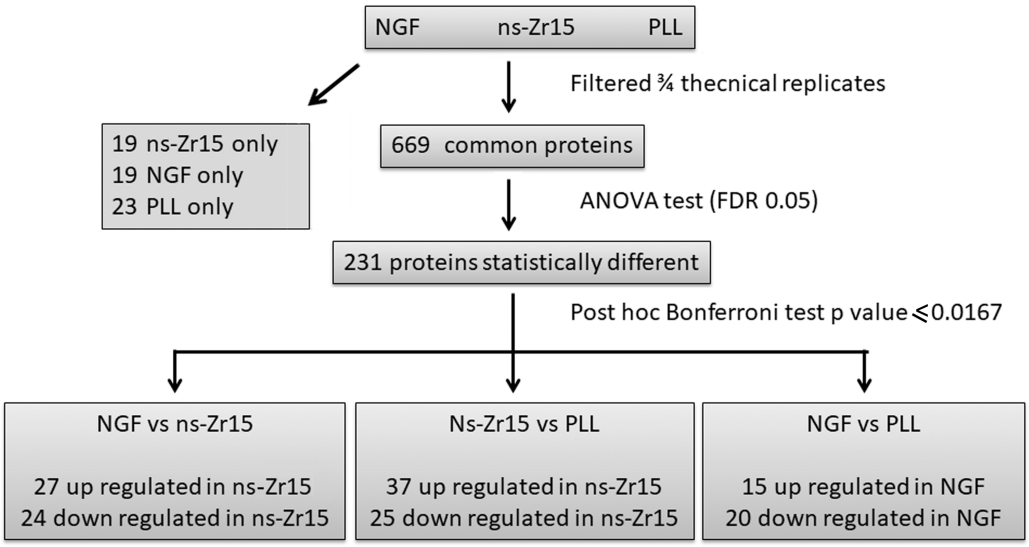

Figure 20: workflow of comparison of PLL, NGF and ns-Zr15. Numbers are referred to expressed proteins.

The proteomic analysis of NGF vs PLL compared to ns-Zr15 vs PLL highlights the common outcome of neuronal differentiation, independent of whether initiated canonically by NGF stimulation (NGF) or instead by mechanotransductive processes (ns-Zr15). 11 out of 35 proteins found to be significantly altered in NGF vs PLL are differentially expressed in the same manner also in ns-Zr15 vs PLL. Several of these proteins indeed have prominent and versatile known roles in the regulation of neuronal functioning and neurogenic processes (such as e.g., Htra1 [231, 232]; Vps35 [233, 234]; Fasn [235]; Pdia3/ERp57 [236, 237]; C3 [238]; RPL19 [239].)

The comparison of ns-Zr15 vs PLL with ns-Zr15 vs flat-Zr [153] shows that the impact of ns-Zr15 on the protein expression profile is very similar (24 proteins altered in the same manner; marked X in Table 1) with respect to the two flat surfaces (flat-Zr and PLL).

Pointing instead more specifically toward the differences between ns-Zr15 and NGF (ns-Zr15 vs NGF, Table 2), the comparison reveals that 19 proteins (37%) are involved in cell proliferation and differentiation, 11 (22%) are receptors or players in signal transduction processes and 4 (8%) are related to Ca^{2+} signaling. Moreover, the ClueGo analysis highlights that these proteins are mainly involved in neurofilament formation and assembly (e.g., vimentin, an intermediate filament protein

needed during initiation of neuritogenesis; [240]) and some in protection against oxidative damage (Figure 21).

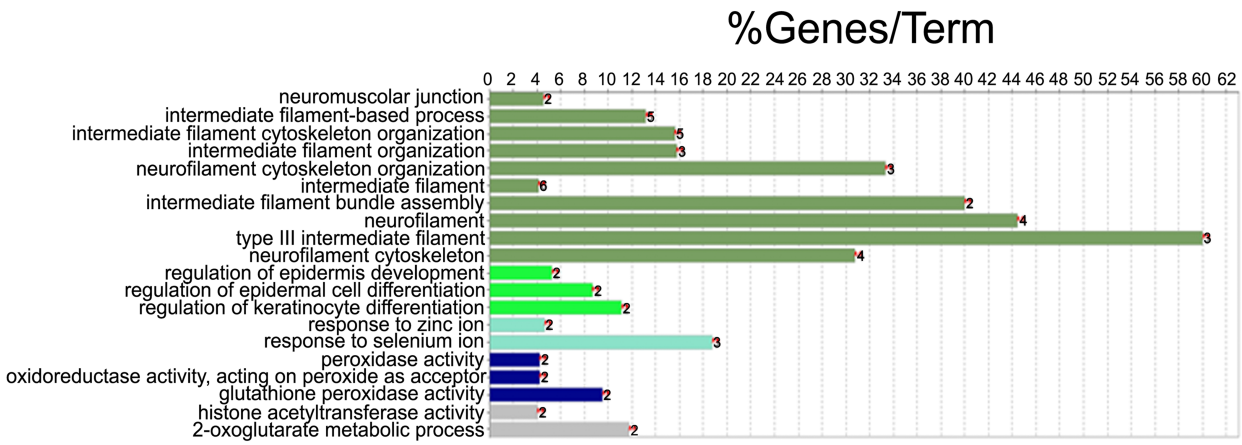

Figure 21: ClueGo analysis of proteins upregulated or expressed only in cells grown on ns-Zr15 vs NGF.
Functional grouping was based on $p \leq 0.05$ and at least two counts. Numbers represent genes numerosity.

For some of these proteins crucial and versatile functions in (post-)transcriptional and epigenetic regulation have been observed (e.g., DDB1 [241], Nedd4 [242, 243, 244]; Dpy30 [245]; Nsun2 [246, 247], HMGB2 [248], hnRNP A1 [249, 250], Vbp1/prefoldin 3 [251].). Moreover, various proteins are of particular interest regarding a potential connection of mechanotransductive signaling and neuronal differentiation processes in the nanotopography- induced setting (e.g., Fat4 [252-254], Versican [255, 256], Thrombospondin [257-260, 256], ADAM12 [261, 262], Talin [263, 264], NCoa2 [265-274], Ran(bp3/GAP) [275]). This information is additionally validated by the IPA bioinformatics analysis of the proteins differentially expressed in ns-Zr15 vs NGF. This evaluation detected relevant protein networks modulated by the surface nanotopography related to: cell morphology, cellular assembly and organization, cellular movement, molecular transport, cell signaling, vitamin and mineral metabolism, cancer and invasion (Table 4).

Table 2 Proteins differently expressed comparing ns-Zr15 vs PLL. X = proteins differentially expressed in the same manner in ns-Zr15 vs flat-Zr and ns-Zr15 vs PLL. In gray, proteins differentially expressed in the same manner in NGF vs PLL and ns-Zr15 vs PLL.

Welch Difference	Protein IDs	Protein names	Gene names	Comparison ns-Zr15vsflat-Zr with ns-Zr15vsPLL
-3,79609	P63312	Thymosin beta-10	Tmsb10	X
-1,98755	F1LP80;P20156;M0RDR2	Neurosecretory protein VGF	Vgf	
-1,82048	P00787;Q6IN22	Cathepsin B	Ctsb	X
-1,59084	F1LXK8	Protein Kmt2d (Histone-lysine N-methyltransferase)	LOC100362634	X
-1,47791	P11232;R4GNK3	Thioredoxin	Txn	X
-1,4192	Q4KM49	Tyrosine--tRNA ligase, cytoplasmic (YARS)	Yars	
-1,32253	B2RYM3;CON__Q0VCM5	Inter-alpha trypsin inhibitor, heavy chain 1	Itih1	X
-1,21926	Q7TP54;D4A8D3;P02793;M0R5T8;M0R6L9;M0R597;M0RCS3;F1M5T1;D3ZUZ5;D4ADM5	Ferritin;Ferritin light chain 1	Fam65b;Ftl;Ftl1	
-1,18024	P25236	Selenoprotein P;Selenoprotein Se-P10;Selenoprotein Se-P6;Selenoprotein Se-P2;Selenoprotein Se-P1	Sepp1	
-1,13526	M0R9G2;P06238	Alpha-2-macroglobulin	A2m	X
-0,9431	D4A9V4	Protein E2f4	LOC100360427	X
-0,92619	Q5U216	ATP-dependent RNA helicase DDX39A	Ddx39a	
-0,82184	G3V7K3;P13635	Ceruloplasmin	Cp	
-0,79789	M0RBF1;M0RBJ7	Complement C3	C3	
-0,75414	M0R685;D3ZSS4;D4ADQ0;D3Z875;D3Z888	Ulk4	Ulk4	X
-0,70887	P13668;A0A096MK73;P21818	Stathmin	Stmn1	
-0,67426	Q6AXU6	Hematological and neurological expressed 1 protein	Hn1	X
-0,6597	Q5U328;P13383	Nucleolin	Ncl	X
-0,63929	F7FEZ6;P04256;M0R584;F1M6M1;D4A2D2;F1LUF2;F1M6C7;D4ACJ7	Heterogeneous nuclear ribonucleoprotein A1	Hnrnpa1	X
-0,62126	M0R7B4	Protein LOC684828	LOC684828	
-0,61327	Q6P7A7;P07153	Dolichyl-diphosphooligosaccharide--protein glycosyltransferase subunit 1	Rpn1	
-0,58489	D3ZC07;Q63945;Q63945-2;F6Q1X3;D4ADL2;P80349	Protein SET	Pkn3;Set	

-0,53705	P04937;P04937-3;P04937-2;P04937-4;A0A096P6L8;F1LST1	Fibronectin	Fn1	**X**
-0,42766	Q64268;CON__ENSEMBL:ENSBTAP00000018574	Heparin cofactor 2	Serpind1	**X**
-0,19459	P11598	Protein disulfide-isomerase A3	Pdia3	**X**
0,28212	P11980-2;P11980;M0R4B8;M0RD14;M0RBT1;M0R5T1;D3ZH80;P12928;P12928-2;D4ADU8	Pyruvate kinase isozymes M1/M2	Pkm2	
0,29285	P85845	Fascin	Fscn1	**X**
0,344429	Q08163	Adenylyl cyclase-associated protein 1	Cap1	**X**
0,355151	G3V8C3;P31000;F1M7P4;P48675;Q6P725;P21807;P16884;F1LRZ7;P12839;G3V8Q2;P23565	Vimentin	Vim	
0,383326	P34058;F1LTA7;F1M2F7;F1LYW7	Heat shock protein HSP 90-beta	Hsp90ab1	
0,459751	M0R9D5	Protein Ahnak	Ahnak	
0,50837	F1LQQ1;P13697	Malic enzyme	Me1	
0,541918	M0R4M2	Olfactory receptor	Olfr1320	
0,548924	Q499N6	UBX domain-containing protein 1	Ubxn1	
0,549268	G3V852	Protein Tln1	Tln1	
0,569478	P06214;M0RDE7	Delta-aminolevulinic acid dehydratase	Alad	
0,597732	P85973;D3ZXK9	Purine nucleoside phosphorylase	Pnp	**X**
0,61237	P13471;Q6PDV6	40S ribosomal protein S14	Rps14	
0,661978	P12785	Fatty acid synthase	Fasn	
0,678424	Q4FZU6	Annexin A8	Anxa8	
0,685157	P25235	Dolichyl-diphosphooligosaccharide--protein glycosyltransferase subunit 2	Rpn2	
0,748252	F1MA18;Q62764;D4A0L4;Q62764-2	Y-box-binding protein 3	Csda	**X**
0,759332	G3V6W6	Protein Psmc6	LOC100365869	
0,800036	G3V8A5	Vacuolar protein sorting-associated protein 35	Vps35	
0,824451	E9PU16;Q6NYB7	Ras-related protein Rab-1A	Rab1;Rab1A	
0,835074	Q5XIM5;Q6QI67	Protein CDV3 homolog	Cdv3;LOC499235	
0,839502	B1WC34	Protein Prkcsh	Prkcsh	
0,842592	F1LR10	Epithelial protein lost in neoplasm	Lima1	
0,880544	D3ZM33;P62271;M0R5K9;D3ZAU6;D3ZII2;F1M6D1;D4AA93	40S ribosomal protein S18	LOC100362298;Rps18;RGD1561919;RGD1562404	
0,959727	Q4G061	Eukaryotic translation initiation factor 3 subunit B	Eif3b	
1,02124	Q920J4	Thioredoxin-like protein 1	Txnl1	**X**

1,12943	F1LNI5	Ppm1g (Protein phosphatase 1G)	Ppm1g	
1,18258	D4A3S8	NOL1/NOP2/Sun domain family, member 2	Nsun2	
1,24811	Q9QZK5	Serine protease HTRA1	Htra1	
1,5611	Q62658	Peptidyl-prolyl cis-trans isomerase FKBP1A	Fkbp1a	**X**
1,56464	P62634	Cellular nucleic acid-binding protein	Cnbp	**X**
1,60303	Q63207	Coagulation factor X;Factor X light chain;Factor X heavy chain;Activated factor Xa heavy chain	F10	
2,03314	P84100	60S ribosomal protein L19	Rpl19	**X**
2,04107	M0R979	Protein Thbs1	Thbs1	
2,10847	P61314;D3ZF52;D3ZXA2;M0R6I6	60S ribosomal protein L15;Ribosomal protein L15	Rpl15;RGD 1565767;RGD1565131	**X**
2,29659	Q920Q3	Spermatogenesis-associated protein 19, mitochondrial	Spata19	
2,37902	P61515	Putative 60S ribosomal protein L37a	Rpl37a-ps1	**X**

Table 3 Proteins differently expressed comparing NGF vs ns-Zr15. Proteins that are of particular interest regarding a potential connection of IAC/mechanotransductive signaling and neuronal differentiation processes in the nanotopography-induced setting are marked in gray.

Welch Difference	Protein IDs	Protein names	Gene names
-7,12165	P25427	Beta-nerve growth factor	Ngf
-3,37741	P63312	Thymosin beta-10	Tmsb10
-2,88836	F1LP80;P20156;M0RDR2	Neurosecretory protein VGF;VGF(24-63);VGF(180-194);VGF(375-407);Neuroendocrine regulatory peptide-1;Neuroendocrine regulatory peptide-2;TLQP-11;TLQP-21;TLQP-30;TLQP-62;HFHH-10;AQEE-30;LQEQ-19	Vgf
-2,24729	Q3T1J1;G3V7J7	Eukaryotic translation initiation factor 5A-1	Eif5a;Eif5a2
-1,5625	P25236	Selenoprotein P;Selenoprotein Se-P10;Selenoprotein Se-P6;Selenoprotein Se-P2;Selenoprotein Se-P1	Sepp1
-1,517	P31232	Transgelin	Tagln
-1,39688	F1LUM5	Protein Tubal3	Tubal3
-1,36922	F1M9Z9	Protein Adam12	Adam12
-1,31466	Q6AXU6	Hematological and neurological expressed 1 protein	Hn1
-1,31205	P52925;D3ZS25	High mobility group protein B2	Hmgb2
-1,30598	P11232;R4GNK3	Thioredoxin	Txn
-1,23615	D3ZN59	Protein RGD1559962	LOC100911856
-1,22788	F1LRN8	Protein Nedd4l	Nedd4l

-0,998347	P00787;Q6IN22	Cathepsin B;Cathepsin B light chain;Cathepsin B heavy chain	Ctsb
-0,98734	F1LXK8	Protein Kmt2d	LOC100362634
-0,927585	Q7TP54;D4A8D3;P02793;M0R5T8;M0R6L9;M0R597;M0RCS3;F1M5T1;D3ZUZ5;D4ADM5	Ferritin;Ferritin light chain 1	Fam65b;Ftl;Ftl1
-0,903233	Q5PQL2	Cell differentiation protein RCD1 homolog	Rqcd1
-0,82259	D4A9V4	Protein E2f4	LOC100360427
-0,819237	P13084;P13084-2;F7FKF2;D3ZXI2	Nucleophosmin	Npm1
-0,773041	F7FEZ6;P04256;M0R584;F1M6M1;D4A2D2;F1LUF2;F1M6C7;D4ACJ7	Heterogeneous nuclear ribonucleoprotein A1	Hnrnpa1
-0,726569	G3V7K3;P13635	Ceruloplasmin	Cp
-0,654307	A0A096MK30;O35763;F1LP60;E9PT65	Moesin	Msn
-0,634319	M0R919	Protein Vbp1	Vbp1
-0,577521	P15865;D4A3K5;P06349	Histone H1.2	Hist1h1c
0,311619	M0R9D5	Protein Ahnak	Ahnak
0,44417	G3V8C3;P31000;F1M7P4;P48675;Q6P725;P21807;P16884;F1LRZ7;P12839;G3V8Q2;P23565	Vimentin	Vim
0,447913	M0R9X8;P38650;F1LRT9	Cytoplasmic dynein 1 heavy chain 1	Dync1h1
0,488957	F1MA61;Q9WUI9	Nuclear receptor coactivator 2	Ncoa2
0,490331	P06214;M0RDE7	Delta-aminolevulinic acid dehydratase	Alad
0,49894	Q9EPQ0;F1LN72	Sodium/potassium/calcium exchanger 3	Slc24a3
0,49986	P23764;Q64625;D3ZH29	Glutathione peroxidase 3;Glutathione peroxidase 6;Glutathione peroxidase	Gpx3;Gpx6
0,504105	D3ZPL5;D3ZU22;P62425;F1M013;D3ZWM2;F1M1M2;D3ZJH5;D4A6B9;F1M0R8;D3ZNA3;F1M4C7;D4A8X2;F1M300;M0R6L1;M0R3M3;F1M4Z6;F1M394;F1LV49;F1LUI8;F1M0S7;D4A2J1;F1LU72;M0R9T3;D3ZD15;M0RDP4	60S ribosomal protein L7a	RGD1562953;LOC100361311;Rpl7a;RGD1559149;RGD1563220;RGD1562409;LOC680161;LOC685027;RGD1563045
0,613201	G3V852	Protein Tln1	Tln1
0,628405	M0R4M2	Olfactory receptor	Olfr1320
0,674795	F1LQS3;P21533;H7C5Y5;F1LVJ5	60S ribosomal protein L6	Rpl6
0,681933	Q9QZK5	Serine protease HTRA1	Htra1
0,683081	G3V9K0	Cysteinyl-tRNA synthetase (Predicted), isoform CRA_b	Cars
0,71095	B1WC34	Protein Prkcsh	Prkcsh
0,74149	P18331	Inhibin beta A chain	Inhba
0,816835	D3ZP02	Olfactory receptor	Olr552
0,860588	Q920J4	Thioredoxin-like protein 1	Txnl1

0,909781	P61314;D3ZF52;D3ZXA2;M0R6I6	60S ribosomal protein L15;Ribosomal protein L15	Rpl15;RGD1565767;RGD1565131
0,970465	Q641X8	Eukaryotic translation initiation factor 3 subunit E	Eif3e
0,973167	G3V8T4;Q9ESW0	DNA damage-binding protein 1	Ddb1
1,04444	P13221	Aspartate aminotransferase, cytoplasmic	Got1
1,15907	P62634	Cellular nucleic acid-binding protein	Cnbp
1,20349	P18291	Granzyme B	Gzmb
1,2938	D3ZEH1	Protein Fat4	Fat4
1,38075	G3V9R2;F1M983	Protein Cfh	Cfh
1,99062	M0R979	Protein Thbs1 (Fragment)	Thbs1
2,41476	Q63207		F10

Table 4 IPA bioinformatics analysis of the proteins differentially expressed in ns-Zr15 vs NGF**.**

Networks	Molecules in network	Score
Cell Morphology, Cellular Assembly and Organization, Cellular Movement	Actin, AHNAK, Akt, Ap1, API5, caspase, CD3, Cg, CNIH4, Creb, ERK, estrogen receptor, FSH, GOT1, Gsk3, GZMB, HDLBP, Histone h3, HN1, IDH2, Lh, MAP2K1/2, MCAM, NCOA2, NGF, p85 (pik3r), PARP, Pkc(s), PLC gamma, RANGAP1, ROCK2, TMSB10/TMSB4X, Vegf, VGF, VIM	34
Cancer, Neurological Disease, Organismal Injury and Abnormalities	26sProteasome, ACADL, ALAD, CD163, CFH, DDB1, DYNC1H1, EML2, HISTONE, Histone h4, IgG, IL1, IL12 (complex), IL12 (family), Immunoglobulin, ING3, Insulin, Jnk, NEDD4L, NFkB, (complex), Nr1h, P38 MAPK, PI3K (complex), Pka, PSMA1, PSMD11, Ras, Ras homolog, RNA polymerase II, RPA2, RPL6, RPL15,Tnf (family), TUBB2A,TXNL1	34
Cancer, Organismal Injury and Abnormalities, Reproductive System Disease	ACY1, Alpha Actinin, collagen, Collagen Alpha1, Collagen type I, Collagen type IV, Collagen(s), CTGF, ERK1/2, F10, F Actin, Focal adhesion kinase, HTRA1, INHBA, Integrin, Laminin, LDL, Mek, Mmp, Myosin, NEB, Pdgf (complex), PDGF BB, RANBP3, Rock, SELP, SERPINB8, Smad, Smad2/3, Sphk, TAGLN, Tgf beta, THBS1, TLN1, VCAN	26
Molecular Transport, Cell Signaling, Vitamin and Mineral Metabolism	12-hydroxyeicosatetraenoic acid, ADGRB2, AMT, ATP6V1A, C1QBP, Ca2+, CHAT, CNBP, CYP2D6, DLD, EGF, FAM136A, FFAR4, GCSH, GPX3, growth factor receptor, Hmgb2 (includes others), HNF4A, HTT, ILK, MGST3, MYC, Nefm, Neurotrophin, Ntrk1 dimer, PNPLA6, potassium channel, quinolinic acid, S1PR2, SCG2,SHC1, SLC24A3, sn-glycero-3-phosphocholine, TUBAL3, VGF	23
Cell Cycle, Cellular Development, Hair and Skin Development and Function	12-hydroxyeicosatetraenoic acid, ADAM12, CARS, CCDC80, CDK4, CDKN2A, CHRNB4, CTNND2, DPY30, DUSP4, E2F4, EIF5A, KIF3C, KRAS, LIFR, Mapk, mir-1260a, miR-1913 (and other miRNAs w/seed CUGCCCC), miR-378a-3p (and other miRNAs w/seed CUGGACU), neuroprotectin D1, NPM1, PRKCSH, Rac, RALB, Rho gdi, ROR1, RPS15, S100A12, S1PR2, SH3RF1, STMN2, TGFB1, TNF, TRIO, VTA1	14
Cardiovascular Disease, Connective Tissue Disorders, Dermatological Diseases and Conditions	LBR, Olfr1320	2

3.2 Influence of the surface nanotopography roughness on the protein expression

As shown in Figure 22, the higher surface roughness Rq 25 nm RMS (ns-Zr25) also induced neuritogenesis in PC12 but to a lower degree [153].

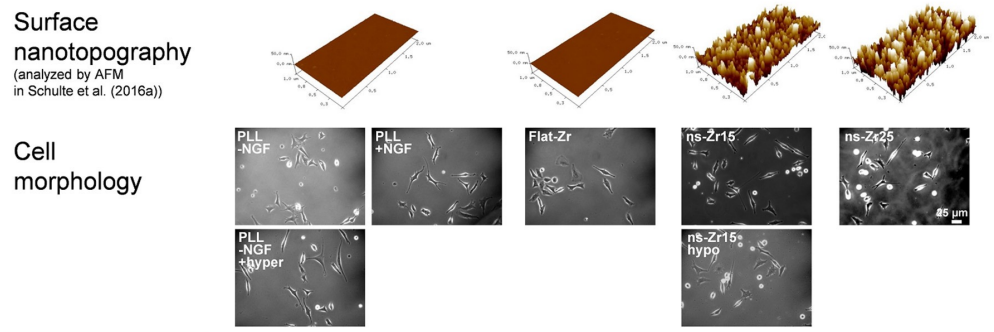

Cellular parameter (Schulte et al. (2016a))	PLL		Flat-Zr	ns-Zr15	ns-Zr25
	-NGF	+NGF			
Induction of Neuritogenesis	Baseline Neurite outgrowth after hyperosmotic shock (Fig. S1)	Yes Biochemically induced	No not even with NGF	Yes Mechanotransductively induced Reduction in hypoosmotic condition	Partial Mechanotransductively induced
IAC	Large (FA)	Small (FC)	Large (FA)	Small (FC)	n.a.
Stress fibre formation	Yes	No	Yes	No	n.a.
Cellular rigidity	Intermediate	Low	Increased	Low	n.a.

Figure 22: representations of the cell morphology in the different conditions and a summary of the results presented in Schulte et al., 2016a [153]. The figure summarizes the results of publication by Schulte et al., 2016a [153] which provided the basis for the selection of the experimental conditions of the extended phosphoproteomic analyses of this work. In the upper row representations of the surface nanotopographies are displayed which were also used in this work (PLL-coated glass, flat-Zr, ns-Zr15, and ns-Zr25). Underneath example photos demonstrate the morphology of PC12 cells in the indicated conditions. In the table the impact of these different conditions on examined cellular parameter are recapitulated (FA, focal adhesions; FC, focal complexes; IAC, integrin adhesion complex; n.a., not analyzed).

The rationale of this phenomenon is not completely clear yet. Therefore, in addition to the mentioned ns-Zr15, we have included ns-Zr25 into this proteomic approach. The Venn diagram and work flow for the comparison of NGF, ns-Zr15, ns-Zr25 are shown in Figures 23 A, B respectively.

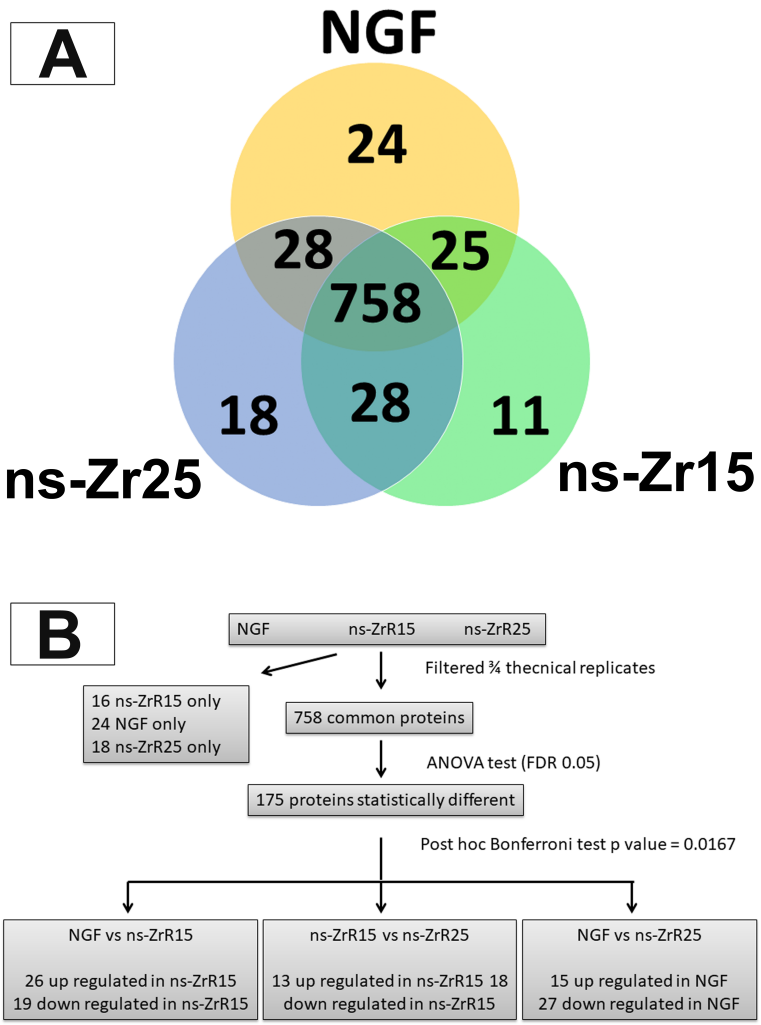

Figure 23: comparison of NGF, ns-Zr15, ns-Zr25. (A) Venn diagram; **(B)** work flow

Several proteins (7 out of 26) found to be upregulated in ns-Zr25 vs NGF are also upregulated in the comparison ns-Zr15 vs NGF (Table 3) or ns- Zr15 vs PLL (Table 2), suggesting that the biological processes triggered by the cell/nanostructure interaction are partially similar, even if the roughness parameter is increasing.

The proteins upregulated only in ns-Zr25 vs NGF, and not in the other conditions, are e.g., stress-induced proteins (such as CASC5, GPX3, A1M, and HSP90) and proteins involved in transport and trafficking. The data further demonstrates that the interaction of PC12 cells with higher roughness is accompanied by an increase of proteins related to formation/degradation of atherosclerosis plaques (APOB, SERPIND1), secretion, anti-inflammation activity and stress response (HMOX1,

LOC681468, TXN, HMGN1, Cybasc3) while others are directly involved in gene expression control. Accordingly, the enrichment analysis of GO biological processes carried out by Panther on the proteins upregulated or only expressed in ns-Zr25 (Table 5) shows that the roughness increase triggers the expression of proteins involved in response to oxygen-containing compounds.

Table 5 Comparison of ns-Zr15vsns-Zr25 with respect to biological processes.

GO biological process complete	**Fold enrichment**	***p-value***
Regulation of peptidase activity (GO:0052547)	11.55	1.68E-02
Response to oxygen-containing compound (GO:1901700)	4.82	2.37E-02
Regulation of biological quality (GO:0065008)	3.29	4.24E-02
Negative regulation of cellular process (GO:0048523)	3.02	2.48E-02
Negative regulation of biological process (GO:0048519)	2.96	1.40E-02

The proteome analysis of cells grown on ns-Zr25 also displays an increased expression of proteins involved in regulation of cell proliferation, differentiation and apoptosis, adhesion and trafficking, as well as intercellular signaling pathways. Some of these proteins indicate a strong neuronal differentiation- promotive effect also for this substrate (e.g., syntaxin 4 [276, 277], clathrin [278, 279], HMGN1 [280, 281], and SCN1B [282]), consistent with our results in primary hippocampal neurons where ns-Zr25 had the most significant effect on neuron differentiation and maturation [283]. However, the induction of many stress- related proteins suggests that the substrate situation is becoming suboptimal for PC12 cells leading to the altered expression of proteins that are essential for the regulation of neuronal survival (e.g., CREM [284, 285], NPM1 [286, 287]).

Compared to ns-Zr15, in ns-Zr25 there was decreased protein expression of tumor suppressors involved in apoptosis (PARK7, GZMB, SRSF1, FAT4) and cytoskeletal proteins that play essential roles in the integrin signaling. The IPA confirms the latter observation by identifying ILK (integrin-linked kinase) signaling as the only canonical pathway significantly decreased on ns-Zr25 (Z score-1, proteins CDH1, FN1, ACTN4, TMSB10/TMSB4X) (Table 6).

Table 6 IPA bioinformatics comparison of ns-Zr15 vs ns-Zr25.

Ingenuity canonical pathways	*p*-Value	*z-score*	Molecules
Epithelial Adherens Junction Signaling	5,37E-03	NaN	CDH1, ACTN4, TUBB
Germ Cell-Sertoli Cell Junction Signaling	8,71E-03	NaN	CDH1, ACTN4, TUBB
Sertoli Cell-Sertoli Cell Junction Signaling	1,02E-02	NaN	CDH1, ACTN4, TUBB
GIalpha12/13 Signaling	3,98E-02	NaN	CDH1, ARHGEF1
ILK Signaling	1,32E-03	-1	CDH1, FN1, ACTN4, TMSB10/TMSB4X
Actin Cytoskeleton Signaling	2,34E-03	0	FN1, ARHGEF1, ACTN4, TMSB10/TMSB4X
Heme Degradation	3,09E-04	NaN	HMOX1, BLVRB
IL-10 Signaling	1,29E-02	NaN	HMOX1, BLVRB
Unfolded protein response	7,41E-03	NaN	P4HB, EIF2AK3
Acute Phase Response Signaling	7,59E-04	NaN	PLG, HMOX1, FN1, SERPIND1
Coagulation System	3,24E-03	NaN	PLG, SERPIND1
Insulin Receptor Signaling	4,90E-02	NaN	PTPN1, STX4

Intriguingly, this pathway has been reported to be pivotal in the regulation of IAC architecture/composition and to be sensitive to integrin ligand density of the substrate [288]. In the context of mechanosensing, lysophosphatidylcholine acyltransferase (Lpcat2b) expression only in the ns-Zr25 condition is intriguing. This protein converts lysophosphatidylcholine in phosphatidylcholine; a process essential in the regulation of membrane dynamics (i.e., curvature/bending, tension), recruitment of F-BAR proteins and membrane/f-actin linkage [289]. Also regarding cell/cell contact, IAC and actomyosin organization some changes are noteworthy (such as Rab14 [290], clathrin [291], nischarin [292-296], ArhGEF1/P115-RhoGEF [297-299]). In addition, SF3B2 and 5 (upregulated in the cells on ns-Zr15), are components of the spliceosomal U2 small nuclear ribonucleoprotein particle that has an important role in neuronal transcriptional regulation [300]. In conclusion, it emerges that several critical proteins for membrane dynamics and configuration, integrin activation, IAC assembly and linkage to the f-actin are affected even by relatively subtle differences in the nanotopographical characteristics [153].

This impact suggests a prominent role of the mentioned proteins in mechanosensing of topographical surface features.

3.3 Impact of the cellular interaction with the neuritogenesis-inducing cluster-assembled zirconia surface on protein phosphorylation

The proteomic data presented here are complemented by an analysis of the phosphorylation state of proteins in the outlined experimental conditions, providing more profound information on the signaling pathways and potential specific key mediators. A detailed analysis of individually identified phosphorylated proteins with interesting functions in the framework of this study is displayed in Table 7.

Table 7: comparison of the conditions ns-Zr15, ns-Zr25, NGF, PLL and flat-Zr to analyse the impact of the cellular interaction with the neuritogenesis-inducing cluster-assembled zirconia surface on protein phosphorylation.

Protein name	Reported protein functions	References
Nidogen-1	The basement membrane protein nidogen-1 is known to be important in the regulation of hippocampal synaptic plasticity and network excitability.	Vasudevan et al., 2010 [301]
Brorin	Brorin has been reported to favor neurogenesis and to inhibit astrogenesis contributing to axon guidance in the zebrafish forebrain.	Myyake et al., 2017 [302]
Galectin-8	Galectin-8 is a secreted ECM protein and matricellular modulator of cell adhesion that is bound by integrins which regulates cell adhesion and survival, promoting or inhibiting, dependent on whether it is present in a soluble or immobilized manner.	Hadari et al., 2000 [303]; Zick et al., 2004 [304]
Ptprf (receptor-type tyrosine-protein phosphatase F)/LAR (leukocyte common antigen-related)	The Ptprf/LAR receptor, a neuronal adhesion molecule essential in synapse maturation, is particularly interesting with respect to IAC, mechanotransduction and calcium signaling. The presence of this receptor in focal adhesions (FA) is controlled in a negative manner by myosin II-generated force and has been shown to have the capacity to regulate FAs (in mouse embryonic fibroblasts). It interacts in a CaMKII (Ca^{2+}/calmodulin-dependent protein kinase II)-regulated way with liprin-α 1. The liprin-α 1/LAR interaction determines LAR distribution and therefore synapse morphogenesis. Moreover, Ptprf/LAR can be found, to a minor extent, tyrosine-phosphorylated in the adult brain. The function of this phosphorylation is yet unknown but could be important for the binding of SH2/SH3 domain-containing adaptor proteins.	den Hertog et al., 1994 [305]; Johnson and Van Vactor, 2003 [306]; Dunah et al., 2005 [307]; Kuo et al., 2011 [308]; Um and Ko, 2013 [309]; Sarhan et al., 2016 [310].
Gpr56 (G protein-coupled receptor 56)	Malfunctions of Gpr56 can cause the neurodevelopmental disease polymicrogyria. In the brain it is predominantly expressed in neuronal progenitor cells (NPC) in regions of postnatal neurogenesis where it is involved in the control of brain convolution/patterning in the cerebral cortex in an integrin α3β1-dependent manner. Moreover, Gpr56 operates together with Gα13 in the Rho-mediated regulation of NPC adhesion/migration. Gα13 again is essential in integrin signaling.	Piao et al., 2004[311]; Iguchi et al., 2008 [312]; Gong et al., 2010 [313]; Shen et al., 2012 [314]; Jeong et al., 2013 [315]; Bae et al., 2014 [316]
ROCK (Rho-associated, coiled-coil-containing protein kinase)	ROCK/RhoA activity has a complex role in neuritogenesis. Although on the one hand it is known to be inhibitory for neuritogenesis, and in particular for the initial neurite formation, on the other hand spatially restricted ROCK/RhoA activity is also essential to suppress lamellipodial protrusions, thereby consolidating neurites/axons by maintaining the growth cone polarity. ROCK and its RhoA binding activity is tightly regulated by phosphorylation	Yamaguchi et al., 2001[317]; Loudon et al., 2006 [318]; Lee et al., 2010 [319]; Schulte et al., 2010 [320]

	downstream of src and contributes to the modulation of focal adhesion turnover.	
GFRA1 (GDNF family receptor α-1)	GFRA1 was found to form a complex with β1 integrin, together with Ret and NCAM-140, and to play an important role in the differentiation of neurons in the olfactory system and the survival of glutamatergic cortical neurons.	Cao et al., 2008 [321]; Marks et al., 2012 [322]; Konishi et al., 2014 [323]
G3BP1 (Ras GTPase-activating protein-binding protein 1)	G3BP1 has been reported to have an impact on neuronal sprouting by promoting the formation of tau mRNA ribonucleoprotein granules and can be found associated with α5β1 integrin-containing complexes. Moreover, G3BP1 deficiency impairs the synaptic plasticity and calcium homeostasis in hippocampal neurons.	Meng et al., 2004 [324]; Martin et al., 2013 [325]; Moschner et al., 2014 [326]
ArhGAP18 (Rho GTPase activating protein 18)	ArhGAP18 has been shown to be involved, as negative regulator, in the control of RhoA activity and stress fiber formation by increasing the GTPase activity of Rho and stabilizing the RhoA-GDP inactive form. The protein, interacting with RhoA, has been described recently as YAP effector in the actomyosin-dependent regulation of tissue tension. A specific role of this protein in neurons has not been reported so far, but its expression level decreases in neurospheres during differentiation and it appeared as a gene associated with schizophrenia in a screening for single nucleotide polymorphisms. For another ArhGAP family member, ArhGAP15, a contribution in the neurogenesis of hippocampal neurons has been shown very recently.	Gurok et al., 2004 [327]; Potkin et al., 2009 [328]; Maeda et al., 2011 [329]; Porazinski et al., 2015 [330]; Zamboni et al., 2016 [331]
ASPM (Abnormal spindle-like microcephaly-associated protein)	ASPM is known to contribute to the regulation of neuronal differentiation processes by actomyosin-dependent actions. As the protein name indicates, this protein is involved in the control of brain size and mutations of this protein can be responsible for developing the neural disorder microcephaly. ASPM is a positive regulator for Wnt signaling and its expression is essential for accurate neurogenesis. Furthermore, recently it has been found that the drosophila ortholog of this protein interacts with and regulates myosin II localization, thereby controlling neuroepithelium morphogenesis by mechanobiological events.	Buchman et al., 2011 [332]; Rujano et al., 2013 [333]
Cofilin/destrin/ ADF (actin depolymerising factor)	Cofilin is essential for actin cytoskeletal organization by regulating the severing of f-actin and the turnover rate of actin and therewith, in the neuronal context, the actin retrograde flow in neurite growth cones of the developing brain. Phosphorylation negatively regulates its actin binding and thereby controls the f-actin homeostasis.	Hawkins et al., 1993 [334]; Jovceva et al., 2007 [335]; Flynn et al., 2012 [336]
Septin-2	Septin-2 modulates actomyosin contractility by binding myosin II and recruiting regulatory proteins. Septin phosphorylation controls the assembly of septins into highly ordered polymers. Interestingly, septin-2 has been found to be phosphorylated in post-mitotic neurons.	Spiliotis and Nelson, 2006 [337]; Joo et al., 2007 [338]
KMT2D (histone-lysine N-methyltransferase 2D)/MLL4 (mixed-lineage leukemia 4)	This protein is a mammalian histone H3 lysine 4 (H3K4) mono-methyltransferase essential in differentiation-specific gene activation. It has been shown to participate in the regulation of neuronal differentiation, facilitating the activation of differentiation-specific genes (e.g., nestin).	Dhar et al., 2012 [339]
RTCB (RNA 2′,3′-cyclic phosphate and 5′-OH ligase)	This RtcB RNA ligase participates in tRNA ligation and it is involved in the regulation of neuronal growth and axon regeneration.	Kosmaczewski et al., 2015 [340]
E2F4	This transcription factor has been shown to play a role in neuronal differentiation and neuritogenesis.	Persengiev et al., 1999 [341]
Rab23 (Ras-related protein 23)	Rab23 participates to endocytic vesicle trafficking and is involved in the regulation of sonic hedgehog signaling in neural tube patterning.	Eggenschwiler et al., 2001[342]; Evans et al., 2003 [343]

Specifically, the phosphoproteomic data shows that the cell/nanotopography interaction (ns-Zr15) leads to a differential phosphorylation of various proteins reported to be important in controlling IAC dimension/composition, the actin cytoskeleton, and the cellular mechanics (e.g., ADAM12 [261, 262] nidogen-1 [301], brorin [302], Ptprf/LAR [305-310], Gpr56 [311-316], ROCK [317-320], GFRA1 [321-323], G3BP1 [324-326], ArhGAP18 [327-331], ASPM [332, 333], cofilin [334-336], septin-2 [337, 338]). Furthermore, several proteins essential in epigenetic and (post-)transcriptional regulation of gene expression are modulated at the phosphorylation level (e.g., KMT2D [339], RtcB [340], E2F4 [341]). Regarding this latter aspect, it is noteworthy that lipin-1 phosphorylation is affected by the interaction with ns-Zr15. This phosphatidic acid phosphatase is important in lipid synthesis and SREBP-mediated transcriptional regulation. Its phosphorylation is regulated by mTOR which thereby also controls its intracellular localisation and the lamin A-dependent nuclear organization [344, 345].

The alterations (regarding expression and phosphorylation levels) extend in a consistent manner our previous results [153], accentuating additionally the impact of the cell/nanotopography interaction on mechanotransductive processes and defining more precisely nanotopography-sensitive signaling hubs (Figure 24).

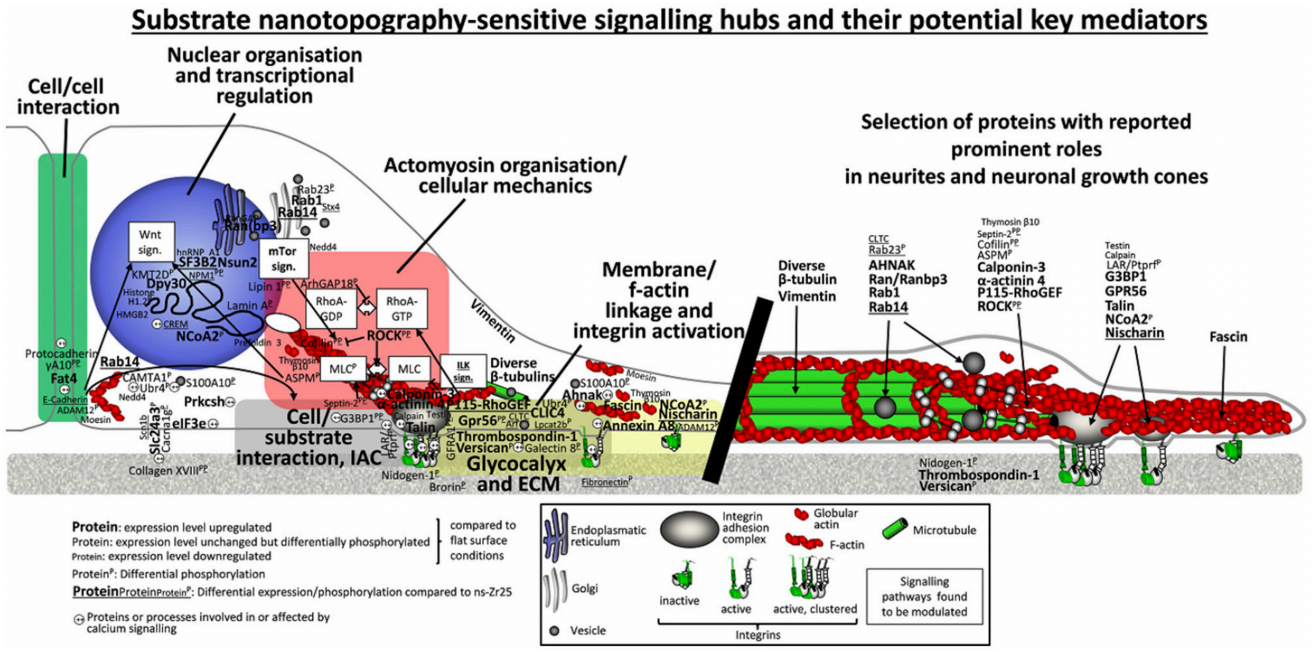

Figure 24: schematic representation of the potential relation and crosstalk among different signaling pathways modulated by the neuron/nanotopography interaction. On the left the illustration arranges proteins dissected from the whole (phospho)proteomic data set into several categories and sets them into a (potential) relation to each other with respect to their reported cell biological function and context. The main categories are visualized as follows; cell/cell interaction (green box), glycocalyx and ECM (box with gray patterned filling), cell substrate interaction and IAC (gray box, gray oval represents the IAC), membrane/f-actin linkage and integrin activation (yellow box), actomyosin organization/cellular mechanics (red box), nuclear organization, and transcriptional regulation (blue circle, representing the nucleus). Further information on the reported specific functions of the individual proteins, justifying their categorization, can be found in the corresponding tables throughout the manuscript. Moreover, on the right a selection of proteins is listed with association to their functions in neuronal differentiation processes, particularly in neurite growth cones.

To find relevant patterns and specific differences in signaling processes related to the diverse conditions (PLL, NGF, ns-Zr15, ns-Zr25, and flat-Zr) a principal component analysis (PCA) was carried out on the corresponding phosphoproteomes. The analysis, applied to all the peptides found phosphorylated in these 5 conditions, reveals at a glance that the phosphoproteomes of NGF and ns-Zr15 cluster together (confirming again the common outcome of a differentiated cell). Flat-Zr and PLL instead are at the opposite ends of the plot (Figure 25 A), suggesting that the cells on these two substrates behave very differently as far as protein phosphorylation concerns, in agreement with the other data reported so far. If the same analysis is carried out focusing only on the sequence phospho-motifs present in the phosphoproteome data, a similar plot can be obtained (Figure 25 B), but in this case a more evident separation can be observed between NGF and ns-Zr15, indicating that the kinases and phosphatases involved are, at least in part, different. Figure 25 C reports in green all the substrate

motifs that are more relevant in the PCA analysis, accounting for the 16% of all the phospho-motifs present in the phosphopeptides.

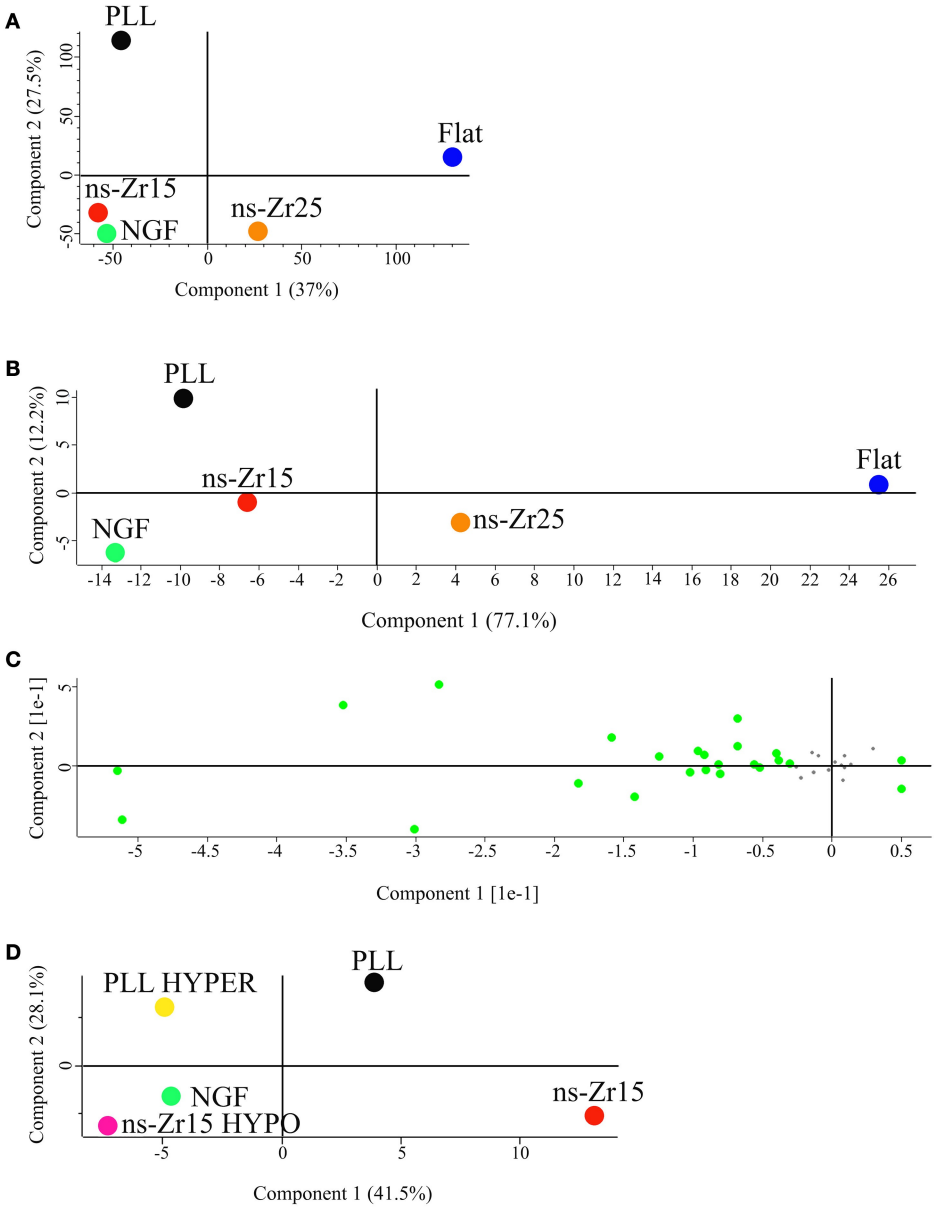

Figure 25: principal component analysis (PCA) on the phosphoproteome of PC12 cells grown in different experimental conditions. (A) PCA analysis of the phosphopeptides of PC12 cells in the experimental conditions PLL, NGF, ns-Zr15, ns-Zr25, and flat-Zr. **(B)** PCA analysis of the sequence phospho-motifs present in the phosphoproteome data of PLL, NGF, ns-Zr15, ns-Zr25, and flat-Zr. **(C)** Visual representation of the PCA analysis of the sequence phospho-motifs. All the substrate motifs that are more relevant in the PCA analysis are marked in green. **(D)** PCA analysis of the phosphopeptides of PC12 cells in the experimental conditions PLL, NGF, ns-Zr15, PLL hyper, and ns-Zr15 hypo.

The enrichment analysis of these phospho-motifs, carried out by Panther and David, shows that there is a highly significant enrichment ($p \leq 0.05$) of few signaling pathways in the cells on ns-Zr15 (Table 8).

Table 8 Enrichment analysis of the kinases substrate motifs that are more relevant in the PCA analysis of phospho-sites differently expressed in ns-Zr15$_{VS}$ NGF.

PANTHER PATHWAYS	**Fold enrichment**	***p*-value**
Heterotrimeric G-protein signaling pathway-rod outer segment phototransduction	>100	1.47E-02
VEGF signaling pathway	78.4	4.40E-02
Parkinson disease	64.84	1.72E-03
CCKR signaling map	54.74	8.16E-05
Angiogenesis	45.05	5.07E-03
Wnt signaling pathway	22.45	3.96E-02
DAVID PATHWAYS		
Wnt signaling pathway	27,58865	1.93E-04
VEGF signaling pathway	48,625	1.198-03
GABAergic synapse	33,53448	2.503-03
Gap junction	33,15341	2.56-03
GnRH signaling pathway	31,71196	2.795-03
Inflammatory mediator regulation of TRP channels	25,36957	4.333-03
Thyroid hormone signaling pathway	25,36957	4.333-03
Tight junction	20,54577	6.542-03
Oxytocin signaling pathway	18,23438	8.247-03

The angiogenesis and VEGF signaling pathways are in line with the processes mentioned throughout this work as they comprise many players also involved in focal adhesion, MAPK and Ca^{2+} signaling. In addition, the results suggest that the differences between PC12 cells grown on ns-Zr15 (compared to the NGF condition) could be partially ascribed to a modulation within the Wnt pathway (Table 8). An indicator is e.g., the downregulation of E-cadherin in the cells on ns- Zr15, considering the known crosstalk between (E-)cadherin cell adhesion and canonical Wnt signaling by release of β-catenin [346]. Interestingly, Wnt expression in PC12 cells leads to an upregulation of E-cadherin and a flat epithelial-like cell morphology associated with unresponsiveness to NGF-induced neuritogenesis [347]. In epithelial cells E-cadherin-mediated cell/cell adhesions are essential in mechanically connecting the intercellular actomyosin machineries to regulate tissue organization [348]. Moreover, it has been demonstrated in human embryonic stem cells that the surface nanotopography has an impact on E-cadherin expression level [349]. The potential impact of the

substrate nanotopography on Wnt signaling in a neuronal setting is therefore an interesting issue for further investigations.

In the comparison ns-Zr15 vs ns-Zr25, apart from various already mentioned proteins, lamin A appeared as differentially phosphorylated. This protein is particularly interesting in the context of mechanotransduction representing one of the intermediate filaments that forms the interior of the nuclear envelope. It was found to be involved in the regulation of nuclear architecture/biophysics, chromatin organization, and transcription regulation at the end of mechanotransductive signaling cascades that influence differentiative processes [350]. Its differential expression during adult neurogenesis proposes a potential role in it; however, to date details remain still unclear [351]. Further proteins found to be phosphorylated on ns-Zr25 are Galectin-8 [303, 304], and Rab23 [342, 343] which have essential reported functions in cell adhesion/survival and neuronal development, respectively (Table 8).

Altogether, many proteins that are important in neurogenic and/or mechanotransductive processes are differentially expressed and/or phosphorylated upon cellular interaction with the cluster-assembled zirconia surface that promotes neuritogenesis. Combining the analysis of our proteomic data with information available on these proteins and their functions, suggests a dynamic and complex modulation of an entire signaling network by the cell/nanotopography interaction that is in control of cellular behavior and fate, i.e., in this case neuronal differentiation. We were able to dissect potential nanotopography-sensitive key elements regulated within a mechanotransductive sequence, identifying many proteins that can be assigned to these principal categories: cell/cell adhesion, ECM and glycocalyx, cell/substrate interaction and IAC, integrin activation and membrane/f-actin linkage, integrin adhesion complexes, actomyosin organization/cellular mechanics and nuclear organization and transcriptional regulation (Figure 24).

3.4 Alterations in cellular processes and signaling by the modulation of cellular tension

In our paper Schulte et al., 2016 we identified the alteration of the cellular nanomechanical properties as critical for the signal integration within the nanotopography-dependent mechanotransductive sequence that fostered neuronal differentiation. The interaction with the nanostructured surface dictated the IAC nanoarchitecture/dynamics and cytoskeletal organization in a manner that consequentially resulted in a softer membrane/cytoskeletal layer of the neuronal cell. Compensating this effect by a hypoosmotic gradient (causing cell swelling and an increase of cell tension) counteracted gradually the nanostructure-induced neuritogenesis on the morphological level [153].

The mechanotransduction dependency of the nanotopography-promoted differentiation was broadly validated by a proteomic comparison of PC12 cells interacting with the ns-Zr15 in the isoosmotic standard medium (ns-Zr15) or instead in the presence of hypoosmotic medium (ns-Zr15 hypo). Many proteins found to be expressed only in ns-Zr15 or to be downregulated in ns-Zr15 hypo can be classified as proteins involved in RhoGTPase-controlled cytoskeletal organization according to the IPA canonical pathways enrichment analysis (Figure 26). Consistent with the hypoosmotic manipulation of the membrane tension, clathrin- and caveolar-mediated endocytosis appeared among the five most affected pathways in this evaluation (Figure 26).

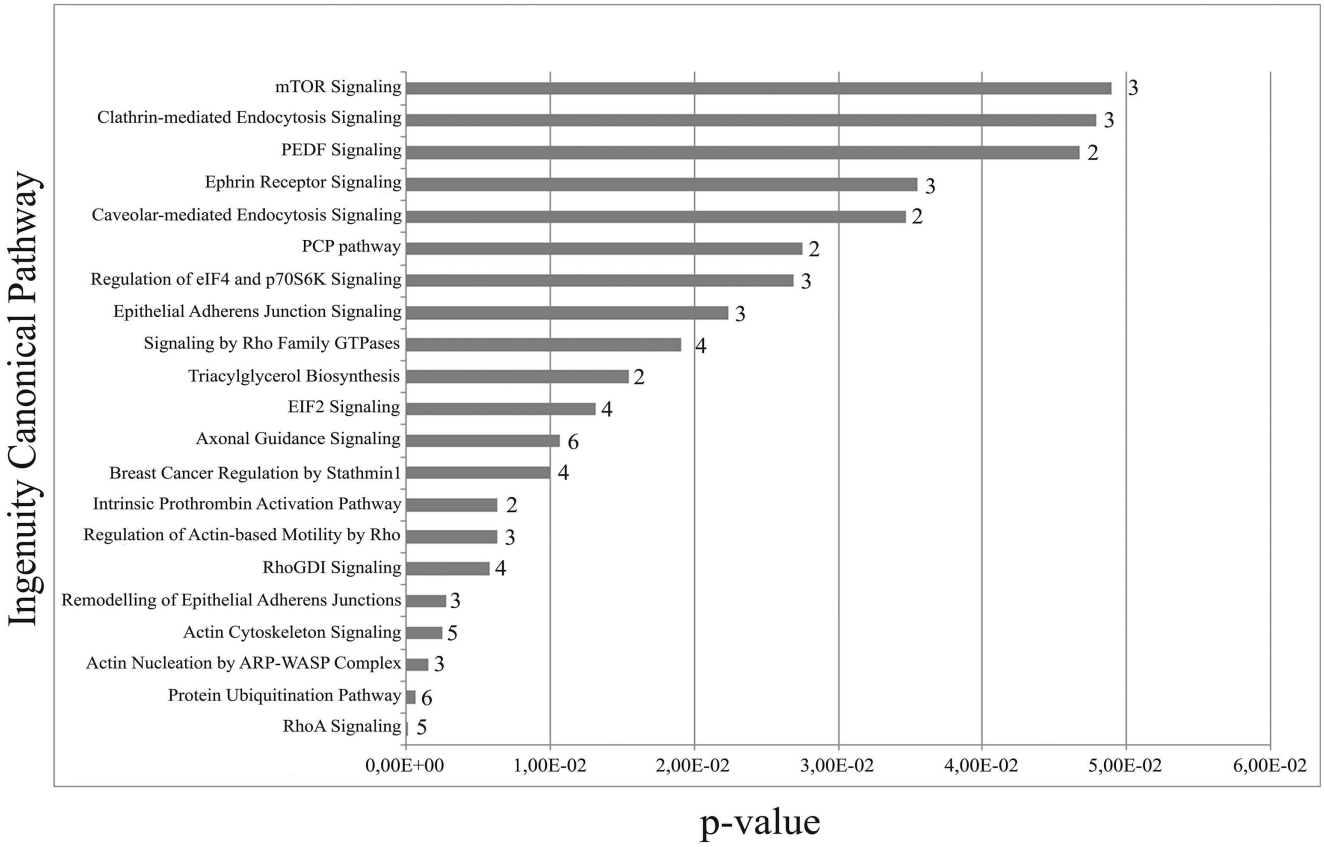

Figure 26: comparison of ns-Zr15$_{VS}$ns-Zr15 hypo. IPA canonical pathways enrichment analysis of ns-Zr15$_{VS}$ns-Zr15 hypo.

These pathways are regulated by and respond to modulations of the membrane tension and are crucially involved in cell volume and shape control [352-354].

Intriguingly, mTOR signaling emerged as the strongest modulated pathway in this analysis (Figure 26). mTOR signaling represents a highly conserved pathway known to be an integrative master regulator of many cellular processes/pathways at the interface of intracellular and extracellular signals [355], also in regard to neurogenic events [356]. Inhibition of mTOR(C1) with rapamycin had different effects on flat and nanostructured substrates. On PLL there was an increase of neurite outgrowth upon rapamycin inhibition both in the absence, or presence, of NGF. In the latter, the effect was additive to the NGF- induced increase, reproducing data reported by others [357]. On ns-Zr15 instead no significant impact, neither promotive nor inhibitory, with respect to neurite outgrowth was observable (Figure 27).

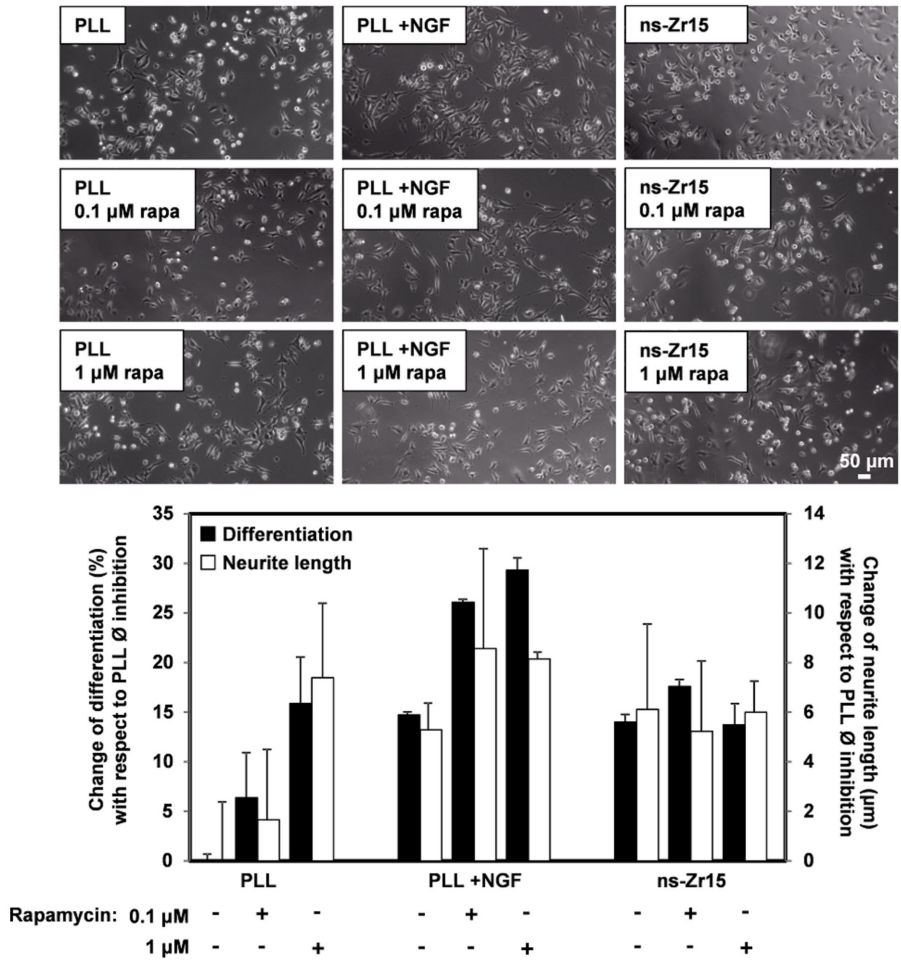

Figure 27: effect of rapamycin inhibition on neurite outgrowth of PC12 cells on PLL and ns-Zr15. The phase contrast images and the graph display the reaction of PC12 cells on PLL (± NGF) or on ns-Zr15 after rapamycin treatment at two different concentrations: 0.1 and 1 µM. The graph summarizes the global statistics of two independent experiments showing the change of the differentiation rate and neurite length compared to the PLL –NGF Ø inhibition, with in total 367–943 cells and 216–661 neurites quantified for the differentiation rate (black bars), respectively neurite length (white bars). The bars show the average (mean ± s.d.) of the two experiments.

It can be speculated that the boosted neuritogenesis on PLL is due to an induction of mTORC2 activation triggered by the rapamycin-mediated inhibition of mTORC1 as a negative feedback between the two mTORCs is known [358]. Moreover, mTORC2 has been shown to be involved in the regulation of actin dynamics and morphology of neurons in a Rac/PAK-dependent signaling pathway that controls cofilin phosphorylation [359, 360]. Very recently, it has been demonstrated in DRG neurons that topographical features can potentiate mTORC2 guiding neurite outgrowth [361]. On ns-Zr15 the mTORC2 might already be induced by the cell/nanotopography interaction and thus rapamycin treatment does not further affect neurite outgrowth. The altered cofilin phosphorylation (Table 8) is in line with this [359]. The varying impact of mTOR(C1) inhibition by rapamycin

depending on whether the cells interact with a flat or a nanotopographical surface makes mTOR signaling an interesting and promising target for further studies in this context but goes beyond the scope of this work.

Moreover, prominent markers for (developing) neurons and neurite outgrowth, such as BASP1, MAP1B, or β-tubulin (TUBB5), are strongly downregulated in the hypoosmotic condition. The same is true for many proteins involved in the actin polymerisation machinery and the cytoskeletal organization (e.g., Capg, Arpc1b, 3 and 5, Capzb, fascin) which are crucial for the realization of neuritogenesis [362, 363]. The alterations in the protein expression profile are largely mirror-inverted to those seen in the comparison ns-Zr15 vs flat-Zr [153]. 37 proteins have an opposite expression level in these two comparisons, whereas only 5 proteins are altered in the same way.

On the other hand, a hyperosmotic shock applied to cells on PLL-coated glass (resulting in a decrease of membrane tension) led morphologically to the outgrowth of neurites (Figure 22). The proteomic data disclosed that the neuritogenesis was accompanied by a modification of the protein profile similar to those found in ns-Zr15 vs flat-Zr [153]. 39 proteins had the same alteration of the expression level. However, proteins known to be involved in IAC are basically missing here. In addition, 16 proteins also showed an opposite expression level modification.

The PCA analysis carried out on the phosphopeptides differentially expressed in these conditions (ns-Zr15, ns-Zr15 hypo, NGF, PLL hyper, PLL) indicates that either hypoosmotic swelling on ns-Zr15, as well as the hyperosmotic shock on PLL, moves the profiles partially closer to the NGF condition. This emphasizes again that ns-Zr15 hypo basically lost its nanotopography-specific features, whereas PLL hyper has gained at least some characteristics of the NGF condition (Figure 25 D).

Overall, these proteomic data further reinforce that the modulation of the cellular nanomechanical properties is a key integrating signal causally linked to the change of the cellular

program and the differentiation processes that we discussed in our previous work [153], with a potential involvement of mTOR signaling constituents.

3.5 Calcium signaling/homeostasis-related proteins affected by the cell/nanotopography interaction

Alterations of the integrin/ECM interaction (e.g., in growth cone filopodia) [364, 365] and cellular biomechanics can modulate another important mechanotransduction-susceptible pathway; that is calcium signaling regulated by Ca^{2+} influx passing mechanosensitive membrane channels [366,178]. In turn, it has long been known that integrin/ligand binding is affected by divalent cations (also Ca^{2+}) [367]. Local changes in calcium concentration influence integrin adhesion dynamics in growth cones and axon guidance in a calpain/talin-dependent manner [368], mediated e.g., by Piezo1/Fam38A [369]. However, despite this acknowledged role of calcium signals in neuronal differentiative processes, the exact spatiotemporal regulation and impact of calcium signaling is rather complex and intricate with many details still elusive [370-373]. To study the involvement of mechanosensitive channel types in our experimental context, we used the inhibitors SKF- 96365 for transient receptor potential cation channels (TRPC) and GsMTx4 for stretch-activated channels (SAC, such as e.g., Piezo) in collaboration with CIMAINA, Physics Department of University of Milan. With respect to the canonical NGF-stimulated outgrowth our results were in line with findings published by others, i.e., the two inhibitors showed opposing effects on neurite outgrowth [374, 375, 372]. SKF-96365 impeded differentiation and neurite outgrowth, whereas GsMTx4 had a minor differentiation- enhancing effect (Figure 28).

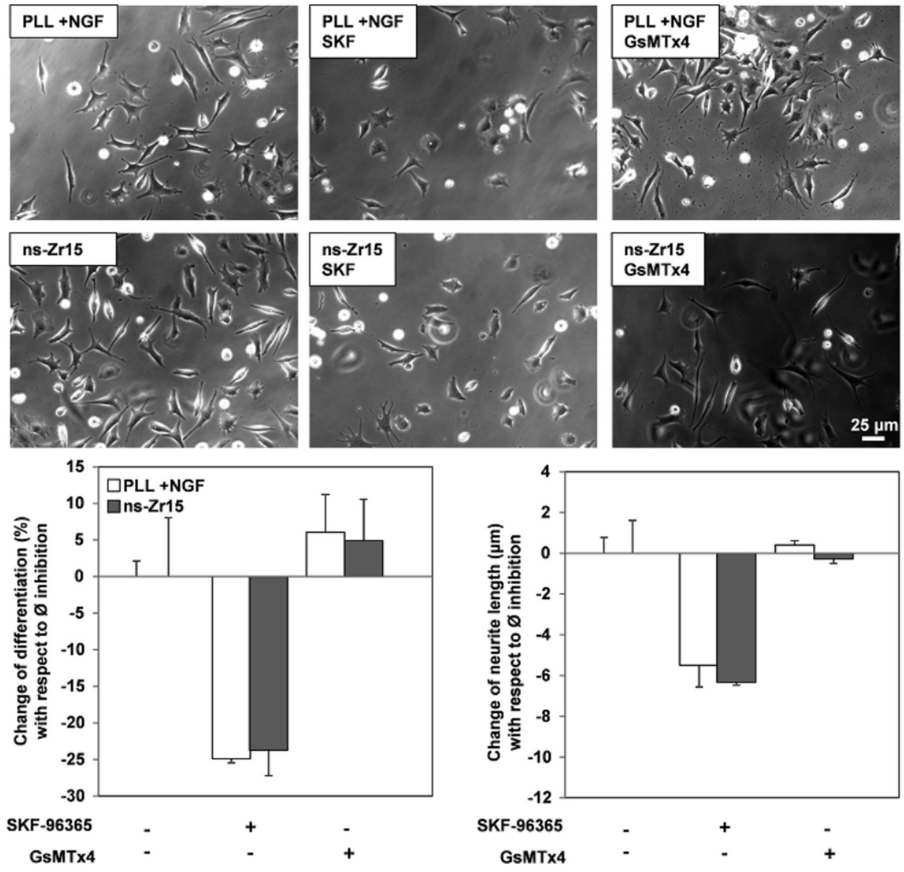

Figure 28: impact of treatment with drugs affecting different types of calcium channels (SKF-96365 and GsMTx4). The phase contrast and the graph show the effect of the drugs SKF-96365 (15 µM) and GsMTx4 (10 µM), affecting transient receptor potential cation channels (TRPC), respectively stretch-activated channels (SAC), on PC12 differentiation grown in the PLL +NGF and ns-Zr15 condition. The graph represents the global statistics of two independent experiments with the change of differentiation rate (left graph) and neurite length (right graph) in comparison to the corresponding condition Ø inhibition (white bars: PLL + NGF, gray bars: ns-Zr15). The bars represent the average (mean ± s.d.) of the two experiments (comprising in total 434–650 cells and 108–387 neurites quantified).

This is consistent with the reported crosstalk between NGF/TrkA and TRPC-mediated calcium signaling [376, 377]. More interestingly and despite its independence of NGF/TrkA activation [153], the outcome was practically in the same range for the nanotopography-promoted neuritogenesis (Figure 28) suggesting a contribution of calcium signaling also in this mechanotransductively fostered differentiation.

This reflected in the phosphoproteomic analysis. Independent of whether the neuritogenesis-inducing stimulus was NGF or the nanotopography, numerous proteins with reported roles in the regulation of calcium signaling or homeostasis were differentially expressed and/or phosphorylated in the differentiated cells, compared to the PLL condition. However, the phosphoproteomic data

insinuate potential differences in calcium signaling-involved proteins between the ns-Zr15 and the NGF condition. Some proteins e.g., are only upregulated in ns-Zr15vsPLL and not in NGFvsPLL, such as annexin A8, thrombospondin-1, and versican. Annexin A8 is particularly interesting regarding mechanotransduction due to the fact that this protein is recruited in a Ca^{2+} -dependent manner to PIP2 -rich membrane domains at F-actin accumulation sites. It might therefore be important in the organization of specific membrane/cytoskeleton contacts [378]. To our best knowledge, roles of annexin A8 in neuronal cells have not been reported yet. The ECM glycoproteins thrombospondin-1 and versican; beyond the already mentioned involvement in IAC dynamics and neurito/synaptogenesis, bind calcium which affects their structure/function and participates in the regulation of calcium concentration [379, 380].

Other proteins related to calcium signaling can be found upregulated comparing directly ns-Zr15 vs NGF, such as Ahnak, Fat4 (protocadherin 4) and Prkcsh/PKC substrate 80K- H. Ahnak is a scaffolding protein that partakes in versatile cellular processes, many in fact related to calcium signaling [381] and/or membrane morphogenesis (together with S100A10) [382, 383]. In the neuronal context, it is also a marker of enlargeosomes. These exocytic vesicles can contribute to the membrane supply for neurite outgrowth in a REST-regulated manner [384, 385, 320]. Fat/Protocadherin 4 belongs to the calcium-dependent cadherin cell adhesion protein family and has been reported to be involved in the regulation of neuroprogenitor proliferation and differentiation upstream of YAP. Fat4 downregulation lowers differentiation of neuroprogenitors into neurons in the cerebellum [386]. Prkcsh/PKC substrate 80K-H, which colocalises with IP3 R1, modulates IP3 -induced calcium release and might therefore have a role in synaptic plasticity [387].

In comparison to ns-Zr25 the S100 calcium-binding protein A10 [382, 388, 389] differentially phosphorylated in the cells on ns-Zr15.

In summary, Ca^{2+} signaling is important for both, NGF- and nanotopography-triggered neuritogenesis, but the proteomic data suggest that the cell/nanotopography interaction might influence some specific proteins prominently involved in calcium homeostasis and/or signaling.

The presently adopted quantitative proteomic approach (associated to a systematic characterization) challenges PC12 cells with diverse experimental situations that address the impact of substrate nanotopography and/or cellular biomechanics on neuronal cell fate. The analyzed conditions comprised the canonical PC12 cell differentiation setting with a biochemical stimulus (PLL ±NGF; i.e., PLL and NGF), three different zirconia surface topographies with distinct nanoscale roughness parameters (flat-Zr, ns-Zr15, ns-Zr25) and treatments that affect the tensional state of the cell (ns-Zr15 hypo, PLL hyper). This approach enabled us to acquire an extensive molecular image of the processes and pathways that are sensitive to changes in the microenvironmental nanotopography and/or cellular nanomechanical properties, and to identify potential key elements therein. The data thus provide various starting points and indications on how the nanotopographical sensitivity is achieved and integrated into signaling pathways.

A robust engagement of proteins involved in cell morphology, cellular assembly and organization, and cellular movement (see IPA, Table 4) was observed and many proteins with acknowledged roles related to IAC/mechanotransduction were altered. In addition, versatile proteins with tasks in neuronal functioning and differentiation have been identified to be modulated in the nanotopography setting; as well as several proteins essentially involved in epigenetic and (post-)transcriptional regulation during neuronal differentiation. This is in line with the hypothesis of a potential epigenetic regulation of cell reprogramming and differentiation dependent on cellular mechanics and microenvironmental cues (such as in this case surface nanotopography) [389, 390].

We have seen on the morphological level that only specific roughness parameters of the cluster-assembled zirconia surfaces (for PC12 cells ns-Zr15) provide appropriate biophysical cues to gain full neuritogenesis. An increased nanotopography roughness (ns-Zr25) instead leads to an only

partial effect on neuritogenesis [153]. In line with this, the proteomic analysis demonstrated that there is a partial overlap in the molecular alterations between ns-Zr15 and ns-Zr25, compared to NGF. Yet, the comparison revealed and specified also some decisive differences regarding proteins important for integrin activation and cytoskeletal organization. Notably, the IPA emphasized the importance of IAC in the mechanosensing to interpret the distinct natures of the topographies as ILK (integrin-linked kinase) signaling is the only decreased pathway (Table 6). This is striking because ILK signaling is essentially involved in determining the molecular architecture of IAC and its signaling is sensitive to variations in ligand spacing/density. The proteomic data suggests furthermore that the increase in roughness starts to cause cellular stress in this PC12 cell model.

In summary, many of the proteins found to be altered at the expression and/or phosphorylation level can be associated with the following categories which all have high relevance with respect to mechanotransductive signaling: cell/cell adhesion, glycocalyx and ECM, integrin activation and membrane/f-actin linkage, cell/substrate interaction and IAC, actomyosin organization/cellular mechanics, and nuclear organization and transcriptional regulation. By integrating the dissected alterations into a potential context, a complex nanotopography-sensitive network with broad crosstalk opportunities crystallizes, capable of regulating the cell/microenvironment interface and consequentially cellular cytoskeletal mechanics and signaling, here in control of neuronal differentiation processes (Figure 24).

This comprehensive proteomic analysis insinuates that other pathways with strong correlation to mechanotransduction, such as Wnt (Table 8), mTOR (Figures 26, 27) and Ca^{2+} signaling (Figure 28), might also be affected by, and involved in, the nanotopography-triggered cellular processes. However, more profound future studies are required regarding these pathways.

Altogether, this proteomic-based analysis defined nanotopography-sensitive signaling hubs and key elements potentially important in the promotion of neuronal differentiation by nanotopographical cues. It delivered several interesting starting points to evaluate in more specific

studies, and in a wider context with respect to the role of certain proteins in mechanotransductive signalin that regulates neuron development and maturation. In the framework of biomaterials that are based on nanoscale surface features, an in-depth understanding of the impact of cell/nanotopography interaction on cellular processes and fate is the indispensable prerequisite. An improved insight might help to harness and effectively control the potential of these biomaterials in biomedical applications. Vice versa, information obtained by advanced biomaterial approaches could provide conclusions for a better comprehension of the difficult to access in vivo mode of operation of microenvironmental and cellular mechanobiological processes, e.g., regarding epigenetic regulation.

Proteomic analysis of GM1 Oligosaccharide, II3Neu5Ac-Gg4, in Neuroblastoma Cells

1. INTRODUCTION

1.2 Structural lipids membrane: sphingolipids

The structure of biological membranes consists in a lipid bilayer which acts as a barrier for polar molecules and ions. Membrane lipids are amphipathic so they have an hydrophilic head, polar and soluble in water, and an hydrophobic end, nonpolar and soluble in fat.

Among this group of different lipids there are sphingolipids, also composed by a polar head and two nonpolar tail, but they differ from other glycerophospholipids for the absence of glycerol.

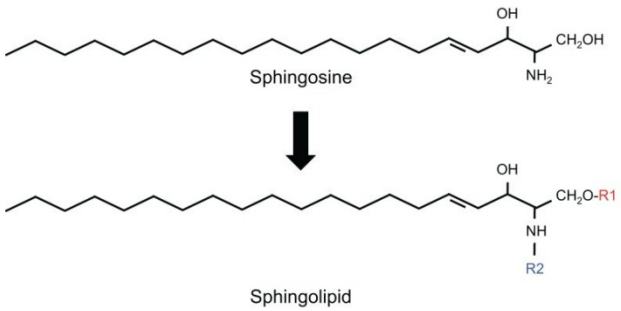

Figure 29: Structure of sphingolipids. In sphingolipids, the hydrophobic region consists of a longchain sphingoid base with generally 18 carbons, such as sphingosine, which is linked to the acyl group of a fatty acid via an amide bond (R2). The hydrophilic region (R1) consists in the simplest case of a hydroxyl group in the case of ceramide [figure and legend from 392].

Sphingolipids are composed by a molecule of sphingosine, a long chain amino alcohol, also known as 4-sphingenin, or by its derivative, by a molecule of long chain fatty acid and by a polar head joined, in some cases, by a glycosidic bond, in other, by a phosphodiesteric bridge. The fundamental unit, common to all sphingolipids, is ceramide, formed when sphingosine reacts with long fatty acid. There are three subclasses of sphingolipids:

- Sphingomyelins: phosphocholine or phosphoethanolamine are bounded at OH in C1, forming a polar head. They are in plasmatic membrane of animals and they are abundant in myelin.

- Glycosphingolipids: Localized in abundance on the outer surface of the plasma membrane, they have polar head, composed by a one or more sugar directly bound to -OH of ceramide C1, they don't contain phosphate. Cerebroside and globoside are two neutral glycosphingolipids, the first is form by a single saccharidic unit bound to ceramide, the second are with two or more sugar, usually D-glucose, D- galattose or N-acetyl-D-galactosammin. They have pH 7, therefore are neutral at physiological pH, equal to 7.
- Ganglioside: they are the most complex sphingolipids whit polar head formed by complex oligosaccharides, which end with one or more residues of N-acetylneuraminic acid (Neu5Ac) and sialic acid. The latter gives to ganglioside a negative charge at pH 7 which distinguishes them from globosides. Gangliosides with only one residue of sialic acid belong to GM series, where M is for mono; those with two residues are GD (D for di-) series and so on.

When sphingolipids where discovered, more than 100 years ago, their function seemed enigmatic like Sphinx, their name comes from this consideration. Many of these are particular abundant in plasmatic membrane of neurons, others are recognition sites on the surface of the cell, but only for few of them it's been recognized a specific function.

1.3 Gangliosides GM1

Gangliosides are the major sialoglycoconjugate type in the nervous system and they have defined roles in signaling and/or regulatory mechanisms. It's a molecule composed of a glycosphingolipid (ceramide and oligosaccharide) with N-acetylneuraminic acid linked on the sugar chain.

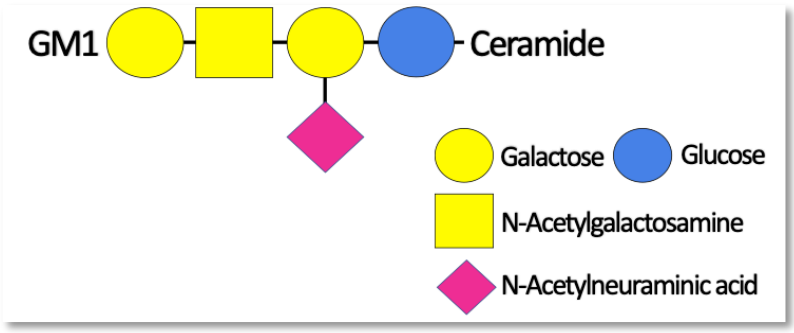

Figure 30: structure of ganglioside GM1

GM1 ganglioside has been of special interest with regards to its unusually heavy burden of signaling and regulatory assignments [393]. The list of cellular duties is guaranteed by the collaboration of GM1 with biomolecules that drive cellular functions such as:

- microdomain regulation;
- ion transport modulation;
- neuronal differentiation;
- immune cell reactivity;
- neurotrophin signaling.

The essential role of ganglioside GM1 (II3Neu5Ac-Gg4Cer) in neuronal differentiation, protection, and restoration is a milestone as demonstrated by the disastrous consequences deriving from its genetic deletion and, on the other hand, by its therapeutic potential in relation to neurodegenerative diseases [394-398]. The molecular mechanism explaining its physiological function and its pathological implication still remain to be clarify. For many years in vivo and in vitro

studies have suggested that oligo portion of GM1 could have a key role in promotion of neuritogenesis process, starting from results of Schengrund and Prouty paper (1988). To reinforce this evidence, two semisynthetic derivatives, LIGA4 and LIGA20, were produced through chemical modification in the GM1 ceramide structure. These two GM1 analogs maintained the neurotrophic potency, suggesting that the ceramide structure is not critical in determining the GM1 modulatory effects.

Recently, Chiricozzi et al. proved, in the neuroblastoma cell line Neuro2a (N2a), that within the entire molecule, the oli- gosaccharide chain, β-Gal-(1-3)-β-GalNAc-(1-4)-[α- Neu5Ac-(2-3)]-β-Gal-(1-4)-Glc-, II3 Neu5Ac-Gg4 (OligoGM1), is actually the moiety responsible for GM1 neurodifferentiative properties by directly interacting with NGF-specific receptor TrkA at the plas-ma membrane (PM), leading to the activation of the ERK1/2 downstream pathway [399]. The hydrophilic head protrudes in the extracellular environment and acts at the cell surface level across the interaction with PM proteins, in this way GM1 exerts its bioactive feature.

1.4 Neuroblastoma cell line, Neuro2a (N2a)

Neuro 2A (N2a) is a mouse neural crest-derived cell line that has been extensively used to study neuronal differentiation, axonal growth and signaling pathway [400]. These cells have neuronal and ameboid stem cells morphology.

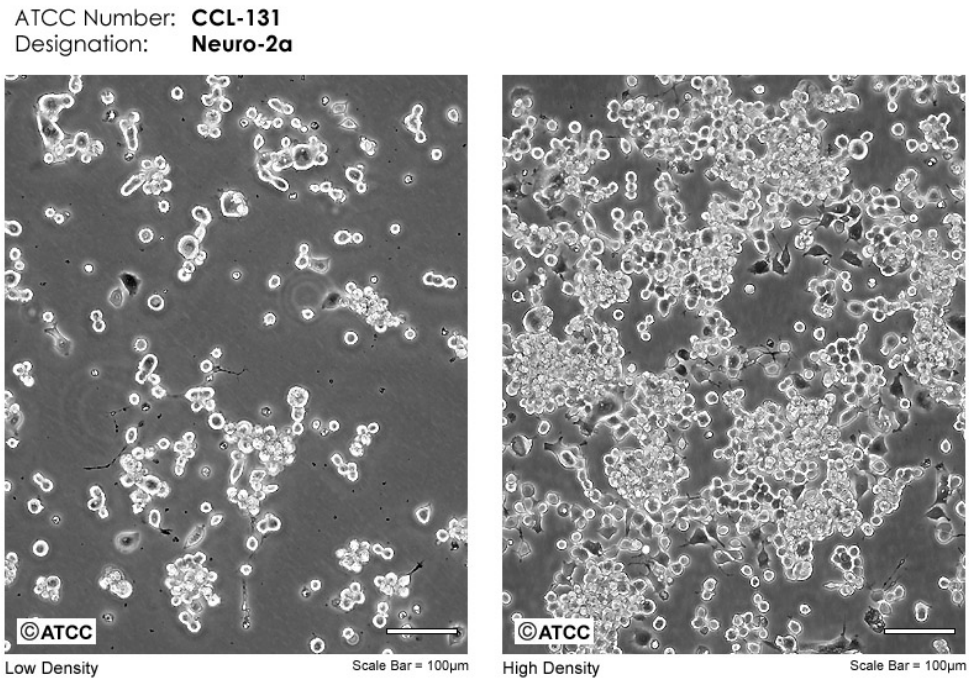

Figure 31: Neuro-2a at phase contrast microscopy

These cells are able to differentiate in a few days into neurons of different type. Neurite outgrowth is a requisite for an accurate functional network of neurons during development [401, 402] and N2a cell have the advantage of responding quickly to environmental stimuli, e.g. serum deprivation by expressing signaling molecules that lead to neuronal differentiation and neurite growth.

The neuroblastoma cell line Neuro2a (N2a) could differentiate under the influence of oligoGM1 by directly interacting with NGF-specific receptor TrkA at the plasma membrane (PM), leading to the activation of the ERK1/2 downstream pathway [19].

1.5 Nerve growth factor (NGF)

In 1954 a nucleoprotein particle was isolated from mouse sarcomas, it was called Nerve growth factor for its property of enhancing growth and differentiation in sensory and sympathetic nerve cells. This important discovery is to be attributed to Rita Levi-Montalcini and collaborators and for this in the 1986 she was awarded the Nobel prize for Medicine, together with Stanley Cohen. Several studies demonstrate that NGF administered to primary cultured neurons prevents neuronal apoptosis and reduces neuronal degeneration in animal models of neurodegenerative diseases.

NGF is a member of neurotrophins family formed by growth and survival factors, it has trkA as receptor, expressed primarily on nociceptors giving to NGF a prominent role in nociception, the sensory nervous system's response to certain harmful or potentially harmful stimuli. Neurotrophins are fundamental for neuronal survival, they innervate peripheral tissue and compete for the appropriate trophic molecules. Sensory and sympathetic neurons expressing trkA, bind NGF available, if they win survive instead they die through apoptosis. This is the mechanism through which is matched the number of central neurons to the size of the periphery to be innervated.

NGF is produce after the cleavage of Pro-NGF, its precursor protein; however they have different and opposite roles. Pro-NGF administered to cervical ganglia neurons, expressing both NGF receptors p75NTR and trkA, leads them to programmed cell death instead NGF treatment of the same neurons results in survival and axonal growth. Free NGF have several physiological actions in the central nervous system. It exerts neurotrophic effects being critical for the neurite outgrowth and survival and maintenance of neurons, moreover NGF has also a strong antiapoptotic effect. NGF could also circulates throughout the body playing roles in different organs. It’s been demonstrated that NGF dysregulation could be involved in various neuronal degeneration diseases such as Alzheimer’s disease and multiple sclerosis [403-405]. Moreover, the dysfunction of NGF is linked to mental and psychiatric disorder, like schizophrenia, depression and autism [406-408].

NGF plays its role through binding with its receptors located on the cell surface. NGF exerts its trkA-mediated effects by becoming internalized and activating diverse signaling pathways [409]. Clathrin is essential for the internalization of NGF/trkA complex into endosomes that are transported to cell body where the cell signaling takes place. Trka is a 140 kDa glycoprotein which bind NGF. The receptor activated by NGF undergoes dimerization and autophosphorylation at several tyrosine residues activating its downstream targets, such as protein kinase B (Akt) or extracellular signal regulated protein kinase 1/2 (ERK1/2), which could cause neural differentiation and prevention of apoptosis. The other NGF low affinity receptor is p75NTR. Even if its distribution is wider the affinity of NGF for trkA is stronger. This receptor is mainly expressed in peripheral sensory neurons, sympathetic neurons, and basal forebrain cholinergic neurons [410].

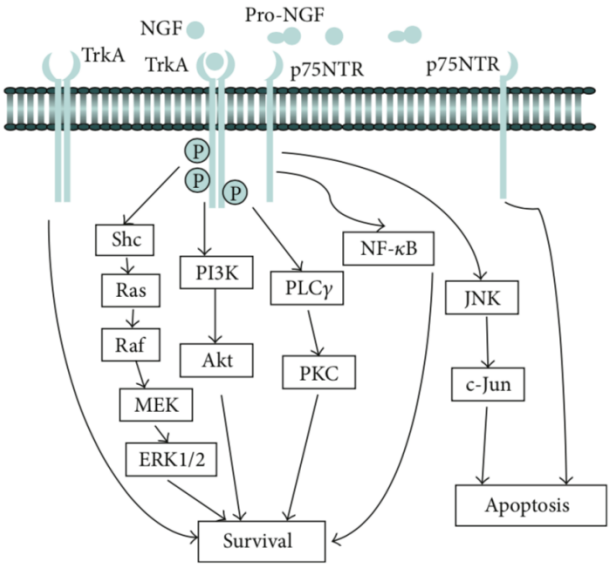

Figure 32: Signaling of NGF receptors. NGF is formed by cleavage from Pro-NGF, which is the precursor protein form of NGF. TrkA receptor is the high affinity receptor for NGF; NGF binding to TrkA causes the phosphorylation of TrkA and activation of multiple signaling pathways such as the PI3K/Akt, Ras/Raf/MEK/ERK1/2, or PLCγ/PKC signaling pathways. Activation of these pathways eventually leads to different biological functions including the prevention of apoptosis. The other NGF receptor, p75NTR, is a low affinity receptor. The precise role of p75NTR depends upon the cellular context; it can enhance cell survival through NF-κB pathway or promote cell death through JNK/c-Jun signal pathway [Figure and legend from 405].

TrkA is the high affinity catalytic receptor for the NGF and it mediates the main effects of NGF, which include cell growth, the formation and regeneration of neurites, and avoidance of programmed cell death [411]. The complex NGF-trkA leads to receptor dimerization and activation

thanks to phosphorylation of its tyrosine residues. When trkA is active it works as docking site for effector molecules such as Sch which in turn induces the recruitment of a complex of Shc/Grb2, subsequent to which several downstream signaling cascades are initiated and propagated [412]. The phosphorylation of Shc is the first step of activation of Ras-mediated activation of the mitogen-activated protein kinase (MAPK) pathway. The membrane-associated G protein, Ras, binds and phosphorylates the protooncogene Raf, which in turn activates MAPK kinase (MEK) and phosphorylated MEK activates ERK1/2 [413]. Phosphorylated ERK1/2 could regulate the activity of many transcription factors, when it enters into the nucleus, like ETS domain-containing protein ELK1. ERK1/2 may also phosphorylate ribosomal S6 kinase (S6K), which leads to the phosphorylation of cyclic adenosine monophosphate response element binding protein, eventually affecting the regulation of the expression of NGF-inducible genes and, thus, contributing to neuronal differentiation or neurite outgrowth [414].

1.6 1-methyl-4-phenyl-1,2,3,6- tetrahydropyridine hydrochloride (MPTP)

In this thesis we investigated the OligoGM1 role in the protection from 1-methyl-4-phenyl-1,2,3,6- tetrahydropyridine hydrochloride (MPTP)-mediated cytotoxicity [415-417]. Biochemical analysis highlighted that the GM1 oligosaccharide protects neuroblastoma cells from MPTP toxic effect as well as from mitochondrial oxidative stress starting with PM activation of TrkA- ERK1/2 signaling pathway.

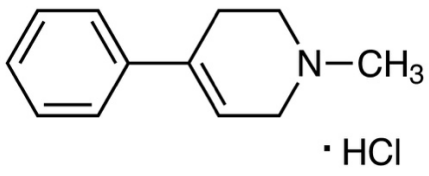

Figure 33: chemical structure of MPTP **[figure from 418]**

The MPTP is a secondary compound that is formed during meperidine synthesis. Meperidine is a synthetic piperidine ester with opioid analgesic activity. Meperidine mimics the actions of endogenous neuropeptides via opioid receptors, thereby producing the characteristic morphine-like effects on the mu-opioid receptor, including analgesia, euphoria, sedation, respiratory depression, miosis, bradycardia and physical dependence [537].

MPTP exerts its neurotoxic effect through biological activation by the catecholaminergic enzyme monoamine oxidase [419], producing an unstable intermediate 1-methyl-4-phenyl-2,3-dihydropyrdinium ion ($MPDP^+$), prior to forming the toxic metabolite 1-methyl-4-phenyl pyridinium (MPP^+) [415]. MPTP, via complex I, can inhibit mitochondrial respiration [420, 421] causing mitochondrial energy deprivation and eventual cell death [422]. In addition, MPTP is thought to mediate the generation of toxic reactive oxygen species [423] causing lethal damage to critical biomolecules. This is supported by the protective capacity of various antioxidants to alleviate MPTP-induced cell death [424]. Even if the mechanism of action of MPTP is still not totally clear, the cell's response to stress involves multiples signaling pathways. MAPK pathways plays important role in mediating neurotoxicity indeed *in vivo* studies have recently suggested that MPTP-induced cell death can be attenuated by inhibition of the stress-activated protein kinase (SAPK) [425].

2. MATERIALS AND METHODS

2.1 Preparation of OligoGM1

OligoGM1 was prepared by ozonolysis followed by alkaline degradation [399, 426] from GM1 ganglioside, which was purified from the total ganglioside mixture extracted from pig brains [427, 428]. Briefly, GM1 was dissolved in methanol and slowly saturated with ozone at 23 °C. The solvent was then evaporated under vacuum and the residue brought immediately to pH 10.5–11.0 by addition of triethylamine. After solvent evaporation, GM1 oligosaccharide was purified by flash chromatography using chloroform/methanol/2-propanol/water 60:35:5:5 v/v/v/v as eluent. GM1 oligosaccharide was dissolved in methanol and stored at 4 °C.

NMR, mass spectrometry (MS), and HPTLC analyses [429] showed a purity over 99% for the prepared oligosaccharide (Fig 35).

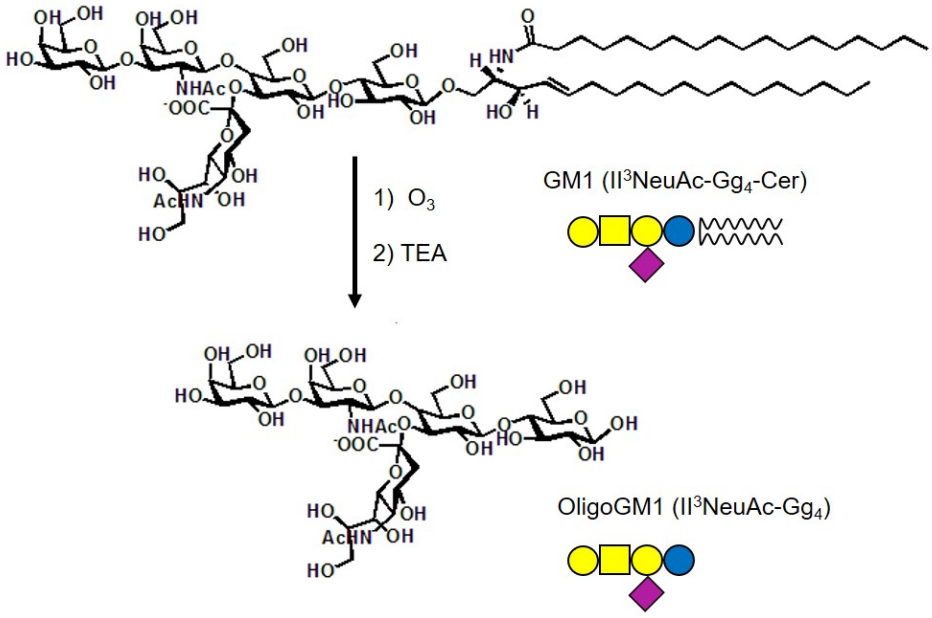

Figure 34 OligoGM1 structure and chemical synthesis. GM1 was purified from a mixture of bovine extract gangliosides using the ion-exchange chromatography technique. Subsequently, GM1 underwent catalytic ozonolysis and basic treatment with triethylamine to cleave the apolar chain from the oligosaccharide core. OligoGM1 was purified from the reaction mixture using standard chromatographic procedures and its purity was proved by MS analysis. Glycoconjugates representation is according to Varki *et al*. 2015 [430] (TEA, triethylamine)

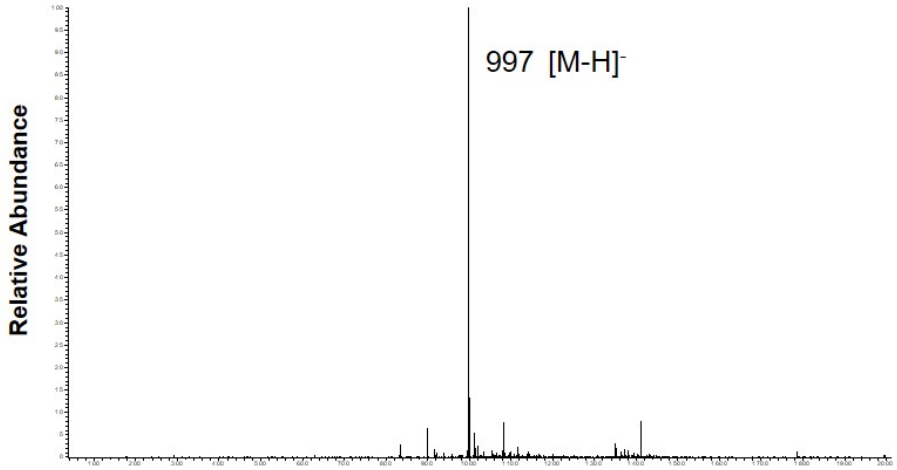

Figure 35 MS profile ESI-MS (negative-ion mode): m/z= 997 $[M - H]^-$.

2.2 Cell Cultures

Murine neuroblastoma N2a cells (RRID: CVCL_0470) were cultured and propagated as monolayer in DME high glucose medium supplemented with 10% heat-inactivated FBS, 1% L-glutamine, and 1% penicillin/streptomycin all from EuroClone (Paignton, UK), at 37 °C in a humidified atmosphere of 95% air/5% CO_2. Cells were subcultured to a fresh culture when growth reached the 80–90% confluence (i.e., every 3–4 days).

2.3 Cell Treatments

N2a cells were plated at 5 × 103/cm^2 and incubated for 24 h to allow cell attachment and recovery in complete medium before treatments.

2.3.1 OligoGM1 or RA Treatment

To induce neurodifferentiation, growth medium was removed and N2a cells were pre-incubated in pre-warmed (37 °C) Transfectagro medium (Corning, NY, USA) containing 2% FBS, 1% L-glutamine, and 1% penicillin/streptomycin (EuroClone Paignton, UK), for 30 min at 37 °C. Sequentially, cells were incubated at 37 °C with 50 μM OligoGM1 [399] or 20 μM RA (Sigma-

Aldrich, St. Louis, MO, USA) [431]. Control cells were incubated under the same experimental conditions but omitting any addition of OligoGM1 or RA.

2.3.2 MPTP Treatment

To induce neurotoxicity, following 24 h from OligoGM1 or RA treatment, cells were incubated with MPTP (250 μM) [415] (Figure 36). Control experiments were carried out under the same experimental conditions.

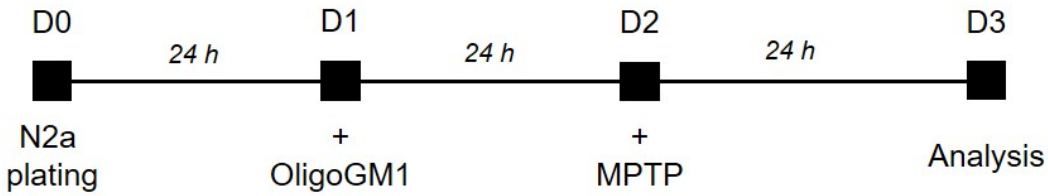

Figure 36 Paradigm of OligoGM1 treatment**.** N2a cells were plated at 5 x 10^3/cm^2 in complete medium and incubated for 24 h. After, cells were preincubated with 50 μM OligoGM1 for 24 h prior to exposure to MPTP (250 μM) for 24 h (Transfectagro medium containing 2% FBS).

2.3.3 Inhibition of TrkA Receptor

To block TrkA activity in N2a cells, TrkA inhibitor (CAS 388626-12-8 from Merck Millipore Billerica, MA, USA) (120 nM) was added to the incubation medium 1 h before the addition of OligoGM1 [432, 433].

2.4. Proteomic analysis

N2a cells were incubated in the absence (control) or in the presence of 50 μM OligoGM1 for 24 h. Then, medium was removed and cells were rinsed twice with 1 mM Na_3VO_4, 1 mM PMSF, 2% (v/v) aprotinin, and 1% (v/v) IP in cold PBS (Sigma-Aldrich St. Louis, MO, USA). Cells were scraped in the same buffer and centrifuged 800×g for 5 min at 4 °C. Pellets were immediately frozen by liquid nitrogen and conserved at − 80 °C before proteomic analysis by a shotgun label-free proteomic approach for the identification and quantification of expressed proteins.

Sample treatment and mass parameters of mass spectrometric analysis remain the same described in chapter 2.4 Protein identification by mass spectrometry and 2.5 Mass Spectrometry of PC12 section.

2.5 Data processing and analysis

MS spectra were searched against the mouse Uniprot sequence database (release 31.07.2017) by MaxQuant (version 1.3.0.5) [437]. The following parameters were used: initial maximum allowed mass deviation of 15 ppm for monoisotopic precursor ions and 0.5 Da for MS/MS peaks, trypsin enzyme specificity, a maximum of two missed cleavages, carbamidomethyl cysteine as fixed modification, N-terminal acetylation, methionine oxidation, asparagine/glutamine deamidation, and serine/threonine/tyrosine phosphorylation as variable modifications. False protein identification rate (5%) was estimated by searching MS/MS spectra against the corresponding reversed-sequence (decoy) database. The minimum required peptide length was set to 6 amino acids and the minimum number of unique peptide supporting protein identification was set to 1. Quantification in MaxQuant was performed using the built-in label-free quantification (LFQ) algorithms based on extracted ion intensity of precursor ions.

Three biological replicates, each one replicated twice, were carried out for treated and control cells. Only proteins present and quantified in at least 2 out of 3 biological repeats were considered as positively identified in a sample and used for statistical analyses performed by the Perseus software module (version 1.5.5.3, www.biochem.mpg.de/mann/tools/). A t test (p value ≤ 0.01) was carried out to identify proteins differentially.

3. RESULTS AND DISCUSSION

3.1 Proteomic profile of oligoGM1-treated cells

The information on TrkA-MAPK cascade activation by the OligoGM1 on N2a cells [399] suggests the triggering of other biochemical signaling processes besides that of cellular differentiation. To verify such hypothesis, we performed a proteomic analysis of cells treated with 50 μM OligoGM1 for 24 h.

Proteins were identified by a shotgun proteomic approach, using label free for the relative quantification of their expression levels. The proteomic analysis led to the identification of 3166 proteins in treated cells and 3132 in control cells with Pearson's correlation of 0.94, suggesting that the two data sets are very similar in terms of protein composition (figure 37a).

In accordance, the Venn diagram (figure 37b) shows that 2842 proteins are commonly expressed both in control and OligoGM1-treated cells, among which 70 proteins are differently expressed, 23 up and 47 downregulated, in treated cells in comparison to controls (Table 9), while 350 (Table 10) and 324 (Table 11) proteins are expressed only in control cells and in OligoGM1-treated cells, respectively.

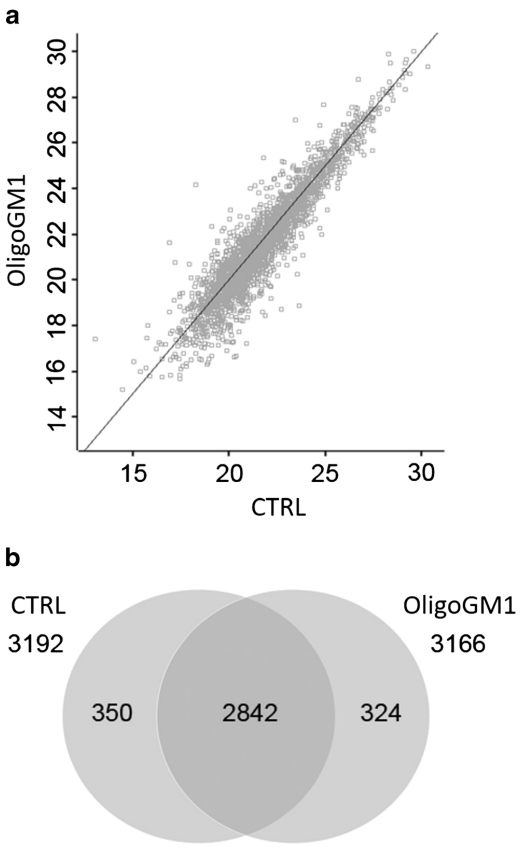

Figure 37 Proteomic characterization of OligoGM1-treated cells and control cells. **a** Scatter plot of the proteome of N2a cells treated (OligoGM1) and untreated (CTRL) with OligoGM1. Pearson's correlation coefficient R = 0.94. **b** Venn diagram showing the proteins identified in at least 2/3 replicates. Proteins common to both data sets were considered for differential expression.

Table 9 List of the proteins statistically differentially expressed in OligoGM1 vs CONTROL N2a cells

Student's T-test Difference OLIGO_CTR	Majority protein IDs	Protein names	Gene names
-3,97953	E9QMV2	Costars family protein ABRACL	3110003A17Rik
-3,19309	Q9CQR2	40S ribosomal protein S21	Rps21
-3,07356	Q9CQZ1	Heat shock factor-binding protein 1	Hsbp1
-3,00908	Q3TIX9	U4/U6.U5 tri-snRNP-associated protein 2	Usp39
-2,89295	P60710	Actin, cytoplasmic 1	Actb
-2,47279	Q9CWZ3	RNA-binding protein 8A	Rbm8a
-2,46072	P55105	Bone morphogenetic protein 8B	Bmp8b
-2,12761	Q6ZWV3	60S ribosomal protein L10	Rpl10
-2,00293	A6H6S0	Hect domain and RLD 3	Herc3
-1,92439	Q8BJA2	Solute carrier family 41 member 1	Slc41a1
-1,91339	Q9ESW4	Acylglycerol kinase, mitochondrial	Agk
-1,75705	Q8VIB5	BarH-like 2 homeobox protein	Barhl2
-1,68246	P11157	Ribonucleoside-diphosphate reductase subunit M2	Rrm2
-1,61967	A0A0R4J0I2	Transmembrane protein 132D	Tmem132d
-1,5279	E9Q2G7	Solute carrier family 2, facilitated glucose transporter member 3	Slc2a3

-1,51962	P54103	DnaJ homolog subfamily C member 2	Dnajc2
-1,49549	P58389	Serine/threonine-protein phosphatase 2A activator	Ppp2r4
-1,40454	E9PW66	Nucleosome assembly protein 1-like 1	Nap1l1
-1,37956	Q9Z1R2	Large proline-rich protein BAG6	Bag6
-1,37446	Q8VEH6	COBW domain-containing protein 1	Cbwd1
-1,37404	Q9CWF2	Tubulin beta-2B chain	Tubb2b
-1,31362	Q924T2	28S ribosomal protein S2, mitochondrial	Mrps2
-1,31199	Q9QZD8	Mitochondrial dicarboxylate carrier	Slc25a10
-1,23455	G3X8Y3	N-alpha-acetyltransferase 15, NatA auxiliary subunit	Naa15
-1,21106	A0A0R4J008	Histone deacetylase 2	Hdac2
-1,14768	E9Q6G4	ATP-binding cassette sub-family A member 7	Abca7
-1,13689	Q9Z2Q6	Septin-5	Sept5
-1,12486	Q4FE56	Ubiquitin carboxyl-terminal hydrolase	Usp9x
-1,09299	Q0VBD2	Protein MCM10 homolog	Mcm10
-1,0627	Q6P1J1	Crmp1 protein	Crmp1
-0,961719	A2AFI6	Transmembrane 9 superfamily member	Gm364
-0,908271	D3Z780	Translation initiation factor eIF-2B subunit delta	Eif2b4
-0,878172	E9QM77	Ataxin-2	Atxn2
-0,840163	Q9R0P4	Small acidic protein	Smap
-0,831308	Q9Z0V8	Mitochondrial import inner membrane translocase subunit Tim17-A	Timm17a
-0,814648	I1E4X0	Disks large-associated protein 4	Dlgap4
-0,801263	E9Q1P8	Interferon regulatory factor 2-binding protein 2	Irf2bp2
-0,750502	Q62465	Synaptic vesicle membrane protein VAT-1 homolog	Vat1
-0,7079	E9Q616	AHNAK nucleoprotein (desmoyokin)	Ahnak
-0,703338	Q9CQ22	Ragulator complex protein LAMTOR1	Lamtor1
-0,64407	P56480	ATP synthase subunit beta, mitochondrial	Atp5b
-0,641168	Q9DAP7	Histone chaperone ASF1B	Asf1b
-0,509192	Q9Z1N5	Spliceosome RNA helicase Ddx39b	Ddx39b
-0,448086	Q8BTW3	Exosome complex component MTR3	Exosc6
-0,387215	Q6PAM1	Alpha-taxilin	Txlna
-0,368086	Q9WTM5	RuvB-like 2	Ruvbl2
-0,316293	Q3UHJ0	AP2-associated protein kinase 1	Aak1
0,272641	Q99LC8	Translation initiation factor eIF-2B subunit alpha	Eif2b1
0,309552	Q8VE73	Cullin-7	Cul7
0,450782	Q9EQI8	39S ribosomal protein L46, mitochondrial	Mrpl46
0,484953	G5E8R4	Serine/threonine-protein phosphatase 6 regulatory subunit 3	Ppp6r3
0,550471	Q60790	Ras GTPase-activating protein 3	Rasa3
0,657146	E9Q0S6	Tensin 1	Tns1
0,700328	Q3U9G9	Lamin-B receptor	Lbr
0,71614	A0A087WPU8	Transcription factor Dp-2	Tfdp2
0,724323	P53994	Ras-related protein Rab-2A	Rab2a
0,868009	Q6PDI6	Protein FAM63B	Fam63b
0,886094	Q64378	Peptidyl-prolyl cis-trans isomerase FKBP5	Fkbp5
0,972225	P36552	Coproporphyrinogen-III oxidase, mitochondrial	Cpox
1,02418	P62827	GTP-binding nuclear protein Ran	Ran

1,11385	P61514	60S ribosomal protein L37a	Rpl37a
1,21209	A0A0U1RNX8	B-cell CLL/lymphoma 7 protein family member C	Bcl7c
1,25283	Q6GQT9	Nodal modulator 1	Nomo1
1,33364	P29595	NEDD8	Nedd8
1,35297	P62281	40S ribosomal protein S11	Rps11
1,53449	P35550	rRNA 2-O-methyltransferase fibrillarin	Fbl
1,60853	P62889	60S ribosomal protein L30	Rpl30
1,7774	Q6PIU9	Uncharacterized protein FLJ45252 homolog	N/A
1,84351	Q8CBB6	Histone H2B	Gm13646
2,89154	P02301	Histone H3.3C	H3f3c

Table 10 List of the proteins only expressed in CONTROL cells in the comparison OligoGM1 vs CONTROL N2a cells

Majority protein IDs	Protein names	Gene names
A0A075B5Z7	T cell receptor alpha variable 5-1	Trav5-1
A0A087WPL5	ATP-dependent RNA helicase A	Dhx9
Q9CWU4	UPF0690 protein C1orf52 homolog	2410004B18Rik
Q8BXK8	Arf-GAP with GTPase, ANK repeat and PH domain-containing protein 1	Agap1
A0A087WRX8	Serine/arginine repetitive matrix protein 2	Srrm2
Q60862	Origin recognition complex subunit 2	Orc2
A0A087WSQ9	Zinc finger CCHC domain-containing protein 2	Zcchc2
G3UZM1	Probable JmjC domain-containing histone demethylation protein 2C	Jmjd1c
B7ZCJ1	Rho GTPase-activating protein 21	Arhgap21
A0A0A6YVS2	Transmembrane and coiled-coil domain-containing protein 1	Tmco1
Q64735	Complement component receptor 1-like protein	Cr1l
A0A0A6YVW3	Immunoglobulin heavy variable V1-23	Ighv1-23
A0A0A6YXG9	Uridine-cytidine kinase 2	Uck2
A0A0B4J1J5	Immunoglobulin heavy variable V9-3	Ighv9-3
E9PZ43	Microtubule-associated protein	Mtap4
A0A0G2JEG1	Serine/arginine-rich-splicing factor 11	Srsf11
O54946	DnaJ homolog subfamily B member 6	Dnajb6
A0A0G2JFP4	Ferric-chelate reductase 1	FRRS1
Q8BXV2	BRI3-binding protein	Bri3bp
A0A0G2LB90	Tubulin polyglutamylase TTLL7	Ttll7
A0A0J9YTZ5	Protein FAM193A	Fam193a
O35427	DNA-directed RNA polymerase III subunit RPC9	Crcp
F7BJB9	MORC family CW-type zinc finger protein 3	Morc3
Q3UEZ8	Sodium/bile acid cotransporter 4	Slc10a4
Q4VC33	Macrophage erythroblast attacher	Maea
P17183	Gamma-enolase	Eno2
Q80V62	Fanconi anemia group D2 protein homolog	Fancd2
Q9CQR6	Serine/threonine-protein phosphatase 6 catalytic subunit	Ppp6c
A0A0N4SVR5	RasGEF domain family, member 1A	Rasgef1a

A0A0R4J023	Methylglutaconyl-CoA hydratase, mitochondrial	Auh
A0A0R4J0D1	Store-operated calcium entry-associated regulatory factor	Tmem66
A0A0R4J0H8	Fibronectin type III domain-containing protein 3B	Fndc3b
A0A0R4J0J4	Atypical chemokine receptor 1	Ackr1
A0A0R4J0P1	Isobutyryl-CoA dehydrogenase, mitochondrial	Acad8
A0A0R4J0T5	CUGBP Elav-like family member 1	Celf1
A0A0R4J1C6	Butyrophilin-like protein 10	Btnl10
A0A0R4J1K1	CCR4-NOT transcription complex subunit 4	Cnot4
Q9QZR5	Homeodomain-interacting protein kinase 2	Hipk2
A0A0R4J220	Atypical chemokine receptor 1	Kifc3
A0A0R4J259	Heterogeneous nuclear ribonucleoprotein Q	Syncrip
Q8BX09	Retinoblastoma-binding protein 5	Rbbp5
A0A0U1RNX4	Unconventional prefoldin RPB5 interactor	Uri1
A0A140LJ04	Zinc finger ZZ-type and EF-hand domain-containing protein 1	Zzef1
A0A140LJ70	Protein arginine N-methyltransferase 1	Prmt1
O55222	Integrin-linked protein kinase	Ilk
Q6PD31	Trafficking kinesin-binding protein 1	Trak1
Q3TIR3	Synembryn-A	Ric8a
G5E8I8	Calcium homeostasis endoplasmic reticulum protein	Cherp
E9PZW8	Unconventional myosin-IXb	Myo9b
O54833	Casein kinase II subunit alpha	Csnk2a2
Q7TR45	Olfactory receptor	Olfr1131
Q9WU63	Heme-binding protein 2	Hebp2
Q8R4S0	Protein phosphatase 1 regulatory subunit 14C	Ppp1r14c
A0A1L1SUG9	Cadherin EGF LAG seven-pass G-type receptor 3	Celsr3
Q4VBF2	R3H domain-containing protein 4	R3hdm4
K3W4Q9	Golgi-associated PDZ and coiled-coil motif-containing protein	Gopc
Q8VHR5	Transcriptional repressor p66-beta	Gatad2b
A2A432	Cullin-4B	Cul4b
P02535	Keratin, type I cytoskeletal 10	Krt10
A2A654	Bromodomain PHD finger transcription factor	Bptf
A2AE27	AMP deaminase 2	Ampd2
Q9D711	Pirin	Pir
A2AIR7	Voltage-dependent N-type calcium channel subunit alpha-1B	Cacna1b
A2AMD0	Predicted gene 12666	Gm12666
A2AML7	Zinc finger protein 352	Zfp352
Q8JZX4	Splicing factor 45	Rbm17
A2APR8	Mitotic checkpoint serine/threonine-protein kinase BUB1	Bub1
Q80TY0	Formin-binding protein 1	Fnbp1
A2ASI5	Sodium channel protein type 3 subunit alpha	Scn3a
A2AUD5	Tumor protein D54	Tpd52l2
A2AVR2	HEAT repeat-containing protein 8	Heatr8
A2AWI7	Endophilin-B2	Sh3glb2
Q9D868	Peptidyl-prolyl cis-trans isomerase H	Ppih
A3KFM7	Chromodomain-helicase-DNA-binding protein 6	Chd6
A4FUP9	Glycosyltransferase 1 domain-containing protein 1	Glt1d1
A6H630	UPF0364 protein C6orf211 homolog	Armt1

Q9D3L3	Synaptosomal-associated protein	Snap23
Q9WTT4	V-type proton ATPase subunit G 2	Atp6v1g2
B1AQW2	Microtubule-associated protein	Mapt
Q9QWI6	SRC kinase signaling inhibitor 1	Srcin1
B1AUN2	Eukaryotic translation initiation factor 2B, subunit 3	Eif2b3
B1AVB2	Scm polycomb group protein-like 2	Scml2
B1AZM2	Predicted gene 15091	Gm15091
O35317	Pre-B-cell leukemia transcription factor 3	Pbx3
B2M1R6	Heterogeneous nuclear ribonucleoprotein K	Hnrnpk
B2RXS4	Plexin-B2	Plxnb2
B7ZC40	Glutaredoxin-2, mitochondrial	Glrx2
P47934	Carnitine O-acetyltransferase	Crat
B8JJZ4	Zinc finger protein 808	Zfp808
G3UZF7	Centrosomal protein C10orf90 homolog	D7Ertd443e
P62843	40S ribosomal protein S15	Rps15
E9Q425	Tubulin polyglutamylase TTLL5	Ttll5
P17515	C-X-C motif chemokine 10	Cxcl10
Q9Z1M4	Ribosomal protein S6 kinase beta-2	Rps6kb2
D3YXS5	Kinesin-like protein KLP6	Klp6
D3YXW1	Protein LLP homolog	Llph
Q99MN9	Propionyl-CoA carboxylase beta chain, mitochondrial	Pccb
Q9D6K7	Tetratricopeptide repeat protein 33	Ttc33
D3Z2J4	AKT-interacting protein	Aktip
Q9WTZ1	RING-box protein 2	Rnf7
Q9CQB5	CDGSH iron-sulfur domain-containing protein 2	Cisd2
D3Z4U8	DDB1- and CUL4-associated factor 11	Dcaf11
D3Z6B7	DNA damage-regulated autophagy modulator protein 2	Dram2
D3Z7P4	Glutaminase kidney isoform, mitochondrial	Gls
P97785	GDNF family receptor alpha-1	Gfra1
Q8CIG9	F-box/LRR-repeat protein 8	Fbxl8
D6RJI8	TBC1 domain family member 13	Tbc1d13
Q5SUQ9	CST complex subunit CTC1	Ctc1
E0CXT7	Cleavage and polyadenylation specificity factor subunit 4	Cpsf4
E9PU87	Serine/threonine-protein kinase SIK3	Sik3
P70170	ATP-binding cassette sub-family C member 9	Abcc9
E9PUR1	Opticin	Optc
P48774	Glutathione S-transferase Mu 5	Gstm5
E9PVN6	Synaptojanin-2-binding protein	Gm20498
E9PVZ8	Golgi autoantigen, golgin subfamily b, macrogolgin 1	Golgb1
E9PWQ7	Zonadhesin	Zan
Q8CCB4	Vacuolar protein sorting-associated protein 53 homolog	Vps53
E9PXU1	Integrator complex subunit 6-like	Ddx26b
E9PYD5	Transcription elongation factor A protein 1	Tcea1
Q6NZN0	RNA-binding protein 26	Rbm26
E9Q430		Gm2832
O08532	Voltage-dependent calcium channel subunit alpha-2/delta-1	Cacna2d1
Q8R0F3	Sulfatase-modifying factor 1	Sumf1

E9Q2E4	HECT domain E3 ubiquitin protein ligase 4	Gm15800
E9Q2N4	Vomeronasal type-1 receptor	Vmn1r184
E9Q394	A-kinase anchor protein 13	Akap13
E9Q4K7	Kinesin family member 13B	Kif13b
E9Q4R1	Protein FAM102B	Fam102b
E9Q545	Olfactory receptor	Olfr552
E9Q5L3	Short/branched chain specific acyl-CoA dehydrogenase, mitochondrial	Acadsb
G5E8P0	Gamma-tubulin complex component 6	Tubgcp6
E9Q7E2	AT-rich interactive domain-containing protein 2	Arid2
Q3UQ84	Threonine--tRNA ligase, mitochondrial	Tars2
E9Q7P5	Olfactory receptor	Olfr640
E9Q9J4	Inositol hexakisphosphate and diphosphoinositol-pentakisphosphate kinase 2	Ppip5k2
Q6ZPL9	ATP-dependent RNA helicase DDX55	Ddx55
H3BJQ9	Homeobox protein cut-like 1	Cux1
F6QYZ5	Peptidase inhibitor 16	Pi16
F6S169	Tankyrase-2	Tnks2
O88384	Vesicle transport through interaction with t-SNAREs homolog 1B	Vti1b
Q810U5	Coiled-coil domain-containing protein 50	Ccdc50
Q6DFZ2	Nesprin-2	Syne2
F6XVH0	Predicted gene 12830	Gm12830
Q9CR21	Acyl carrier protein, mitochondrial	Ndufab1
F6ZGR6	RIKEN cDNA D430041D05 gene	D430041D05Rik
J3QPW1	Phosphatidylinositol transfer protein alpha isoform	Pitpna
Q69ZR2	E3 ubiquitin-protein ligase HECTD1	Hectd1
Q99N84	28S ribosomal protein S18b, mitochondrial	Mrps18b
P19426	Negative elongation factor E	Rdbp
Q80VJ2	Steroid receptor RNA activator 1	Sra1
G3X9H5	Huntingtin	Htt
G3X9Z8	Innate immunity activator protein	5730559C18Rik
G5E852	Tyrosine-protein kinase	Jak2
H3BLL4	Heterogeneous nuclear ribonucleoprotein K	Hnrnpk
Q60766	Immunity-related GTPase family M protein 1	Irgm1
K4DI67	Condensin-2 complex subunit D3	Ncapd3
K7N678	Olfactory receptor	Olfr893
M9MMK5	Olfactory receptor	Olfr329-ps
O08675	Proteinase-activated receptor 3	F2rl2
O35350	Calpain-1 catalytic subunit	Capn1
O54732	Matrix metalloproteinase-15	Mmp15
O54774	AP-3 complex subunit delta-1	Ap3d1
O70456	14-3-3 protein sigma	Sfn
P01649	Ig kappa chain V-V regions	
P01897	H-2 class I histocompatibility antigen, L-D alpha chain	H2-L
P01942	Hemoglobin subunit alpha	Hba
P02772	Alpha-fetoprotein	Afp
P08122	Collagen alpha-2(IV) chain	Col4a2
P10922	Histone H1.0	H1f0

P13542	Myosin-8	Myh8
P15533	Tripartite motif-containing protein 30A	Trim30a
P20060	Beta-hexosaminidase subunit beta	Hexb
P22437	Prostaglandin G/H synthase 1	Ptgs1
P31938	Dual specificity mitogen-activated protein kinase kinase 1	Map2k1
P35585	AP-1 complex subunit mu-1	Ap1m1
P42227	Signal transducer and activator of transcription 3	Stat3
P43247	DNA mismatch repair protein Msh2	Msh2
P48432	Transcription factor SOX-2	Sox2
P49586	Choline-phosphate cytidylyltransferase A	Pcyt1a
Q922U2	Keratin, type II cytoskeletal 5	Krt5
P51125	Calpastatin	Cast
P51807	Dynein light chain Tctex-type 1	Dynlt1
P51943	Cyclin-A2	Ccna2
P55200	Histone-lysine N-methyltransferase MLL	Mll
P57716	Nicastrin	Ncstn
P58058	NAD kinase	Nadk
P58871	182 kDa tankyrase-1-binding protein	Tnks1bp1
P59017	Bcl-2-like protein 13	Bcl2l13
P61967	AP-1 complex subunit sigma-1A	Ap1s1
P61971	Nuclear transport factor 2	Nutf2
P63147	Ubiquitin-conjugating enzyme E2 B	Ube2b
P70279	Surfeit locus protein 6	Surf6
P70333	Heterogeneous nuclear ribonucleoprotein H2	Hnrnph2
P70388	DNA repair protein RAD50	Rad50
P81117	Nucleobindin-2	Nucb2
Q6P4T3	Eyes absent homolog 3	Eya3
P97481	Endothelial PAS domain-containing protein 1	Epas1
Q0VBL3	RNA-binding protein 15	Rbm15
Q14AX6	Cyclin-dependent kinase 12	Cdk12
Q14CH7	Alanine--tRNA ligase, mitochondrial	Aars2
Q32KG4	Retrotransposon gag domain-containing protein 1	Rgag1
Q3TC93	HCLS1-binding protein 3	Hs1bp3
H9H9T1	Protein FAM107B	Fam107b
Q3TMP1	General transcription factor IIIC, polypeptide 3	Gtf3c3
Q3TTY0	Phospholipase B1, membrane-associated	Plb1
Q3TZR9	Cyclic AMP-dependent transcription factor ATF-7	Atf7
Q3U186	Probable arginine--tRNA ligase, mitochondrial	Rars2
Q3UHI4	Protein TMED8	Tmed8
Q6PDG5	SWI/SNF complex subunit SMARCC2	Smarcc2
Q3UM18	Large subunit GTPase 1 homolog	Lsg1
Q3UMR5	Calcium uniporter protein, mitochondrial	Mcu
Q3UMU9	Hepatoma-derived growth factor-related protein 2	Hdgfrp2
Q3USJ8	FCH and double SH3 domains protein 2	Fchsd2
Q64458	Cytochrome P450 2C29	Cyp2c29
Q3UWX6	RIKEN cDNA E330034G19 gene	E330034G19Rik

Q561M1	Acp1 protein	Acp1
Q68FF6	ARF GTPase-activating protein GIT1	Git1
Q5ND29	Rab-interacting lysosomal protein	Rilp
Q8BFY7	Protein FAM64A	Fam64a
Q5RJG1	Nucleolar protein 10	Nol10
Q99N89	39S ribosomal protein L43, mitochondrial	Mrpl43
Q5SSW2	Proteasome activator complex subunit 4	Psme4
Q7TNE3	Sperm-associated antigen 7	Spag7
Q60596	DNA repair protein XRCC1	Xrcc1
Q60778	NF-kappa-B inhibitor beta	Nfkbib
Q60886	Olfactory receptor 147	Olfr147
Q61025	Intraflagellar transport protein 20 homolog	Ift20
Q61048	WW domain-binding protein 4	Wbp4
Q61136	Serine/threonine-protein kinase PRP4 homolog	Prpf4b
Q61838	Alpha-2-macroglobulin	A2m
Q63886	UDP-glucuronosyltransferase 1-1	Ugt1a1
Q641P0	Actin-related protein 3B	Actr3b
Q64676	2-hydroxyacylsphingosine 1-beta-galactosyltransferase	Ugt8
Q6A037	NEDD4-binding protein 1	N4bp1
Q6A152	Cytochrome P450 4X1	Cyp4x1
Q6DID3	Protein SCAF8	Scaf8
Q6NV83	U2 snRNP-associated SURP motif-containing protein	U2surp
Q6NXJ0	Protein WWC2	Wwc2
Q6NZR5	Superkiller viralicidic activity 2-like (S. cerevisiae)	Skiv2l
Q6P1C6	Leucine-rich repeats and immunoglobulin-like domains protein 3	Lrig3
Q6P5E6	ADP-ribosylation factor-binding protein GGA2	Gga2
Q6P9J9	Anoctamin-6	Ano6
Q6PGC1	ATP-dependent RNA helicase Dhx29	Dhx29
Q6V4S5	Protein sidekick-2	Sdk2
Q6ZQ73	Cullin-associated NEDD8-dissociated protein 2	Cand2
Q7TMM9	Tubulin beta-2A chain	Tubb2a
Q7TPM6	Fibronectin type III and SPRY domain-containing protein 1	Fsd1
Q7TQA6	Taste receptor type 2 member 38	Tas2r38
Q7TQT7	Olfactory receptor	Olfr1371
Q7TQZ0	Olfactory receptor	Olfr32
Q7TR71	Olfactory receptor	Olfr1062
Q7TRI9	Olfactory receptor	Olfr129
Q80X59	Transmembrane and coiled-coil domain-containing protein 5B	Tmco5b
Q80X71	Transmembrane protein 106B	Tmem106b
Q80X98	DEAH (Asp-Glu-Ala-His) box polypeptide 38	Dhx38
Q80ZX2	Zfp790 protein	Zfp790
Q8BFQ4	WD repeat-containing protein 82	Wdr82
Q8BGD6	Putative sodium-coupled neutral amino acid transporter 9	Slc38a9
Q8BGR9	Ubiquitin-like domain-containing CTD phosphatase 1	Ublcp1
Q9EQ28	DNA polymerase delta subunit 3	Pold3
Q8BH79	Anoctamin-10	Ano10

Q8BHF7	CDP-diacylglycerol--glycerol-3-phosphate 3-phosphatidyltransferase, mitochondrial	Pgs1
Q8BJ03	Cytochrome c oxidase assembly protein COX15 homolog	Cox15
Q8BP48	Methionine aminopeptidase 1	Metap1
Q9CTN4	Rho-related BTB domain-containing protein 3	Rhobtb3
Q8BVG4	Dipeptidyl peptidase 9	Dpp9
Q8BYL4	Tyrosine--tRNA ligase, mitochondrial	Yars2
Q8C052	Microtubule-associated protein 1S	Map1s
Q8C0L8	Conserved oligomeric Golgi complex subunit 5	Cog5
Q8C263	Spindle and kinetochore-associated protein 3	Ska3
Q8C3Y4	Kinetochore-associated protein 1	Kntc1
Q8C9W3	A disintegrin and metalloproteinase with thrombospondin motifs 2	Adamts2
Q8CD10	EF-hand domain-containing family member A1	Efha1
Q8CD92	Tetratricopeptide repeat protein 27	Ttc27
Q8CDA1	Phosphatidylinositide phosphatase SAC2	Inpp5f
Q8CE46	Pseudouridylate synthase 7 homolog-like protein	Pus7l
Q8CEC6	Peptidylprolyl isomerase domain and WD repeat-containing protein 1	Ppwd1
Q8CI03	FLYWCH-type zinc finger-containing protein 1	Flywch1
Q8CI61	BAG family molecular chaperone regulator 4	Bag4
Q8CIL4	Uncharacterized protein C1orf131 homolog	
Q8CJ27	Abnormal spindle-like microcephaly-associated protein homolog	Aspm
Q8CJG0	Protein argonaute-2	Eif2c2
Q8K202	DNA-directed RNA polymerase I subunit RPA49	Polr1e
Q8K248	4-hydroxyphenylpyruvate dioxygenase-like protein	Hpdl
Q8K4P0	pre-mRNA 3 end processing protein WDR33	Wdr33
Q8R000	Organic solute transporter subunit alpha	Osta
Q8R080	G2 and S phase-expressed protein 1	Gtse1
Q8R0A0	General transcription factor IIF subunit 2	Gtf2f2
Q8R293	Vomeronasal type-1 receptor	Vmn1r73
Q8R322	Nucleoporin GLE1	Gle1
Q8R3H7	Heparan sulfate 2-O-sulfotransferase 1	Hs2st1
Q8R3K3	Pentatricopeptide repeat-containing protein 2	Ptcd2
Q8R3N6	THO complex subunit 1	Thoc1
Q8R480	Nuclear pore complex protein Nup85	Nup85
Q8R4H4	Carboxypeptidase A5	Cpa5
Q8R5A6	TBC1 domain family member 22A	Tbc1d22a
Q8VCV2	Protein NDRG3	Ndrg3
Q8VDK1	Nitrilase homolog 1	Nit1
Q8VED5	Keratin, type II cytoskeletal 79	Krt79
Q8VGW6	Olfactory receptor	Olfr124
Q8VHZ7	U3 small nucleolar ribonucleoprotein protein IMP4	Imp4
Q8VI47	Canalicular multispecific organic anion transporter 1	Abcc2
Q8VIH1	Homeobox protein NOBOX	Nobox
Q91UZ5	Inositol monophosphatase 2	Impa2
Q91WG2	Rab GTPase-binding effector protein 2	Rabep2
Q91XL3	UDP-glucuronic acid decarboxylase 1	Uxs1
Q920G5	Olfactory receptor	Olfr713

Q99J10	Cytoplasmic tRNA 2-thiolation protein 1	Ctu1
Q99L85	Dermal papilla-derived protein 6 homolog	Derp6
Q99LB2	Dehydrogenase/reductase SDR family member 4	Dhrs4
Q99NI3	General transcription factor II-I repeat domain-containing protein 2	Gtf2ird2
Q99P31	Hsp70-binding protein 1	Hspbp1
Q99PL6	UBX domain-containing protein 6	Ubxn6
Q9CQA6	Coiled-coil-helix-coiled-coil-helix domain-containing protein 1	Chchd1
Q9CQT7	Desumoylating isopeptidase 1	Pppde2
Q9CWE0	Protein FAM54B	Fam54b
Q9CZH7	Matrix-remodeling-associated protein 7	Mxra7
Q9D0N7	Chromatin assembly factor 1 subunit B	Chaf1b
Q9D1M4	Eukaryotic translation elongation factor 1 epsilon-1	Eef1e1
Q9D2F1	PRAME family member 12	Pramef12
Q9D2H8	Fibronectin type III domain-containing protein 8	Fndc8
Q9D2R8	28S ribosomal protein S33, mitochondrial	Mrps33
Q9D6X6	Serine protease 23	Prss23
Q9D771	Transmembrane protein 206	Tmem206
Q9D7A8	Armadillo repeat-containing protein 1	Armc1
Q9D9S2	Transmembrane protein 225	Tmem225
Q9DC33	High mobility group protein 20A	Hmg20a
Q9DC70	NADH dehydrogenase [ubiquinone] iron-sulfur protein 7, mitochondrial	Ndufs7
Q9DCC4	Pyrroline-5-carboxylate reductase 3	Pycrl
Q9EP97	Sentrin-specific protease 3	Senp3
Q9EPQ8	Transcription factor 20	Tcf20
Q9EQG9	Collagen type IV alpha-3-binding protein	Col4a3bp
Q9ER38	Torsin-3A	Tor3a
Q9ER81	Torsin-1A-interacting protein 2, isoform IFRG15	Tor1aip2
Q9ESN1	Double C2-like domain-containing protein gamma	Doc2g
Q9JKS4	LIM domain-binding protein 3	Ldb3
Q9JL35	High mobility group nucleosome-binding domain-containing protein 5	Hmgn5
Q9QWV9	Cyclin-T1	Ccnt1
Q9QXV1	Chromobox protein homolog 8	Cbx8
Q9QXW0	F-box/LRR-repeat protein 6	Fbxl6
Q9QYC1	Pecanex-like protein 1	Pcnx
Q9QYX7	Protein piccolo	Pclo
Q9QZI8	Serine incorporator 1	Serinc1
Q9WTP7	GTP:AMP phosphotransferase, mitochondrial	Ak3
Q9WUK4	Replication factor C subunit 2	Rfc2
Q9WUN2	Serine/threonine-protein kinase TBK1	Tbk1
Q9WVL0	Maleylacetoacetate isomerase	Gstz1
Q9Z2U2	Zinc finger protein 292	Zfp292
S4R1D6	H-2 class I histocompatibility antigen, TLA(B) alpha chain	H2-T3
Z4YKJ7	Excitatory amino acid transporter 5	Slc1a7

Table 11 List of the proteins expressed only in OligoGM1 cells in the comparison OligoGM1 vs CONTROL N2a cells

Majority protein IDs	Protein names	Gene names
A0A075B607	T cell receptor alpha variable 14-3	Trav14d-2
A0A075B6D5	Immunoglobulin kappa chain variable 19-93	Igkv19-93
A0A087WQ44	Snf2-related CREBBP activator protein	Srcap
Q5DTW7	Uncharacterized protein C12orf35 homolog	Kiaa1551
A0A087WR36	Vomeronasal type-1 receptor	Vmn1r90
A0A1L1SQU7	FAT atypical cadherin 1	Fat1
A0A0A0MQA5	Tubulin alpha-4A chain	Tuba4a
A0A0A0MQD1	Tudor domain-containing protein 7	Tdrd7
P09925	Surfeit locus protein 1	Surf1
Q3TRR0	Microtubule-associated protein 9	Map9
A0A0A6YVV8	Muscleblind-like protein 1	Mbnl1
Q8VBV3	Exosome complex component RRP4	Exosc2
Q99PJ1	Protocadherin-15	Pcdh15
A0A0A6YX01	Protocadherin beta-6	Pcdhb6
A0A0A6YY47	Neural cell adhesion molecule 1	Ncam1
A0A0B4J1I7	Immunoglobulin kappa variable 4-68	Igkv4-68
A0A0G2JDF6	RIKEN cDNA I830077J02 gene	I830077J02Rik
A0A0G2JDW9	Immunoglobulin kappa variable 4-62	Igkv4-62
A0A0G2JE49	Paired immunoglobulin-like type 2 receptor alpha	Pilra
A0A0G2JEK2	Cysteine-rich protein 1	Crip1
A0A0G2JEY5	Immunoglobulin kappa variable 4-81	
Q920L5	Elongation of very long chain fatty acids protein 6	Elovl6
A0A0G2JFV8	Polypyrimidine tract-binding protein 2	Ptbp2
Q5DW34	Histone-lysine N-methyltransferase EHMT1	Ehmt1
A0A0J9YUP9	Transcription factor 4	Tcf4
Q91YP3	Putative deoxyribose-phosphate aldolase	Dera
A0A1N9MDH9	Probable G-protein coupled receptor 19	Gpr19
B2RPV6	Multimerin-1	Mmrn1
Q91WI7	Integrin-alpha FG-GAP repeat-containing protein 2	Itfg2
F6V2U0	Type I inositol 3,4-bisphosphate 4-phosphatase	Inpp4a
A0A0R4J0U3	Period circadian protein homolog 2	Per2
A0A0R4J187	X-ray repair cross-complementing protein 6	Xrcc6
A0A0R4J1N7	Ankyrin-1	Ank1
Q8R2Q6	Tectonic-3	Tctn3
A0A0U1RPA0	Pleckstrin homology domain-containing family A member 7	Plekha7
Q8BMB0	Protein EMSY	Emsy
A0A0U1RQ37	Ubiquitin-conjugating enzyme E2 S	Ube2s
Q9Z179	SHC SH2 domain-binding protein 1	Shcbp1
E9QPQ8	39S ribosomal protein L48, mitochondrial	Mrpl48
Q571B6	WASP homolog-associated protein with actin, membranes and microtubules	Whamm
Q9CQG6	Transmembrane protein 147	Tmem147
A0A140LIT2	7-dehydrocholesterol reductase	Dhcr7

A0A140LIW7	Ankyrin-repeat and fibronectin type III domain-containing 1	Ankfn1
Q8CG73	Protein fantom	Rpgrip1l
Q9D6T0	Nitric oxide synthase-interacting protein	Nosip
Q8JZK6	MCG22896, isoform CRA_b	Trim61
A0A1D5RLF0	F-box and WD-40 domain protein 27	Fbxw27
A0A1D5RLL4	Transformation/transcription domain-associated protein	Trrap
F8WI85	Leucine-rich repeat-containing protein 36	Lrrc36
A0A1L1SRQ8	Olfactory receptor	Olfr251
Q91XE8	Transmembrane protein 205	Tmem205
Q9DCU6	39S ribosomal protein L4, mitochondrial	Mrpl4
A0A1L1SSZ5	Olfactory receptor 1248	Olfr1248
Q9D083	Kinetochore protein Spc24	Spc24
A0A1W2P7F9	MCG50764, isoform CRA_a	Btg1
Q9CWV7	Zinc finger SWIM domain-containing protein 1	Zswim1
Q3TB48	Transmembrane protein 104	Tmem104
Q9D7S1	Transmembrane protein 54	Tmem54
A2A9L3	Serine/threonine-protein kinase PDIK1L	Pdik1l
E9Q0J2	Ral GTPase-activating protein subunit beta	Ralgapb
A2ACM0	Regulatory-associated protein of mTOR	Rptor
Q9ER67	Maged2 protein	Maged2
A2AI92	Predicted gene 9112	Gm9112
Q6P2L7	Protein CASC4	Casc4
A2AT37	UPF2 regulator of nonsense transcripts homolog (Yeast)	Upf2
Q80YN3	Breast carcinoma-amplified sequence 1 homolog	Bcas1
A2AX52	Collagen alpha-4(VI) chain	Col6a4
A4QPD3	Proto-oncogene c-Rel	Rel
A6PWV5	AT-rich interactive domain-containing protein 3C	Arid3c
A7TZG3	Selection and upkeep of intraepithelial T-cells protein 9	Skint9
B2RQS1	Striatin-3	Strn3
B2RXC1	Trafficking protein particle complex subunit 11	Trappc11
Q8BXQ2	GPI transamidase component PIG-T	Pigt
J3QQ27	Coiled-coil domain-containing 191	2610015P09Rik
B8QI34	Liprin-alpha-2	Ppfia2
D3YU71	3 beta-hydroxysteroid dehydrogenase type 7	Hsd3b7
D3YUK0	Predicted gene 3259	Gm3259
D3YUP1	Histone-arginine methyltransferase CARM1	Carm1
Q3TQR0	Post-GPI attachment to proteins factor 2	Pgap2
Q99LG0	Ubiquitin carboxyl-terminal hydrolase 16	Usp16
P30285	Cyclin-dependent kinase 4	Cdk4
Q9JIY5	Serine protease HTRA2, mitochondrial	Htra2
D3YYL7	40S ribosomal protein S29	Gm10126
D3YZP5	Ras-related protein Rab-3A	Rab3a
D3Z0X5	Pleckstrin homology-like domain family B member 1	Phldb1
Q9DCL8	Protein phosphatase inhibitor 2	Ppp1r2
D3Z3G0	Uncharacterized protein C12orf56 homolog	D930020B18Rik
D3Z3S5	Predicted gene 4744	Gm4744

Q9CXK9	RNA-binding protein 33	Rbm33
D3Z6C4	Carbonyl reductase family member 4	Cbr4
Q9D8N6	Protein lin-37 homolog	Lin37
Q9Z120	tRNA (guanine-N(7)-)-methyltransferase	Mettl1
D6RFB0	Adhesion G protein-coupled receptor L3	Lphn3
E9Q2M9	WD repeat and FYVE domain-containing 4	Wdfy4
E9PXJ8	Vomeronasal 2, receptor 90	Vmn2r90
Q8C2B3	Histone deacetylase 7	Hdac7
Q9CQJ6	Density-regulated protein	Denr
E9Q0J5	Kinesin-like protein KIF21A	Kif21a
E9Q0N0	Intersectin-1	Itsn1
E9Q163	X-ray repair cross-complementing protein 6	Xrcc6
E9Q1P2	Olfactory receptor	Olfr288
A7RDN6	Renalase	Rnls
Q9QVP9	Protein-tyrosine kinase 2-beta	Ptk2b
Q8BMQ2	General transcription factor 3C polypeptide 4	Gtf3c4
E9Q5A3	Histone-lysine N-methyltransferase EHMT1	Ehmt1
E9Q622	Protocadherin 11 X-linked	Pcdh11x
Q6ZQE4	Transmembrane protein 194A	Tmem194a
E9Q7Q3	Tropomyosin alpha-3 chain	Tpm3
E9Q876	ATP-binding cassette, sub-family A (ABC1), member 12	Abca12
E9Q912	RAP1, GTP-GDP dissociation stimulator 1	Rap1gds1
E9Q9M1	Cytosolic purine 5-nucleotidase	Nt5c2
E9QAN2	Poly(A) polymerase alpha	Papola
Q6RT24	Centromere-associated protein E	Cenpe
E9QKK4	Glucocorticoid-induced transcript 1 protein	Glcci1
Q70KF4	Cardiomyopathy-associated protein 5	Cmya5
Q8VEH3	ADP-ribosylation factor-like protein 8A	Arl8a
Q3UQN2	FCH domain only protein 2	Fcho2
F6UK53	MCG62900	4933403O08Rik
P10493	Nidogen-1	Nid1
F6VWU8	Zinc finger protein 946	Zfp946
Q8BND4	Protein DDX26B	Ddx26b
Q8K3A9	7SK snRNA methylphosphate capping enzyme	Mepce
F8VPP8	Zinc finger CCCH type-containing 7B	Zc3h7b
F8WIN2	AT-rich interactive domain-containing protein 3B	Arid3b
V9GX74	Zinc finger transcription factor Trps1	Trps1
Q9QUS9	Reg III delta	Reg3d
Q3UW64	Bifunctional UDP-N-acetylglucosamine 2-epimerase/N-acetylmannosamine kinase	Gne
H3BJU3	Mitoguardin 2	Fam73b
Q4VGL6	Roquin	Rc3h1
Q549C9	Cellular tumor antigen p53	Trp53
Q9D572	UBX domain-containing protein 11	Ubxn11
J3QMK1	Shugoshin 2B	Sgo2b
J3QNW4	UPF0533 protein C5orf44 homolog	Trappc13
K3W4Q5	Protein FAM186A	FAM186A

O55057	Retinal rod rhodopsin-sensitive cGMP 3,5-cyclic phosphodiesterase subunit delta	Pde6d
O08643	Granzyme M	Gzmm
O35257	Prolactin-6A1	Prl6a1
O35615	Zinc finger protein ZFPM1	Zfpm1
O35654	DNA polymerase delta subunit 2	Pold2
O35943	Frataxin, mitochondrial	Fxn
O54786	DNA fragmentation factor subunit alpha	Dffa
O54988	STE20-like serine/threonine-protein kinase	Slk
O55142	60S ribosomal protein L35a	Rpl35a
O55183	Stanniocalcin-1	Stc1
O88495	Melatonin-related receptor	Gpr50
O88574	Histone deacetylase complex subunit SAP30	Sap30
O88630	Golgi SNAP receptor complex member 1	Gosr1
O89001	Carboxypeptidase D	Cpd
P01325	Insulin-1	Ins1
P01639	Ig kappa chain V-V region MOPC 41	Gm5571
P08508	Low affinity immunoglobulin gamma Fc region receptor III	Fcgr3
P11438	Lysosome-associated membrane glycoprotein 1	Lamp1
P11930	Nucleoside diphosphate-linked moiety X motif 19, mitochondrial	Nudt19
P12367	cAMP-dependent protein kinase type II-alpha regulatory subunit	Prkar2a
P16330	2,3-cyclic-nucleotide 3-phosphodiesterase	Cnp
P16382	Interleukin-4 receptor subunit alpha	Il4r
P19137	Laminin subunit alpha-1	Lama1
P22339	Growth arrest and DNA damage-inducible protein GADD45 beta	Gadd45b
P30549	Substance-K receptor	Tacr2
P34152	Focal adhesion kinase 1	Ptk2
P35546	Proto-oncogene tyrosine-protein kinase receptor Ret	Ret
P45952	Medium-chain specific acyl-CoA dehydrogenase, mitochondrial	Acadm
P46414	Cyclin-dependent kinase inhibitor 1B	Cdkn1b
P48455	Serine/threonine-protein phosphatase 2B catalytic subunit gamma isoform	Ppp3cc
P48542	G protein-activated inward rectifier potassium channel 2	Kcnj6
P54726	UV excision repair protein RAD23 homolog A	Rad23a
P61027	Ras-related protein Rab-10	Rab10
P61458	Pterin-4-alpha-carbinolamine dehydratase	Pcbd1
P61957	Small ubiquitin-related modifier 2	Sumo2
P62071	Ras-related protein R-Ras2	Rras2
P62911	60S ribosomal protein L32	Rpl32
P63166	Small ubiquitin-related modifier 1	Sumo1
P63328	Serine/threonine-protein phosphatase 2B catalytic subunit alpha isoform	Ppp3ca
P70213	Friend virus susceptibility protein 1	Fv1
P70298	Homeobox protein cut-like 2	Cux2
P97489	Transcription factor GATA-5	Gata5
P97496	SWI/SNF complex subunit SMARCC1	Smarcc1
Q02614	SAP30-binding protein	Sap30bp
Q03402	Cysteine-rich secretory protein 3	Crisp3
Q04447	Creatine kinase B-type	Ckb

Q07563	Collagen alpha-1(XVII) chain	Col17a1
Q0V8T7	Contactin-associated protein like 5-3	Cntnap5c
Q0VAV1	Muc6 protein	Muc6
Q8BZH4	Pogo transposable element with ZNF domain	Pogz
Q3TCU5	Tapasin	Tapbp
Q3TDD9	Protein phosphatase 1 regulatory subunit 21	Ppp1r21
Q80W82	Mitogen-activated protein kinase 10	Mapk10
Q3TSN9	BTB/POZ domain-containing protein 3	Btbd3
Q3UDW8	Heparan-alpha-glucosaminide N-acetyltransferase	Hgsnat
Q3UQ17	MCG3834	Zbtb16
Q3UVL4	Protein fat-free homolog	Ffr
Q3UY93	Melanin-concentrating hormone receptor 1	Mchr1
Q3V3G9	Nardilysin, N-arginine dibasic convertase, NRD convertase 1	Nrd1
Q3V3Q4	Pyrin domain-containing protein 3	Pydc3
Q4ZGD9	Nuclear RNA export factor 3	Nxf3
Q569L8	Centromere protein J	Cenpj
Q91YI4	Beta-arrestin-2	Arrb2
A2AH25	Rho GTPase-activating protein 1	Arhgap1
Q5I043	Ubiquitin carboxyl-terminal hydrolase 28	Usp28
Q5SSE9	ATP-binding cassette sub-family A member 13	Abca13
E9Q284	Coilin	Coil
Q5SXG7	Vitelline membrane outer layer protein 1 homolog	Vmo1
Q60707	T-box transcription factor TBX2	Tbx2
Q61687	Transcriptional regulator ATRX	Atrx
Q61781	Keratin, type I cytoskeletal 14	Krt14
Q62048	Astrocytic phosphoprotein PEA-15	Pea15
Q62095	ATP-dependent RNA helicase DDX3Y	Ddx3y
Q62172	RalA-binding protein 1	Ralbp1
Q640M1	U3 small nucleolar RNA-associated protein 14 homolog A	Utp14a
Q64505	Cholesterol 7-alpha-monooxygenase	Cyp7a1
Q6DFV1	Condensin-2 complex subunit G2	Ncapg2
Q9WV80	Sorting nexin-1	Snx1
Q6P1G0	HEAT repeat-containing protein 6	Heatr6
Q6P539	Uncharacterized protein C17orf63 homolog	Fam222b
Q6P6J9	Thioredoxin domain-containing protein 15	Txndc15
Q6P8K3	Predicted gene 7978	BC061212
Q6P9R1	ATP-dependent RNA helicase DDX51	Ddx51
Q6PGF7	Exocyst complex component 8	Exoc8
Q6PR54	Telomere-associated protein RIF1	Rif1
Q6UJY2	Sodium/hydrogen exchanger 10	Slc9c1
Q6ZPY5	Zinc finger protein 507	Znf507
Q704Y3	Transient receptor potential cation channel subfamily V member 1	Trpv1
Q7M721	Taste receptor type 2 member 120	Tas2r120
Q7TS04	Olfactory receptor 301	Olfr301
Q80UW8	DNA-directed RNA polymerases I, II, and III subunit RPABC1	Polr2e
Q80WQ2	Protein VAC14 homolog	Vac14
Q8BHE0	Proline-rich protein 11	Prr11

Q8BHG9	CGG triplet repeat-binding protein 1	Cggbp1
Q8BLY2	Probable threonine--tRNA ligase 2, cytoplasmic	Tarsl2
Q8BNY6	Neuronal calcium sensor 1	Ncs1
Q8R2L5	28S ribosomal protein S18c, mitochondrial	Mrps18c
Q8BU03	Periodic tryptophan protein 2 homolog	Pwp2
Q8BUJ9	Low-density lipoprotein receptor-related protein 12	Lrp12
Q8BVT7	RIKEN cDNA 4921511C20 gene	4921511C20Rik
Q8BXZ1	Protein disulfide-isomerase TMX3	Tmx3
Q8BZR0	Probable G-protein coupled receptor 82	Gpr82
Q8C2E4	Pentatricopeptide repeat-containing protein 1	Ptcd1
Q8C5R8	Ribose-phosphate pyrophosphokinase	Prps1l1
Q8C754	Vacuolar protein sorting-associated protein 52 homolog	Vps52
Q8C845	EF-hand domain-containing protein D2	Efhd2
Q8CBF3	Ephrin type-B receptor 1	Ephb1
Q8CCX5	Keratin-like protein KRT222	Krt222
Q8CDK2	Cytosolic carboxypeptidase 2	Agbl2
Q8CF66	UPF0539 protein C7orf59 homolog	Lamtor4
Q8CH09	SURP and G-patch domain-containing protein 2	Sugp2
Q8CIV2	Membralin	ORF61
Q8JZM8	Mucin-4	Muc4
Q8JZR0	Long-chain-fatty-acid--CoA ligase 5	Acsl5
Q8K0Z7	Translational activator of cytochrome c oxidase 1	Taco1
Q8K394	Inactive phospholipase C-like protein 2	Plcl2
Q8K3H0	DCC-interacting protein 13-alpha	Appl1
Q8K3V4	Protein-arginine deiminase type-6	Padi6
Q8N7N5	DDB1- and CUL4-associated factor 8	Dcaf8
Q8R054	Sushi repeat-containing protein SRPX2	Srpx2
Q8R105	Vacuolar protein sorting-associated protein 37C	Vps37c
Q8R2E3	Vomeronasal type-1 receptor	Vmn1r36
Q8R2P1	Ectoderm-neural cortex protein 2	Klhl25
Q8R3F5	Malonyl-CoA-acyl carrier protein transacylase, mitochondrial	Mcat
Q8R420	ATP-binding cassette sub-family A member 3	Abca3
Q8R4Y8	Rotatin	Rttn
Q8VDV8	MIT domain-containing protein 1	Mitd1
Q8VFJ7	Olfactory receptor	Olfr1012
Q8VFV9	Olfactory receptor	Olfr1459
Q8VFZ3	Olfactory receptor	Olfr513
Q8VG32	Olfactory receptor	Olfr1408
Q8VGE3	Olfactory receptor	Olfr160
Q8VGL3	Olfactory receptor	Olfr535
F8WJ23	Hornerin	Hrnr
Q8VHP6	Cadherin-related family member 1	Cdhr1
Q8VHY0	Chondroitin sulfate proteoglycan 4	Cspg4
Q91XC9	Peroxisomal membrane protein PEX16	Pex16
Q91YP0	L-2-hydroxyglutarate dehydrogenase, mitochondrial	L2hgdh
Q91ZP4	MCG3105, isoform CRA_a	Slc5a4b

Q91ZZ3	Beta-synuclein	Sncb
Q921Y2	U3 small nucleolar ribonucleoprotein protein IMP3	Imp3
Q922B1	O-acetyl-ADP-ribose deacetylase MACROD1	Macrod1
Q99L04	Dehydrogenase/reductase SDR family member 1	Dhrs1
Q99LI5	Zinc finger protein 281	Zfp281
Q99LJ0	CTTNBP2 N-terminal-like protein	Cttnbp2nl
Q99MR1	PERQ amino acid-rich with GYF domain-containing protein 1	Gigyf1
Q99MZ3	Carbohydrate-responsive element-binding protein	Mlxipl
Q99N05	Membrane-spanning 4-domains subfamily A member 4D	Ms4a4d
Q99N96	39S ribosomal protein L1, mitochondrial	Mrpl1
Q9CPN9	RIKEN cDNA 2210010C04 gene	2210010C04Rik
Q9CQ54	NADH dehydrogenase [ubiquinone] 1 subunit C2	Ndufc2
Q9CQQ7	ATP synthase subunit b, mitochondrial	Atp5f1
E9PW43	Protein transport protein Sec61 subunit beta	Gm10320
Q9CR02	Translation machinery-associated protein 16	Tma16
Q9CXR1	Dehydrogenase/reductase SDR family member 7	Dhrs7
Q9CY97	RNA polymerase II subunit A C-terminal domain phosphatase SSU72	Ssu72
Q9CZN8	Glutamyl-tRNA(Gln) amidotransferase subunit A, mitochondrial	Qrsl1
Q9CZX5	PIN2/TERF1-interacting telomerase inhibitor 1	Pinx1
Q9D0M5	Dynein light chain 2, cytoplasmic	Dynll2
Q9D1C8	Vacuolar protein sorting-associated protein 28 homolog	Vps28
Q9D1H8	39S ribosomal protein L53, mitochondrial	Mrpl53
Q9D1N9	39S ribosomal protein L21, mitochondrial	Mrpl21
Q9D1Z3	Protein FAM173B	Fam173b
Q9D267	Epididymal-specific lipocalin-9	Lcn9
Q9D3Z8	RIKEN cDNA 4933425L06	4933425L06Rik
Q9D411	Testis-specific serine/threonine-protein kinase 4	Tssk4
Q9D9V3	Ethylmalonyl-CoA decarboxylase	Echdc1
Q9DAT2	MRG-binding protein	Mrgbp
Q9DBE0	Cysteine sulfinic acid decarboxylase	Csad
Q9DBG1	Sterol 26-hydroxylase, mitochondrial	Cyp27a1
Q9DBJ3	Brain-specific angiogenesis inhibitor 1-associated protein 2-like protein 1	Baiap2l1
Q9DCA5	Ribosome biogenesis protein BRX1 homolog	Brix1
Q9DCF9	Translocon-associated protein subunit gamma	Ssr3
Q9DD18	D-tyrosyl-tRNA(Tyr) deacylase 1	Dtd1
Q9EQ06	Estradiol 17-beta-dehydrogenase 11	Hsd17b11
Q9ERN0	Secretory carrier-associated membrane protein 2	Scamp2
Q9ES83	Blood vessel epicardial substance	Bves
Q9JIK9	28S ribosomal protein S34, mitochondrial	Mrps34
Q9JIX0	Enhancer of yellow 2 transcription factor homolog	Eny2
Q9JJ28	Protein flightless-1 homolog	Flii
Q9JJ78	Lymphokine-activated killer T-cell-originated protein kinase	Pbk
Q9JJ94	Sjoegren syndrome nuclear autoantigen 1 homolog	Ssna1
Q9JJT0	RNA 3-terminal phosphate cyclase-like protein	Rcl1
Q9R0H0	Peroxisomal acyl-coenzyme A oxidase 1	Acox1
Q9R0K2	Olfactory receptor	Olfr1264

Q9WTR1	Transient receptor potential cation channel subfamily V member 2	Trpv2
Q9WV54	Acid ceramidase	Asah1
Q9Z262	Claudin-6	Cldn6
Q9Z2X2	26S proteasome non-ATPase regulatory subunit 10	Psmd10
V9GXI9	Striatin-4	Strn4

3.2 Classification of the differentially expressed proteins based on bioinformatic analysis

In order to understand the effect of OligoGM1, we focused on the proteins expressed in OligoGM1-treated cells. The bioinformatic analyses by DAVID (p value ≤ 0.05, at least 2 counts) showed that in these cells, there is a significant enrichment of gene ontology terms related to endocytic trafficking, ribosome biogenesis, and regulation of transcription, regulation of cell cycle, mitochondrion, fatty acid metabolism, and cell adhesion (Table 12).

Table 12 Bioinformatic analysis by David of the proteins exclusively expressed in OligoGM1 cells in the comparison OligoGM1 vs CONTROL N2a cells

DAVID analysis p-value ≤ 0.05 counts ≥ 2

	Category	Term	Count	p-value	Genes
endosome/endocytic trafficking	**Annotation Cluster 1**	**Enrichment Score: 1.9283871903046559**			
	UP_KEYWORDS	Endosome	14	7,27E-03	RET, SCAMP2, VAC14, VPS52, SNX1, VPS37C, MITD1, APPL1, EPHB1, LAMP1, CDKN1B, ARL8A, VPS28, RAB10
	GOTERM_CC_DIRECT	GO:0010008~endosome membrane	7	8,49E-03	LAMP1, RET, VAC14, VPS52, SNX1, VPS28, APPL1
	GOTERM_CC_DIRECT	GO:0005768~endosome	15	2,66E-02	RAB3A, RET, SCAMP2, VAC14, VPS52, SNX1, VPS37C, MITD1, APPL1, EPHB1, LAMP1, CDKN1B, ARL8A, RAB10, VPS28
	Annotation Cluster 5	**Enrichment Score: 1.2682691071296288**			
	SMART	SM00282: LamG	4	1,77E-02	LAMA1, FAT1, CSPG4, CNTNAP5C
	INTERPRO	IPR001791: Laminin G domain	4	4,92E-02	LAMA1, FAT1, CSPG4, CNTNAP5C
	Annotation Cluster 8	**Enrichment Score: 1.0091254512435084**			
	UP_KEYWORDS	Coated pit	4	2,82E-02	ARRB2, LRP12, ITSN1, FCHO2
ribosome biogenesis and regulation of transcription	**Annotation Cluster 2**	**Enrichment Score: 1.5686242450542756**			
	GOTERM_CC_DIRECT	GO:0005840~ribosome	10	1,65E-03	MRPL53, MRPL1, RPL35A, MRPS34, MRPL4, MRPL21, MRPS18C, RPL32, TMA16, DENR
	UP_KEYWORDS	Ribosomal protein	9	6,36E-03	MRPL53, MRPL1, RPL35A, MRPS34, MRPL4, MRPL21, MRPS18C, RPL32, MRPL48
	UP_KEYWORDS	Ribonucleoprotein	10	2,42E-02	MRPL53, MRPL1, RPL35A, IMP3, MRPS34, MRPL4, MRPL21, MRPS18C, RPL32, MRPL48
	GOTERM_CC_DIRECT	GO:0030529~intracellular ribonucleoprotein complex	10	4,28E-02	MRPL53, MRPL1, RPL35A, IMP3, MRPS34, MRPL4, MRPL21, MRPS18C, RPL32, TDRD7
	Annotation Cluster 3	**Enrichment Score: 1.561905533986465**			
	UP_KEYWORDS	Ribosome biogenesis	5	8,66E-03	RCL1, IMP3, BRIX1, UTP14A, DDX51
	GOTERM_BP_DIRECT	GO:0006364~rRNA processing	6	3,71E-02	RCL1, RPL35A, IMP3, EXOSC2, UTP14A, DDX51
	GOTERM_BP_DIRECT	GO:0042254~ribosome biogenesis	5	4,09E-02	RCL1, IMP3, BRIX1, UTP14A, DDX51
	KEGG_PATHWAY	mmu03008: Ribosome biogenesis in eukaryotes	5	4,31E-02	RCL1, IMP3, NXF3, UTP14A, PWP2
	Annotation Cluster 24	**Enrichment Score: 0.586830761089792**			

	GOTERM_MF_DIRECT	GO:0001085~RNA polymerase II transcription factor binding	4	4,51E-02	TRP53, GATA5, TRPS1, ZFPM1
	Annotation Cluster 28	**Enrichment Score: 0.547197473552621**			
	GOTERM_BP_DIRECT	GO:0000122~negative regulation of transcription from RNA polymerase II promoter	19	2,07E-02	TRP53, EHMT1, TBX2, TRPV1, MLXIPL, ZBTB16, MAPK10, SAP30, REL, CGGBP1, PSMD10, TRPS1, PER2, ZFP281, CUX2, ZFPM1, TCF4, MEPCE, …
cell cycle	**Annotation Cluster 9**	**Enrichment Score: 0.9624582129177877**			
	GOTERM_BP_DIRECT	GO:0051301~cell division	11	4,77E-02	SPC24, POGZ, NCAPG2, ARL8A, CENPE, MITD1, MAP9, USP16, CDK4, CENPJ, UBE2S
	Annotation Cluster 11	**Enrichment Score: 0.8865229236222075**			
	GOTERM_BP_DIRECT	GO:0051726~regulation of cell cycle	6	2,39E-02	TRP53, PRR11, PER2, USP16, CDK4, GADD45B
mitochondrion, fatty acid metab.	**Annotation Cluster 4**	**Enrichment Score: 1.2776717793217818**			
	UP_KEYWORDS	Mitochondrion	23	2,91E-02	TRP53, MRPL53, MRPL1, MRPS34, MRPL4, ACADM, MCAT, ATP5F1, NDUFC2, CBR4, MAPK10, TACO1, QRSL1, MRPL21, MRPS18C, HTRA2
	Annotation Cluster 6	**Enrichment Score: 1.0521935305885302**			
	KEGG_PATHWAY	mmu01212: Fatty acid metabolism	5	8,61E-03	ACOX1, ACADM, MCAT, ELOVL6, ACSL5
	UP_KEYWORDS	Fatty acid metabolism	6	2,63E-02	ACOX1, ACADM, MCAT, CBR4, ELOVL6, ACSL5
	GOTERM_BP_DIRECT	GO:0006631~fatty acid metabolic process	7	2,67E-02	ACOX1, ACADM, MCAT, PER2, CBR4, ELOVL6, ACSL5
	KEGG_PATHWAY	mmu03320: PPAR signaling pathway	5	3,84E-02	ACOX1, ACADM, CYP27A1, CYP7A1, ACSL5
	Annotation Cluster 12	**Enrichment Score: 0.8062496294708845**			
	INTERPRO	IPR026082:ABC transporter A, ABCA	3	2,11E-02	ABCA3, ABCA13, ABCA12
cell adhesion	**Annotation Cluster 7**	**Enrichment Score: 1.0256913451821696**			
	INTERPRO	IPR002126: Cadherin	6	3,29E-02	RET, PCDHB6, PCDH11X, FAT1, CDHR1, PCDH15
	INTERPRO	IPR015919: Cadherin-like	6	3,48E-02	RET, PCDHB6, PCDH11X, FAT1, CDHR1, PCDH15
	Annotation Cluster 21	**Enrichment Score: 0.6276318581765036**			
	GOTERM_BP_DIRECT	GO:0030155~regulation of cell adhesion	4	2,30E-02	LAMA1, RET, PTK2, PTK2B

	Annotation Cluster 18	**Enrichment Score: 0.6872907708951744**			
various	UP_KEYWORDS	Nucleotide-binding	36	1,25E-02	RAB3A, GNE, TRPV1, XRCC6, ABCA3, EPHB1, CKB, QRSL1, PRKAR2A, PTK2, SLK, PTK2B, NT5C2, DDX3Y, 4933425L06RIK, KIF21A, …
	UP_SEQ_FEATURE	active site:Proton acceptor	19	1,51E-02	HSD17B11, ACOX1, RET, ACADM, HSD3B7, NRD1, CNP, CBR4, PBK, MAPK10, CDK4, EPHB1, DHRS7, DHRS1, PDIK1L, PTK2, SLK, PTK2B, TSSK4
	UP_KEYWORDS	ATP-binding	27	4,62E-02	TRPV1, GNE, XRCC6, ABCA3, EPHB1, CKB, QRSL1, PTK2, SLK, PTK2B, DDX3Y, KIF21A, TARSL2, ABCA13, ABCA12, ACSL5, RET, ATRX, …
	GOTERM_MF_DIRECT	GO:0000166~nucleotide binding	38	4,64E-02	RAB3A, RBM33, GNE, TRPV1, XRCC6, ABCA3, EPHB1, CKB, QRSL1, PRKAR2A, PTK2, SLK, PTK2B, NT5C2, DDX3Y, 4933425L06RIK, PTBP2, …
	Annotation Cluster 25	**Enrichment Score: 0.5793190221422585**			
	UP_SEQ_FEATURE	binding site:S-adenosyl-L-methionine; via carbonyl oxygen	3	4,30E-02	METTL1, CARM1, MEPCE

Panther analysis on the same data set suggested a significant enrichment of proteins related to organelle bio- genesis and maintenance (R-MMU-1852241) (p value 0.006). In accordance, IPA showed, among the top biofunctions in terms of p value, cellular assembly and organization, cell and organism survival, tissue morphology, and nervous system development and function (Table 13).

Table 13 Bioinformatic analysis by IPA of the proteins exclusively expressed in OligoGM1 cells in the comparison OligoGM1 vs CONTROL N2a cells

Molecular and Cellular Functions		
	p-value	**Molecules**
Cell Death and Survival	1.24E-02-2.37E-06	86
Cell Morphology	1.16E-02-1.18E-05	54
Cellular Assembly and Organization	1.28E-02-1.18E-05	76
DNA Replication, Recombination, and Repair	1.18E-02-2.09E-05	28
Carbohydrate Metabolism	1.15E-02-3.99E-05	12
Physiological System Development and Function		
	p-value	**Molecules**
Organismal Survival	3.56E-03-1.29E-05	75
Nervous System Development and Function	1.28E-02-4.21E-05	54
Tissue Morphology	1.24E-02-1.62E-04	33
Connective Tissue Development and Function	1.15E-02-1.89E-04	25
Embryonic Development	1.25E-02-3.14E-04	60

We then compared by IPA the proteins that are upregulated or only expressed in treated cells (347 proteins) with the proteins that are downregulated in treated cells or expressed only in the control (397 proteins) to highlight differences that may be triggered by the presence of OligoGM1 (Table 14).

Table 14 Bioinformatic analysis by IPA of the proteins differentially expressed in the comparison OligoGM1 vs CONTROL N2a cells

TOP BIOFUNCTION		
Molecular and Cellular Functions		
	p-value	**Molecules**
Cell Death and Survival	1.24E-02-2.37E-06	86
Cell Morphology	1.16E-02-1.18E-05	54
Cellular Assembly and Organization	1.28E-02-1.18E-05	76
DNA Replication, Recombination, and Repair	1.18E-02-2.09E-05	28
Carbohydrate Metabolism	1.15E-02-3.99E-05	12
Physiological System Development and Function		
	p-value	**Molecules**
Organismal Survival	3.56E-03-1.29E-05	75
Nervous System Development and Function	1.28E-02-4.21E-05	54
Tissue Morphology	1.24E-02-1.62E-04	33
Connective Tissue Development and Function	1.15E-02-1.89E-04	25
Embryonic Development	1.25E-02-3.14E-04	60

Interestingly, the proteome of OligoGM1-treated cells presents upregulation or exclusive expression of proteins involved in the biochemical mechanism of neuronal differentiation, protection, and restoration, such as suppression of proinflammatory molecules and inhibition of oxidative stress. Sirtuins, for example, are described as a protein family whose activities cause activation of anti-apoptotic, anti- inflammatory, anti-stress responses, and the modulation of the aggregation of proteins involved in neurodegenerative disorders [435]. SUMOylation has emerged as a potential therapeutic target for neuroprotection in brain ischemia, including both global and focal brain ischemia (ischemic stroke) [436]. EIF2 is a signaling pathway involved in cell proliferation and protein translation whose dysregulation is associated with a number of pathologies, including neurodegenerative diseases, metabolic disorders, and cancer [437]. In the central nervous system, the phosphatase and tensin homolog deleted on chromosome ten (PTEN) plays a fundamental role in development, in

synaptogenesis and synaptic plasticity, and in neuronal death [438]. The renin-angiotensin pathway is involved in neurodevelopment and participates in cell growth inhibition, fetal tissue development, extracellular matrix modulation, neuronal regeneration, apoptosis, and cellular differentiation [439]. Mostly, the proteomic analysis pointed out an increased expression of proteins typically involved in mitochondria bioenergetic and in oxidative stress protection in N2a treated with OligoGM1. Among them, we found the expression of

- mitochondrial ribosome (mitoribosome) proteins (MRPL53, MRPL1, MRPS34, MRPL4, MRPL21, MRPS18C, MRPL48), which synthesize essential components of the oxidative phosphorylation machinery [440, 441];
- proteins involved in the mitochondrial bioenergetics (i.e., ACADM, MCAT, ATP5F1, NDUFC2, CBR4, TACO1, CYP27A1, L2HGDH, SURF1, ACSL5, ACOX1, SNCB, CKB, PPP3CA, ACSL5, NUT19, RAP1GDS1, NDUFC2, DHRS1);
- frataxin (FXN) protein, whose loss of function activates an iron/sphingolipid/PDK1/Mef2 pathway leading to a neurodegeneration [442];
- CYP27A1 enzyme, a member of the cytochrome P450 superfamily, whose functions are related to iron ion binding, to oxidoreductase activity, and to vitamin D metabolism in the brain [443].

In addition, we found the expression of the mitochondrial serine protease HtrA2, which negatively correlates with mitochondrial dysfunction leading to neurodegenerative disease with Parkinson's feature [444].

3.3 OligoGM1 protection in MPTP-treated cells

All the subsequent results are obtained thanks to the collaboration with the group the Prof. Sandro Sonnino at the Department of Medical Biotechnology and Translational Medicine of University of Milan.

MPTP is a lipophilic compound which easily crosses the blood- brain barrier inducing in vivo selective degeneration of nigrostriatal neurons, thereby mimicking the Parkinson's disease. MPTP is converted by mitochondria MAO-B enzyme to its toxic metabolite MPP^+ [415-417]. Although, the mechanisms of cell death induced by MPP^+ are not fully clear, it is known that MPP^+ exerts its neurotoxic effect by the inhibition of mitochondrial respiration via complex I, leading to mitochondrial energy deprivation and eventual cell death. An additional mechanism of MPTP-induced toxicity involves oxidative stress resulting in generation of toxic mitochondrial reactive oxygen species (ROS) causing damage to critical biomolecules [415, 417]. Considering the reported GM1 efficacy in vitro, in mouse and non-human primate MPTP models [396, 445-447], its ability to protect PC12 cells by the activation of MAPK against hydrogen peroxide toxicity [445], and what the proteomic analysis highlighted, we chose to verify whether the GM1 oligosaccharide has a neuroprotective potential in MPTP-treated cells.

3.4 OligoGM1 protects from MPTP-induced cell death

N2a cells were exposed to 50 μM OligoGM1 which leads to activation of the TrkA-ERK1/2 pathway and differentiation in neuron-like cells (figure 38).

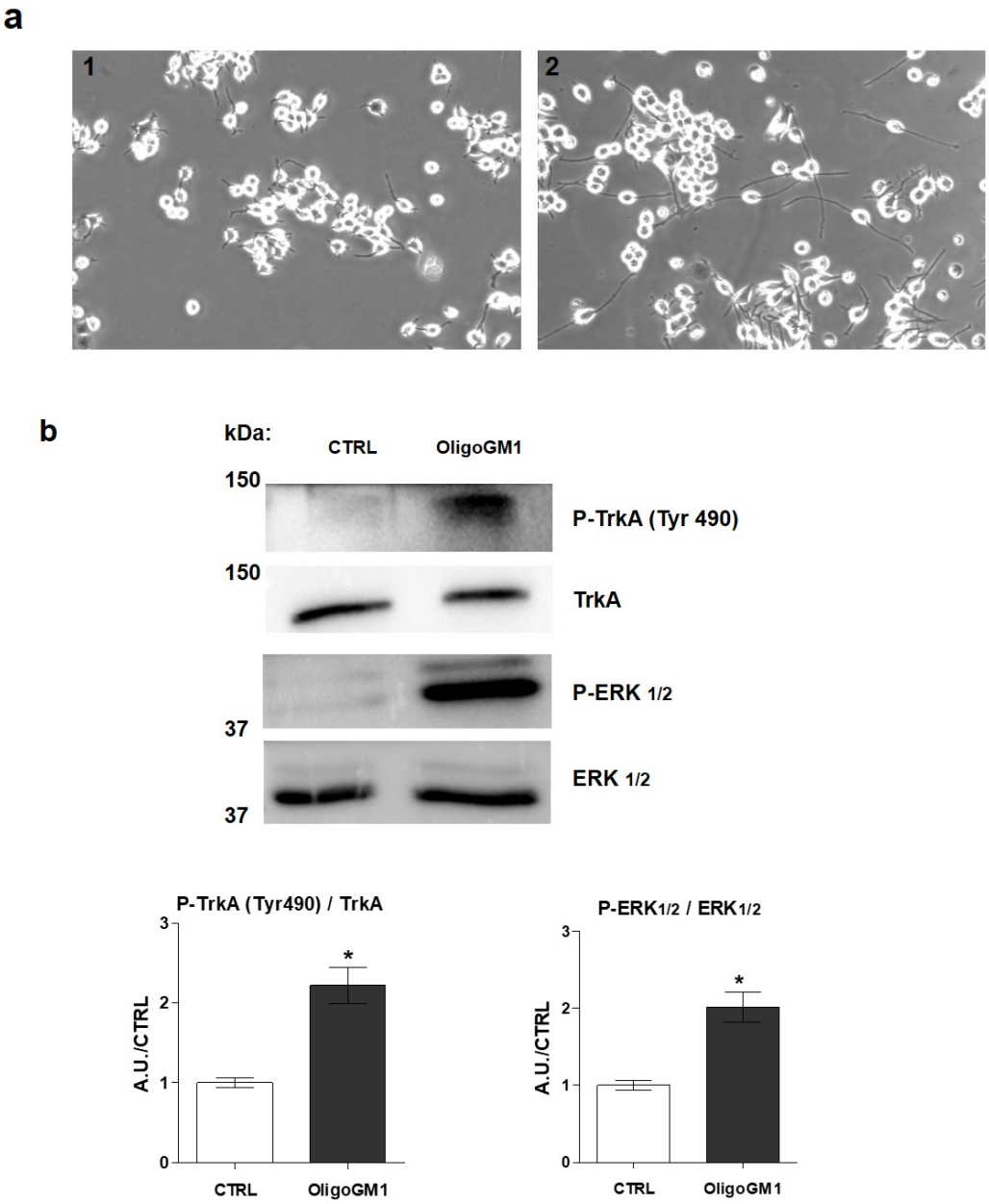

Figure 38 OligoGM1 neurodifferentiative effect on N2a cells. **a)** Morphological analysis of N2a cells. 1, control; 2, OligoGM1. Following 24 h incubation, cells were analyzed by contrast phase microscopy with 200x magnification. Images are representative of ten independent experiments (*n*=10). **b)** Expression of TrkA, phosphorylated TrkA (Tyr490), total ERK1/2 and phosphorylated ERK1/2 in cell lysate by means of specific antibodies and reveled by enhanced chemiluminescence. Top: immunoblotting images are shown. Bottom: Semi-quantitative analysis of phosphorylated TrkA and ERK1/2 related to total level of TrkA and ERK1/2, respectively. Data are expressed as fold increase over control of the mean ± SEM from five different experiments (*$p < 0.05$, Student's *t*-test, *n*=5).

After 24 h from OligoGM1 treatment, N2a cells were exposed to MPTP (250 μM). MPTP-treated cells showed a morphological dam- age immediately after 24-h treatment, while the OligoGM1 pretreatment induced identifiable dose-dependent signal of survival in the presence of MPTP (Figure 39a).

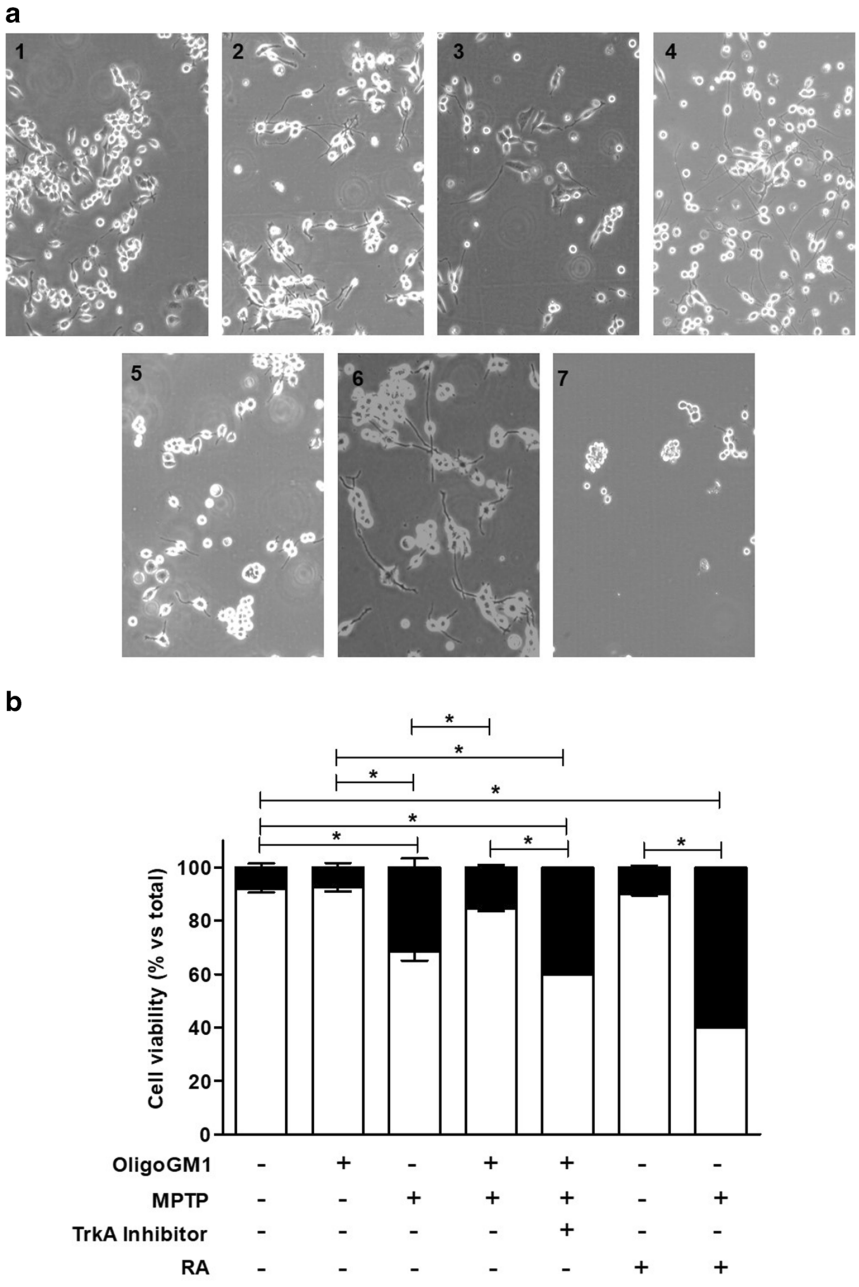

Figure 39 OligoGM1 neuroprotective effect versus MPTP treatment. **a** Morphological analysis of N2a cells. 1, control; 2, OligoGM1; 3, MPTP; 4, OligoGM1 + MPTP; 5, TrkA-Inh + OligoGM1 + MPTP; 6, RA; 7, RA + MPTP. Following 24-h treatment with MPTP, cells were evaluated at × 200 magnification with phase- contrast microscopy. Images are representative of five independent experiments (n = 5). **b** Viability of cells under different treatments. The number of living (white square) and dead (black square) cells was determined by trypan blue exclusion assay. Values represent the percentage mean of living (trypan blue negative) and dead (trypan blue positive) cells for three different experiments (*$p < 0.01$; one-way ANOVA, followed by Bonferroni's post hoc, n = 3)

Trypan blue assay showed that the pretreatment with 50 μM OligoGM1 was effective in preventing the MPTP-mediated cell death (Figure 39b), with a significant reduction in cell death over 50% with respect to MPTP-treated cells.

To clarify if the OligoGM1 neuroprotective effect against MPTP was due only to the OligoGM1-induced neuro-like phenotype, N2a cells were incubated with RA, a well- known neurodifferentiative agent. The RA treatment induced cell differentiation but did not prevent from the MPTP toxic effect (Figure 39), supporting OligoGM1 specificity in activating proper signal pathways.

3.5 OligoGM1 protective effect is abolished by TrkA inhibitor

To understand if the OligoGM1 protective effect is mediated by TrkA activation at the PM by the GM1 oligosaccharide interaction, we blocked TrkA activity using a specific inhibitor able to fit in the ATP pocket [399, 433]. The presence of inhibitor together with OligoGM1 abolished the OligoGM1 protective effect against MPTP (figure 39), suggesting that the OligoGM1 neuroprotective effect is associated to the TrkA-ERK1/2 pathway activation.

3.6 OligoGM1 protects from MPTP-induced mitochondrial oxidative stress

N2a cells were pretreated with OligoGM1 for 24 h before MPTP. After 6, 10, and 24 h from MPTP administration, using the fluorescent probe MitoSOX Red, we carried out measurements of mitochondrial ROS levels via live-cell microscopy (Figure 40).

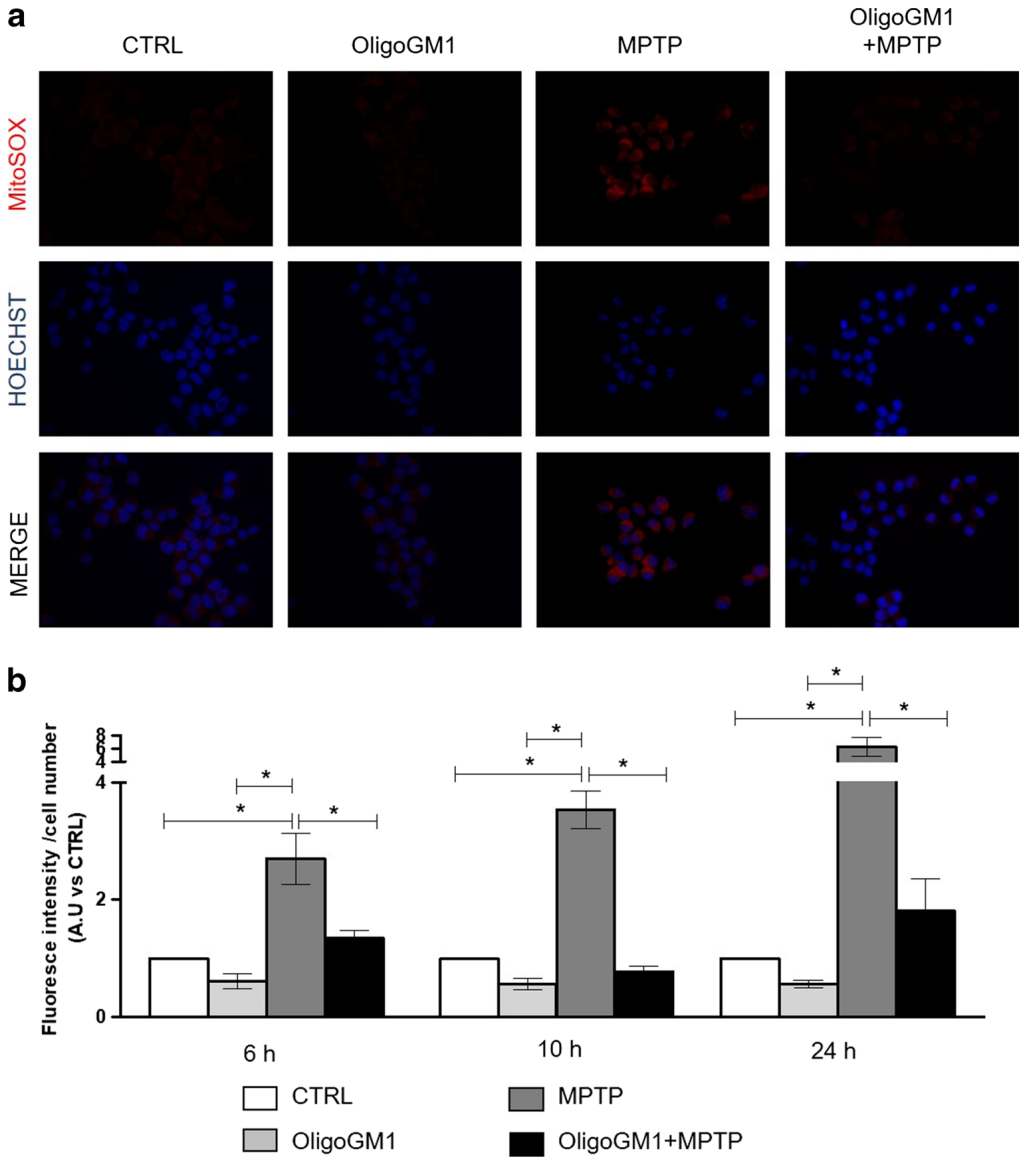

Figure 40 OligoGM1 effect on ROS production induced by MPTP. **a** Representative fluorescence images showing mitochondrial superoxide (MitoSOX Red fluorescence), nuclei (Hoechst blue fluorescence), and overlay of the two signals (merge) with × 400 magnification. Images are representative of three indepen- dent experiments (n = 3). **b** MitoSOX Red signal was quanti- fied using ImageJ software in percentage pixel intensity nor- malized on cell number. Data are the mean of three independent experiments and are expressed as fold increase over CTRL of mean ± SEM from three different ex- periments (*p < 0.01; one-way ANOVA, followed by Bonferroni's post, n = 3)

Interestingly, we observed reduced MitoSOX Red signal in pretreated OligoGM1 cells compared to controls, for every time point analyzed (Figure 40), suggesting that OligoGM1 limits MPTP-ROS production.

From the latter result, we can infer that the molecular mechanism underlying the OligoGM1 neuroprotective property relies on the modulation of mitochondrial ROS production conferring a protection against oxidative stress induced by MPTP.

Comparing the protein patterns of OligoGM1-treated and untreated cells, we found restricted but significant differences of basal protein content, depending on the differential expression of specific groups of genes as a consequence of the down- stream molecule cascade promoted by OligoGM1-induced TrkA activation (Table 9; Figure 38). In addition, we found 324 proteins present exclusively in cells treated with the OligoGM1. Some of these are known to be involved in neuroprotection and survival processes (Tables 12, 13, and 14). Thus, we examined more in detail the protective potential of OligoGM1 against neurotoxicity induced by MPTP. MPTP- mediated toxicity is related to the inhibition of electron transport chain and to oxidative stress [415-417]. It has been reported, for example, that MPTP caused H_2O_2 accumulation and inhibited catalase activity. Hydrogen peroxide can react with Fe^{2+} via Fenton reaction to generate $OH^{\bullet}$, a strong reactive oxidant.

For the first time, here, we showed that OligoGM1 pretreatment for 24 h before exposure of cells to MPTP reduces mitochondrial ROS production conferring a protection against oxidative stress and reduces the cell death (Figures. 39 and 40).

To confirm that OligoGM1-induced TrkA activation represents the trigger event underling MPTP protection, we specifically inhibited the TrkA activity: the administration of OligoGM1 together with TrkA inhibitor abolished the OligoGM1 protective effect against MPTP treatment (Figure 39). On the other hand, to exclude that the OligoGM1 effect was simply due to the acquisition of a neuron-like phenotype, N2a cells were differentiated with retinoic acid and 24 h later were treated

with MPTP. Retinoic acid was not able to confer any protection against MPTP toxicity. The latter result strengthened the specificity of OligoGM1 effect (Figure 39).

The neuroprotective properties of GM1 ganglioside have been reported in many papers. Now, as for the GM1 differentiative properties [399], we confirm that the GM1 neuroprotection, at least in N2a cells, derives from a direct interaction between the GM1 oligosaccharide and the TrkA receptor, and the following signaling cascade capable to overexpress specific neuroprotective proteins.

Although much experimental work is needed to fully clarify the GM1 mechanism of action with respect to its potential, our findings sustain the idea that the oligosaccharide chain is the key molecular portion and the starting point for GM1- mediated protective function at the plasma membrane level.

We propose that GM1 oligosaccharide may stabilize the TrkA-NGF complex on the cell surface triggering the phosphorylation of Tyr490 promoting the MAPK differentiation signaling. This induces the activation of a complex network of signaling processes that are involved in the biochemical pathway of neuroprotection and neurorestoration (Figure 41).

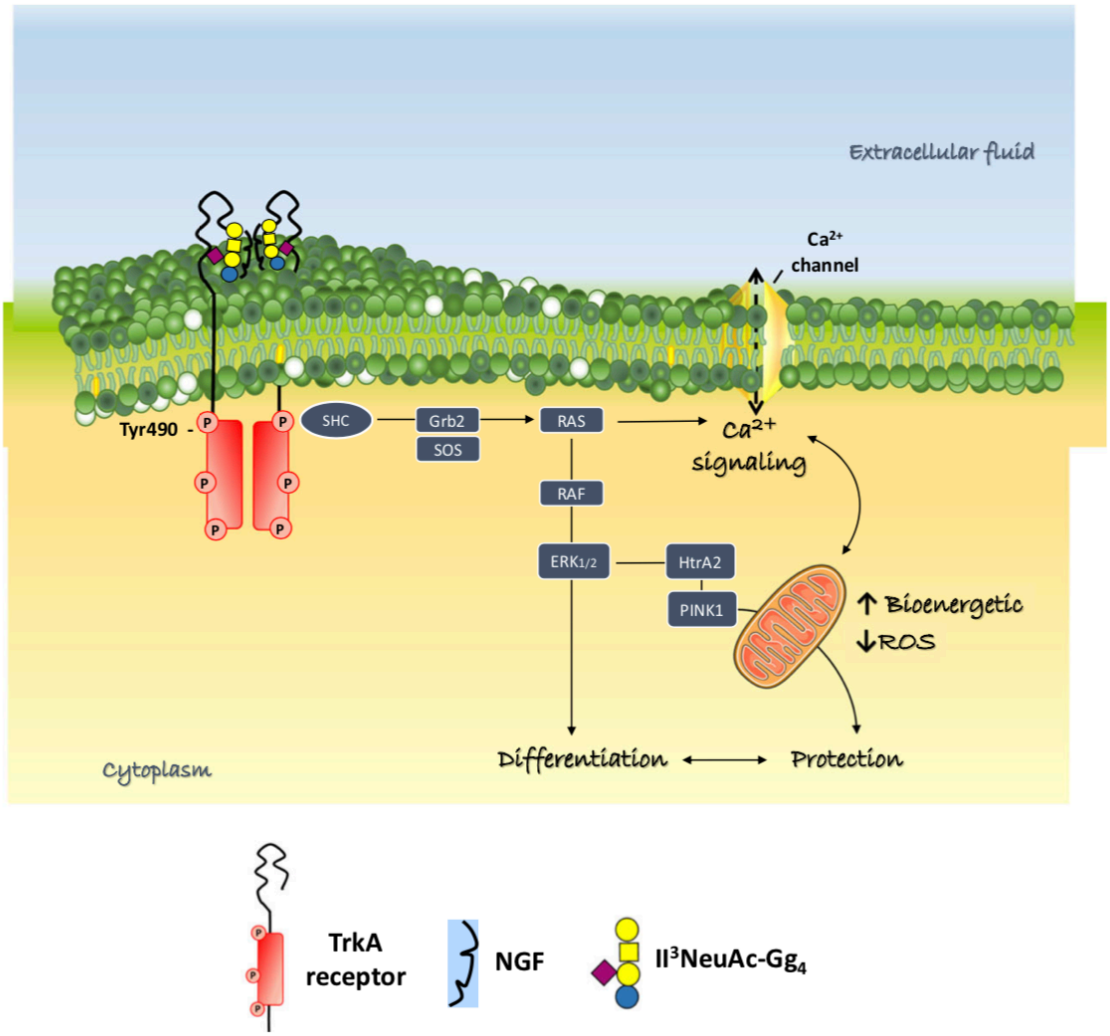

Figure 41 Diagram of the proposed mechanism for GM1-mediated neuroprotection in N2a cells. On the cell plasma membrane, ganglioside GM1 induces the TrkA activation by autophosphorylation. GM1 enhances TrkA activity stabilizing the TrkA-NGF com- plex by a direct interaction with its oligosaccharide chain. GM1 promotes the phosphorylation of Tyr490 triggering the differentiation, mitochondrial neuroprotective, and calcium signaling. This image is updated from [399]. GM1 representation is according to [430]. ERK, extracellular signal- regulated protein kinases 1 and 2; Grb2, growth factor receptor- bound protein 2; Gab1, Grb2- associated binder-1; HrtA2, serine protease; PINK1, PTEN (phosphatase and tension homolog)-induced putative kinase 1; RAS, GTP-binding protein; RAF, serine/threonine kinase; SHC, transforming protein 1; SOS, son of sevenless.

Proteomic and behavioural analysis of thermal stress effects on zebrafish brain

1. INTRODUCTION

1.1 Global warming

Global warming is the long-term warming of the planet's overall temperature, as defined by National geographic. This phenomenon is amplified by anthropic action, the release of CO_2 and other greenhouse gases, higher now than at any time in the last 800,000 years. Indeed, the increase of human population caused the augmented volume of fossil fuels burned; they are form by coal, oil and natural gas and from their burning originates the so called "greenhouse effect" in Earth's atmosphere. The greenhouse effect is realized when the Sun's ray which penetrate the atmosphere aren't reflected off the surface in the space because of the presence of gases derived from the burning of fossil fuels. Among these carbon dioxide, chlorofluorocarbons, water vapor, methane and nitrous oxide were found.

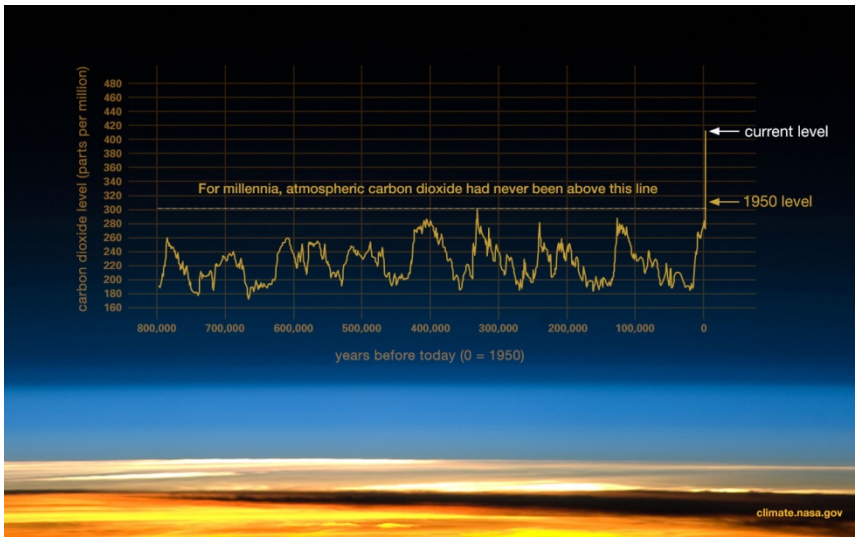

Figure 42: This graph, based on the comparison of atmospheric samples contained in ice cores and more recent direct measurements, provides evidence that atmospheric CO2 has increased since the Industrial Revolution. [448]

The situation just described has caused the average global temperature to rise overtime, presenting another issue called climate change. Indeed global warming and climate change are not synonyms, the second is used for the complex shifts now affecting our planet's weather and climate systems. The Earth's climate responds to changes in greenhouse gas levels as demonstrate from ice

cores drawn from Greenland, Antartica, and tropical mountain glaciers. Ancient evidence can also be found in tree rings, ocean sediments, coral reefs, and layers of sedimentary rocks. This ancient, or paleoclimate, evidence reveals that current warming is occurring roughly ten times faster than the average rate of ice-age-recovery warming [449]. The evidences of climate changes are:

- global temperature rise;
- warming of oceans;
- shrinking of ice sheets;
- glacial retreat;
- decreased snow cover;
- sea level rise;
- declining arctic sea ice;
- extreme events;
- ocean acidification.

The most worrying aspect for the species that inhabit the earth, human and animal, is the overheating of the waters of our planet. Indeed the oceans have absorbed much of this increased heat, with the top 700 meters of ocean showing warming of more than 0.4 degrees Celsius since 1969 [450]. Climate changes can deeply alter the habitat of the species and impact on all levels of biological life from that of the population to the molecule affecting the survival and longevity of the organism [17]. The poikiloterm animals such as fish, whose body temperature varies considerably with the environmental temperature, are particularly sensitive to thermal variations and in aquatic ectotherms, water temperature is considered the major ecophysiological variable, influencing the physiology, behaviour and the distribution of organisms [451].

1.2 The response of fish to climate changes

The potential evolutionary and plastic responses to physical fish drivers are widely documented in the literature. However, predicting actual responses in natural populations remains a core challenge because observed responses typically fail to match predictions based on theory or laboratory experiments [452]. The first response to climate changes of fish is the modulation of its behaviour migrating to areas where the environmental factors favor the biological fitness [453], otherwise it has to adapt and acclimatize to new environment. The prolonged exposure to altered conditions could lead to phenotypic changes, through an acclimatory response which is triggered by different conditions among species. In zebrafish (*Danio rerio*), developmental plasticity affects acclimation to temperature substantially later in life [454].

A common physiological effect of rising temperatures in fish is the increase of metabolic rates, however there are many factors from which ecological and evolutionary consequences of rising temperature depend, like population-specific proximity to lethal limits or growth optima [455, 456], interspecific dynamics [457] and disease impacts [458]. Thermoregulation can reduce expression of physiological responses or increase them because of concomitant stressors like diseases.

The thermal acclimatization is based on complex yet not fully understood physiological processes known as temperature compensation that allow acclimated (or adapted) animals to change their thermal sensitivity [459]. An important role in this phenomenon is play by the variation of enzymatic concentration trough the regulation of transcription and translation.

1.3 Animal model: Danio Rerio (Zebrafish)

The zebrafish (*Danio rerio*) is a small, tropical, freshwater fish, native to river of South Asia, which has become known as an excellent model organism for studies of vertebrate biology, vertebrate genetics, embryonal development, diseases and drug screening [460]. It is also usefull in behavioural studies associated with feeding, predator evasion, habituation and memory. *Danio rerio* became a

model for research in the late 1960s thanks to the researcher George Streisinger, of Oregon University, who used it for developmental biology studies.

Figure 43: Some adults wild-type zebrafish with normal body length, eyes and pigmentation [figure from 539]

Adult reach 2.5 cm of dimension and have a generation time of 3-4 months, they can lay hundreds of transparent eggs in very short time, at weekly intervals, which make them useful for different type of research. Their maintenance is cheaper than that for rats and mice and required little space. Zebrafish' immune system is well developed and similar to mammalian one.

The species is an annual species. Adults inhabit streams, canals, ditches, and they slowly move to stagnant standing water, like rice-fields and lower reaches of streams. They eat worms and small crustaceans, even insect larvae. Spawning is induced by temperature and commences at the onset of the monsoon season. Food availability also acts as cue for breeding. The ZF is an ectotherm and poikiloterm, so its internal temperature depends on the temperature of the surroundings and varies considerably, it's a cyprinid characterized by a wide thermal tolerance in the range of 6.7 to 41.7°C [461, 462]. *Danio* prefers to live in shallow water at temperatures ranging from 24 °C to 30°C, suitable for its development, reproduction and growth, and pH 6.0–8.0.

Before electing zebrafish as the perfect animal model for human research it is important to understand the extent to which zebrafish genes and gene structures are related to orthologous human genes [463]. Zebrafish genome sequencing project, started in 2001 at the Sanger Institute, allowed the annotation of more than 26000 protein-coding genes, the largest gene set of any vertebrate so far

sequenced. As a result of comparison with the human genome, 70% of human genes have at least one obvious zebrafish orthologue. Moreover, zebrafish genome displays several interesting features like:

- unique repeat content;
- scarcity of pseudogenes;
- enrichment of zebrafish-specific genes on chromosome 4;
- chromosomal regions that influence sex determination

1.3.1 Nervous system development and organization

The first step in building the nervous system is the specification of the neural plate, a process called neural induction. The neural plate, through neurulation, give rise to neural tube, this process involved the formation of a neural rod followed by the establishment of a lumen. Except these two events, the morphogenetic movements and molecular mechanisms involved in Danio rerio are almost the same of those of other vertebrates. The Planar Cell Polarity (PCP) pathway, mediated by non-canonical Wnt signaling, is the responsible for the convergence of dorsal tissues, a critical point for the formation of a single neurulation center. At this point, the activity of genes directly involved in cytoskeletal organization, like *Zic* genes and cadherins, play important role in neuro development phenomena, as the maturation of the neural plate. The commitment of neuroepithelial progenitors towards neuronal or glial differentiation is initiated concomitantly to neural plate formation and neurulation [464]. The early phase of neurogenesis, consists in the recruitment of early proneural clusters to build the first larval neuronal scaffold, which will permit autonomous larval behavior, and it is controlled by the "lateral inhibition" process.

As the neuronal numbers increase and the diversification of neuronal subtypes occours, there is the onset of "secondary neurogenesis".

Positional cues, first established during gastrulation, concomitant to neural induction, and refined later on, guide the perfect organization of the neurogenesis pattern. These cues involve signaling from the Hh, Nodal, BMP and Wnt pathways and have been extensively reviewed [465].

These signaling processes have two major outcomes, the definition of brain subdivision (tel-, di-, mes- and rhombencephalon) and the definition of roof, alar, ventral and basal plate which give rise to the major organization of the adult brain. Thanks to co-regulation of patterning and neurogenesis some important features were found:

- a stereotyped organization of the primary neuronal scaffold;
- specific characteristics to the neurons and neural progenitors of the different central nervous system subdivisions;
- a very similar organization of the body plan to other vertebrates at the mid-embryogenesis stage.

Despite the similarities between zebrafish and other vertebrates, some differences can be noted like the absence of serotonergic neurons and the diencephalic (and not mesencephalic) localization of dopaminergic neurons with ascending projections [466, 467].

Cholinergic cranial and spinal motoneurons, interneurons of various subtypes and large spinal cord glutamatergic sensory neurons composed the primary neuronal scaffold, which controls the escape response. Visually guided behavior, feeding, sleep, refined locomotion, mechanosensation and escape are ensured by modulatory neurons that appear within the first 5-6 days of life. Instead, reticulospinal ‘‘functional groups’’ rather than individual neurons are involved in sensory–motor connection. Their identity and localization within the brainstem renders them sensitive to distinctly localized stimuli [468]. Zebrafish central nervous system is organized in a very similar way to that of other vertebrates and it is divided into four parts:

- spinal cord;
- rhombencephalon;
- forebrain or prosencephalon;
- mesencephalon.

These four parts are subdivided into morphological and functional areas, for example the forebrain is divided into diencephalon and secondary prosencephalon, which give rise to the hypothalamus.

1.4 Behavioural test: Y-Maze

In the last decade, zebrafish have been gaining popularity in behavioural brain research [456]. The extensive literature demonstrates the cognitive and mnemonic capabilities of zebrafish and this allows the use of this animal as development of disease models that affect the central nervous system and also permits the evaluation of toxic or neuroprotective agents on cognition [457].

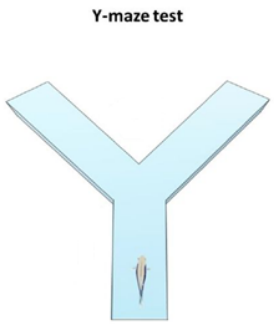

Figure 44: Schematic representation of the experimental design and the behavioral tasks [457].

To study learning and memory in zebrafish protocols are available based on longer training periods and/or on reward or avoidance. Y-Maze represent an alternative approach, firstly developed for rats but also useful for zebrafish, showing many advantages:

- it does not involve conditioned learning and thus enables specific testing of memory [457];
- it minimizes motivational and emotional states that influences the results;
- it is based on natural tendency to explore novelty, starting form a short training-test interval (TTI) to establish a preferential exploration, moving to longer TTIs;
- retention does not last longer than a few hours, so performance could be repeated several times in the same animal;

- through the record of the number of arm visits or distance traveled locomotor activity can be evaluated;
- measurement of behavior is quick, precise, and entirely automated.

The Y-maze was built by replicating exactly the same features of the maze successfully used on ZF by Cognato and collaborators [470]. Briefly, the Y-Maze is built with three arms of glass (25 × 8 × 15 cm width × depth × height) in which the single arm is identified by the presence of geometric shapes (square, circle and triangle) made of white paper and placed on the external walls and visible from the inside. The work by Cognato et al. [470] demonstrated the ability to recognize, distinguish and not to be feared by the geometric shapes chosen. In their work they wanted to evaluate the learning and memory, without using place preference, establishing appropriate visual cues for each arm, in a way that the fish did not show signs of avoidance or preference. During the test they measure the time spent by the fish in each arm, associated to a specific geometric form. In the first trial they used squares, triangles and crosses; the zebrafish spent less time in the arm with crosses passing most of it in that with squares or triangles cues. After this result, crosses were substituted by circles, and the preference between circles, squares or triangles was evaluated. The zebrafish spent statistically comparable times in each arm, so the final Y-Maze apparatus consisted of squares, triangles and circles for arm cues.

1.5 Aim of the project

The aim of this study is to determine the effects of environmental temperature on the zebrafish brain proteome, through a shotgun proteomic approach, and the behavioural responses of animals thanks to Y-Maze apparatus in collaboration with University La Sapienza in Rome, to analyze swimming performance, response to novelty and spatial memory. For such purpose 99 fish were maintained for 21 days at two test temperatures 18°C and 34°C and animals kept at 26°C were used as controls. At the end of thermal treatments, the proteome of 9 brains for each condition not subjected to behavioural tests was analyzed by a shotgun label free proteomic approach for the identification

and quantification of expressed proteins. Instead 20 individuals were subjected to the behavioural test performed by Mattia Toni. At the end we try to verify if proteomic results could explain at the molecular level what we observe thanks to the behavioural test, and also if a proteomic approach could be useful to analyze the impact of temperature variation on proteome.

2. MATERIALS AND METHODS

2.1 Subjects

A total of 99 adult (6–7 months old) wild type ZF, purchased from commercial dealers, was used in the present study. Sex ratio was about 50:50 male:female and the mean weight was 0.4 g. Fish were randomly placed in three tanks (40×30×30 cm, width×depth×height) of 33 l (hometanks) and maintained at 26 °C (control temperature) for 10 days to acclimate to the tank (adaptation period). Fish, 33 for each tank, were maintained under an artificial photoperiod (12:12 light/dark cycle) and fed three times a day (10 am, 2 pm and 6 pm) with commercial dry granular food (TropiGranMIX, Dajanapet) by using automatic fish feeders (Eden 90, Eden Water paradise, Germany). 1.3 g/day of food, corresponding to 10% of body mass, were administrated to each tank. The water used throughout the experimental phase was produced by reverse osmosis pumps (Reverse Osmosis AquiliOS2) and reported to the appropriate salinity adding aquarium salt (1 g/l, Aqua Medic 301.01).

In order to ensure good water quality, a constant flow of filtered water (600 l/h) was maintained by external filter systems (Eden 511 h) in each tank and water was also continuously aerated (7.20 mgO_2/l) by aerator for aquaria (SicceAIRlight, 3300 cc/min 200 l/h). The chemical/physical characteristics of tank water were checked at least two times per week by measuring the values of water hardness, pH, ammonium (NH_4), ammonia (NH_3), nitrate (NO_3), nitrite (NO_2), phosphate (PO_4), copper (Cu) and calcium (Ca^{2+}) with the Sera aqua-test box kit (Sera Italia srl). The salinity was checked with a hand-held refractometer. Faeces and the remaining food waste were removed from the animal tanks at least three times per week. During the tank-cleaning operations, a water exchange of about 20–30% per week was performed to restore the correct volume of water and to maintain its chemical–physical parameters.

2.2. Thermal treatment

Subjects were exposed to thermal treatment. In two of the three hometanks the water temperature was gradually brought from 26 °C to 18 °C or 34 °C in 72 h. Fish were then maintained at the two experimental temperatures, 18 ± 1 °C and 34 ± 1 °C, for 21 days. Fish maintained at 26± 1 °C were used as control. The three temperature values were chosen according to Vergauwen et al. [472] within the ZF vital range and correspond to temperatures the fish cope with in the natural environment. The water temperature was kept constant by external water chiller (TK 150 Teco) or digital thermostats (Eden 430) connected to a heating coil (Eden 415, 230 V, 50/60 Hz, 80 W). The water temperature was further checked daily using a hand thermometer. The interior enrichment of each tank (consisting of a heating coil, inlet and outlet pipes of the filters and aerator) was replicated identical in all the tanks. During the thermal treatment only three fishes died: two at 18 °C and one at 34 °C. All the experimental procedures were approved by the Animal Care Committee and authorized by the Italian Ministry of Health (protocol number 290/2017-PR).

At the end of the thermal treatment, of the total of 33 fishes present in each hometank, 20 individuals were subjected to the behavioural test, 9 were used for proteomic analysis and the remaining fish were stored for mRNA expression analysis. All the individuals enrolled in the study were euthanised individually by a prolonged immersion in a solution of the anaesthetic tricaine methanesulfonate MS-222 (300 mg/l). All the procedures were performed between March and May 2017.

2.3. Proteomic analysis

Total protein expression in fish brain homogenates was analysed and compared under the three thermal regimes. Although this analysis is not able to discriminate proteins expressed in the different cell populations of the brain (neurons, glial cells, endothelial cells), it provides a useful tool for assessing the impact of thermal treatment on the brain function and neurochemistry.

2.3.1 Sample homogenization

At the end of thermal treatments, the brain proteome from ZF adapted at the three temperatures (not subjected to behavioural tests) was analysed by a shotgun label free proteomic approach for the identification and quantification of expressed proteins. At each temperature, 9 whole brains were homogenized using a Potter homogenizer in 500 µl of extraction buffer (8M urea, 20mM Hepes pH 8, with protease inhibitors Complete Mini) at full speed for 1–3 min. The homogenate was centrifuged at 10000 rpm for 10 min to sediment unhomogenized tissue and large cellular debris. The pellet was discarded and the protein content was determined by a bicinchoninic acid assay (Thermo Fisher Scientific).

2.3.2 Bicinchoninic acid (BCA) assay

The concentration of each sample was determined using the bicinchoninic acid method. The BCA protein assay is used for quantitation of total protein in a sample. The principle of this method is that proteins can reduce Cu^{+2} to Cu^{+1} in an alkaline solution (the biuret reaction) and result in a purple color formation by bicinchoninic acid. The reduction of copper is mainly caused by four amino acid residues including cysteine or cystine, tyrosine, and tryptophan that are present in protein molecules. However, unlike the Coomassie dye-binding methods, the universal peptide backbone also contributes to color formation, helping to minimize variability caused by protein compositional differences. The assay is monitored at 562 nm in a Du® 730 Life Science Uv/vis Spectrophotometer (Beckman Coulter), and determines the purple-colored complex formed by two molecules of

bicinchoninic acid chelate with each Cu^{+} ion. Bovine plasma immunoglobulin was used as standard protein.

2.4 Protein identification by mass spectrometry

Proteins were subjected to reduction with 13mM dithioerythritol (30 min at 55 °C) and alkylation with 26mM iodoacetamide (IAA; 30 min at RT). Peptide digestion was conducted using sequence-grade trypsin (Roche) for 16h at 37°C using a protein:trypsin ratio of 20:1 [473].

2.4.1 Zip-Tip C18

The proteolytic digest was desalted using Zip-Tip C18 (Millipore) before mass spectrometric (MS) analysis [434]. The protocol is the same described in chapter 2.4 of PC12 section.

2.5 Mass Spectrometry

Mass spectrometry theory is already reported in the chapter 2.5 of PC12 section. The only clarification concerns the gradient, that in this case is 2% ACN in 0.1% formic acid for 10min, 2–4% ACN in 0.1% formic acid for 6min, 4–30% ACN in 0.1% formic acid for 147 min and 30–50% ACN in 0.1% formic for 3 min at a flow rate of 0.3 μl/min. All the other parameters remain the same.

2.6 Data processing and analysis

MS spectra were searched against the ZF Uniprot sequence database (release 01.04.2015) by MaxQuant (version 1.3.0.5). The following parameters were used: initial maximum allowed mass deviation of 15 ppm for monoisotopic precursor ions and 0.5 Da for MS/MS peaks, trypsin enzyme specificity, a maximum of two missed cleavages, carbamidomethyl cysteine as fixed modification, N-terminal acetylation, methionine oxidation, asparagine/glutamine deamidation and serine/ threonine/tyrosine phosphorylation as variable modifications. False protein identification rate (5%) was estimated by searching MS/MS spectra against the corresponding reversed-sequence (decoy)

database. Minimum required peptide length was set to 6 amino acids and minimum number of unique peptide supporting protein identification was set to 1.

Quantification in MaxQuant was performed using the built-in label- free quantification algorithms (LFQ) based on extracted ion intensity of precursor ions [474, 475].

Four replicates were carried out for each group: 18 °C, 34 °C and 26 °C used as the control. Only proteins present and quantified in at least 3 out of 4 technical repeats were considered as positively identified in a sample and used for statistical analyses. Statistical analyses of Max Quant results were performed using the Perseus software module (version 1.4.0.6, www.biochem.mpg.de/mann/tools/). A one-way analysis of variance (ANOVA) test was carried out to identify proteins differentially expressed among the different conditions. Proteins were considered to be differentially expressed if they were present only in 18 °C, 34 °C, or 26 °C samples or showed significant t-test difference p- value (cut-off at 0.05 FDR). Focusing on specific comparisons, namely 26 °C vs 18 °C and 26 °C vs 34 °C, proteins were considered differentially expressed if they were present only in one condition or showed significant t-test difference (Welch's test p value = 0.05). Bioinformatic analyses were carried out by Panther software (Version 10.0) [488] and Revigo to reduce redundant GO terms [489], DAVID software (release 6.7) [490], BINGO and Enriched Map [491] to cluster enriched annotation groups of Molecular Function, Biological Processes, Pathways and Networks within the set of identified proteins. Functional grouping was based on p value ≤ 0.05 and at least two counts.

2.7 Y-maze apparatus

The Y-maze was built by replicating exactly the same features of the maze successfully used on ZF by Cognato and collaborators [470]. Briefly, the Y-Maze was built with three arms of glass (25 × 8 × 15 cm width × depth × height) in which the single arm was identified by the presence of geometric shapes (square, circle and triangle) made of white paper and placed on the external walls and visible from the inside. The work by Cognato et al. [470] demonstrated the ability to recognize,

distinguish and not to be feared by the geometric shapes chosen. In addition, in our setting, the external walls of the maze were coated by a 2 cm thick polystyrene panel to ensure the heat insulation and to keep constant the water temperature for the entire duration of behavioural tests.

Preliminary tests were carried out to ensure that the water temperature remained constant during behavioural testing. The difference in water temperature measured at the beginning and at the end of each experimental test was 1 °C at maximum. A diffuse light was present in the room to avoid directional lighting that could interfere with the fish behaviour. All tests were video recorded by a webcam (Logitech C170) placed 1 m above the maze.

2.8 Behavioural testing

The maze was filled with 4 l of water at the same temperature at which the animal had been acclimated and the water depth was 6.5 cm, enough to submerge the geometric shapes present on the sides of the arms. The total number of experimental subjects was 60 (20 for each temperature). Each single fish was captured by using a beaker and transferred from the hometank to waiting tank (size 15 × 10 × 10 cm, width × depth × height) for 30 min until the beginning of the behavioural test.

One single task consisted of four trials (T1, T2, T3 and T4) separated by a one-hour interval. Each trial consisted of a training phase (Tr) in which the fish could freely swim in the start (S) arm and in the other (O) arm for 5 min but it could not have access to the novel (N) arm for the presence of a dividing wall, and of a testing phase (Te) in which the wall was removed and the fish was free of swimming for 5 min all over the maze also exploring the novel environment constituted by the N arm. The assignment of circle, square, and triangle to the S, O and N arm was randomized for each experimental subject.

The behaviour was analysed using the ANY-Maze® software (Stoelting Co., Wood Dale, IL, USA). Locomotor activity was evaluated by measuring the mean speed, the total distance travelled, and the rotations of the body (clockwise, CW and counterclockwise, CCW). The exploratory activity and the interest in the novel environment were evaluated by quantifying the time spent in each arm,

the number of passages among arms and the degree of exploration of the novel arm. In order to determine whether the temperature influences fish tendency to explore the novel environment in its entirety, the N arm was virtually divided into three equal parts named as sector 1, 2 and 3 starting from the centre of the maze. At the end of each trial the experimental subject was transferred to the waiting tank for one hour until the next trial. The temperature of the water contained in the waiting tank was the same to which the fish had been acclimated. After each trial the water contained in the maze was removed and the apparatus was rinsed and filled with clean water.

2.9 Statistical analysis of functional behavioural data

Results were expressed as mean ± SEM. Data were subjected to ANOVA analysis with a post hoc test utilizing Bonferroni correction by ORIGIN® 2018 software. Depending on the data considered among swimming activity and behaviour measured as time spent in the Start arm, mean speed, total distance travelled, number of total rotations of the body, number of right (CW) and left (CCW) rotations, number of passages between Start and Other arms, one-, two- or three- way ANOVA analyses were performed. Differences were considered to be statistically significant at $p \leq 0.05$ and $p \leq 0.01$.

3. RESULTS AND DISCUSSION

3.1. Proteomic analysis

To evaluate the possible effects of temperature on protein expression, we have adopted a quantitative label free shotgun proteomic approach. This method allows to examine the impact of different conditions by achieving the simultaneous identification of thousands of proteins and their quantification in each sample.

Therefore, it is well suited for studying differences in global protein expression between samples and provides substantial information to delineate cell signalling pathways involved in thermal responses. The whole brains of ZF acclimated for 21 days to three temperatures (18 °C, 26 °C and 34 °C) were homogenized and submitted to tandem mass spectrometry analysis.

The identification of the proteins from the MS/MS data was then achieved using a database search by MaxQuant which compares acquired mass spectra to a database of known sequences to identify the proteins. This strategy allowed the identification of 1735, 2077 and 1817 proteins at 18 °C, 26 °C and 34 °C, respectively. The comparison of the three data sets highlights the presence of proteins exclusively expressed at a single temperature, as well as 1499 proteins present at all temperatures, among which 125 are differentially expressed at the thermal regimes tested (figure 45).

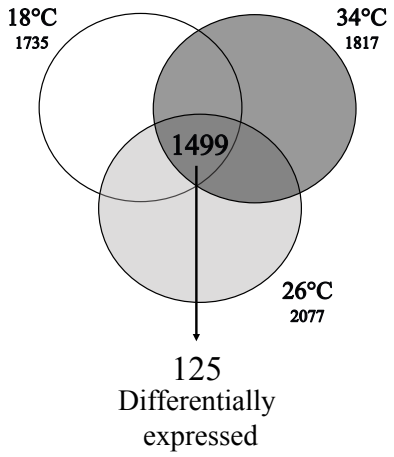

Figure 45 Veen Diagram of the proteins identified in ZF brains acclimated at 26°C (Control Condition), 18°C and 34°C). An Anova test (FDR 0.05) was carried out to identify proteins differentially expressed among the different conditions: 1735, 1817 and 2077 proteins are exclusively expressed in 18°C, 34°C and 26°C, respectively, while 125 out of 1499 common proteins differ with statistical significance.

Bioinformatic analysis carried out on these proteins by DAVID software suggested that different temperatures affect mainly cytoskeleton and ribosome and, to a lesser extent, carbon metabolism and mitochondrion related categories (Table 15).

Table 15 DAVID functional grouping of the proteins differentially expressed at 18 °C, 34 °C and 26 °C. The Table reports the proteins statistically differentially expressed among the three different conditions (ANOVA test FDR 0.05). The column "Counts" indicates the number of genes present in each category. Functional grouping was based on $p \leq 0.05$ and at least two counts.

Term	Count	PValue	Genes
Enrichment Score: 2.53			
GO:0005509~calcium ion binding	9	1.57E-02	SRI, PVALB6, HPCAL4, MYLZ3, PVALB5, CALB2A, ANXA3B, LCP1, CELSR1A
Enrichment Score: 2.49			
GO:0005882~intermediate filament	4	2.06E-03	PRPH, KRT18, KRT5, KRT8
GO:0005198~structural molecule activity	4	3.49E-02	PRPH, KRT18, KRT5, KRT8
Enrichment Score: 2.12			
GO:0005874~microtubule	5	1.45E-03	PAFAH1B1B, LOC100149074, MAP2, TUBA8L2, TUBA8L3
GO:0005856~cytoskeleton	5	3.72E-02	PAFAH1B1B, MAP2, TUBA8L2, LCP1, TUBA8L3
Enrichment Score: 1.66			
GO:0006412~translation	7	1.47E-03	TUFM, RPS8B, MRPL12, RPS19, EIF4A2, RPL4, EIF5A2
GO:0030529~intracellular ribonucleoprotein complex	5	8.94E-03	HNRPDL, RPS8B, MRPL12, RPS19, RPL4
GO:0005840~ribosome	4	2.84E-02	RPS8B, MRPL12, RPS19, RPL4
dre03010:Ribosome	4	4.32E-02	RPS8B, MRPL12, RPS19, RPL4
Enrichment Score: 0.96			
dre01200:Carbon metabolism	4	3.63E-02	SDHB, TPI1B, IDH3G, PGAM1B
Enrichment Score: 0.84			
GO:0000166~nucleotide binding	14	3.85E-02	TUFM, MYHC4, RBM4.2, HSPA4A, ADRBK2, SYNCRIP, NCL, TUBA8L2, TUBA8L3, HNRPDL, SRSF5B, UBE2D3, EIF4A2, ACTA1A
Enrichment Score: 0.75			
GO:0005739~mitochondrion	8	4.77E-03	TUFM, SDHB, IDH3G, COX6B1, CHCHD2, ACADL, VDAC2, TIMM8A

Specific analyses were carried out by comparing 18 °C and 34 °C with 26 °C, kept as the control condition. Figures 45A and B reports the corresponding Volcano plots.

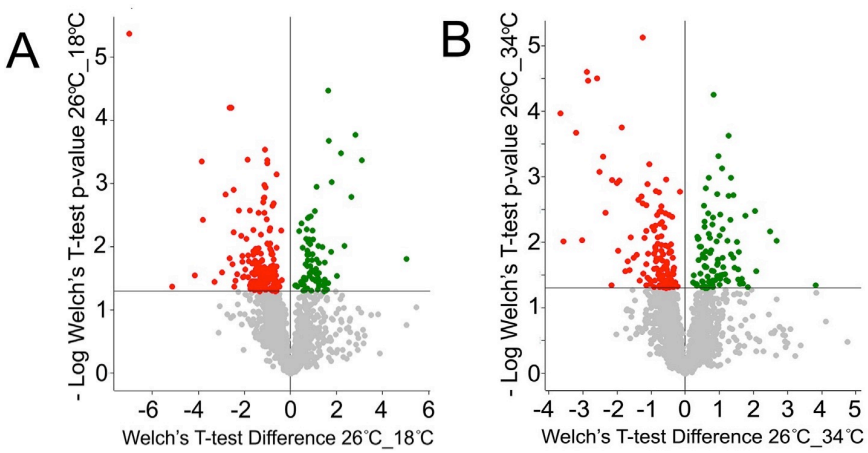

Figure 45 Volcano plot of the proteins differentially expressed in the comparison 26 °C vs 18 °C (A) and 26 °C vs 34 °C (B). Proteins were considered differentially expressed if they were present only in one condition or showed significant t-test difference (Welch's test p = 0.05). The proteins up- or down- regulated are indicated in green and red, respectively.

According to our results, 290 proteins are exclusively expressed at 18°C or down-regulated at 26°C whereas 225 proteins are exclusively expressed at 34 °C or down-regulated at 26 °C.

To disclose the effect of temperature treatment on the ZF brain proteome, the proteins differentially expressed in the comparison 26 °C vs 18°C and 26°C vs 34°C were analysed for functional grouping. Interestingly, most proteins whose expression decreased in response to thermal changes (18 and/or 34 °C) are associated to different steps of protein synthesis, from RNA translation to protein folding, localization and degradation (Table 16).

Table 16 DAVID functional grouping of the proteins differentially expressed at 26 °Cvs18°C and 26 °Cvs34°C. The table reports the proteins up-regulated or exclusively expressed at 26 °C. The column "Counts" indicates the number of genes present in each category. The first column reports a manual clustering of the Terms reported in column 2. Functional grouping was based on $p \leq 0.05$ and at least two counts.

Increased at 26 °C					
		26 °C vs 18 °C_26°Cup_only26°C		26 °C vs 34 °C_26°Cup_only26°C	
Clustering	**Term**	**Counts**	**Genes**	**Counts**	**Genes**
RNA translation	Nucleotide binding	51	CKBA, PSMC1A, SYNCRIP, ATP2B1B, LONP1, LARSA, DHX37, U2AF1, ADCK3, AGAP1, GLULA, RABL3, ARL16, ABCC12, SARS2, EIF4A3, NME3, EIF4BA,	43	HNRNPH1L, SEPT3, PSMC1A, ATL1, MYO10L3, SYNJ1, SYNCRIP, SEPT7A, CHEK2, SF3B4, GMPPAB, ATP2B1B, SRSF5B, LARSA, EIF3G, DHX37, TUBB5, U2AF1,

			CAMK4, EIF4BB, GNAS, GNAI3, MYO10L3, SNRPB2, MYO10L1, SEPT7A, CHEK2, GMPPAB, SF3B4, IARS, UBE2D3, EIF3G, GSK3AB, SEPT8A, PRKCDA, SNRNP70, YES1, RHOAA, DHX9, MATR3L1.1, MYO6A, RBM4.2, ADCY1A, MAPK10, TIA1L, GNA15.3, PSMC2, HUG, PABPC1A, MAP2K2A, ATP8A2		SNRNP70, YES1, MARS, RPS24, MATR3L1.1, DHX9, MYO6A, SI:ZFOS-588F8.1, HNRNPA0L, OLA1, ARL16, ELAVL3, ABCC12, MAPK10, NCL, TUBA8L2, SARS2, HNRPDL, NME3, ZGC:63587, MAP2K2A, PFKMB, EIF4BB, ATP8A2, KATNAL2
	Intracellular ribonucleoprotein complex	9	RPS25, DHX9, LSM6, HUG, RPL24, RPS10, SNRNP70, MRPL46, RPL28	11	HNRPDL, DHX9, RPS28, LSM6, RPS12, SNRPC, ELAVL3, SNRNP70, MRPL46, RPS24, RPS7
	Nucleosome assembly	8	ZGC:153405, HISTH1L, NAP1L1, SETB, H1FX, ZGC:163061, ZGC:110216, SI:CH211-103 N10.5		
	Chromosome	7	ZGC:153405, HISTH1L, H1FX, ZGC:163061, ZGC:110216, SI:CH211-103 N10.5, SMC3		
	Ribonucleoprotein			10	HNRPDL, RPS28, LSM6, RPS12, SNRPC, ELAVL3, SNRNP70, MRPL46, RPS24, RPS7
	Cytosolic small ribosomal subunit			5	RPS28, RPS12, ZGC:114188, RPS24, RPS7
Protein folding	Protein folding	7	ERP44, PFDN1, PPIFB, PFDN6, PPID, VBP1, AIP	7	PFDN1, GRPEL1, TXNDC5, PPID, PPIAA, VBP1, PDIA4
	Prefoldin complex	3	PFDN1, PFDN6, VBP1		
Protein localization	Protein transport			10	SEC23A, BC2, SLC7A6OS, AP1G1, TOM1L2, TIMM10, AP3S1, VPS26BL, AP4S1
	Protein transport			10	SCAMP1, SEC23A, BC2, SLC7A6OS, AP1G1, TIMM10, EXOC4, AP3S1, VPS26BL, AP4S1
	Protein transporter activity			5	AP1G1, TIMM10, AP3S1, VPS26BL, AP4S1

PT modification	Phosphoprotein phosphatase activity	7	PPM1BB, PGAM5, PPM1BA, PTPRNB, PPP3CB, UBLCP1, PPP1CAB	8	PPP3CCB, PPM1BB, PGAM5, PPM1BA, PTPRNB, PPP3CB, UBLCP1, PPP1CAB
	Protein serine/threonine phosphatase activity			4	PPM1BB, PPM1J, PPM1BA, UBLCP1
	Protein phosphatase			5	PPM1BB, PPM1BA, PTPRNB, UBLCP1, PPP1CAB
Degradation	Proteasome complex	7	PSMB7, PSMB6, PSMC1A, PSMC2, PSMB2, PSMD7, PSMA6B	5	PSMB7, PSMC1A, PSMB3, PSMA3, PSMD7
	Proteasome core complex	4	PSMB7, PSMB6, PSMB2, PSMA6B		
	Proteolysis involved in cellular protein catabolic process	5	PSMB7, PSMB6, PSMB2, CTSH, PSMA6B		
	Protein catabolic process	4	LONP1, PSMC1A, PSMC2, CTSD		
Redox balance	Cell redox homeostasis			5	TXNDC5, PRDX2, PDIA4, SH3BGRL3, GLRX
	Mitochondrial respiratory chain complex I			3	NDUFS5, NDUFS4, NDUFB9
	Oxidoreductase activity			16	HADHAA, GLUD1B, GMPR2, AIFM2, AKR1A1B, CBR1L, FDXR, PRDX2, GPD1L, SDHB, IDH3G, MICAL2A, CAT, CYP8B1, GPX1A, GLYR1
Other	Endopeptidase activity	5	PSMB7, PSMB6, PSMB2, SI:DKEY-21C19.3, PSMA6B		
	Threonine-type endopeptidase activity	4	PSMB7, PSMB6, PSMB2, PSMA6B		
	ATP-dependent RNA helicase activity	5	DHX9, EIF4A3, DDX39AB, DHX37, DDX39B		
	Calcium ion binding			19	SRI, CALUA, LRP1AA, HPCAL4, PVALB6, PVALB5, SI:DKEY-110 K5.6, NID1B, ANXA4, EFHD2, SCGN, NCALDA, NCALDB, CAPNS1A, SYT1B, F2, CELSR1B, S100A10B, LCP1
	Isomerase activity			5	TXNDC5, PPID, PPIAA, PGAM1B, PDIA4

All these proteins are more expressed or only expressed at 26 °C suggesting that heat or cold temperatures may hamper the normal protein synthesis cascade.

GO enrichment analysis according to Panther software, BINGO and Enriched Map (Figure 46) suggests that this effect is possibly mediated by a significant impact on the cytoskeleton.

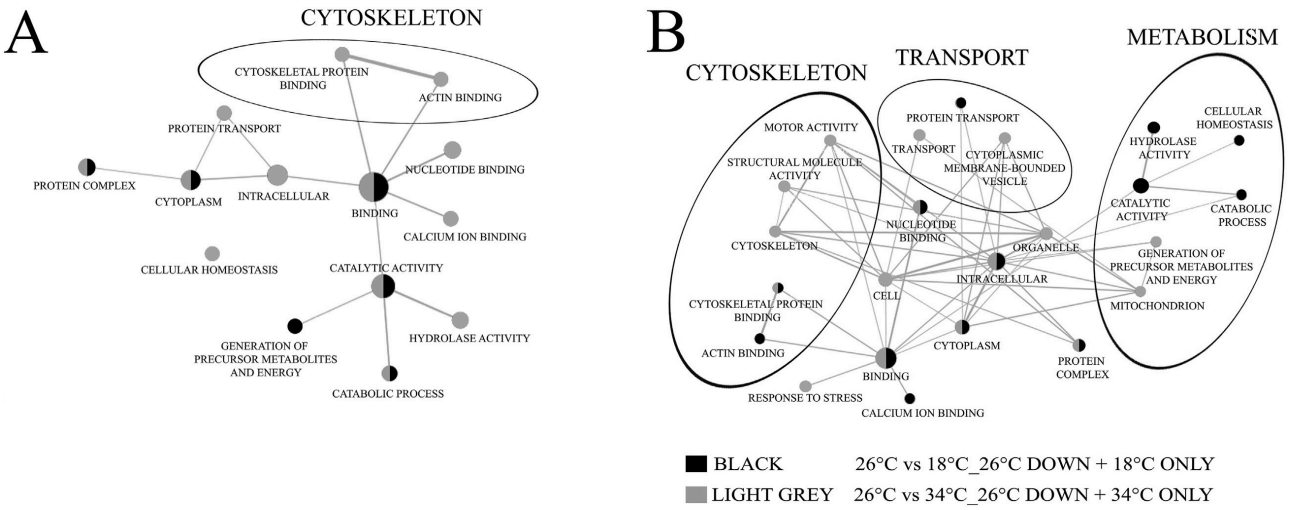

Figure 46 (A) Enriched Map analysis of gene sets up-regulated or only expressed at 26 °C in the comparison 26 °C vs 18 °C and 26°C vs 34°C (increased at 26°C). The differentially ex- pressed proteins were classified into different biological processes according to the Gene Ontology Slim classification system using BINGO and Enriched Map software. Functional grouping was based on $p \leq 0.05$. Nodes represent gene-sets and edges represent GO defined relations. Gene-sets that did not pass the enrichment significance threshold are not shown. Nodes are colored according to samples: black represents enrichment in the comparison 26°C vs 18°C whereas light grey represents the gene sets in the comparison 26 °C vs 34 °C. **(B)** Enriched map analysis of gene sets down-regulated at 26 °C or only expressed at 18 °C or 34 °C in the comparison 26°C vs 18°C and 26°C vs 34°C (decreased at 26°C).

GO Slim Biological Processes (GOBP), GO Slim Molecular Function (GOMF) and GO Slim Cellular Component (GOCC) highlight changes in structural cytoskeleton constituents, cellular morphogenesis and organization at extreme temperature conditions and a more pronounced effect on motor activity, transmembrane movement and vesicle mediated transport at 18 °C and 34 °C. This finding is in agreement with the functional grouping analysis by DAVID that shows a decrease at 26 °C of proteins related to cytoskeleton and transport or motor activity (Table 17).

Table 17 DAVID functional grouping of the proteins differentially expressed at 26 °Cvs18°C and 26 °Cvs34°C. The Table reports the proteins down-regulated at 26° C or exclusively expressed in stress conditions. The column "Counts" indicates the number of genes present in each category. The first column reports a manual clustering of the Terms reported in column 2. Functional grouping was based on $p \leq 0.05$ and at least two counts.

Decreased at 26 °C					
		26 °C vs 18 °C_26°Cdown_only18°C		26 °C vs 34 °C_26°Cdown_only34°C	
Clustering	**Term**	**Counts**	**Genes**	**Counts**	**Genes**
Cytoskeleton	Structural molecule activity	9	SI:DKEY-178 K16.1, PRPH, COPG2, KRT18, KRT5, COPB1, CLTCA, CLDNK, INAB	5	GFAP, KRT5, CLTCB, KRT8, KRT4
	Intermediate filament	4	PRPH, KRT18, KRT5, INAB	4	GFAP, KRT5, KRT8, KRT4
	Microtubule	8	FSD1, PAFAH1B1B, LOC100149074, MAP2, TUBA8L, SI:DKEY-77A20.5, TUBA8L2, TUBA8L3		
	Cytoskeleton	12	FSD1, SI:DKEY-178 K16.1, PAFAH1B1B, MYO15AA, ACTB1, MAP2, TUBA8L, SI:DKEY-77A20.5, LCP1, TUBA8L2, TUBA8L3, PLECA		
	Microtubule-based process	4	DYNLL1, TUBA8L, TUBA8L2, TUBA8L3		
	Structural constituent of cytoskeleton	4	SI:DKEY-178 K16.1, TUBA8L, TUBA8L2, TUBA8L3		
	Keratin filament			3	KRT5, KRT8, KRT4
	Actin-binding			7	MYHC4, SYNE2B, SPTBN5, MYO18AB, CAPZA1B, FLNA, MYH10
	Myosin complex			4	MYHC4, MYO15AA, MYO18AB, MYH10
Transport/motor activity	Vesicle-mediated transport	7	COPG2, ZGC:92912, COPB1, CLTCA, AP3B2, STXBP1A, STXBP3		
	Intracellular protein transport	8	COPG2, NAPG, CSE1L, COPB1, CLTCA, AP3B2, VPS35, ADPRH		
	Lipid transporter activity			3	VTG4, VTG7, VTG5
	Motor activity			4	MYHC4, MYO15AA, MYO18AB, MYH10
Ion binding	Magnesium ion binding	5	IDH3G, PGM1, ENO2, ENO3, ADPRH		
	Calcium ion binding			12	PVALB4, PCDH1A3, MYLPFA, HMCN1, LRP2A, MYLZ3, MYL1, PCDH1B, SPNA2, NOTCH1B, CELSR1A, CAPN2B
Other	Nucleotide binding	30	TUFM, GNA11A, ATL1, ACTB1,	28	MYHC4, TUFM, HSP90AB1,

		CKMB, ADRBK2, IARS2, SI:DKEY-172 J4.3, SRSF5B, SRSF2A, HNRNPM, MARK4A, PRKAA1, CSNK1A1, CSTF2, TUBA8L, ATP1A3B, RNPS1, NCL, TUBA8L2, TUBA8L3, SRSF6A, PSMC3, RARS, UBA2, EIF4A2, GSK3B, PFKMB, ACTA1A, CARS2		ADRBK2, IARS2, HNRNPM, ACTR1, MYO18AB, GSK3AB, PRKAA1, HSPA5, HSPA9, HSPA4A, SSB, ABCA4A, EIF4A3, ATP2A3, RARS, UBA2, RRAS2, EIF4A2, REM2, ACTA1A, CCT8, FGFR1B, RHEB, KIF19, MYH10
Ribosome	10	RPS8B, MRPL12, RPS19, RPS16, RPS15, RPL10, RPL4, RPL10A, RPLP2L, RPS3		
Sm01391	4	PRPH, KRT18, KRT5, INAB		
Glycolytic process	4	ALDOAB, PFKMB, ENO2, ENO3		
Proteasome complex	5	PSMB4, PSMD13, PSMD12, PSMC3, PSMD6		
Oxidation-reduction process	15	SQRDL, KCNH6B, CYP2V1, FDXR, DLAT, ACADL, GLDC, SDHB, G6PD, IDH3G, YWHABL, UQCRH, ALDH4A1, GLYR1, RTN4IP1		
Mitochondrion	12	TUFM, SDHB, IDH3G, UQCRH, OTC, FDXR, SIRT5, ALDH4A1, IARS2, ACADL, RTN4IP1, FH		
Tricarboxylic acid cycle	3	SDHB, IDH3G, FH		
Gtpase activity	6	TUFM, GNA11A, ATL1, TUBA8L, TUBA8L2, TUBA8L3		
ATP binding			26	MYHC4, HSP90AB1, ADRBK2, TTNB, IARS2, ACTR1, MYO18AB, GSK3AB, PRKAA1, HSPA5, DYNC1H1, HSPA9, HSPA4A, DDX1, ABCA4A, EIF4A3, MYO15AA, ATP2A3, RARS, UBA2, EIF4A2, ACTA1A, CCT8, FGFR1B, KIF19, MYH10
Stress response			4	HSP90AB1, HSPA4A, HSPA5, HSPA9

At low temperature the GO enrichment analysis reveals a profound impact on morphogenesis, cytoskeleton organization and synaptic transmission, as well cell communication all de- creased. Cold also induces a marked alteration of the actin cytoskeleton and actin binding proteins (Figure 46).

The fold enrichment analysis gave more information on cold and heat effects. There are pathways exclusively enriched at 34 °C or 18 °C (Figure 47) and most pathways altered at the two temperatures decreased in comparison to controls at 26 °C (Figure 47).

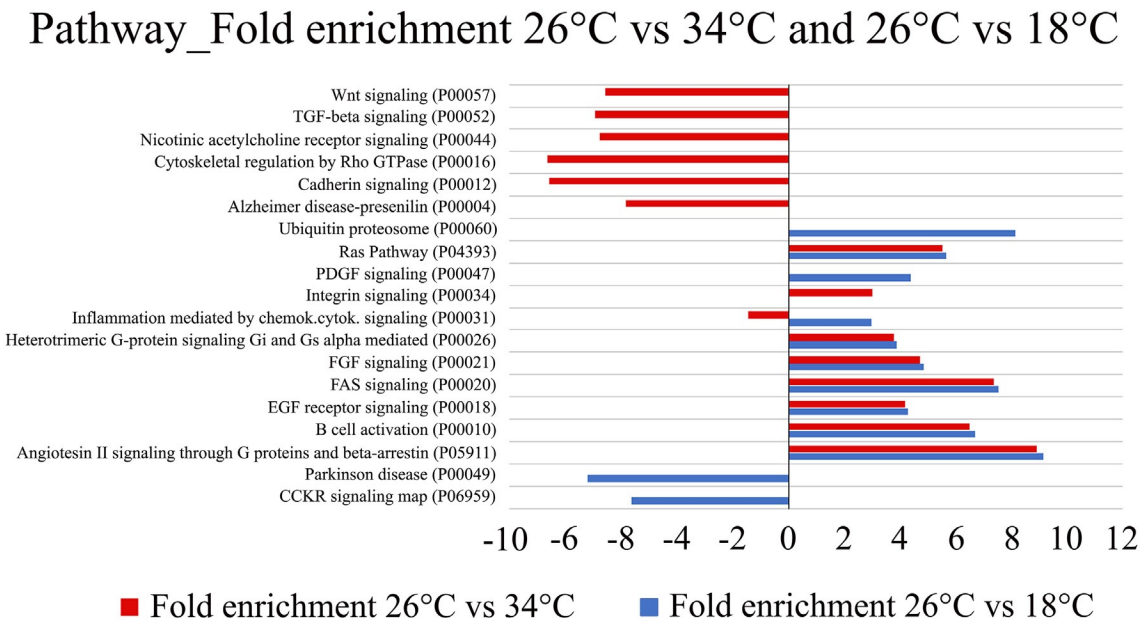

Figure 47 Gene Ontology Pathway classification of proteins differentially expressed in the comparison 26 °C vs 18 °C and 26 °C vs 34 °C. The differentially expressed proteins were classified into different GO Pathways using the Panther software. Functional grouping was based on $p \leq 0.05$ and minimum two counts. Negative values refer to fold enrichment of proteins less expressed at 26 °C or only expressed at 18 °C or 34 °C (decreased at 26 °C) whereas positive value refer to proteins more or only expressed at 26 °C in the comparison 26 °C vs 18 °C and 26 °C vs 34 °C (increased at 26 °C).

The effects on WNT signalling pathways are quite interesting. Beside the canonical WNT pathway that leads to the regulation of gene transcription, two non canonical WNT pathways were described: the planar cell polarity pathway that regulates the cytoskeleton, and the WNT/calcium pathway that regulates calcium levels inside the cell [479]. By targeting the cytoskeleton directly or through Rho GTPase [480], WNT signalling alteration may be related to a significant impact of temperature on the cytoskeleton in ZF brain (Figure 47).

3.2. Temperature treatment: impact on metabolism and transport

Data show an increase in the transketolase and transaminase activity suggesting that the pentose metabolism (PPP) prevails at 34 °C in keeping with the decrease of the oxidative phosphorylation at 34 °C compared to 26 °C (Table 16). The need of the cell to counteract the oxidative stress induced by high temperatures could explain the increase associated with the PPP which produces NADPH necessary both for DNA production and for the regeneration of reduced glutathione, which in turn plays an important role in the regulation of the intracellular redox state by providing reduced equivalents for antioxidative pathways (Table 17, Fig. 46B) [481]. However, the cell redox balance is hampered by heat due to a decrease of the antioxidant and peroxidase activity (Table 16).

The alteration of mitochondrion-associated proteins found at 34 °C suggests a perturbed cell energy metabolism that may compromise cell physiology and brain functioning. Most of the energy produced in the brain (75% -80%) is consumed by neurons [482] that are highly dependent on ATP amounts necessary to support synaptic vesicle mobilization, to generate the membrane action potential [483] and to ensure calcium homeostasis at the synaptic level [484, 485]. The different cellular districts need different amounts of energy and the synapse has a high energy requirement for restoration of neuronal membrane potentials following depolarization [486]. For these reasons, a reduced energy availability in the neuronal cells may induce synaptic impairments [487]. Moreover, the reduction of proteins involved in the mitochondrial transport at 34 °C may suggest a defective mitochondria positioning in synaptic terminals [488] where they are involved in regulating neurotransmission [489-492] and synaptic plasticity [493, 494]. The defective transport of mitochondria is believed to contribute to the onset of neurodegenerative diseases [495-498]. Our proteome results are consistent with literature data showing that high temperature induces mitochondrial uncoupling and dysfunction by the reduction of cristae, oxidative phosphorylation and ATP synthesis [499-501]. Experimental evidence shows that the impairment of mitochondrial

function can lead to synaptic degeneration [488, 493, 502, 503]; consistently, our results show a reduction in proteins associated to synapse, neurotransmitter secretion, receptor-mediated endocytosis and endosome suggesting an impairment of intercellular communication.

Heat also induces the increase of ion transporter activity and transmembrane movement of substances, muscle contraction, motor activity, nuclear and protein transport and the increase in lipid and fatty acids metabolic processes (Table 17, Fig. 46B).

At 18 °C, the data reported in figure 46 clearly show an increase of catalytic activity, catabolic processes and TCA cycle (figure 46B), in accordance with findings suggesting that cold stress increases the cellular content in ATP and ADP as possible strategy for offsetting kinetic effects of low temperatures on the reaction rates [504].

The increase in proteins associated with catalytic activity, catabolic processes, carbohydrate metabolism and TCA cycle (figure 46B) found at 18 °C might be related to cellular production of a greater amount of ATP to counteract the reduced enzyme kinetics and vesicular mobility occurring at low temperatures [505-507]. The increased expression of proteins involved in the transport of vesicles and polypeptides could be also related to the restoring of the axon flow slowed by low temperatures. However, the reduction of proteins associated to synapse and neurosecretion was detected at both 18 °C and 34 °C.

Consequently, the exposure to thermal extremes both determines synaptic function impairments that, associated with the modulation of signal transduction pathways, might be responsible for functional alterations of the CNS.

3.3. Temperature treatment: impact on cytoskeleton

As shown in Table 17 and figure 46, heat treatment has a profound impact on cytoskeleton, mitochondrial organization and chromatin remodelling. We then asked if the temperature itself may lead to a change in cytoskeleton that can reverberate on cell signalling. It is known that temperature modulates stiffness and elasticity of cells and recent findings in rat demonstrated that neurons display

a significant drop in the average elastic modulus with increasing temperature [508]. The decrease in neuron stiffness is linked to an increase in myosin II activity at high temperature since active myosin II fluidizes the cells while inactive myosin II acts as a cross linker for F-actin. Moreover, metabolic activity of the myosin II motor is dependent on the temperature and availability of ATP [508-511], as well as on the length and orientation of actin filaments. In accordance, our GO analysis at 34 °C shows a significant enrichment of proteins involved in muscle contraction, structural activity, intermediate and actin cytoskeleton while at 18 °C the effect on microtubules are prevalent (Tables 16, 17).

Interestingly, at 18 °C and 34 °C there is also an increase of proteins involved in calcium binding (Table 17, figure 46B). This finding is in line with the data reported in Amato & Christner [504] which suggest that the link between thermoregulation and neurotransmission is largely dependent on intracellular calcium homeostasis [512].

Therefore, the temperature treatment effects on proteins involved in actin rearrangements and calcium binding observed in ZF brains at 18 °C and at 34 °C can be framed in the mechano-biological interplay between cytoskeleton and calcium concentration.

3.4. Signal transduction pathway modulation

Several proteins involved in fundamental signalling pathways are modulated at both thermal extremes. Interestingly, many of the down-regulated pathways are involved in cognitive processes (figure 47).

The expression of proteins involved in the integrins pathway was reduced at 34 °C in comparison to 26 °C. Integrins are a large family of heterodimeric transmembrane cell adhesion receptors involved in processes that can modify the brain cytoarchitecture by affecting axon growth and guidance, dendritic spine morphology, synaptogenesis [514], synaptic plasticity [517, 514, 515], cell migration and regeneration [516] and by supporting the differentiation and maintenance of neural stem cells [518]. Integrins are also engaged in learning mechanisms and their reduced expression in

mice determined the impairment of long term potentiation (LTP) stabilization, memory acquisition and long- term storage of several kinds of memories, including spatial and working memory [517], long-term object-location memory and novel- object recognition [517, 519].

The down-regulation of the arrestin pathway at 18 °C and 34 °C could provoke alterations of ZF cognitive abilities in analogy to β arrestin 1 KO-mice that showed deficits in learning tasks suggesting spatial learning deficiencies and general alteration in reward processing [520].

The down-regulation of the Ras pathway at 18 °C and 34 °C suggests that the exposition to the extreme temperatures could affect the cognitive abilities of the animals, as the Ras signalling is implicated in synaptic events leading to formation of long-term memories [521].

Focusing on pathways exclusively altered at 18 °C or altered in the same way at 18 °C and 34 °C (Figure 47), cold acclimation leads to a lower expression of EGF and PDGF signalling in comparison to 26°C. Although these growth factors belong to different families and drive different biological roles, they share some overlapping targets. Both EGF and PDGF engage several well-characterized pathways as the Ras- MAPK, PI3K, and PLCG that are deeply involved in diverse cellular responses, and their dysregulation is common during oncogenesis and pathophysiological tissue remodelling [522]. The reduced expression of the PDGF pathway observed at 18 °C suggests that ZF brain acclimated to low temperatures may be more susceptible to environmental stressors considering the neuroprotective role of the PDGF pathway demonstrated in different animal models during ischemy [523, 524], oxidative stress [525] and glutamate- or NMDA-induced excitotoxicity [526]. Moreover, PDGF increases neuronal cell survival, neurogenesis, angio- genesis and gliosis and its neuroprotective effect on dopaminergic neurons is well documented [527]. The reduced expression of the PDGF pathway could have a negative impact on animal cognitive abilities being PDGF involved in the regulation of synaptic plasticity and function, in the hippocampal LTP and hippocampus-dependent memory [528]. The EGF pathway down-regulation detected in fish at 18 °C and 34 °C could contribute to the altered cognitive performances on considering that EGF

administration ameliorates the cognitive decline [529] and memory deficit [530], and prevents brain injury upon hypoxia in mice [531].

The down-regulation of the ubiquitin pathway observed at 18 °C could further contribute to the CNS impairment as the failure of the ubiquitin-proteasome system has been found in Parkinson's disease [532].

3.5. Behavioural data analysis

With the aim of verifying if the adaptation to thermal extremes determines impairments of cognitive abilities of the animals, experimental and control subjects maintained for 21 days at the three temperatures were subjected to behavioural tests by using a Y-Maze apparatus. The Behavioural analysis was performed by Mattia Toni at University La Sapienza in Rome. The Y-Maze task is widely used on mouse model and has been also successfully used in ZF [470]. It allows evaluating both physical performances related to the locomotor activity and cognitive abilities related to the response to novelty and spatial orientation.

Behavioural parameters were analysed in both Training phase (Tr) and Testing phase (Te) in order to evaluate the swimming performances and the dynamism of the fish together with its tendency to explore the novel environment.

During Tr, fish did not show preference for one or the other of the two arms, spending approximately the 50% of the total time in each arm. Neither temperature nor trial replication influenced these results (figure. 48A).

As indicated by mean speed and distance travelled, animals maintained at 18 °C and 34 °C respectively showed a decrease and an increase in locomotor activity compared to controls (figure 48B, C). In the intra-temperature analysis, no differences were detected in mean speed and distance travelled between Tr and Te at 18 °C and 26 °C. At 34 °C fish in Te showed higher values of mean speed and distance. The number of body rotations, which is the number of 360° rotations, was respectively lower and higher in fish at 18 °C and 34 °C compared to controls (figure 48D). The

three-way ANOVA analysis among temperatures (18 °C, 26 °C and 34 °C), experimental phases (Tr and Te) and directions of rotation (clockwise, CW and counter-clockwise, CCW) did not show significant differences in intra-test phase analysis between CW and CCW rotations, except at 34 °C in which a higher number of CW rotations was detected in Te (figure 48E). The swimming activity and the dynamism of fish were also estimated by measuring the number of passages between the S and O arms. At both 26 °C and 34 °C, fish increased the number of passages from T1 to T4, whereas no differences were detected in fish at 18 °C (figure 48F).

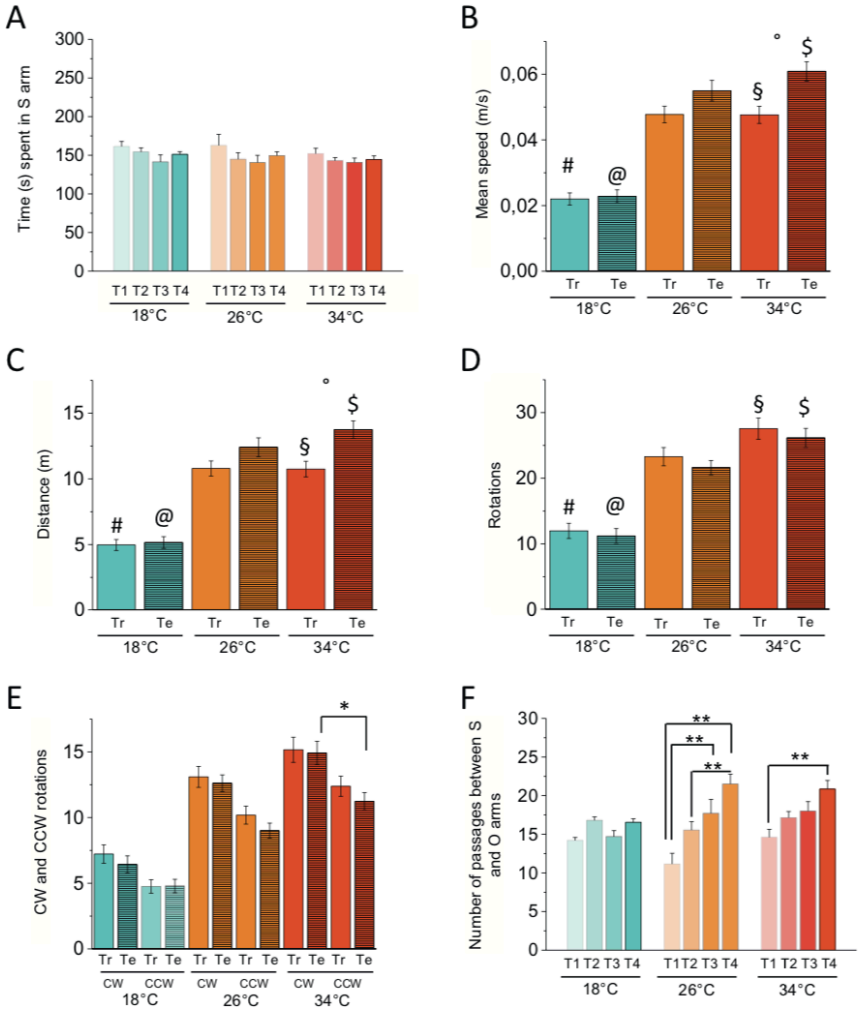

Figure 48 Behavioural response to thermal treatment on Y-Maze test observed in Training phase (Tr) and Testing phase (Te). Swimming activity and behaviour measured as time spent in the Start arm **(A)**, mean speed **(B)**, total distance travelled **(C)**, number of total rotations of the body **(D)**, number of right (CW) and left (CCW) rotations **(E)**, number of passages between Start and Other arms **(F)**. Data were analysed by two-way ANOVA (A-D, F) and three-way ANOVA (E) with a post hoc test that utilizes a Bonferroni correction. #, $p \leq 0.05$ between Tr at 18 °C and 26 °C; @, $p \leq 0.05$ between Te at 18 °C and 26 °C; §, $p \leq 0.05$ between Tr at 34 °C and 26 °C; $, $p \leq 0.05$ between Te at 34 °C and 26 °C; °, $p \leq 0.05$ in intra-temperature Tr vs Te comparison; *, $p \leq 0.05$; **, $p \leq 0.01$.

The lower swimming performances showed by fish at 18°C in comparison to those kept at 26 °C or acclimated to 34 °C are consistent with literature data showing the increase in swimming activity at higher temperatures [533-535].

In Te, fish could freely swim in the three arms of the maze exploring the novel environment of the N arm for 5 min. Fish acclimated at 34 °C showed the tendency to carry out a greater number of passages among the arms than those at 26 °C and 18 °C in all the trials, although only the comparison between 18 °C and 34 °C in T2 was statistically significant. No statistically significant differences were measured in the intra-temperature analysis (figure 49A).

The number of times that fish entered into the N arm reaching the sector 3 was measured to evaluate whether temperature affects the exploration of the novel environment. Fish acclimated to the 34°C entered more often in the sector 3 of the N arm than fish at 18 °C and 26 °C. The number of entries was significantly higher at 34 °C than at 26°C in T1 and T2 and at 34°C than 18°C in T1, T2, T3 (figure 49B). Intra- temperature analysis revealed differences in number of entries in the sector 3 of the N arm only at 18 °C between T4 and the other trials (figure 49C). To better evaluate the temperature effect on the exploration of the novel environment, the ratio between the number of times the animal reached the sector 3 of the N arm and the number of total entries in the N arm was calculated. No statistically significant differences were found both in the intra-trial and intra-temperature analysis (figure 49D): in all conditions tested, fish tended to fully explore the N arm reaching the sector 3 the 60–80% of time.

The total time spent by the experimental subjects in each arm was also measured in Te to estimate the animal's interest in the novel environment. Fish maintained to the control temperature (26 °C) during T1 spent most of the time in the N arm (54% of total time) (figure 49E). This result demonstrates fish interest for the N arm, where they spent most of the time and is coherent with findings by Cognato and co-workers [470] thus confirming that control fish are able in spatial orientation and distinguish the unexplored from the explored arms. As expected from the results of proteomic analysis, fish acclimated to 18 °C and 34 °C showed a different behaviour compared to

controls as they showed no preference for the N arm where they spent only 25–30% of the time. Different phenomena could explain the reduced interest in novelties such as the compromised ability in recognizing the geometric figures that distinguish the arms, difficulties in spatial orientation and the inability in recognizing the N arm like a novel environment.

In the subsequent trials at 26 °C, there was a progressive significant reduction in the time spent in the N arm that gradually declines from T1 to T4 (45% in T2, 36% in T3 and 29% in T4) (figure 49E, F), demonstrating a progressively lowered interest in the N arm that is no longer a novelty for the fish, as it has already been explored previously.

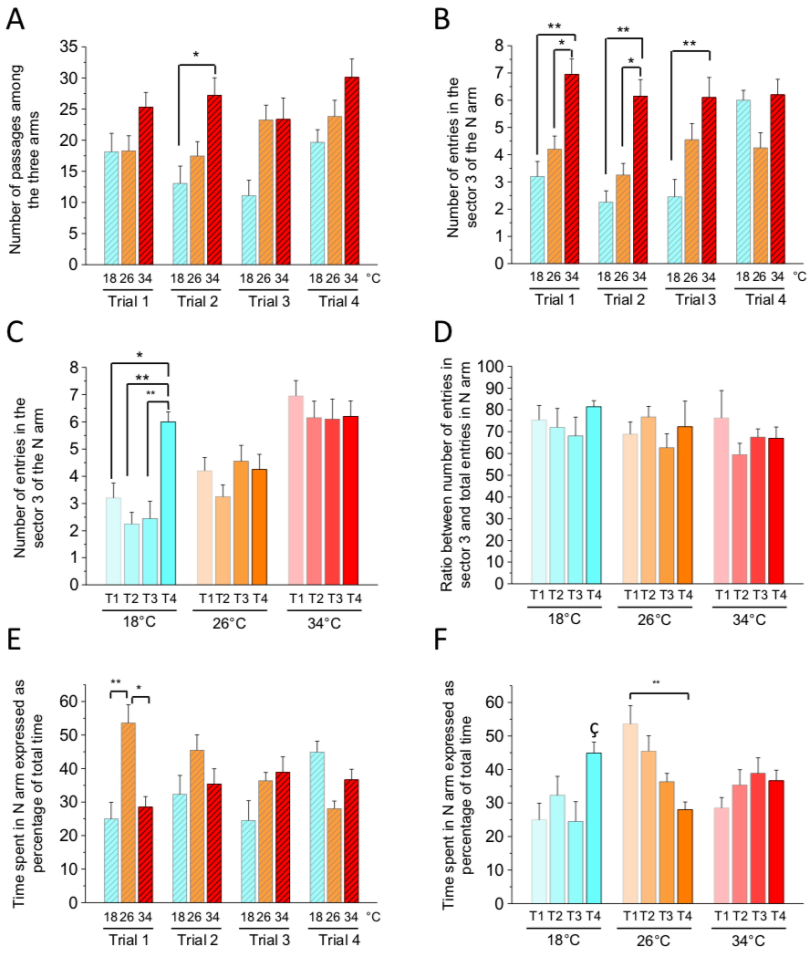

Figure 49 Behavioural response to thermal treatment on Y-Maze test observed in Testing phase (Te). Total number of passages among the three arms **(A)**, total number entries in the sector 3 of the N arm **(B, C)**, ratio between the number of entries in sector 3 and the number of total entries in N arm expressed as percentage **(D)**, time spent in N arm expressed as percentage of the total time **(E, F)** are represented. Data are shown as mean ± SEM and analysed by two-way ANOVA with a post hoc test that utilizes a Bonferroni correction. Test with $p \leq 0.05$ and $p \leq 0.01$ represented by * and ** respectively. Ç refers to the comparison T4 vs T1 at 18 °C with a $p \leq 0.05$ in a one-way ANOVA among values at 18 °C.

These data indicate that past experiences affect behaviour of control fish. Therefore, they suggest that fish memorise experience made in previous trials. Differently, fish acclimated at 18 °C and 34 °C continued to exhibit a scarce interest in the N arm also in the following trials (figure 49E, F). Their behaviour appears not to be modulated by past experiences and this may be related to an impairment of learning abilities due to thermal treatment. Both the extreme temperatures seem to induce a similar effect on the exploratory behaviour. However, it is interesting that the number of entries in sector 3 of the N arm (figure 49C) and the time spent in the N arm (figure 49F) showed higher values in T4 compared to T1 at 18 °C, while no differences were found at 34 °C. This result may suggest differences in behavioural effects of the exposure to 18 °C and 34 °C, as if specimens acclimated to 18 °C in T4 could recognize the N arm as a novel environment with a sort of delay in comparison to fish at 26 °C. Further studies will be devoted to deeply investigate physiological and behavioural differences between low and high temperature acclimation.

The GOBP, GOMF, GOCC and Pathway enrichment analysis showed a strong impact of environmental temperature on the brain proteome. Overall, present results suggest that, in adult ZF, the exposure at 18 °C and 34 °C for 21 days provokes detectable alterations in the brain proteome possibly causing functional alterations of the CNS which can impair the exploratory behaviour of the animal (figure 50).

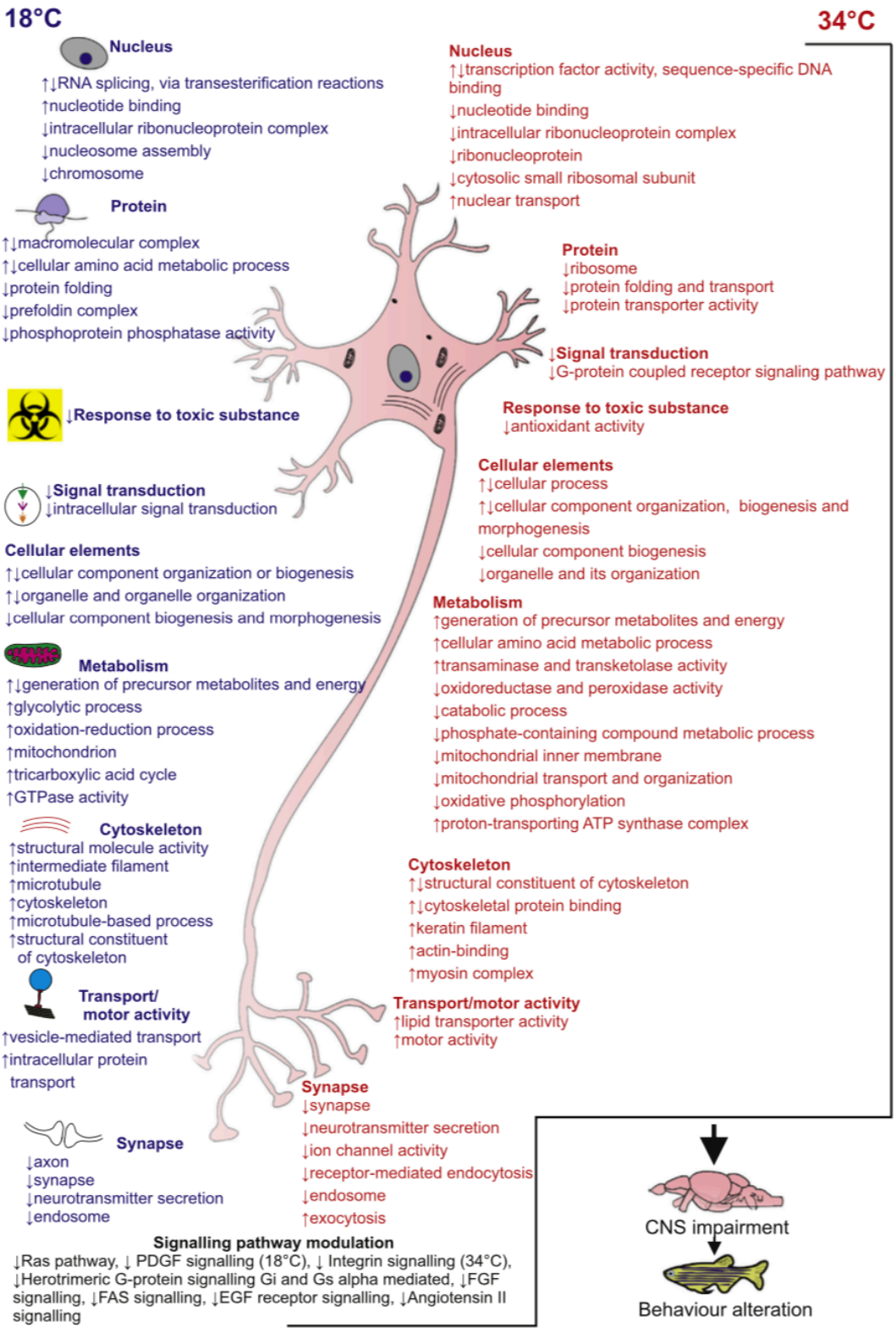

Figure 50 Schematic summary of Gene Ontology classification of brain proteins expressed after thermal treatment fully reported in Tables 2, 3. Down-regulation ↓, Up-regulation ↑ and general variation ↑↓ of proteins are reported at 18 °C on the left and at 34 °C on the right.

Both thermal extremes induce quantitative alterations of proteins associated with metabolism, cytoskeleton organization and cellular transport suggesting a strong impact of environmental temperature on the cytoarchitecture and the energy state of the brain. In particular, the reduced expression of synaptic proteins and the down-regulation of pathways positively correlated to cognitive functions in fish acclimated to 18 °C and 34 °C, suggest that thermal treatment may alter the animal's cognitive abilities. This alteration is suggested by the Y-Maze tests in which the interest in novelties and spatial orientation abilities appear significantly reduced in specimens maintained at 18 °C and at 34 °C compared to controls.

The reduced interest in novelty at the extreme temperatures may be due to the compromised ability in recognizing the geometric figures that distinguish the Y-Maze arms. Thermal treatment may cause a stress condition that prevent or impair fish from distinguishing new objects and recognizing familiar from unfamiliar parts of the environment.

In conclusion, although temperatures tested fall within the ZF vital range, present results demonstrate that long term acclimation to extreme temperatures strongly influences brain protein expression and the exploratory behaviour of animals suggesting the impairment of some cognitive abilities. Under a global warming scenario such temperature-dependent cognitive alterations could seriously compromise the survival of wild fish in the long-term perspective.

4. CONCLUSIONS

Proteome is the entire complement of proteins, protein-protein interaction and post-translational modification within an organism. Since protein modifications, such as phosphorylation, acetylation, glycosylation and methylation, are state-dependent, the proteome is constantly changing in response to cellular cues. Proteomics involves the applications of technologies for the identification and quantification of overall proteins present content of a cell, tissue or an organism. It supplements the other "omics" technologies to expound the identity of proteins of an organism, and to cognize the structure and function of a particular protein [536]. The complexity of proteome could be elucidated thanks to the modern proteomics that benefits from the ability to assess the modification state of proteins directly. In this thesis I present three different projects in which, beside canonical biochemical techniques and a behavioural analysis, a shotgun label free proteomic approach is used to understand how change in protein expression or protein state could explain the results obtained or observed by other analytical methods.

In the first project the proteomic-based analysis defined nanotopography-sensitive signaling hubs and key elements potentially important in the promotion of neuronal differentiation by nanotopographical cues. It gives new information on the mechanotransductive signaling that regulates neuron development and maturation.

We found distinctive features in the protein expression and phosphorylation profiles comparing the canonical biochemically (NGF-)induced neuronal differentiation and the one triggered by the cell/nanotopography interaction. In this neuron-like PC12 cell model the mechanotransductive stimulus provided by an appropriate nanotopography is alone sufficient to achieve the necessary

change in the cellular program that implements the neuronal differentiation. There are indications in the phosphoproteomic data that the nanotopographical stimulus is even more effective.

In the second project, we confirmed that in N2a cells the GM1 neuroprotection, derives from a direct interaction between the GM1 oligosaccharide and the TrkA receptor, activating the following signaling cascade capable to overexpress specific neuroprotective proteins. Our results suggest that the oligosaccharide chain is the key molecular portion and the starting point for GM1- mediated protective function at the plasma membrane level. However more experimental work is needed to fully clarify the GM1 mechanism of action with respect to its potential.

And finally, thanks to proteomics used in combination to a behavioural approach, we were able to demonstrate that, in adult ZF, the exposure at 18 °C and 34 °C for 21 days provokes detectable alterations in the brain proteome possibly causing functional alterations of the CNS which can impair the exploratory behaviour of the animal. Further studies will be devoted to deeply investigate physiological and behavioural differences between low and high temperature acclimation.

BIBLIOGRAPHY

1. Zhu W, Smith JW, Huang CM. Mass spectrometry-based label-free quantitative proteomics. J Biomed Biotechnol. 2010;2010:840518. doi: 10.1155/2010/840518. Epub 2009 Nov 10
2. Washburn MP. Driving biochemical discovery with quantitative proteomics. Trends Biochem Sci. 2011 Mar;36(3):170-7. doi: 10.1016/j.tibs.2010.09.001. Epub 2010 Sep 27.
3. Etsuro E. Uemura. Foundamentals of Canine Nauroanatomy and Neoruphysiology, First Edition. 2015 John Wiley & Sons, Inc.
4. Joan S, Terry L J. The Basics of Brain Development Neuropsychol Rev (2010) 20:327–348"
5. Bystron I, Blakemore C, et al. Development of the human cerebral cortex: boulder committee revisited. Nature Reviews (2008). Neuroscience, 9(2), 110–122.
6. Stiles, J. The fundamentals of brain development: Integrating nature and nurture. (2008) Cambridge: MA, Harvard University Press.
7. Pakkenberg B, Gundersen HJ. Neocortical neuron number in humans: effect of sex and age. The Journal of Comparative Neurology (1997), 384(2), 312–320.
8. Morell P, Quarles RH. Basic Neurochemistry: Molecular, Cellular and Medical Aspects 6th edition. Characteristic Composition of Myelin. Siegel GJ, Agranoff BW, Albers RW, et al., editors. Philadelphia: Lippincott-Raven; 1999.
9. Molyneaux BJ, Arlotta P, et al. Neuronal subtype specification in the cerebral cortex. Nature Reviews. (2007) Neuroscience, 8(6), 427–437.
10. Brown M, Keynes R, et al. The developing brain. Oxford: Oxford University Press. (2001)
11. Sharma N, Classen J, Cohen LG. Neural plasticity and its contribution to functional recovery. Handb Clin Neurol. 2013;110:3–12. doi:10.1016/B978-0-444-52901-5.00001-0
12. Grefkes C, Nowak DA, Eickhoff SB, et al. Cortical connectivity after subcortical stroke assessed with functional magnetic resonance imaging. Ann Neurol. 2008; 63:236–246. [PubMed: 17896791]
13. Clarkson AN, Huang BS, Macisaac SE, et al. Reducing excessive GABA-mediated tonic inhibition promotes functional recovery after stroke. Nature. 2010; 468:305–309. [PubMed: 21048709]

14. Li S, Overman JJ, Katsman D, et al. An age-related sprouting transcriptome provides molecular control of axonal sprouting after stroke. Nat Neurosci. 2010; 13:1496–1504. [PubMed: 21057507]
15. Calford MB, Tweedale R. Immediate expansion of receptive fields of neurons in area 3b of macaque monkeys after digit denervation. Somatosens Mot Res. 1991b; 8:249–260. [PubMed: 1767621]
16. Liu HH, McClatchy DB, Schiapparelli L, Shen W, Yates III JR, Cline HT. Role of the visual experience-dependent nascent proteome in neuronal plasticity Elife. 2018 Feb 7;7. pii: e33420. doi: 10.7554/eLife.33420.
17. Toni M, Angiulli E, Miccoli G, Cioni C, Alleva E, Frabetti F, Pizzetti F, Grassi Scalvini F, Nonnis S, Negri A, Tedeschi G, Maffioli E. Environmental temperature variation affects brain protein expression and cognitive abilities in adult zebrafish (Danio rerio): a proteomic and behavioural study. Journal of Proteomics (2019). Accepted 24 May 2019
18. Maffioli E, Schulte C, Nonnis S, Grassi Scalvini F, Piazzoni C, Lenardi C, Negri A, Milani P, Tedeschi G. Proteomic Dissection of Nanotopography-Sensitive Mechanotransductive Signaling Hubs that Foster Neuronal Differentiation in PC12 Cells. Front Cell Neurosci. 2018 Jan 4;11:417 I.F 4,555;
19. Chiricozzi E, Maggioni M, di Biase E, Lunghi G, Fazzari M, Loberto N, Maffioli E, Grassi Scalvini F, Tedeschi G. The Neuroprotective Role of the GM1 Oligosaccharide, II3Neu5Ac-Gg4, in Neuroblastoma Cells. Mol Neurobiol. 2019 March 26 doi.org/10.1007/s12035-019-1556-8;
20. Wu CC, MacCoss MJ. Shotgun proteomics: tools for the analysis of complex biological systems. Curr. Opin. Mol. Ther. 2002, 4: 242– 250.
21. Langley RJ, Tsalik EL, van Velkinburgh JC, Glickman SW, Rice BJ, Wang C, Chen B, Carin L, Suarez A, Mohney RP, Freeman DH, Wang M, You J, Wulff J, Thompson JW, Moseley MA, Reisinger S, Edmonds BT, Grinnell B, Nelson DR, Dinwiddie DL, Miller NA, Saunders CJ, Soden SS, Rogers AJ, Gazourian L, Fredenburgh LE, Massaro AF, Baron RM, Choi AM, Corey GR, Ginsburg GS, Cairns CB, Otero RM, Fowler VG Jr, Rivers EP, Woods CW, Kingsmore SF.An integrated clinico-metabolomic model improves prediction of death in sepsis. Sci Transl Med. 2013, 24; 5(195):195ra95

22. Motoyama A, Yates JR III. Multidimensional LC separations in shotgun proteomics. Analytical Chemistry. 2008, vol.80, no.19, pp. 7187-7193.
23. Domon B, Aebersold R. Mass spectrometry and protein analysis. Science 2006, vol.312, no. 5771, pp. 212-217.
24. Washburn MP, Wolters D, Yates III JR. Large-scale analysis of the yeast proteome by multidimensional protein identification technology. Nature Biotechnology. 2001, vol. 19, no. 3, pp. 242–247.
25. Voyksner RD, Lee H. Investigation the use of an octupole ion guide for ion storage and high-pass mass filtering to improve the quantitative performance of electrospray ion trap mass spectrometry. Rapid communication in Mass Spectrometry. 1999, Vol.13, no.14, pp. 1427-1437.
26. Wiener MC, Sachs JR, Deyanova EG, Yates NA. Differential mass spectrometry: a label-free LC-MS method for finding significant differences in complex peptide and protein mixture. Analytical Chemistry. 2004, Vol.76, no.20, pp. 6085-6096.
27. Higgs RE, Knierman MD, Gelfanova V, Butler JP, Hale JE. Comprehensive label-free method for the relative quantification of proteins from biological samples. Journal of Proteome Research. 2005, Vol.4, no. 4, pp. 1442-1450.
28. Tamplenizza M, Lenardi C, Maffioli E, Nonnis S, Negri A, Forti S, Sogne E, De Astis S, Matteoli M, Schulte C, Milani P and Tedeschi G. (2013) Nitric oxide synthase mediates PC12 differentiation induced by the surface topography of nanostructured TiO_2. Journal of Nanobiotechnology.
29. Huang C, Borchers CH, Schaller MD, Jacobson K: Phosphorylation of paxillin by p38MAPK is involved in the neurite extension of PC12 cells. J Cell Biol 2004, 26:593–602.
30. Woo S, Gomez TM: Rac1 and RhoA promote neurite outgrowth through formation and stabilization of growth come point contacts. J Neurosci 2006, 27:730–742.
31. D'Arcandelo G, Halegoua S: A branched signaling pathway for nerve growth factor is revealed by Src-, Ras-, and Raf-mediated gene inductions. Mol Cell Biol 1993, 13:3146 3155.
32. Klesse LJ, Meyers KA, Marshall CJ, Para LF: Nerve growth factor induces survival and differentiation through two distinct signaling cascades in PC12 cells. Oncogene 1999, 18:2055–2068.

33. Rakhit S, Pyne S, Pyne NJ: Nerve growth factor stimulation of p42/p44 mitogen activated protein kinase in PC12 cells: Role of G(i/o), G protein –coupled receptor kinase 2, beta-arrestin I, and endocytic processing. Mol Pharmacol 2001, 60:63–70.
34. Waetzig V, Herdegen T: The concerted signaling of ERK1/2 and JNKs is essential for PC12 cell neuritogenesis and converges at the level of target proteins. Mol Cell Neurosci 2003, 24:238–249.
35. Peunova N, Enikolopov G: Nitric oxide triggers a switch to growth arrest during differentiation of neuronal cells. Nature 1995, 375:68–73.
36. Yamazaki M, Chiba K, Mohri T: Fundamental role of nitric oxide in neuritogenesis of PC12. h cells. Br J Pharmacol 2005, 146:662–669.
37. Gerdin MJ, Eiden LE: Regulation of PC12 cell differentiation by cAMP signaling to ERK independent of PKA: do all the connections add up? Sci STKE 2007, 382:pe15.
38. Lutolf MP, Hubbell JA: Synthetic biomaterials as instructive extracellular microenvironments for morphogenesis in tissue engineering. Nat Biotechnol 2005, 23:47–55.
39. Kleinman HK, Philp D, Hoffman MP: Role of the extracellular matrix in morphogenesis. Curr Opin Biotechnol 2003, 14:526–532.
40. Chen C, Jiang X: Microengineering the environment of mammalian cells in culture. MRS Bull 2005, 30:194–201.
41. Wheeldon I, Farhadi A, Bick AG, Jabbari E, Khademhosseini A: Nanoscale tissue engineering: spatial control over cell-materials interactions. Nanotechnology 2011, 22:212001.
42. Abrams GA, Goodman SL, Nealey PF, Franco M, Murphy CJ: Nanoscale topography of the basement membrane underlying the corneal epithelium of the rhesus macaque. Cell Tissue Res 2000, 299:39–46.
43. Dalby MJ, Riehle MO, Johnstone H, Affrossman S, Curtis AS: In vitro reaction of endothelial cells to polymer demixed nanotopography. Biomaterials 2002, 23:2945–2954.
44. Andersson AS, Backhed F, Von Euler A, Richter-Dahlfors A, Sutherland D, Kasemo B: Nanoscale features influence epithelial cell morphology and cytokine production. Biomaterials 2003, 24:3427–3436.

45. Thapa A, Webster TJ, Haberstroh KM: Polymers with nano-dimensional surface features enhance bladder smooth muscle cell adhesion. J Biomed Mater Res 2003, 67:1374–1383.
46. Dalby MJ, Gadegaard N, Riehle MO, Wilkinson CD, Curtis AS: Investigating filopodia sensing using arrays of defined nano-pits down to 35 nm diameter in size. Int J Biochem Cell Biol 2004, 36:2015–2025.
47. Dalby MJ, Riehle MO, Johnstone HJ, Affrossman S, Curtis AS: Polymer-demixed nanotopography: control of fibroblast spreading and proliferation. Tissue Eng 2002, 8:1099–1108.
48. Humphries J.D, Paul N.R, Humphries M.J, and Morgan M.R: Emerging properties of adhesion complexes: what are they and what do they do? Trends in Cell Biology July 2015, Vol. 25, No. 7.
49. Dityatev A, Seidenbecher CI, Schachner M. Compartmentalization from the outside: the extracellular matrix and functional microdomains in the brain. Trends Neurosci. 2010, 33:503–12
50. Ruoslahti E. Brain extracellular matrix. Glycobiology 1996, 6:489–92
51. Veznedaroglu E, Van Bockstaele EJ, O'ConnorMJ. Extravascular collagen in the human epileptic brain: a potential substrate for aberrant cell migration in cases of temporal lobe epilepsy. J. Neurosurg. 2002, 97:1125–30
52. Comley K, Fleck NA. A micromechanical model for the Young's modulus of adipose tissue. Int. J. Solids Struct. 2010, 47:2982–90
53. Yamaguchi Y. Lecticans: organizers of the brain extracellular matrix. Cell. Mol. Life Sci. 2000, 57:276–89
54. Georges PC, Miller WJ, Meaney DF, Sawyer ES, Janmey PA. Matrices with compliance comparable to that of brain tissue select neuronal over glial growth in mixed cortical cultures. Biophys. J. 2006, 90:3012–18
55. Keung AJ, Asuri P, Kumar S, Schaffer DV. Soft microenvironments promote the early neurogenic differentiation but not self-renewal of human pluripotent stem cells. Integr. Biol. 2012, 4:1049–58
56. Her GJ, Wu HC, Chen MH, Chen MY, Chang SC, Wang TW. Control of three-dimensional substrate stiffness to manipulate mesenchymal stem cell fate toward neuronal or glial lineages. Acta Biomater. 2013, 9(2):5170–80

57. Ju YE, Janmey PA, McCormick ME, Sawyer ES, Flanagan LA. Enhanced neurite growth from mammalian neurons in three-dimensional salmon fibrin gels. Biomaterials 2007, 28:2097–108
58. Matyash M, Despang F, Mandal R, Fiore D, Gelinsky M, Ikonomidou C. Novel soft alginate hydrogel strongly supports neurite growth and protects neurons against oxidative stress. Tissue Eng. Part A 2012, 18:55–66
59. Sharp KG, Dickson AR, Marchenko SA, Yee KM, Emery PN, et al. Salmon fibrin treatment of spinal cord injury promotes functional recovery and density of serotonergic innervation. Exp. Neurol. 2012, 235:345–56
60. Khaing ZZ, Milman BD, Vanscoy JE, Seidlits SK, Grill RJ, Schmidt CE. High molecular weight hyaluronic acid limits astrocyte activation and scar formation after spinal cord injury. J. Neural Eng. 2011, 8:046033
61. Crapo PM, Medberry CJ, Reing JE, Tottey S, van derMerwe Y, et al. Biologic scaffolds composed of central nervous system extracellular matrix. Biomaterials 2012, 33:3539–47
62. Evolution of Cell Culture Surfaces By: John A. Ryan, BioFiles 2008, 3.8, 21
63. Jaiswal N, Haynesworth SE, Caplan AI, Bruder SP. Osteogenic differentiation of purified, cultureexpanded human mesenchymal stem cells in vitro. J Cell Biochem 1997, 64(2):295–312.
64. Schnaper HW, Grant DS, Stetlerstevenson WG, Fridman R, Dorazi G, Murphy AN, Bird RE, Hoythya M, Fuerst TR, French DL, Quigley JP, Kleinman HK. Type IV collagenase(s) and TIMPs modulate endothelial cell morphogenesis in vitro. J Cell Physiol 1993, 156(2):235–246.
65. Engler AJ, Sen S, Sweeney HL, Discher DE. Matrix elasticity directs stem cell lineage specification. Cell 2006, 126(4):677–689.
66. Chen CS, Mrksich M, Huang S, Whitesides GM, Ingber DE. Geometric control of cell life and death. Science 1997, 276(5317):1425–1428.
67. Zhang, S.; Zhao, X.; Spirio, L. PuraMatrix: Self-assembling peptide nanofiber scaffolds. In: Ma, PX.; Elisseeff, J., editors. Scaffolding in tissue engineering. Boca Raton, FL: CRC Press; 2005, p.217-238.
68. Gieni RS, Hendzel MJ. Mechanotransduction from the ECM to the genome: Are the pieces now in place? J Cell Biochem 2008, 104(6):1964–1987.
69. Ashe HL, Briscoe J. The interpretation of morphogen gradients. Development 2006, 133(3):385–394.

70. Le Beyec J, Xu R, Lee SY, Nelson CM, Rizki A, Alcaraz J, Bissell MJ. Cell shape regulates global histone acetylation in human mammary epithelial cells. Exp Cell Res 2007, 313(14):3066–3075.
71. Birgersdotter A, Sandberg R, Ernberg I. Gene expression perturbation in vitro—A growing case for three-dimensional (3D) culture systems. Semin Cancer Biol 2005, 15(5):405–412.
72. Bell E, Ehrlich HP, Buttle DJ, Nakatsuji T. Living tissue formed in vitro and accepted as skin-equivalent tissue of full thickness. 1981, Science 211, 1052–1054.
73. Yannas IV, Lee E, Orgill DP, Skrabut EM, Murphy GF. Synthesis and characterization of a model extracellular matrix that induces partial regeneration of adult mammalian skin. Proc. Natl. Acad. Sci. USA 86 1989, 933–937.
74. Patino MG, Neiders ME, Andreana S, Noble B, Cohen RE. Collagen as an implantable material in medicine and dentistry. J. Oral Implantol. 28 2002, 220–225.
75. Currie LJ, Sharpe JR, Martin R. The use of fibrin glue in skin grafts and tissue-engineered skin replacements: A review. Plast. Reconstr. Surg. 108 2001, 1713–1726.
76. Hubbell JA. Bioactive biomaterials. Curr. Opin. Biotechnol. 10 1999, 123–129.
77. Griffith LG. Emerging design principles in biomaterials and scaffolds for tissue engineering. Ann. N. Y. Acad. Sci. 961 2002, 83–95.
78. Holmes TC et al. Extensive neurite outgrowth and active synapse formation on self-assembling peptide scaffolds. Proc. Natl. Acad. Sci. USA 97 2000, 6728–6733.
79. Kisiday J et al. Self-assembling peptide hydrogel fosters chondrocyte extracellular matrix production and cell division: Implications for cartilage tissue repair. Proc. Natl. Acad. Sci. USA 99 2002, 9996–10001.
80. Semino CE, Merok JR, Crane GG, Panagiotakos G, Zhang S. Functional differentiation of hepatocyte-like spheroid structures from putative liver progenitor cells in three-dimensional peptide scaffolds. Differentiation 71 2003, 262–270.
81. Butcher JT, Nerem RM. Porcine aortic valve interstitial cells in three-dimensional culture: Comparison of phenotype with aortic smooth muscle cells. J Heart Valve Dis 2004, 13:478–485.
82. Eyrich D, Brandl F, Appel B, Wiese H, Maier G, Wenzel M, Staudenmaier R, Goepferich A, Blunk T. Long-term stable fibrin gels for cartilage engineering. Biomaterials 2007, 28(1):55–65.

83. Masters KS, Shah DN, Walker G, Leinwand LA, Anseth KS. Designing scaffolds for valvular interstitial cells: Cell adhesion and function on naturally derived materials. J Biomed Mater Res A 2004, 71(1):172–180.
84. Azab AK, Orkin B, Doviner V, Nissan A, Klein M, Srebnik M, Rubinstein A. Crosslinked chitosan implants as potential degradable devices for brachytherapy: In vitro and in vivo analysis. J Control Release 2006, 111(3):281–289.
85. Barralet JE, Wang L, Lawson M, Triffitt JT, Cooper PR, Shelton RM. Comparison of bone marrow cell growth on 2D and 3D alginate hydrogels. J Mater Sci Mater Med 2005, 16:515–519.
86. Dawson E, Mapili G, Erickson K, Taqvi S, Roy K. Biomaterials for stem cell differentiation. Adv Drug Deliv Rev 2008, 60(2):215–228.
87. Cushing MC, Anseth KS. Hydrogel cell cultures. Science 2007, 316(5828):1133–1134.
88. Sawhney AS, Pathak CP, Hubbell JA. Bioerodible hydrogels based on photopolymerized poly(ethylene glycol)-co-poly(a-hydroxy acid) diacrylate macromers. Macromolecules 1993, 26(4):581–587.
89. Martens P, Anseth KS. Characterization of hydrogels formed from acrylate modified poly(vinyl alcohol) macromers. Polymer 2000, 41(21):7715–7722.
90. Chirila TV, Constable IJ, Crawford GJ, Vijayasekaran S, Thompson DE, Chen YC, Fletcher WA, Griffin BJ. Poly(2-hydroxyethel methacrylate) sponges as implant materials: In vivo and in vitro evaluation of cellular invasion. Biomaterials 1993, 14(1):26–38.
91. Bryant SJ, Anseth KS. Hydrogel properties influence ECM production by chondrocytes photoencapsulated in poly(ethylene glycol) hydrogels. J Biomed Mater Res 2002, 59(1):63–72.
92. Massia SP, Hubbell JA. An RGD spacing of 440 nm is sufficient for integrin alpha v beta 3-mediated fibroblast spreading and 140 nm for focal contact and stress fiber formation. J. Cell Biol. 1991, 114, 1089–1100.
93. DiMilla PA, Barbee K, Lauffenburger DA. Mathematical model for the effects of adhesion and mechanics on cell migration speed. Biophys. J. 1991, 60, 15–37.

94. Palecek SP, Loftus JC, Ginsberg MH, Lauffenburger DA, Horwitz AF. Integrin-ligand binding properties govern cell migration speed through cell-substratum adhesiveness. Nature 1997, 385, 537–540.

95. Kuntz RM, Saltzman WM. Neutrophil motility in extracellular matrix gels: Mesh size and adhesion affect speed of migration. Biophys. J. 1997, 72, 1472–1480.

96. Burgess BT, Myles JL, Dickinson RB. Quantitative analysis of adhesion-mediated cell migration in three-dimensional gels of RGD-grafted collagen. Ann. Biomed. 2000, Eng. 28, 110–118.

97. Schense JC, Hubbell JA. Three-dimensional migration of neurites is mediated by adhesion site density and affinity. J. Biol. Chem. 2000, 275, 6813–6818.

98. Gobin AS, West JL. Cell migration through defined, synthetic ECM analogs. FASEB J. 2002, 16, 751–753.

99. Maheshwari G, Brown G, Lauffenburger DA, Wells A, Griffith LG. Cell adhesion and motility depend on nanoscale RGD clustering. J. Cell Sci. 2000, 113, 1677–1686.

100. Irvine DJ, Hue KA, Mayes AM, Griffith LG. Simulations of cell-surface integrin binding to nanoscale-clustered adhesion ligands. Biophys. J. 2002, 82, 120–132.

101. Brandley BK, Schnaar RL. Tumor cell haptotaxis on covalently immobilized linear and exponential gradients of a cell adhesion peptide. Dev. Biol. 1989, 135, 74–86.

102. Maheshwari G, Wells A, Griffith LG, Lauffenburger DA. Biophysical integration of effects of epidermal growth factor and fibronectin on fibroblast migration. Biophys. J. 1999, 76, 2814–2823.

103. Koo LY, Irvine DJ, Mayes AM, Lauffenburger DA, Griffith LG. Co-regulation of cell adhesion by nanoscale RGD organization and mechanical stimulus. J. Cell Sci. 2002, 115, 1423–1433.

104. Zisch AH, Schenk U, Schense JC, Sakiyama-Elbert SE, Hubbell JA. Covalently conjugated VEGF–fibrin matrices for endothelialization. J. Control. 2001, Release 72, 101–113.

105. Silva GA et al. Selective differentiation of neural progenitor cells by high-epitope density nanofibers. Science 2004, 303, 1352–1355.

106. Zhang S. Fabrication of novel biomaterials through molecular self-assembly. Nat. Biotechnol. 2003, 21, 1171–1178.

107. Lutolf MP, Raeber, G.P., Zisch, A.H., Tirelli, N. & Hubbell, J.A. Cell-responsive synthetic hydrogels. Advanced Materials 2003, 15, 888–892.

108. van Hest JC, Tirrell DA. Protein-based materials, toward a new level of structural control. Chem Commun (Cams) 2001, 1897–1904 ().

109. Urry DW. Elastic molecular machines in metabolism and soft-tissue restoration. Trends Biotechnol. 17, 249–257 (1999).

110. Kopecek J. Smart and genetically engineered biomaterials and drug delivery systems. Eur. J. Pharm. Sci. 20, 1–16 (2003).

111. Liu JC, Heilshorn SC, Tirrell DA. Comparative cell response to artificial extracellular matrix proteins containing the RGD and CS5 cell-binding domains. Biomacromolecules 5, 497–504 (2004).

112. Halstenberg S, Panitch A, Rizzi S, Hall H, Hubbell JA. Biologically engineered protein-graft-poly(ethylene glycol) hydrogels: A cell adhesive and plasmindegradable biosynthetic material for tissue repair. Biomacromolecules 2002, 3,710–723.

113. Welsh ER, Tirrell DA. Engineering the extracellular matrix: A novel approach to polymeric biomaterials. I. Control of the physical properties of artificial protein matrices designed to support adhesion of vascular endothelial cells. Biomacromolecules 2000, 1, 23–30.

114. Urry DW et al. Elastic protein-based polymers in soft tissue augmentation and generation. J. Biomater. Sci. Polym. 1998, Ed. 9, 1015–1048.

115. Petka WA, Harden JL, McGrath KP, Wirtz D, Tirrell DA. Reversible hydrogels from self-assembling artificial proteins. Science 1998, 281, 389–392.

116. Roduner E. Size matters: why nanomaterials are different. Chemical Society Reviews 2006, 35(7):583–592.

117. Li H, Liu S, Dai Z, Bao J, Yang X. Applications of nanomaterials in electrochemical enzyme biosensors. Sensors 2009, 9(11):8547–8561.

118. Hasanzadeh M, Shadjou N, de la Guardia M, Eskandani M, Sheikhzadeh P, Mesoporous silica-based materials for use in biosensors. TrAC Trends in Analytical Chemistry 2012, 33:117–129.

119. Sagadevan S, Periasamy M. Recent trends in nanobiosensors and their applications-a review. Rev. Adv. Mater. Sci 2014, 36:62–69.

120. Hrapovic S, Liu Y, Male KB, Luong JHT. Electrochemical biosensing platforms using platinum nanoparticles and carbon nanotubes. Analytical chemistry 2004, 76(4):1083–1088.

121. Li Y, Schluesener HJ, Xu S. Gold nanoparticle-based biosensors. Gold Bulletin 2010, 43(1):29–41.

122. Biju V. Chemical modifications and bioconjugate reactions of nanomaterials for sensing, imaging, drug delivery and therapy. Chemical Society Reviews 2014, 43(3):744–764.

123. Wijaya E, Lenaerts C, Maricot S, Hastanin J, Habraken S, Vilcot JP, Boukherroub R, Szunerits S. Surface plasmon resonance-based biosensors: from the development of di↵erent SPR structures to novel surface functionalization strategies. Current Opinion in Solid State and Materials Science 2011, 15(5):208–224.

124. Guo X. Surface plasmon resonance based biosensor technique: A review. Journal of Biophotonics 2012, 5(7):483–501.

125. Kelly KL, Coronado E, Zhao LL, Schatz GC. The optical properties of metal nanoparticles: the influence of size, shape, and dielectric environment. The Journal of Physical Chemistry B 2003, 107(3):668–677.

126. Reynolds RA, Mirkin CA, Letsinger RL. Homogeneous, nanoparticle based quantitative colorimetric detection of oligonucleotides. Journal of the American Chemical Society 2000, 122(15):3795–3796.

127. Xu W, Xue X, Li T, Zeng H, Liu X. Ultrasensitive and selective colorimetric DNA detection by nicking endonuclease assisted nanoparticle amplification. Angewandte Chemie International Edition 2009, 48(37):6849–6852.

128. Oldenburg SJ, Genick CC, Clark KA, Schultz DA. Base pair mismatch recognition using plasmon resonant particle labels. Analytical Biochemistry, 2002, 309(1):109–116.

129. Liu J, Lu Y. Colorimetric biosensors based on DNAzyme-assembled gold nanoparticles. Journal of Fluorescence 2004, 14(4):343–354.

130. He X, Huo H, Wang K, Tan W, Gong P, Ge J. Plasmid DNA isolation using amino-silica coated magnetic nanoparticles (ASMNPs). Talanta 2007, 73(4):764–769.

131. Li K, Lai Y, Zhang W, Jin L. Fe_2O_3 Au core/shell nanoparticle-based electrochemical DNA biosensor for Escherichia coli detection. Talanta, 2011, 84(3):607–613.

132. Min JH, Woo MK, Yoon HY, Jang JW, Wu JH, Lim CS, Kim YK. Isolation of DNA using magnetic nanoparticles coated with dimercaptosuccinic acid. Analytical Biochemistry 2014, 447:114–118.

133. Tamanaha CR, Mulvaney SP, Rife JC, Whitman LJ. Magnetic labeling, detection, and system integration. Biosensors and Bioelectronics 2008, 24(1):1–13.

134. Mujika M, Arana S, Castano E, Tijero M, Vilares R, Ruano-Lopez JM, Cruz A, Sainz L, Berganza J. Magnetoresistive immunosensor for the detection of Escherichia coli O157: H7 including a microfluidic network. Biosensors and Bioelectronics 2009, 24(5):1253–1258.

135. Liebana S, Lermo A, Campoy S, Barb´e J, Alegret S, Pividori MI. Magneto immunoseparation of pathogenic bacteria and electrochemical magneto genosensing of the double-tagged amplicon. Analytical Chemistry 2009, 81(14):5812–5820.

136. Battigelli A, M´enard-Moyon C, Da Ros T, Prato M, Bianco A. Endowing carbon nanotubes with biological and biomedical properties by chemical modifications. Advanced Drug Delivery Reviews 2013, 65(15):1899–1920.

137. M´enard-Moyon C, Kostarelos K, Prato M, Bianco A. Functionalized carbon nanotubes for probing and modulating molecular functions. Chemistry & Biology 2010 17(2):107–115.

138. Wang J. Carbon-nanotube based electrochemical biosensors: A review. Electroanalysis 2005, 17(1):7–14.

139. Le Goff A, Holzinger M, Cosnier S. Enzymatic biosensors based on SWCNT conducting polymer electrodes. Analyst 2011, 136(7):1279–1287.

140. Pandey P, Datta M, Malhotra BD. Prospects of nanomaterials in biosensors. Analytical Letters 2008, 41(2):159–209.

141. Singh SP, Arya SK, Pandey P, Malhotra BD, Saha S, Sreenivas K, Gupta V. Cholesterol biosensor based on rf sputtered zinc oxide nanoporous thin film. Applied Physics Letters 2007, 91(6):063901–063901.

142. Liu J, Li Y, Huang X, Zhu Z. Tin oxide nanorod array-based electrochemical hydrogen peroxide biosensor. Nanoscale Research Letters 2010, 5(7):1177–1181.

143. Gupta AK, Gupta M. Synthesis and surface engineering of iron oxide nanoparticles for biomedical applications. Biomaterials 2005, 26(18):3995–4021.

144. Solanki PR, Kaushik A, Agrawal VV, Malhotra BD. Nanostructured metal oxide-based biosensors. NPG Asia Materials 2011, 3(1):17–24.

145. Martin JY, Dean DD, Cochran DL, Simpson J, Boyan BD, Schwartz Z. Proliferation, differentiation, and protein synthesis of human osteoblast-like cells (MG63) cultured on previously used titanium surfaces. Clin Oral Implants Res 1996, 7(1):27–37.

146. Long M, Rack HJ. Titanium alloys in total joint replacement–a materials science perspective. Biomaterials 1998, 19(18):1621–39.

147. Brunette D, Tengvall P, Textor M, Thomsen P. editors. Titanium in medicine: material science, surface science, engineering, biological responses and medical applications. Berlin: Springer, 2001.

148. Lee CJ, Blumenkranz MS, Fishman HA, Bent SF. Controlling cell adhesion on human tissue by soft lithography. Langmuir 2004, 20(10): 4155–61.

149. Diehl KA, Foley JD, Nealey PF, Murphy CJ. Nanoscale topography modulates corneal epithelial cell migration. J Biomed Mater Res A 2005, 75(3):603–11.

150. Carbone R, Marangi I, Zanardi A, Giorgetti L, Chierici E, Berlanda G, Podestà A, Fiorentini F, Bongiorno G, Piseri P, Pelicci PG, Milani P. Biocompatibility of cluster-assembled nanostructured TiO2 with primary and cancer cells. Biomaterials. 2006 ,27(17):3221-9.

151. Manicone PF, Iommetti PR, Raffaelli L. An overview of zirconia ceramics: basic properties and clinical applications. J Dent. 2007;35:819–26.

152. Wegner K, Piseri P, Tafreshi HV, Milani P. Cluster beam deposition: a tool for nanoscale science and technology. J Phys Appl Phys. 2006;39:R439.

153. Schulte C, Rodighiero S, Cappelluti MA, Puricelli L, Maffioli E, Borghi F, Negri A, Sogne E, Galluzzi M, Piazzoni C, Tamplenizza M, Podestà A, Tedeschi G, Lenardi C, Milani P. Conversion of

nanoscale topographical information of cluster-assembled zirconia surfaces into mechanotransductive events promotes neuronal differentiation. J Nanobiotechnology. 2016 Mar 9;14:18.

154. Podestà A, Borghi F, Indrieri M, Bovio S, Piazzoni C, Milani P.. Nanomanufacturing of titania interfaces with controlled structural and functional properties by supersonic cluster beam deposition. J. Appl. Phys. (2015) 118:234309. doi: 10.1063/1.4937549

155. Liu Y, Medda R, Liu Z, Galior K, Yehl K, Spatz JP, et al. Nanoparticle tension probes patterned at the nanoscale: impact of integrin clustering on force transmission. Nano Lett. 2014.

156. Dalby MJ, Gadegaard N, Oreffo ROC. Harnessing nanotopography and integrin-matrix interactions to influence stem cell fate. Nat Mater.2014;13:558–69.

157. Geiger B, Spatz JP, Bershadsky AD. Environmental sensing through focal adhesions. Nat Rev Mol Cell Biol. 2009;10:21–33.

158. Chen W, Shao Y, Li X, Zhao G, Fu J. Nanotopographical surfaces for stem cell fate control: Engineering mechanobiology from the bottom. Nano Today. 2014.

159. Gardel ML, Schneider IC, Aratyn-Schaus Y, Waterman CM. Mechanical integration of actin and adhesion dynamics in cell migration. Annu Rev Cell Dev Biol. 2010;26:315–33.

160. Klein R, Jing SQ, Nanduri V, O'Rourke E, Barbacid M. The trk proto-oncogene encodes a receptor for nerve growth factor. Cell. 1991;65:189–97.

161. Wang N, Tytell JD, Ingber DE. Mechanotransduction at a distance: mechanically coupling the extracellular matrix with the nucleus. Nat Rev Mol Cell Biol. 2009;10:75–82.

162. Iskratsch T, Wolfenson H, Sheetz MP. Appreciating force and shape – the rise of mechanotransduction in cell biology. Nat Rev Mol Cell Biol. 2014.

163. Franze K, Janmey PA, Guck JG. Mechanics in Neuronal Development and Repair Annual Reviewof Biomedical Engineering, 2013.

164. Chen CS. Mechanotransduction — a field pulling together? J. Cell Sci. 2008 121 , 3285–3292.

165. DuFort CC, Paszek MJ, Weaver VM. Balancing forces: architectural control of mechanotransduction. Nature reviews Molecular cell biology, 12(5):308–319, 2011. I.1.2, I.2

166. Jaalouk DE, Lammerding J. Mechanotransduction gone awry. Nature Rev. Mol. Cell Biol. 2009 10 , 63–73.

167. Vogel V, Sheetz MP. Cell fate regulation by coupling mechanical cycles to biochemical signaling pathways. Curr. Opin. Cell Biol. 2009 21 , 38–46.

168. Geblinger D, Addadi L, Geiger B. Nanotopography sensing by osteoclasts. J. Cell Sci. 2010 123, 1503–1510.

169. Cavalcanti-Adam EA, et al. Cell spreading and focal adhesion dynamics are regulated by spacing of integrin ligands. Biophys. 2007 J. 92, 2964–2974

170. Arnold M et al. Induction of cell polarization and migration by a gradient of nanoscale variations in adhesive ligand spacing. Nano Lett. 2008 8, 2063–2069.

171. Pelham RJ Jr, Wang Y. Cell locomotion and focal adhesions are regulated by substrate flexibility. Proc. Natl Acad. Sci. 1997, 13661–13665.

172. Tan W, Oldenburg AL, Norman JJ, Desai TA, Boppart SA. Optical coherence tomography of cell dynamics in three-dimensional tissue models. Opt. Express 14 2006, 7159–7171.

173. Friedl P, Brocker EB. The biology of cell locomotion within three-dimensional extracellular matrix. Cell. Mol. Life Sci. 2000 57, 41–64.

174. Doyle AD, Wang FW, Matsumoto K, Yamada KM. One-dimensional topography underlies three-dimensional fibrillar cell migration. J. Cell Biol. 2009 184, 481–490.

175. Cukierman E, Pankov R, Stevens DR, Yamada KM. Taking cell-matrix adhesions to the third dimension. Science 294 2001, 1708–1712.

176. Ochsner M, Textor M, Vogel V, Smith ML. Dimensionality controls cytoskeleton assembly and metabolism of fibroblast cells in response to rigidity and shape. PLoS ONE 5 2010, e9445.

177. Weaver VM, et al. β4 integrin-dependent formation of polarized three-dimensional architecture confers resistance to apoptosis in normal and malignant mammary epithelium. Cancer Cell 2 2002, 205–216.

178. Sukharev S, Sachs F. Molecular force transduction by ion channels—diversity and unifying principles. J.Cell Sci. 2012, 125:3075–83.

179. Chalfie M. Neurosensory mechanotransduction. Nat. Rev.Mol. Cell Biol. 2009,10:44–52.

180. Franze K, Gerdelmann J, Weick M, Betz T, Pawlizak S, et al. Neurite b ranch retraction is caused by a t hreshold-dependent mechanical impact. Biophys. J. 2009 97:1883–90.

181. Hardie RC, Franze K. Photomechanical responses inDrosophila photoreceptors. Science 2012, 338:260–63.

182. Lee J, Ishihara A, Oxford G, Johnson B, Jacobson K. Regulation of cell movement is mediated by stretch-activated calcium channels. Nature 1999, 400:382–86

183. Gomez TM, Zheng JQ. The molecular basis for calcium-dependent axon pathfinding. Nat. Rev. Neurosci. 2006, 7:115–25

184. Orr AW, Helmke BP, Lackman BR, Schwartz MA. Mechanisms of mechanotransduction. Dev.Cell 2006, 10:11–20

185. Hynes RO. Integrins: bidirectional, allosteric signaling machines. Cell 2002, 110, 673–687.

186. Desgrosellier JS, Cheresh DA. Integrins in cancer: biological implications and therapeutic opportunities. Nat. Rev. Cancer 2010, 10, 9–22.

187. Avraamides CJ, Garmy-Susini B, Varner JA. Integrins in angiogenesis and lymphangiogenesis. Nat. Rev. Cancer 2008 8, 604–617.

188. Liu H et al. MYC suppresses cancer metastasis by direct transcriptional silencing ofα(v) andβ(3) integrin subunits. Nat. Cell Biol. 2012, 14, 567–574.

189. Humphries JD, Byron A, Humphries MJ. Integrin ligands at a glance. J. Cell Sci. 2006, 119, 3901–3903.

190. Yang JT, Rayburn H, Hynes RO. Embryonic mesodermal defects in α5 integrin-deficient mice. Development 1993, 119, 1093–1105 ().

191. Bader BL, Rayburn H, Crowley D, Hynes RO. Extensive vasculogenesis, angiogenesis, and organogenesis precede lethality in mice lacking allαv integrins. Cell 1998, 95, 507–519.

192. Yang JT et al. Overlapping and independent functions of fibronectin receptor integrins in early mesodermal development. Dev. Biol. 1999, 215, 264–277.

193. Zamir E et al. Dynamics and segregation of cell–matrix adhesions in cultured fibroblasts. Nat. Cell Biol. 2000, 2, 191–196.

194. Ballestrem C, Hinz B, Imhof BA, Wehrle-Haller B. Marching at the front and dragging behind: differential αvβ3-integrin turnover regulates focal adhesion behavior. J. Cell Biol. 2001, 155, 1319–1332.

195. Danen EH, Sonneveld P, Brakebusch C, Fassler R, Sonnenberg A. The fibronectin-binding integrins α5β1 and αvβ3 differentially modulate RhoA–GTP loading, organization of cell matrix adhesions, and fibronectin fibrillogenesis. J. Cell Biol. 2002, 159, 1071–1086.

196. White DP, Caswell PT, Norman JC. αvβ3 and α5β1 integrin recycling pathways dictate downstream Rho kinase signaling to regulate persistent cell migration. J. Cell Biol. 2007, 177, 515–525.

197. Morgan MR, Byron A, Humphries MJ, Bass MD. Giving off mixed signals-distinct functions of α(5)β(1) and α(v)β(3) integrins in regulating cell behaviour. IUBMB Life 2009,61, 731–738.

198. Van der Flier A et al. Endothelial α5 and αv integrins cooperate in remodeling of the vasculature during development. Development 2010, 137, 2439–2449 ().

199. Choi CK et al. Actin andα-actinin orchestrate the assembly and maturation of nascent adhesions in a myosin II motor-independent manner. Nat. Cell Biol. 2008, 10, 1039–1050.

200. Bershadsky A, Kozlov M, Geiger B. Adhesion-mediated mechanosensitivity: a time to experiment, and a time to theorize. Curr. Opin. Cell Biol. 2006, 18, 472–481.

201. Lobert VH et al. Ubiquitination of alpha 5 beta 1 integrin controls fibroblast migration thro ugh lysosomal degradation of fibronectin-integrin complexes. Dev. Cell 2010, 19, 148–1 59.

202. Hsia HC et al. The fate of internalize d alpha5 integrin is regulated by matrix-capable fibronectin. J. Surg. Res 2014, 191, 268–2 79.

203. Bottcher RT et al. Sorting nexin 17 prevents lysosomal degradation of b 1 integrins by binding to the b1-integrin tail. Nat.Cell Biol. 2012, 14, 584–592.

204. Steinberg F et al. SNX17 protects integrins from degradation by sorting between lysosomal and recycling pathways. J. Cell Biol. 2012, 197, 219–2 30.

205. Morgan MR et al. Syndeca n-4 phosphorylation is a control point for integrin recycling. Dev. Cell 2013, 24, 472–485.

206. Bass MD et al. A syndecan-4 hair trigger initiates wound healing thro ugh caveolin- and RhoG -regulated integrin endocytosis. Dev. Cell 2011, 21, 681–693.

207. Wolfenson H et al. Dynamic regulation of the structure and function s of integrin adhesion s. Dev. Cell 2013, 24, 447–458.

208. Morgan MR et al. Synergistic control of cell adhesion by integrins and syndecans. Nat. Rev. Mol. Cell Biol. 2007, 8, 957–9 69.

209. Campbel ID, Humphries MJ. Integrin structure, activation, and interactions. Cold Spring Harb. Perspect. Biol. 2011, 1–15.

210. Morse EM et al. Integrin cytoplasmic tail interactions. Biochemistry 2014, 53, 810–8 20.

211. Calderwood DA et al. Talins and kindlins: partners in integrin -mediated adhesion . Nat. Rev. Mol. Cell Biol. 2013, 14, 503–517.

212. Byron A et al. Adhesion signalling complexes. Curr. Biol. 2010, 20, R1063 –R1067.

213. Ross TD et al. Integrins in mechanotransduction. Curr. Opin. Cell Biol. 2013, 25, 613–618.

214. Schiller HB and Fassler R. Mechanosensitivity and compositional dynamics of cell-matrix adhesions. EMBO Rep. 2013, 14, 509–519.

215. Geiger B et al. Transmembrane crosstalk between the extracellular matrix- cytoskeleton crosstalk. Nat. Rev. Mol. Cell Biol. 2001, 2, 793-805.

216. Mammoto A, Mammoto T, Ingber DE. Mechanosensitive mechanisms in transcriptional regulation. J. CellSci. 2012, 125:3061–73.

217. Miralles F, Posern G, Zaromytidou AI, Treisman R. Actin dynamics control SRF activity by regulation of its coactivator MAL.Cell 2003, 113:329–42.

218. Kalita KK, Kuzniewska BB, Kaczmarek LL. MKLs: co-factors o f s erum response factor (SRF) in neuronal responses.Int.J. Biochem. CellBiol. 2012, 44:1444–47.

219. Dupont S, Morsut L, Aragona M, Enzo E, Giulitti S, et al. Role of YAP/TAZ in mechanotransduction. Nature 2011, 474:179–83.

220. Borghi F, Sogne E, Lenardi C, Podestà A, Merlini M, Ducati C, et al. (2016). Cluster-assembled cubic zirconia films with tunable and stable nanoscale morphology against thermal annealing. J. Appl. Phys. 120:055302. doi: 10.1063/1.4960441

221. Karas M, Hillenkamp F. Laser desorption ionization of proteins with molecular mass exceeding 10000 daltons. Anal. Chem. 1988, 60: 2299-2301.

222. Hillenkamp F, Karas M, Beavis RC, Chait BT. Matrix-assisted laser desorption/ionization mass spectrometry of biopolymers. Anal. Chem. 1991, 63: 1193A-1203A.

223. Fenn JB, Mann M, Meng CK, Wong SF, Whitehouse CM. Electrospray ionization for mass spectrometry of large biomolecules. Science. 1989, 246: 64-71.

224. Makarov A, Denisov E, Kholomeev A, Balschun W, Lange O, Strupat K, Horning S. Performance Evalutation of a Hybrid Linear Ion Trap/ Orbitrap Mass Spectrometer. Anal Chem. 2006, 78: 2113-2120.

225. Hu Q, Noll RJ, Li H, Makarov A, Hardman M, Graham Cooks R. The Orbitrap: a new mass spectrometer. J. Mass Spectrom. 2005, 40: 430-443.

226. Makarov A. Electrostatic axially harmonic orbitrap trapping: a high- performance technique of mass analysis. Anal.Chem. 2000, 72: 1156-1162.

227. Douglas DJ, Frank AJ, Mao D. Linear ion traps in mass spectrometry. Mass. Spectrom. Rev. 2005, 24: 1-29.

228. Hardman M, Makarov A. Cox J, Mann M. MaxQuant enables high peptide identification rates, individualized p.p.b.-range mass accuracies and proteome-wide protein quantification. Nat Biotechnol. 2008, 26 (12):1367-1372

229. Huang da W, Sherman BT, Lempicki RA. Bioinformatics enrichment tools: paths toward the comprehensive functional analysis of large gene lists. Nucleic Acids Res (2009).. 37, 1–13. doi: 10.1093/nar/gkn923

230. Mi H, Huang X, Muruganujan A, Tang H, Mills C, Kang D, et al. PANTHER version 11: expanded annotation data from Gene Ontology and Reactome pathways, and data analysis tool enhancements. Nucleic Acids Res (2017). 45, D183–D189. doi: 10.1093/nar/gkw1138

231. Launay S, Maubert E, Lebeurrier N, Tennstaedt A, Campioni M, Docagne F, et al. HtrA1-dependent proteolysis of TGF-beta controls both neuronal maturation and developmental survival. Cell Death Differ. (2008) 15, 1408–1416. doi: 10.1038/cdd.2008.82

232. Tennstaedt A, Pöpsel S, Truebestein L, Hauske P, Brockmann A, Schmidt N, et al. (2012). Human high temperature requirement serine protease A1 (HTRA1) degrades tau protein aggregates. J. Biol. Chem. 287, 20931–20941. doi: 10.1074/jbc.M111.316232

233. Wang CL, Tang FL, Peng Y, Shen CY, Mei L, Xiong WC. VPS35 regulates developing mouse hippocampal neuronal morphogenesis by promoting retrograde trafficking of BACE1. Biol. Open (2012)1, 1248–1257. doi: 10.1242/bio.20122451

234. Tang FL, Liu W, Hu JX, Erion JR, Ye J, Mei L, et al.. VPS35 deficiency or mutation causes dopaminergic neuronal loss by impairing mitochondrial fusion and function. Cell Rep (2015). 12, 1631–1643. doi: 10.1016/j.celrep.2015.08.001

235. Knobloch M, Braun SMG, Zurkirchen L, von Schoultz C, Zamboni N, Araúzo-Bravo MJ, et al.. Metabolic control of adult neural stem cell activity by Fasn-dependent lipogenesis. Nature (2013) 493, 226–230. doi: 10.1038/nature11689

236. Castillo V, Oñate M, Woehlbier U, Rozas P, Andreu C, Medinas D, et al.. Functional role of the Disulfide Isomerase ERp57 in Axonal Regeneration. PLOS ONE (2015). 10:e0136620. doi: 10.1371/journal.pone. 0136620

237. Bargsted L, Hetz C, Matus S. ERp57 in neurodegeneration and regeneration. Neural Regen. (2016) Res. 11, 232–233. doi: 10.4103/1673-5374.177722

238. Stevens B, Allen NJ, Vazquez LE, Howell GR, Christopherson KS, Nouri N, et al. The classical complement cascade mediates CNS synapse elimination. Cell (2007)131, 1164–1178. doi: 10.1016/j.cell.2007.10.036

239. Zhou L, Lim QE, Wan G, Too HP. Normalization with genes encoding ribosomal proteins but not GAPDH provides an accurate quantification of gene expressions in neuronal differentiation of PC12 cells. BMC Genomics (2010). 11:75. doi: 10.1186/1471-2164-11-75

240. Boyne LJ, Fischer I, Shea TB. Role of vimentin in early stages of neuritogenesis in cultured hippocampal neurons. Int. J. Dev. Neurosci (1996). 14, 739–748. doi: 10.1016/S0736-5748(96)00053-6

241. Cang Y, Zhang J, Nicholas SA, Bastien J, Li B, Zhou P, et al. Deletion of DDB1 in mouse brain and lens leads to p53-dependent elimination of proliferating cells. Cell (2006)127, 929–940. doi: 10.1016/j.cell.2006.09.045

242. Drinjakovic J, Jung H, Campbell DS, Strochlic L, Dwivedy A, Holt CE. E3 ligase Nedd4 promotes axon branching by downregulating PTEN. Neuron. (2010) 65, 341–357. doi: 10.1016/j.neuron.2010.01.017

243. Wiszniak S, Kabbara S, Lumb R, Scherer M, Secker G, Harvey N, et al. The ubiquitin ligase Nedd4 regulates craniofacial development by promoting cranial neural crest cell survival and stem-cell like properties. Dev. Biol. (2013) 383, 186–200. doi: 10.1016/j.ydbio.2013.09.024

244. Hsia HE, Kumar R, Luca R, Takeda M, Courchet J, Nakashima J, et al. Ubiquitin E3 ligase Nedd4-1 acts as a downstream target of PI3K/PTEN-mTORC1 signaling to promote neurite growth. Proc. Natl. Acad. Sci. (2014) U.S.A. 111, 13205–13210. doi: 10.1073/pnas.1400737111

245. Jiang H, Shukla A, Wang X, Chen W, Bernstein BE, Roeder RG. Role for Dpy-30 in ES cell-fate specification by regulation of H3K4 methylation within bivalent domains. Cell (2011) 144, 513–525. doi: 10.1016/j.cell.2011.01.020

246. Blanco S, Dietmann S, Flores JV, Hussain S, Kutter C, Humphreys P, et al. Aberrant methylation of tRNAs links cellular stress to neuro-developmental disorders. EMBO J. (2014) 33, 2020–2039. doi: 10.15252/embj.201489282

247. Hussain S, Bashir ZI. The epitranscriptome in modulating spatiotemporal RNA translation in neuronal post-synaptic function. Front. Cell Neurosci. (2015) 9:420. doi: 10.3389/fncel.2015.00420

248. Abraham AB, Bronstein R, Reddy AS, Maletic-Savatic M, Aguirre A, Tsirka SE. Aberrant neural stem cell proliferation and increased adult neurogenesis in mice lacking chromatin protein HMGB2. PloS ONE (2013) 8:e84838. doi: 10.1371/journal.pone.0084838

249. Han K, Yeo G, An P, Burge CB, Grabowski PJ. A combinatorial code for splicing silencing: UAGG and GGGG motifs. PLoS Biol. (2005) 3:e158. doi:10.1371/journal.pbio.0030158

250. Li Q, Lee JA, Black DL. Neuronal regulation of alternative pre-mRNA splicing. Nat. Rev. Neurosci. (2007) 8, 819–831. doi: 10.1038/nrn2237

251. Millán-Zambrano G, Chávez S. Nuclear functions of prefoldin. Open Biol. (2014) 4:140085. doi: 10.1098/rsob.140085

252. Katoh M. Function and cancer genomics of FAT family genes (review). Int. J. Oncol. (2012) 41, 1913–1918. doi: 10.3892/ijo.2012.1669

253. Zakaria S, Mao Y, Kuta A, de Sousa CF, Gaufo GO, McNeill H, et al. Regulation of neuronal migration by Dchs1-Fat4 planar cell polarity. Curr. Biol. (2014) 24, 1620–1627. doi: 10.1016/j.cub.2014.05.067

254. Ito T, Taniguchi H, Fukagai K, Okamuro S, Kobayashi A. Inhibitory mechanism of FAT4 gene expression in response to actin dynamics during Src-induced carcinogenesis. PloS ONE (2015) 10:e0118336. doi: 10.1371/journal.pone.0118336

255. Wu Y, Sheng W, Chen L, Dong H, Lee V, Lu F, et al. Versican V1 isoform induces neuronal differentiation and promotes neurite outgrowth. Mol. Biol. Cell (2004) 15, 2093–2104. doi: 10.1091/mbc.E03-09-0667

256. Paszek MJ, DuFort CC, Rossier O, Bainer R, Mouw JK, Godula K, et al. The cancer glycocalyx mechanically primes integrin-mediated growth and survival. Nature (2014) 511, 319–325. doi: 10.1038/nature13535

257. Goicoechea S, Orr AW, Pallero MA, Eggleton P, Murphy-Ullrich JE. Thrombospondin mediates focal adhesion disassembly through interactions with cell surface calreticulin. J. Biol. Chem. (2000) 275, 36358–36368. doi: 10.1074/jbc.M005951200

258. Adams JC, Kureishy N, Taylor AL. A role for syndecan-1 in coupling fascin spike formation by thrombospondin-1. J. Cell Biol. (2001) 152, 1169–1182. doi:10.1083/jcb.152.6.1169

259. Barker TH, Pallero MA, MacEwen MW, Tilden SG, Woods A, Murphy-Ullrich JE, et al. Thrombospondin-1-induced focal adhesion disassembly in fibroblasts requires Thy-1 surface expression, lipid raft integrity, and Src activation. J. Biol. Chem. (2004) 279, 23510–23516. doi: 10.1074/jbc.M402169200

260. Xu J, Xiao N, Xia J. Thrombospondin 1 accelerates synaptogenesis in hippocampal neurons through neuroligin 1. Nat. Neurosci. (2010). 13, 22–24. doi: 10.1038/nn.2459

261. Kawaguchi N, Sundberg C, Kveiborg M, Moghadaszadeh B, Asmar M, Dietrich N, et al. ADAM12 induces actin cytoskeleton and extracellular matrix reorganization during early adipocyte differentiation by regulating beta1 integrin function. J. Cell Sci. (2003) 116(Pt 19), 3893–904. doi: 10.1242/jcs.00699

262. Eckert MA, Santiago-Medina M, Lwin TM, Kim J, Courtneidge SA, Yang J. ADAM12 induction by TWIST1 promotes tumor invasion and metastasis via regulation of invadopodia and focal adhesions. J. Cell Sci. (2017)130, 2036-2048. doi:10.1242/jcs.198200

263. Tan CL, Kwok JC, Heller JP, Zhao R, Eva R, Fawcett JW. Full length talin stimulates integrin activation and axon regeneration. Mol. Cell Neurosci. (2015) 68:1–8. doi: 10.1016/j.mcn.2015.03.011

264. Schulte C, Ferraris GMS, Oldani A, Galluzzi M, Podestà A, Puricelli L, et al. Lamellipodial tension, not integrin/ligand binding, is the crucial factor to realise integrin activation and cell migration. Eur. J. Cell Biol. (2016c) 95, 1–14. doi: 10.1016/j.ejcb.2015.10.002

265. Voegel JJ, Heine MJ, Zechel C, Chambon P, Gronemeyer H. TIF2, a 160 kDa transcriptional mediator for the ligand- dependent activation function AF-2 of nuclear receptors. EMBO J. (1996) 15, 3667–3675.

266. Wyszynski M, Kim E, Dunah AW, Passafaro M, Valtschanoff JG, Serra-Pagès C, et al. Interaction between GRIP and liprin- alpha/SYD2 is required for AMPA receptor targeting. Neuron (2002) 34, 39–52. doi: 10.1016/S0896-6273(02)00640-2

267. Spangler SA, Hoogenraad CC. Liprin-alpha proteins: scaffold molecules for synapse maturation. Biochem. Soc. Trans. (2007) 35(Pt 5), 1278–1282. doi: 10.1042/BST0351278

268. Essmann CL, Martinez E, Geiger JC, Zimmer M, Traut MH, Stein V, et al.. Serine phosphorylation of ephrinB2 regulates trafficking of synaptic AMPA receptors. Nat. Neurosci. (2008) 11, 1035–1043. doi: 10.1038/nn.2171

269. Asperti C, Astro V, Totaro A, Paris S, de Curtis I. Liprin-alpha1 promotes cell spreading on the extracellular matrix by affecting the distribution of activated integrins. J. Cell Sci. (2009) 122(Pt 18), 3225–3232. doi: 10.1242/jcs. 054155

270. Asperti C, Pettinato E, de Curtis I. Liprin-alpha1 affects the distribution of low-affinity beta1 integrins and stabilizes their permanence at the cell surface. Exp. Cell Res. (2010) 316, 915–926. doi: 10.1016/j.yexcr.2010. 01.017

271. Selak S, Paternain AV, Aller MI, Aller IM, Picó E, Rivera R, et al. A role for SNAP25 in internalization of kainate receptors and synaptic plasticity. Neuron. (2009) 63, 357–371. doi: 10.1016/j.neuron.2009.07.017

272. Dasgupta S, Lonard DM, O'Malley BW. Nuclear receptor coactivators: master regulators of human health and disease. Annu. Rev. Med. (2014) 65, 279–292. doi: 10.1146/annurev-med-051812-145316"

273. Geiger JC, Lipka J, Segura I, Hoyer S, Schlager MA, Wulf PS, et al. The GRIP1/14-3-3 pathway coordinates cargo trafficking and dendrite development. Dev. Cell (2014) 28, 381–393. doi: 10.1016/j.devcel.2014.01.018

274. Heisler FF, Lee HK, Gromova KV, Pechmann Y, Schurek B, Ruschkies L, et al. GRIP1 interlinks N-cadherin and AMPA receptors at vesicles to promote combined cargo transport into dendrites. Proc. Natl. Acad. Sci. (2014) U.S.A. 111, 5030–5035. doi: 10.1073/pnas.1304301111"

275. Yudin D, Fainzilber M. Ran on tracks – cytoplasmic roles for a nuclear regulator. J. Cell Sci. (2009) 122, 587–593. doi: 10.1242/jcs.015289

276. Kennedy MJ, Davison IG, Robinson CG, Ehlers MD. Syntaxin- 4 defines a domain for activity-dependent exocytosis in dendritic spines. Cell (2010) 141, 524–535. doi: 10.1016/j.cell.2010.02.042

277. Mohanasundaram P, Shanmugam MM. Role of syntaxin 4 in activity-dependent exocytosis and synaptic plasticity in hippocampal neurons. Sci. Signal. (2010) 3:jc7. doi: 10.1126/scisignal.3144jc7

278. Heuser JE, Reese TS. Evidence for recycling of synaptic vesicle membrane during transmitter release at the frog neuromuscular junction. J. Cell Biol. (1973) 57, 315–344. doi: 10.1083/jcb.57.2.315

279. Cosker KE, Segal RA. Neuronal Signaling through Endocytosis. Cold Spring Harb Perspect Biol. (2014) 6:a020669. doi: 10.1101/cshperspect.a020669

280. Deng T, Zhu ZI, Zhang S, Leng F, Cherukuri S, Hansen L, et al. HMGN1 modulates Nucleosome occupancy and DNase I Hypersensitivity at the CpG island promoters of Embryonic stem cells. Mol. Cell Biol. (2013) 33, 3377–3389. doi: 10.1128/MCB.00435-13

281. Nagao M, Lanjakornsiripan D, Itoh Y, Kishi Y, Ogata T, Gotoh Y. High mobility group nucleosome-binding family proteins promote astrocyte differentiation of neural precursor cells. Stem Cells (2014) 32, 2983–2997. doi: 10.1002/stem.1787

282. Namadurai S, Yereddi NR, Cusdin FS, Huang CLH, Chirgadze DY, Jackson AP. A new look at sodium channel β subunits. Open Biol. (2015) 5:140192. doi:10.1098/rsob.140192

283. Schulte C, Ripamonti M, Maffioli E, Cappelluti MA, Nonnis S, Puricelli L, et al. Scale invariant disordered nanotopography promotes hippocampal neuron development and maturation with involvement of mechanotransductive pathways. Front. Cell Neurosci. (2016b) 10:267. doi: 10.3389/fncel.2016.00267

284. Mantamadiotis T, Lemberger T, Bleckmann SC, Kern H, Kretz O, Villalba AM, et al. Disruption of CREB function in brain leads to neurodegeneration. Nat. Genet. (2002) 31, 47–54. doi: 10.1038/ng882

285. Wu X, Jin W, Liu X, Fu H, Gong P, Xu J, et al. Cyclic AMP response element modulator-1 (CREM-1) involves in Neuronal Apoptosis after Traumatic brain injury. J. Mol. Neurosci. (2012) 47, 357–367. doi: 10.1007/s12031-012-9761-1

286. Qing Y, Yingmao G, Lujun B, Shaoling L. Role of Npm1 in proliferation, apoptosis and differentiation of neural stem cells. J. Neurol. Sci. (2008) 266, 131–137. doi: 10.1016/j.jns.2007.09.029

287. Pfister JA, D'Mello SR. Insights into the regulation of neuronal viability by nucleophosmin/B23. Exp. Biol. Med. (2015) 240, 774–786. doi:10.1177/1535370215579168

288. Elad N, Volberg T, Patla I, Hirschfeld-Warneken V, Grashoff C, Spatz JP, et al. The role of integrin-linked kinase in the molecular architecture of focal adhesions. J. Cell Sci. (2013) 126(Pt 18), 4099–4107. doi: 10.1242/jcs. 120295

289. Anitei M, Hoflack B. Bridging membrane and cytoskeleton dynamics in the secretory and endocytic pathways. Nat. Cell Biol. (2012) 14, 11–19. doi: 10.1038/ncb2409

290. Linford A, Yoshimura S, Nunes Bastos R, Langemeyer L, Gerondopoulos A, Rigden DJ, et al. Rab14 and its exchange factor FAM116 link endocytic recycling and adherens junction stability in migrating cells. Dev. Cell (2012) 22, 952–966. doi: 10.1016/j.devcel.2012.04.010

291. Ezratty EJ, Bertaux C, Marcantonio EE, Gundersen GG. Clathrin mediates integrin endocytosis for focal adhesion disassembly in migrating cells. J. Cell Biol. (2009) 187, 733–747. doi: 10.1083/jcb.200904054

292. Alahari SK, Lee JW, Juliano RL. Nischarin, a novel protein that interacts with the integrin alpha5 subunit and inhibits cell migration. J. Cell Biol. (2000) 151, 1141–1154. doi: 10.1083/jcb.151.6.1141

293. Alahari SK, Reddig PJ, Juliano RL. The integrin-binding protein Nischarin regulates cell migration by inhibiting PAK. EMBO J. (2004) 23, 2777–2788. doi: 10.1038/sj.emboj.7600291

294. Zhang J, Abdel-Rahman AA. Nischarin as a functional imidazoline (I1) receptor. (2006) FEBS Lett. 580, 3070–3074. doi: 10.1016/j.febslet.2006.04.058

295. Ding Y, Milosavljevic T, Alahari SK. Nischarin inhibits LIM kinase to regulate cofilin phosphorylation and cell invasion. Mol. Cell Biol. (2008) 28, 3742–3756. doi: 10.1128/MCB.01832-07

296. Pouwels J, Nevo J, Pellinen T, Ylänne J, Ivaska J. Negative regulators of integrin activity. J. Cell Sci. (2012) 125(Pt 14), 3271–3280. doi: 10.1242/jcs.093641

297. Hart MJ, Jiang X, Kozasa T, Roscoe W, Singer WD, Gilman AG, et al. Direct stimulation of the guanine nucleotide exchange activity of p115 RhoGEF by Galpha13. Science (1998). 280, 2112–2114. doi: 10.1126/science.280.5372.2112

298. Kozasa T, Jiang X, Hart MJ, Sternweis PM, Singer WD, Gilman AG, et al. p115 RhoGEF, a GTPase activating protein for Galpha12 and Galpha13. Science. (1998) 280, 2109–2111. doi: 10.1126/science.280.5372.2109

299. Dubash AD, Wennerberg K, García-Mata R, Menold MM, Arthur WT, Burridge K. A novel role for Lsc/p115 RhoGEF and LARG in regulating RhoA activity downstream of adhesion to fibronectin. J. Cell Sci. (2007)120(Pt 22), 3989–98. doi: 10.1242/jcs.003806

300. Jia Y, Mu JC, Ackerman SL. Mutation of a U2 snRNA gene causes global disruption of alternative splicing and neurodegeneration. Cell (2012)148, 296–308. doi: 10.1016/j.cell.2011.11.057

301. Vasudevan A, Ho MSP, Weiergräber M, Nischt R, Schneider T, Lie A, et al. Basement membrane protein nidogen-1 shapes hippocampal synaptic plasticity and excitability. Hippocampus (2010) 20, 608–620. doi: 10.1002/hipo. 20660

302. Miyake A, Mekata Y, Fujibayashi H, Nakanishi K, Konishi M, Itoh N. Brorin is required for neurogenesis, gliogenesis, and commissural axon guidance in the zebrafish forebrain. PLoS ONE (2017) 12:e0176036. doi: 10.1371/journal.pone.0176036

303. Hadari YR, Arbel-Goren R, Levy Y, Amsterdam A, Alon R, Zakut R, et al. Galectin-8 binding to integrins inhibits cell adhesion and induces apoptosis. J. Cell Sci. (2000) 113(Pt 13), 2385–2397.

304. Zick Y, Eisenstein M, Goren RA, Hadari YR, Levy Y, Ronen D. Role of galectin-8 as a modulator of cell adhesion and cell growth. Glycoconj. J. (2004) 19, 517–526. doi: 10.1023/B:GLYC.0000014081. 55445.af

305. den Hertog J, Tracy S, Hunter T. Phosphorylation of receptor protein-tyrosine phosphatase alpha on Tyr789, a binding site for the SH3-SH2- SH3 adaptor protein GRB-2 in vivo. EMBO J. (1994) 13, 3020–3032.

306. Johnson KG, Van Vactor D. Receptor protein tyrosine phosphatases in nervous system development. Physiol. Rev. (2003) 83, 1–24. doi: 10.1152/physrev.00016.2002

307. Dunah AW, Hueske E, Wyszynski M, Hoogenraad CC, Jaworski J, Pak DT, et al. LAR receptor protein tyrosine phosphatases in the development and maintenance of excitatory synapses. Nat. Neurosci. (2005) 8, 458–467. doi: 10.1038/nn1416

308. Kuo JC, Han X, Hsiao CT, Yates JR, Waterman CM. Analysis of the myosin-II-responsive focal adhesion proteome reveals a role for β-Pix in negative regulation of focal adhesion maturation. Nat. Cell Biol. (2011)13, 383–393. doi: 10.1038/ncb2216

309. Um JW, Ko J. LAR-RPTPs: synaptic adhesion molecules that shape synapse development. Trends Cell Biol (2013). 23, 465–475. doi: 10.1016/j.tcb.2013.07.004

310. Sarhan AR, Patel TR, Cowell AR, Tomlinson MG, Hellberg C, Heath JK, et al. LAR protein tyrosine phosphatase regulates focal adhesions through CDK1. J. Cell Sci. (2016) 129, 2962–2971. doi: 10.1242/jcs.191379

311. Piao X, Hill RS, Bodell A, Chang BS, Basel-Vanagaite L, Straussberg R, et al. G protein-coupled receptor-dependent development of human frontal cortex. Science (2004) 303, 2033–2036. doi: 10.1126/science.1092780

312. Iguchi T, Sakata K, Yoshizaki K, Tago K, Mizuno N, Itoh H. Orphan G protein-coupled receptor GPR56 regulates neural progenitor cell migration via a G alpha 12/13 and Rho pathway. J. Biol. Chem. (2008) 283, 14469–14478. doi: 10.1074/jbc.M708919200

313. Gong H, Shen B, Flevaris P, Chow C, Lam SCT, Voyno-Yasenetskaya TA, et al. G protein subunit Galpha13 binds to integrin alphaIIbbeta3 and mediates integrin 'outside-in' signaling. Science (2010) 327, 340–343. doi: 10.1126/science.1174779

314. Shen B, Delaney MK, Du X. Inside-out, outside-in, and inside-outside-in: G protein signaling in integrin-mediated cell adhesion, spreading, and retraction. Curr. Opin. Cell Biol. (2012) 24, 600–606. doi: 10.1016/j.ceb.2012.08.011

315. Jeong SJ, Luo R, Singer K, Giera S, Kreidberg J, Kiyozumi D, et al. GPR56 functions together with α3β1 integrin in regulating cerebral cortical development. PloS ONE (2013) 8:e68781. doi: 10.1371/journal.pone.0068781

316. Bae BI, Tietjen I, Atabay KD, Evrony GD, Johnson MB, Asare E, et al. Evolutionarily dynamic alternative splicing of GPR56 regulates regional cerebral cortical patterning. Science (2014) 343, 764–768. doi: 10.1126/science.1244392

317. Yamaguchi Y, Katoh H, Yasui H, Mori K, Negishi M. RhoA inhibits the nerve growth factor-induced Rac1 activation through Rho- associated kinase-dependent pathway. J. Biol. Chem. (2001) 276, 18977–18983. doi: 10.1074/jbc.M100254200

318. Loudon RP, Silver LD, Yee HF, Gallo G. RhoA- kinase and myosin II are required for the maintenance of growth cone polarity and guidance by nerve growth factor. J. Neurobiol. (2006) 66, 847–867. doi: 10.1002/neu.20258

319. Lee HH, Tien SC, Jou TS, Chang YC, Jhong JG, Chang ZF. Src-dependent phosphorylation of ROCK participates in regulation of focal adhesion dynamics. J. Cell Sci. (2010) 123(Pt 19), 3368–3377. doi: 10.1242/jcs. 071555

320. Schulte C, Racchetti G, D'Alessandro R, Meldolesi J. A new form of neurite outgrowth sustained by the exocytosis of enlargeosomes expressed under the control of REST. Traffic (2010) 11, 1304–1314. doi: 10.1111/j.1600-0854.2010.01095.x

321. Cao JP, Yu JK, Li C, Sun Y, Yuan HH, Wang HJ, et al. Integrin beta1 is involved in the signaling of glial cell line-derived neurotrophic factor. J. Comp. Neurol. (2008) 509, 203–210. doi: 10.1002/cne.21739

322. Marks C, Belluscio L, Ibáñez CF. Critical role of GFRα1 in the development and function of the main olfactory system. J. Neurosci. (2012) 32, 17306–17320. doi: 10.1523/JNEUROSCI.1522-12.2012

323. Konishi Y, Yang LB, He P, Lindholm K, Lu B, Li R, et al.. Deficiency of GDNF Receptor GFRα1 in Alzheimer's neurons results in neuronal death. J. Neurosci. (2014) 34, 13127–13138. doi: 10.1523/JNEUROSCI.2582-13.2014

324. Meng X, Krishnan J, She Y, Ens W, Standing K, Wilkins JA. Association of rasGAPSH3 binding protein 1, G3BP1, and rasGap120 with integrin containing complexes induced by an adhesion blocking antibody. J. Proteome Res. (2004) 3, 506–516. doi: 10.1021/pr0340983

325. Martin S, Zekri L, Metz A, Maurice T, Chebli K, Vignes M, et al. Deficiency of G3BP1, the stress granules assembly factor, results in abnormal synaptic plasticity and calcium homeostasis in neurons. J. Neurochem (2013). 125, 175–184. doi: 10.1111/jnc.12189

326. Moschner K, Sündermann F, Meyer H, da Graca AP, Appel N, Paululat A, et al. RNA protein granules modulate tau isoform expression and induce neuronal sprouting. J. Biol. Chem. (2014) 289, 16814–16825. doi: 10.1074/jbc.M113.541425

327. Gurok U, Steinhoff C, Lipkowitz B, Ropers HH, Scharff C, Nuber UA. Gene expression changes in the course of neural progenitor cell differentiation. J. Neurosci. (2004) 24, 5982–6002. doi: 10.1523/JNEUROSCI.0809-04.2004

328. Potkin SG, Turner JA, Fallon JA, Lakatos A, Keator DB, Guffanti G, et al. Gene discovery through imaging genetics: identification of two novel genes associated with schizophrenia. Mol. Psychiatry (2009) 14, 416–428. doi: 10.1038/mp.2008.127

329. Maeda M, Hasegawa H, Hyodo T, Ito S, Asano E, Yuang H, et al. ARHGAP18, a GTPase-activating protein for RhoA, controls cell shape, spreading, and motility. Mol. Biol. Cell (2011) 22, 3840–3852. doi: 10.1091/mbc.E11-04-0364

330. Porazinski S, Wang H, Asaoka Y, Behrndt M, Miyamoto T, Morita H, et al. YAP is essential for tissue tension to ensure vertebrate 3D body shape. Nature (2015) 521, 217–221. doi: 10.1038/nature14215

331. Zamboni V, Armentano M, Sarò G, Ciraolo E, Ghigo A, Germena G, et al. Disruption of ArhGAP15 results in hyperactive Rac1, affects the architecture and function of hippocampal inhibitory neurons and causes cognitive deficits. Sci. Rep. (2016) 6:34877. doi: 10.1038/srep34877

332. Buchman JJ, Durak O, Tsai LH. ASPM regulates Wnt signaling pathway activity in the developing brain. Genes Dev. (2011) 25, 1909–1914. doi: 10.1101/gad.16830211

333. Rujano MA, Sanchez-Pulido L, Pennetier C, le Dez G, Basto R. The microcephaly protein Asp regulates neuroepithelium morphogenesis by controlling the spatial distribution of myosin II. Nat. Cell Biol. (2013) 15, 1294–1306. doi: 10.1038/ncb2858

334. Hawkins M, Pope B, Maciver SK, Weeds AG. Human actin depolymerizing factor mediates a pH-sensitive destruction of actin filaments. Biochemistry (1993) 32, 9985–9993. doi: 10.1021/bi00089a014"

335. Jovceva E, Larsen MR, Waterfield MD, Baum B, Timms JF. Dynamic cofilin phosphorylation in the control of lamellipodial actin homeostasis. J. Cell Sci. (2007) 120(Pt 11), 1888–1897. doi: 10.1242/jcs. 004366

336. Flynn KC, Hellal F, Neukirchen D, Jacob S, Tahirovic S, Dupraz S, et al. ADF/cofilin-mediated actin retrograde flow directs neurite formation in the developing brain. Neuron (2012) 76, 1091–1107. doi: 10.1016/j.neuron.2012.09.038

337. Spiliotis ET, Nelson WJ. Here come the septins: novel polymers that coordinate intracellular functions and organization. J. Cell Sci. (2006) 119, 4–10. doi: 10.1242/jcs.02746

338. Joo E, Surka MC, Trimble WS. Mammalian SEPT2 Is required for scaffolding nonmuscle Myosin, I. I., and its Kinases. Dev. Cell (2007) 13, 677–690. doi: 10.1016/j.devcel.2007.09.001

339. Dhar SS, Lee SH, Kan PY, Voigt P, Ma L, Shi X, et al. Trans- tail regulation of MLL4-catalyzed H3K4 methylation by H4R3 symmetric dimethylation is mediated by a tandem PHD of MLL4. Genes Dev. (2012) 26, 2749–2762. doi: 10.1101/gad.203356.112

340. Kosmaczewski SG, Han SM, Han B, Irving Meyer B, Baig HS, Athar W, et al. RNA ligation in neurons by RtcB inhibits axon regeneration. Proc. Natl. Acad. Sci. (2015) U.S.A. 112, 8451–8456. doi: 10.1073/pnas.1502948112

341. Persengiev SP, Kondova II, Kilpatrick DL. E2F4 actively promotes the initiation and maintenance of nerve growth factor-induced cell differentiation. Mol. Cell Biol. (1999) 19, 6048–6056. doi: 10.1128/MCB. 19.9.6048

342. Eggenschwiler JT, Espinoza E, Anderson KV. Rab23 is an essential negative regulator of the mouse Sonic hedgehog signalling pathway. Nature (2001) 412, 194–198. doi: 10.1038/35084089

343. Evans TM, Ferguson C, Wainwright BJ, Parton RG, Wicking C. Rab23, a negative regulator of hedgehog signaling, localizes to the plasma membrane and the endocytic pathway. Traffic (2003) 4, 869–884. doi: 10.1046/j.1600-0854.2003.00141.x

344. Peterson TR, Sengupta SS, Harris TE, Carmack AE, Kang SA, Balderas E, et al. mTOR complex 1 regulates lipin 1 localization to control the SREBP pathway. Cell (2011) 146, 408–420. doi: 10.1016/j.cell.2011.06.034

345. Eaton JM, Mullins GR, Brindley DN, Harris TE. Phosphorylation of lipin 1 and charge on the phosphatidic acid head group control its phosphatidic acid phosphatase activity and membrane association. J. Biol. Chem. (2013) 288, 9933–9945. doi: 10.1074/jbc.M112.441493

346. Heuberger J, Birchmeier W. Interplay of Cadherin-Mediated cell Adhesion and Canonical Wnt signaling. Cold Spring Harb Perspect Biol. (2010) 2:a002915. doi: 10.1101/cshperspect.a002915

347. Bradley RS, Cowin P, Brown AM. Expression of Wnt-1 in PC12 cells results in modulation of plakoglobin and E-cadherin and increased cellular adhesion. J. Cell Biol. (1993) 123(6 Pt 2), 1857–65. doi: 10.1083/jcb.123.6.1857

348. Lecuit T, Yap AS. E-cadherin junctions as active mechanical integrators in tissue dynamics. Nat. Cell. Biol. (2015) 17, 533–539. doi: 10.1038/ncb3136

349. Chen W, Villa-Diaz LG, Sun Y, Weng S, Kim JK, Lam RHW, et al. Nanotopography influences adhesion, spreading, and self-renewal of human embryonic stem cells. ACS Nano (2012) 6, 4094–4103. doi: 10.1021/nn3004923

350. Swift J, Ivanovska IL, Buxboim A, Harada T, Dingal PC, Pinter J, et al. Nuclear lamin-A scales with tissue stiffness and enhances matrix- directed differentiation. Science (2013) 341:1240104. doi: 10.1126/science.1240104

351. Takamori Y, Tamura Y, Kataoka Y, Cui Y, Seo S, Kanazawa T, et al. Differential expression of nuclear lamin, the major component of nuclear lamina, during neurogenesis in two germinal regions of adult rat brain. Eur. J. Neurosci. (2007) 25, 1653–1662. doi: 10.1111/j.1460-9568.2007.05450.x

352. Raucher D, Sheetz MP. Membrane expansion increases endocytosis rate during mitosis. J. Cell Biol. (1999) 144, 497–506. doi: 10.1083/jcb.144.3.497

353. Sinha B, Köster D, Ruez R, Gonnord P, Bastiani M, Abankwa D, et al. Cells respond to mechanical stress by rapid disassembly of caveolae. Cell (2011)144, 402–413. doi: 10.1016/j.cell.2010.12.031

354. Gauthier NC, Masters TA, Sheetz MP. Mechanical feedback between membrane tension and dynamics. Trends Cell Biol. (2012) 22, 527–535. doi: 10.1016/j.tcb.2012.07.005

355. Laplante M, Sabatini DM. mTOR signaling at a glance. J. Cell Sci. (2009) 122, 3589–3594. doi: 10.1242/jcs.051011

356. Garza-Lombó C, Gonsebatt ME. Mammalian target of rapamycin: its role in early neural development and in adult and aged brain function. Front. Cell Neurosci. (2016) 10:157. doi: 10.3389/fncel.2016.00157

357. Parker EM, Monopoli A, Ongini E, Lozza G, Babij CM. Rapamycin, but not FK506 and GPI-1046, increases neurite outgrowth in PC12 cells by inhibiting cell cycle progression. Neuropharmacology (2000) 39, 1913–1919. doi: 10.1016/S0028-3908(00)00028-9"

358. Xie J, Proud CG. Crosstalk between mTOR complexes. Nat. Cell Biol. (2013) 15, 1263–1265. doi: 10.1038/ncb2877

359. Huang W, Zhu PJ, Zhang S, Zhou H, Stoica L, Galiano M, et al. mTORC2 controls actin polymerization required for consolidation of long- term memory. Nat. Neurosci. (2013) 16, 441–448. doi: 10.1038/nn.3351

360. Thomanetz V, Angliker N, Cloëtta D, Lustenberger RM, Schweighauser M, Oliveri F, et al. Ablation of the mTORC2 component rictor in brain or Purkinje cells affects size and neuron morphology. J. Cell Biol. (2013) 201, 293–308. doi: 10.1083/jcb.201205030

361. Thomson SE, Charalambous C, Smith CA, Tsimbouri PM, Déjardin T, Kingham PJ, et al. Microtopographical cues promote peripheral nerve regeneration via transient mTORC2 activation. Acta Biomater. (2017) 60, 220–231. doi: 10.1016/j.actbio.2017.07.031"

362. da Silva JS, Dotti CG. Breaking the neuronal sphere: regulation of the actin cytoskeleton in neuritogenesis. Nat. Rev. Neurosci. (2002) 3, 694–704. doi: 10.1038/nrn918

363. Fletcher DA, Mullins RD. Cell mechanics and the cytoskeleton. Nature (2010) 463, 485–492. doi: 10.1038/nature08908

364. Kuhn TB, Williams CV, Dou P, Kater SB. Laminin directs growth cone navigation via two temporally and functionally distinct calcium signals. J. Neurosci. (1998) 18, 184–194.

365. Gui P, Wu X, Ling S, Stotz SC, Winkfein RJ, Wilson E, et al. Integrin receptor activation triggers converging regulation of Cav1.2 calcium channels by c-Src and protein kinase A pathways. J. Biol. Chem. (2006) 281, 14015–14025. doi:10.1074/jbc.M600433200

366. Vogel V, Sheetz M. Local force and geometry sensing regulate cell functions. Nat. Rev. Mol. Cell Biol. (2006) 7, 265–275. doi: 10.1038/nrm1890

367. Zhang K, Chen J. The regulation of integrin function by divalent cations. Cell Adhes. Migr. (2012) 6, 20–29. doi: 10.4161/cam.18702"

368. Kerstein PC, Patel KM, Gomez TM. Calpain-Mediated Proteolysis of Talin and FAK regulates Adhesion Dynamics necessary for Axon guidance. J. Neurosci. (2017) 37, 1568–1580. doi: 10.1523/JNEUROSCI.2769-16.2016

369. McHugh BJ, Buttery R, Lad Y, Banks S, Haslett C, Sethi T. Integrin activation by Fam38A uses a novel mechanism of R-Ras targeting to the endoplasmic reticulum. J. Cell Sci. (2010) 123(Pt 1), 51–61. doi: 10.1242/jcs.0 56424

370. Gomez TM, Zheng JQ. The molecular basis for calcium-dependent axon pathfinding. Nat. Rev. Neurosci. (2006) 7, 115–125. doi: 10.1038/nrn1844

371. Leclerc C, Néant I, Moreau M. The calcium: an early signal that initiates the formation of the nervous system during embryogenesis. Front. Mol. Neurosci. (2012) 5:3. doi: 10.3389/fnmol.2012.00064

372. Kerstein PC, Jacques-Fricke BT, Rengifo J, Mogen BJ, Williams JC, Gottlieb PA, et al. Mechanosensitive TRPC1 channels promote calpain proteolysis of talin to regulate spinal axon outgrowth. J. Neurosci. (2013) 33, 273–285. doi: 10.1523/JNEUROSCI.2142-12.2013

373. Toth AB, Shum AK, Prakriya M. Regulation of neurogenesis by calcium signaling. Cell Calcium (2016) 59, 124–34. doi: 10.1016/j.ceca.2016. 02.011

374. Jacques-Fricke BT, Seow Y, Gottlieb PA, Sachs F, Gomez TM. Ca2+ Influx through Mechanosensitive channels inhibits neurite outgrowth in opposition to other influx pathways and release from intracellular stores. J. Neurosci. (2006) 26, 5656–5664. doi:10.1523/JNEUROSCI.0675-06.2006

375. Gottlieb PA, Barone T, Sachs F, Plunkett R. Neurite outgrowth from PC12 cells is enhanced by an inhibitor of mechanical channels. Neurosci. Lett. (2010) 481, 115–119. doi: 10.1016/j.neulet.2010.06.066

376. De Bernardi MA, Rabins SJ, Colangelo AM, Brooker G, Mocchetti I. TrkA mediates the nerve growth factor-induced intracellular calcium accumulation. J. Biol. Chem. (1996) 271, 6092–6098. doi: 10.1074/jbc.271.1 1.6092

377. Cohen MR, Johnson WM, Pilat JM, Kiselar J, DeFrancesco-Lisowitz A, Zigmond, RE, et al. Nerve growth factor regulates transient receptor potential vanilloid 2 via extracellular signal-regulated kinase signaling to enhance neurite outgrowth in developing neurons. Mol. Cell Biol. (2015) 35, 4238–4252. doi: 10.1128/MCB.00549-15

378. Goebeler V, Ruhe D, Gerke V, Rescher U. Annexin A8 displays unique phospholipid and F-actin binding properties. FEBS Lett. (2006) 580, 2430–2434. doi:10.1016/j.febslet.2006.03.076

379. Ney A, Booms P, Epple G, Mörgelin M, Guo G, Kettelgerdes G, et al. Calcium-dependent self-association of the C-type lectin domain of versican. Int. J. Biochem. Cell Biol. (2006) 38, 23–29. doi: 10.1016/j.biocel.2005.07.007

380. Carlson CB, Lawler J, Mosher DF. Structures of thrombospondins. Cell Mol. Life Sci. (2008) 65, 672–686. doi: 10.1007/s00018-007-7484-1

381. Davis TA, Loos B, Engelbrecht AM. AHNAK: the giant jack of all trades. Cell Signal. (2014) 26, 2683–2693. doi: 10.1016/j.cellsig.2014.08.017"

382. Benaud C, Gentil BJ, Assard N, Court M, Garin J, Delphin C, et al. AHNAK interaction with the annexin 2/S100A10 complex regulates cell membrane cytoarchitecture. J. Cell Biol. (2004) 164, 133–144. doi: 10.1083/jcb.200307098

383. Lorusso A, Covino C, Priori G, Bachi A, Meldolesi J, Chieregatti E. Annexin2 coating the surface of enlargeosomes is needed for their regulated exocytosis. EMBO J (2006). 25, 5443–5456. doi: 10.1038/sj.emboj. 7601419

384. Borgonovo B, Cocucci E, Racchetti G, Podini P, Bachi A, Meldolesi J. Regulated exocytosis: a novel, widely expressed system. Nat. Cell Biol. (2002) 4, 955–962. doi: 10.1038/ncb888

385. Racchetti G, Lorusso A, Schulte C, Gavello D, Carabelli V, D'Alessandro R, et al. Rapid neurite outgrowth in neurosecretory cells and neurons is sustained by the exocytosis of a cytoplasmic organelle, the enlargeosome. J. Cell Sci. (2010) 123(Pt 2), 165–170. doi:10.1242/jcs.059634

386. Cappello S, Gray MJ, Badouel C, Lange S, Einsiedler M, Srour M, et al. Mutations in genes encoding the cadherin receptor-ligand pair DCHS1 and FAT4 disrupt cerebral cortical development. Nat. Genet. (2013) 45, 1300–1308. doi: 10.1038/ng.2765

387. Kawaai K, Hisatsune C, Kuroda Y, Mizutani A, Tashiro T, Mikoshiba K. 80K-H interacts with inositol 1,4,5-trisphosphate (IP3) receptors and regulates IP3-induced calcium release activity. J. Biol. Chem. (2009) 284, 372–380. doi: 10.1074/jbc.M805828200

388. Rescher U, Gerke V. S100A10/p11: family, friends and functions. Pflugers Arch. (2008) 455, 575–582. doi: 10.1007/s00424-007-0313-4

389. Jung MJ, Murzik U, Wehder L, Hemmerich P, Melle C. Regulation of cellular actin architecture by S100A10. Exp. Cell Res. (2010) 316, 1234–1240. doi:10.1016/j.yexcr.2010.01.022

390. Downing TL, Soto J, Morez C, Houssin T, Fritz A, Yuan F, et al. Biophysical regulation of epigenetic state and cell reprogramming. Nat. Mater. (2013) 12, 1154–1162. doi: 10.1038/nmat3777

391. Crowder SW, Leonardo V, Whittaker T, Papathanasiou P, Stevens MM. Material cues as potent regulators of epigenetics and stem cell function. Cell Stem Cell (2016) 18, 39–52. doi:10.1016/j.stem.2015.12.012"

392. Merscher S, Fornoni A. Podocyte pathology and nephropathy – sphingolipids in glomerular diseases. Front Endocrinol (Lausanne). 2014 Jul 30;5:127. doi:10.3389/fendo.2014.00127. eCollection 2014.

393. Ledeen RW, Wu G. Special Issue: The Magic of the Sugar Code The multi-tasked life of GM1 ganglioside, a true factotum of nature. Trends in Biochemical Sciences. Volume 40, Issue 7, July 2015, Pages 407-418

394. Ledeen RW, Wu G. The multi-tasked life of GM1 ganglioside: a true factotum of nature. Trends Biochem Sci. 2015 Jul;40(7):407-18. doi: 10.1016/j.tibs.2015.04.005. Epub 2015 May 26.

395. Ledeen RW, Wu G. Gangliosides of the nervous system. Methods Mol Biol (2018a) 1804:19–55

396. Ledeen RW, Wu G. Gangliosides, α-synuclein, and Parkinson's disease. Prog Mol Biol Transl Sci (2018b) 156:435–454

397. Schengrund CL. Gangliosides: glycosphingolipids essential for normal neural development and function. Trends Biochem Sci. 2015 Jul;40(7):397-406. doi: 10.1016/j.tibs.2015.03.007. Epub 2015 May 1.

398. Schengrund CL, Prouty C. Oligosaccharide portion of GM1 enhances process formation by S20Y neuroblastoma cells. J Neurochem (1988) 51:277–282

399. Chiricozzi E, Pomè YD, Maggioni M, Di Biase E, Parravicini C, Palazzolo L, Loberto N, Eberini I et al Role of GM1 ganglioside oligosaccharide portion in the TrkA-dependent neurite sprouting in neuroblastoma cells. J Neurochem (2017) 143:645–659

400. Tremblay RG, Sikorska M, Sandhu JK, Lanthier P, Ribecco-Lutkiewicz M, Bani-Yaghoub M. Differentiation of mouse Neuro 2A cells into dopamine neurons. J. Neurosci. Methods (2010) 186:60-67

401. Read DE, Gorman AM. Involvement of Akt in neurite outgrowth. Cell Mol Life Sci. 2009; 66(18):2975– 84. doi: 10.1007/s00018-009-0057-8 PMID: 19504044

402. Salto R, Vílchez JD, Girón MD, Cabrera E, Campos N, Manzano M, Rueda R, López-Pedrosa JM (August 2015). "β-Hydroxy-β-Methylbutyrate (HMB) Promotes Neurite Outgrowth in Neuro2a Cells". PLoS ONE. 10 (8): e0135614. doi:10.1371/journal.pone.0135614. PMC 4534402. PMID 26267903

403. Cattaneo A, Calissano P. Nerve growth factor and Alzheimer's disease: new facts for an old hypothesis. Molecular neurobiology (2012), vol. 46, no. 3, pp. 588–604,

404. Biernacki K, Antel JP, Blain M, Narayanan S, Arnold DL, Prat A. Interferon beta promotes nerve growth factor secretion early in the course of multiple sclerosis. Archives of Neurology (2005), vol. 62, no. 4, pp. 563–568.

405. Wang H, Wang R, Thrimawithana T, Little PJ, Xu J, Feng ZP, Zheng W. The nerve growth factor signaling and its potential as therapeutic target for glaucoma. Biomed Res Int. (2014); 2014:759473. doi: 10.1155/2014/759473.

406. McGeary E, Gurel V, Knopik VS, Spaulding J, McMichael J. Effects of nerve growth factor (NGF), fluoxetine, and amitriptyline on gene expression profiles in rat brain. Neuropeptides (2011), vol. 45, no. 5, pp. 317–322.

407. Nelson KB, Grether JK, Croen LA et al. Neuropeptides and neurotrophins in neonatal blood of children with autism or mental retardation. Annals of Neurology (2001) vol. 49, no. 5, pp. 597–606.

408. Zheng W, Wang H, Zeng Z et al. The possible role of the Akt signaling pathway in schizophrenia. Brain Research (2012), vol. 1470, pp. 145–158.

409. Petruska JC, Mendell LM. Nerve Growth Factor. In: LR Squire, Ed. Encyclopedia of Neuroscience. (2008) Vol. 6 P. 71-78, Elsevier.

410. Lee KF, Davies AM, Jaenisch R. p75-deficient embry- onic dorsal root sensory and neonatal sympathetic neurons display a decreased sensitivity to NGF. Development (1994), vol. 120, no. 4, pp. 1027–1033.

411. Niewiadomska G, Mietelska-Porowska A, Mazurkiewicz M. The cholinergic system, nerve growth factor and the cytoskeleton. Behavioural Brain Research (2011), vol. 221, no. 2, pp. 515–526.

412. Mahata SK, Mahata M, Wu H, Parmer RJ, O'Connor DT. Neurotrophin activation of catecholamine storage vesicle protein gene expression: signaling to chromogranin a biosynthesis. Neuroscience (1999), vol. 88, no. 2, pp. 405–424.

413. Oh YT, Yue P, Zhou W et al. Oncogenic Ras and B- Raf proteins positively regulate death receptor 5 expression through co-activation of ERK and JNK signaling. The Journal of Biological Chemistry (2012), vol. 287, no. 1, pp. 257–267.

414. Cheng HC, Shih HM, Chern Y. Essential role of cAMP-response element-binding protein activation by A2*A* adenosine receptors in rescuing the nerve growth factor- induced neurite outgrowth impaired by blockage of the MAPK cascade. The Journal of Biological Chemistry (2002), vol. 277, no. 37, pp. 33930–33942.

415. De Girolamo LA, Hargreaves AJ, Billett EE. Protection from MPTP-induced neurotoxicity in differentiating mouse N2a neuro- blastoma cells. J Neurochem (2001) 76:650–660

416. Nicotra A, Parvez SH. Apoptotic molecules and MPTP- induced cell death. Neurotoxicol Teratol (2002); 24(5):599-605.

417. Meredith GE, Rademacher DJ. MPTP mouse models of Parkinson's disease: an update. J Park Dis (2011) 1:19–33.

418. Stanley Burns R, LeWitt PA, Ebert MH, Pakkenberg H, Kopin IJ. The Clinical Syndrome of Striatal Dopamine Deficiency — Parkinsonism Induced by 1-Methyl-4-Phenyl-1,2,3,6-Tetrahydropyridine (MPTP) N Engl J Med (1985); 312:1418-1421 Doi: 10.1056/NEJM198505303122203

419. Markey SP, Johannessen JN, Chiueh CC, Burns RS, Herkenham MA. Intraneuronal generation of a pyridinium metabolite may cause drug-induced parkinsonism. Nature (1984) 311, 464±467.

420. Nicklas WJ, Vyas I, Heikkila RE. Inhibition of NADH- linked oxidation in brain mitochondria by 1-methyl-4phenyl- 1,2,3,6-tetrahydropyridine. Life Sci. (1985) 36, 2503±2508.

421. Ramsey RR, Salach JI, Dadgar J, Singer TP. Inhibition of mitochondrial NADH dehydrogenase by pyridine derivatives and its possible relation to experimental and idiopathic Parkinsonism. Biochem. Biophys. Res. Commun. (1986) 135, 269±275.

422. DiMonte D, Jewell SA, Ekstrom G, Sandy MS, Smith MT 1-methyl-4-phenyl-1,2,3,6-tetrahydropyridine (mptp) and 1-methyl-4-phenylpyridine (MPPI) cause rapid ATP depletion in isolated hepatocytes. Biochem. Biophys. Res. Commun. (1986)137, 310 ± 315.

423. Sriram K, Pai KS, Boyd MR, Ravindranath V. Evidence for generation of oxidative stress in brain by MPTP: In vitro and in vivo studies in mice. Brain Res. (1997) 749, 44±52.

424. Lai M, Grifths H, Pall H, Williams A, Lunec J. An investigation into the role of reactive oxygen species in the mechanism of 1-methyl-4-phenyl-1,2,3,6-tetrahydropyridine toxicity using neuronal cell-lines. Biochem. Pharmacol. (1993) 45, 927±933.

425. Saporito MS, Brown EM, Miller MS Carswell S. CEP-1347/KT-7515, an inhibitor of c-jun N-terminal kinase activation, attenuates the 1-methyl-4-phenyl tetrahydropyridine-mediated loss of nigrostriatal dopaminergic neurons in vivo. J. Pharmacol. Exp Therap. (1999) 288, 421±427."

426. Wiegandt H, Bücking HW. Carbohydrate components of extraneuronal gangliosides from bovine and human spleen, and bovine kidney. Eur J Biochem (1970) 15:287–292

427. Tettamanti G, Bonali F, Marchesini S, Zambotti V. A new procedure for the extraction, purification and fractionation of brain gangliosides. Biochim Biophys Acta (1973) 296:160–170

428. Acquotti D, Cantu L, Ragg E, Sonnino S. Geometrical and conformational properties of ganglioside GalNAc-GD1a, IV4GalNAcIV3Neu5AcII3Neu5AcGgOse4Cer. Eur J Biochem (1994) 225:271–288

429. Chiricozzi E, Niemer N, Aureli M, Magini A, Loberto N, Prinetti A, Bassi R, Polchi A et al. Chaperone therapy for GM2 gangliosidosis: effects of pyrimethamine on β-hexosaminidase activity in Sandhoff fibroblasts. Mol Neurobiol (2014) 50:159–167

430. Varki A, Cummings RD, Aebi M, Packer NH, Seeberger PH, Esko JD, Stanley P, Hart G et al. Symbol nomenclature for graph- ical representations of glycans. Glycobiology (2015) 25:1323–1324

431. Riboni L, Prinetti A, Bassi R, Caminiti A, Tettamanti G. A mediator role of ceramide in the regulation of neuroblastoma Neuro2a cell differentiation. J Biol Chem (1995) 270:26868–26875

432. Wu G, Lu ZH, Xie X, Ledeen RW. Susceptibility of cerebellar granule neurons from GM2/GD2 synthase-null mice to apoptosis induced by glutamate excitotoxicity and elevated KCl: rescue by GM1 and LIGA20. Glycoconj (2014) J 21:3015–3313

433. Wood ER, Kuyper L, Petrov KG, Hunter RN, Harris PA, Lackey K. Discovery and in vitro evaluation of potent TrkA kinase inhibitors: oxindole and aza-oxindoles. Bioorg Med Chem Lett (2004) 14:953–957

434. Coccetti P, Tripodi F, Tedeschi G, Nonnis S, Marin O, Fantinato S, Cirulli C, Vanoni M, Alberghina L. The CK2 phosphorylation of catalytic domain of Cdc34 modulates its activity at the G1 to S transition in Saccharomyces cerevisiae, Cell Cycle (2008) 7 (10) 1391–1401.

435. Outeiro TF, Marques O, Kazantsev. A Therapeutic role of sirtuins in neurodegenerative disease. Biochim Biophys Acta (2008) 1782: 363–369

436. Yang W, Sheng H, Wang H. Targeting the SUMO pathway for neuroprotection in brain ischaemia. Stroke Vasc Neurol (2016) 1:101– 107

437. Bogorad AM, Lin KL, Marintchev A. Novel mechanisms of eIF2B action and regulation by eIF2phosphorylation. Nucleic Acids Res (2017) 45:11962–11979

438. Grande V, Manassero G, Vercelli A. Neuroprotective and anti-inflammatory roles of the phosphatase and tensin homolog deleted on chromosome ten (PTEN) inhibition in a mouse model of temporal lobe epilepsy. PLoS One (2014) 12:1–20

439. Vian J, Pereira C, Chavarria V, Köhler C, Stubbs B, Quevedo J, Kim SW, Carvalho AF et al. The renin–angiotensin system: a possible new target for depression. BMC Med (2017) 15:144

440. Priesnitz C, Becker T. Pathways to balance mitochondrial translation and protein import. Genes Dev (2018) 32:1285–1296

441. Bieri P, Greber BJ, Ban N. High-resolution structures of mitochondrial ribosomes and their functional implications. Curr Opin Struct Biol (2018) 49:44–53

442. Chen K, Ho TS, Lin G, Tan KL, Rasband MN, Bellen HJ. Loss of frataxin activates the iron/sphingolipid/PDK1/Mef2 pathway in mammals. Elife (2016) 30:5

443. Almokhtar M, Wikvall K, Ubhayasekera SJKA, Bergquist J, Norlin M. Motor neuron-like NSC-34 cells as a new model for the study of vitamin D metabolism in the brain. J Steroid Biochem Mol Biol (2016) 158:178–188"

444. Plun-Favreau H, Klupsch K, Moisoi N, Gandhi S, Kjaer S, Frith D, Harvey K, Deas E et al. The mitochondrial protease HtrA2 is regulated by Parkinson's disease-associated kinase PINK1. Nat Cell Biol (2007) 9:1243–1252"

445. Zakharova IO, Sokolova TV, Vlasova YA, Furaev VV, Rychkova MP, Avrova NF GM1 ganglioside activates ERK1/2 and Akt downstream of Trk tyrosine kinase and protects PC12 cell against hydrogen peroxide toxicity. Neurochem Res (2014) 39:2262–2275

446. Schneider JS, Seyfried TN, Chiu HS, Kidd SK. Intraventricular sialidase administration enhances GM1 ganglioside expression and is partially neuroprotective in a mouse model of Parkinson's disease. PLoS One (2015) 10:12

447. Saulino MF, Schengrund CL. Effects of specific gangliosides on the in vitro proliferation of MPTP-susceptible cells. J Neurochem (1993) 61:1277–1283

448. Lüthi D, Le Floch M, Bereiter B, Blunier T, Barnola J, Siegenthaler U, Raynaud D, Jouzel J, Fischer H, Kawamura K, Stocker TF. High-resolution carbon dioxide concentration record 650,000–800,000 years before present Nature (2008) volume 453, pages 379–382.

449. National Research Council (NRC). Surface Temperature Reconstructions For the Last 2,000 Years. National Academy Press (2006), Washington, D.C.

450. Levitus S, Antonov J, Boyer T, Baranova O, Garcia H, Locarnini R, Mishonov A, Reagan J, Seidov D, Yarosh E, Zweng M. NCEI ocean heat content, temperature anomalies, salinity anomalies, thermosteric sea level anomalies, halosteric sea level anomalies, and total steric sea level

anomalies from 1955 to present calculated from in situ oceanographic subsurface profile data (NCEI Accession 0164586). Version 4.4. NOAA National Centers for Environmental Information. (2017) Dataset. doi:10.7289/V53F4MVP

451. Brett JR, Energetic responses of salmon to temperature. A study of some thermal relations in the physiology and freshwater ecology of sockeye salmon (Oncorhynchus nerkd), American zoologist 11(1) (1971) 99-113.

452. Merila J, Sheldon BC, Kruuk LEB. Explaining stasis: microevolutionary studies in natural populations. Genetica (2001) 112–113:199–222

453. Daufresne M, Lengfellner K, Sommer U. Global warming benefits the small in aquatic ecosystems. Proc Natl Acad Sci (2009) U S A 106(31) 12788-93.

454. Scott GR, Johnston IA. Temperature during embryonic development has persistent effects on thermal acclimation capacity in zebrafish. Proceedings of the National Academy of Sciences of the United States of America (2012) 109:14247–14252.

455. PÖrtner HO, Peck MA. Climate change effects on fishes and fisheries: towards a cause-and-effect understanding. Journal of Fish Biology (2010) 77:1745–1779.

456. Somero GN. The physiology of climate change: how potentials for acclimatization and genetic adaptation will determine ‘winners’ and ‘losers’. Journal of Experimental Biology (2010) 213:912–920.

457. Finstad AG, Forseth T, Jonsson B, Bellier E, Hesthagen T, Jensen AJ, Hessen DO et al. Competitive exclusion along climate gradients: energy efficiency influences the distribution of two salmonid fishes. Global Change Biology (2011) 17:1703–1711.

458. Marcos-Lopez M, Gale P, Oidtmann BC, Peeler EJ. Assessing the impact of climate change on disease emergence in fresh- water fish in the United Kingdom. Transboundary and Emerging Diseases (2010) 57:293–304.

459. Somero GN. Adaptation of enzymes to temperature: searching for basic "strategies", Comp Biochem Physiol B Biochem Mol Biol (2004) 139(3) 321-33.

460. Nowik N, Podlasz P, Jakimiuk A, Kasica N, Sienkiewicz W, Kaleczyc J. Zebrafish: an animal model for research in veterinary medicine. Pol J Vet Sci. (2015);18(3):663-74. doi: 10.1515/pjvs-2015-0086.

461. Cortemeglia C, Beitinger TL. Temperature Tolerances 725 of Wild-Type and Red Transgenic Zebra Danios, Transactions of the American Fisheries Society (2005) 134(6) 1431-1437. http://doi.org/10.1577/T04-197.1

462. Schaefer J, Ryan A. Developmental plasticity in the thermal tolerance of zebrafish Danio rerio. Journal of Fish Biology (2006) 69(3) 722-734.

463. Howe K, Clark MD, Torroja CF, Torrance J, Berthelot C et al. The zebrafish reference genome sequence and its relationship to the human genome. Nature (2013);496;7446;498-503 PUBMED: 23594743; PMC: 3703927.

464. Bally L, Vernier CP. Organization And Physiology Of The Zebrafish Nervous System Fish Physiology. (2010) Doi: 10.1016/S1546-5098(10)02902-X

465. Schier AF, Talbot WS. Molecular genetics of axis formation in Zebrafish. Annu. Rev. Genet. (2005). 39, 561-613.

466. Wullimann MF, Rink E. Detailed immunohistology of Pax6 protein and tyrosine hydroxylase in the early zebrafish brain suggests role of Pax6 gene in development of dopaminergic diencephalic neurons. Brain Res. Dev. Brain Res. (2001)131, 173–191.

467. Rink E, Wullimann MF. The teleostean (zebrafish) dopaminergic system ascending to the subpallium (striatum) is located in the basal diencephalon (posterior tuberculum). Brain Res. (2001) 889, 316–330."

468. Kohashi T, Oda Y. Initiation of Mauthner- or non-Mauthner-mediated fast escape evoked by different modes of sensory input. J. Neurosci. (2008) 28, 10641–10653.

469. Sison M, Gerlai R. Associative learning in zebrafish (Danio rerio) in the plus maze. Behavioural Brain Research, (2010) 207, 99–104.

470. Cognato Gde P, Bortolotto JW, Blazina AR, Christoff RR, Lara DR, Vianna MR, Bonan CD. Y-Maze memory task in zebrafish (Danio rerio): the role of glutamatergic and cholinergic systems on

the acquisition and consolidation periods. Neurobiol Learn Mem. (2012). 98(4):321-8. doi: 10.1016/j.nlm.2012.09.008. Epub 2012 Oct 6.

471. Fontana BD, Cleal M, Clay JM, Parker MO. Zebrafish (Danio rerio) behavioral laterality predicts increased short-term avoidance memory but not stress-reactivity responses. Anim Cogn. 2019 Jul 24. doi: 10.1007/s10071-019-01296-9.

472. Vergauwen L, Benoot D, Blust R, Knapen D. Long-term warm or cold acclimation elicits a specific transcriptional response and affects energy metabolism in zebrafish, Comp. Biochem. Physiol. A Mol. Integr. Physiol. (2010) 157 (2) 149–157.

473. Eberini I, Calabresi L, Wait R, Tedeschi G, Pirillo A, Puglisi L, Sirtori CR, Gianazza E. Macrophage metalloproteinases degrade high-density lipoprotein associated apolipoprotein A-I at both the N- and C-termini. Biochem. J. (2002) 362 (3) 627–634.

474. Cox J, Mann M. MaxQuant enables high peptide identification rates, individualized p.p.b.-range mass accuracies and proteome wide protein quantification. Nat. Biotechnol. (2008) 26 (12) 1367–1372.

475. Zhang J, Xin L, Shan B, Chen W, Xie M, Yuen D, Zhang W, Zhang Z, Lajoie GA, Ma B. PEAKS DB: de novo sequencing assisted database search for sensitive and accurate peptide identification, Mol. Cell. Proteomics (2012) 11 (4).

476. Mi H, Muruganujan A, Thomas PD. PANTHER in 2013: modeling the evolution of gene function, and other gene attributes, in the context of phylogenetic trees, Nucleic Acids Res. 41 (2013) D377–D386.

477. Supek F, Bosnjak M, Skunca N, Smuc T. REVIGO summarizes and visualizes long lists of gene ontology terms, PLoS ONE (2011).

478. Merico D, Isserlin R, Stueker O, Emili A, Bader GD. Enrichment map: a network- based method for gene-set enrichment visualization and interpretation, PLoS ONE (2010).

479. Montcouquiol M, Crenshaw 3rd EB, Kelley MW. Noncanonical Wnt signaling and neural polarity, Annu. Rev. Neurosci. 29 (2006) 363–386.

480. Schlessinger K, Hall A, Tolwinski N. Wnt signaling pathways meet rho GTPases, Genes Dev. 23 (3) (2009) 265–277.

481. Leopold JA, Loscalzo J. Cyclic strain modulates resistance to oxidant stress by increasing G6PDH expression in smooth muscle cells. Am. J. Physiol. Heart Circ.Physiol. 279 (5) (2000) H2477–H2485.

482. Hyder F, Rothman DL, Bennett MR. Cortical energy demands of signaling and nonsignaling components in brain are conserved across mammalian species and activity levels, Proc. Natl. Acad. Sci. U.S.A. 110 (9) (2013) 3549–3554.

483. Attwell D, Laughlin SB. An energy budget for signaling in the grey matter of the brain, J. Cereb. Blood Flow Metab. 21 (10) (2001) 1133–1145.

484. Tang Y, Zucker RS. Mitochondrial involvement in post-tetanic potentiation of synaptic transmission, Neuron. 18 (3) (1997) 483–491.

485. Werth J, Thayer S. Mitochondria buffer physiological calcium loads in cultured rat dorsal root ganglion neurons, J. Neurosci. 14 (1) (1994) 348–356.

486. Harris JJ, Jolivet R, Attwell D. Synaptic energy use and supply, Neuron. 75 (5) (2012) 762–777.

487. Watts ME, Pocock R, Claudianos C. Brain energy and oxygen metabolism: emerging role in Normal function and disease. Front. Mol. Neurosci. 11 (2018) 216.

488. Li Z, Okamoto K, Hayashi Y, Sheng M, The importance of dendritic mitochondria in the morphogenesis and plasticity of spines and synapses. Cell 119 (6) (2004) 873–887.

489. Billups B, Forsythe ID. Presynaptic mitochondrial calcium sequestration influ- ences transmission at mammalian central synapses. J. Neurosci. 22 (14) (2002) 5840–5847 doi:20026597.

490. Medler K, Gleason EL. Mitochondrial Ca^{2+} buffering regulates synaptic trans- mission between retinal amacrine cells, J. Neurophysiol. 87 (3) (2002) 1426–1439.

491. David G, Barrett EF. Mitochondrial Ca^{2+} uptake prevents desynchronization of quantal release and minimizes depletion during repetitive stimulation of mouse motor nerve terminals. J. Physiol. 548 (2) (2003) 425–438.

492. Talbot JD, David G, Barrett EF. Inhibition of mitochondrial Ca^{2+} uptake affects phasic release from motor terminals differently depending on external [Ca^{2+}]. J. Neurophysiol. 90 (1) (2003) 491–502.

493. Levy M, Faas GC, Saggau P, Craigen WJ, Sweatt JD. Mitochondrial regulation of synaptic plasticity in the hippocampus, J. Biol. Chem. 278 (20) (2003) 17727–17734.

494. Kang JS, Tian JH, Pan PY, Zald P, Li C, Deng C, Sheng ZH. Docking of axonal mitochondria by syntaphilin controls their mobility and affects short-term facilitation. Cell 132 (1) (2008) 137–148.

495. Chang DT, Reynolds IJ. Mitochondrial trafficking and morphology in healthy and injured neurons. Prog. Neurobiol. 80 (5) (2006) 241–268.

496. Chan DC. Mitochondria: dynamic organelles in disease, aging, and development. Cell. 125 (7) (2006) 1241–1252.

497. Stokin GB, Goldstein LS. Axonal transport and Alzheimer's disease. Annu. Rev. Biochem. 75 (2006) 607–627.

498. Schon EA, Przedborski S. Mitochondria: the next (neurode)generation. Neuron. 70 (6) (2011) 1033–1053.

499. White MG, Saleh O, Nonner D, Barrett EF, Moraes CT, Barrett JN. Mitochondrial dysfunction induced by heat stress in cultured rat CNS neurons, J. Neurophysiol. 108 (8) (2012) 2203–2214.

500. Zukiene R, Nauciene Z, Ciapaite J, Mildaziene V. Acute temperature resistance threshold in heart mitochondria: febrile temperature activates function but exceeding it collapses the membrane barrier. Int. J. Hyperth. 26 (1) (2010) 56–66.

501. Qian L, Song X, Ren H, Gong J, Cheng S. Mitochondrial mechanism of heat stress-induced injury in rat cardiomyocyte. Cell Stress Chaperones 9 (3) (2004) 281–293.

502. Gilman CP, Chan SL, Guo Z, Zhu X, Greig N, Mattson MP. p53 is present in synapses where it mediates mitochondrial dysfunction and synaptic degeneration in response to DNA damage, and oxidative and excitotoxic insults. NeuroMolecular Med. 3 (3) (2003) 159–172.

503. Mattson MP, Gleichmann M, Cheng A. Mitochondria in neuroplasticity and neurological disorders. Neuron. 60 (5) (2008) 748–766.

504. Amato P, Christner BC. Energy metabolism response to low-temperature and frozen conditions in Psychrobacter cryohalolentis. Appl. Environ. Microbiol. 75 (3) (2009) 711–718.

505. Gaffield MA, Rizzoli SO, Betz WJ. Mobility of synaptic vesicles in different pools in resting and stimulated frog motor nerve terminals. Neuron. 51 (3) (2006) 317–325.

506. Shtrahman M, Yeung C, Nauen DW, Bi GQ, Wu XL. Probing vesicle dynamics in single hippocampal synapses, Biophys. J. 89 (5) (2005) 3615–3627.

507. Bui L, Glavinovic MI. Temperature dependence of vesicular dynamics at excitatory synapses of rat hippocampus, Cogn. Neurodyn. 8 (4) (2014) 277–286.

508. Spedden E, Kaplan DL, Staii C. Temperature response of the neuronal cytoske- leton mapped via atomic force and fluorescence microscopy. Phys. Biol. 10 (5) (2013) 056002.

509. Humphrey D, Duggan C, Saha D, Smith D, Kas J. Active fluidization of polymer networks through molecular motors. Nature. 416 (6879) (2002) 413–416.

510. Le Goff L, Amblard F, Furst EM. Motor-driven dynamics in actin-myosin networks. Phys. Rev. Lett. 88 (1) (2002) 018101.

511. Smith D, Ziebert F, Humphrey D, Duggan C, Steinbeck M, Zimmermann W, Kas J. Molecular motor-induced instabilities and cross linkers determine biopolymer organization. Biophys. J. 93 (12) (2007) 4445–4452.

512. Yarlagadda A, Clayton AH. Thermoregulation and the role of calcium signalling in neurotransmission. Psychiatry (Edgmont) 5 (12) (2008) 51–54.

513. Hama H, Hara C, Yamaguchi K, Miyawaki A. PKC signaling mediates global enhancement of excitatory synaptogenesis in neurons triggered by local contact with astrocytes. Neuron. 41 (3) (2004) 405–415.

514. Chan CS, Weeber EJ, Zong L, Fuchs E, Sweatt JD, Davis RL. Beta 1-integrins are required for hippocampal AMPA receptor-dependent synaptic transmission, synaptic plasticity, and working memory, J. Neurosci. 26 (1) (2006) 223–232.

515. Shi Y, Ethell IM. Integrins control dendritic spine plasticity in hippocampal neurons through NMDA receptor and Ca^{2+}/calmodulin-dependent protein kinase II-mediated actin reorganization. J. Neurosci. 26 (6) (2006) 1813–1822.

516. Eva R, Andrews MR, Franssen EH, Fawcett JW. Intrinsic mechanisms regulating axon regeneration: an integrin perspective. Int. Rev. Neurobiol. 106 (2012) 75–104.

517. Chan CS, Levenson JM, Mukhopadhyay PS, Zong L, Bradley A, Sweatt JD, Davis RL. Alpha3-integrins are required for hippocampal long-term potentiation and working memory. Learn. Mem. 14 (9) (2007) 606–615.

518. Hall PE, Lathia JD, Miller NG, Caldwell MA, ffrench-Constant C. Integrins are markers of human neural stem cells. Stem Cells 24 (9) (2006) 2078–2084.

519. Kerrisk ME, Greer CA, Koleske AJ. Integrin alpha3 is required for late postnatal stability of dendrite arbors, dendritic spines and synapses, and mouse behavior. J. Neurosci. 33 (16) (2013) 6742–6752.

520. Mittal N, Minasyan A, Romaneschi N, Hakimian JK, Gonzalez-Fernandez G, Albert R, Desai N, Mendez IA, Schallert T, Ostlund SB, Walwyn W. Beta-arrestin 1 regulation of reward-motivated behaviors and glutamatergic function. PLoS ONE 12 (10) (2017) e0185796.

521. Brambilla R, Gnesutta N, Minichiello L, White G, Roylance AJ, Herron CE, Ramsey M, Wolfer DP, Cestari V, Rossi-Arnaud C, Grant SGN, Chapman PF, Lipp HP, Sturani E, Klein R. A role for the Ras signalling pathway in synaptic transmission and long-term memory. Nature. 390 (1997) 281.

522. Berlanga-Acosta J, Gavilondo-Cowley J, del Barco-Herrera DG, Martín- Machado J, Guillen-Nieto G. Epidermal growth factor (EGF) and platelet-derived growth factor (PDGF) as tissue healing agents: clarifying concerns about their possible role in malignant transformation and tumor progression, J. Carcinogene. Mutagene. 2 (1) (2011) 100–115.

523. Sakata M, Yanamoto H, Hashimoto N, Iihara K, Tsukahara T, Taniguchi T, Kikuchi H. Induction of infarct tolerance by platelet-derived growth factor against reversible focal ischemia, Brain Res. 784 (1–2) (1998) 250–255.

524. Tang Z, Arjunan P, Lee C, Li Y, Kumar A, Hou X, Wang B, Wardega P, Zhang F, Dong L, Zhang Y, Zhang SZ, Ding H, Fariss RN, Becker KG, Lennartsson J, Nagai N, Cao Y, Li X. Survival effect of PDGF-CC rescues neurons from apoptosis in both brain and retina by regulating GSK3beta phosphorylation. J. Exp. Med. 207 (4) (2010) 867–880.

525. Zheng L, Ishii Y, Tokunaga A, Hamashima T, Shen J, Zhao QL, Ishizawa S, Fujimori T, Nabeshima Y, Mori H, Kondo T, Sasahara M. Neuroprotective effects of PDGF against oxidative stress and the signaling pathway involved. J. Neurosci. Res. 88 (6) (2010) 1273–1284.

526. Tseng HC, Dichter MA. Platelet-derived growth factor-BB pretreatment attenuates excitotoxic death in cultured hippocampal neurons. Neurobiol. Dis. 19 (1–2) (2005) 77–83.

527. shMohapel P, Frielingsdorf H, Haggblad J, Zachrisson O, Brundin P. Platelet- derived growth factor (PDGF-BB) and brain-derived neurotrophic factor (BDNF) induce striatal neurogenesis in adult rats with 6-hydroxydopamine lesions. Neuroscience 132 (3) (2005) 767–776.

528. Shioda N, Moriguchi S, Oya T, Ishii Y, Shen J, Matsushima T, Nishijo H, Sasahara M, Fukunaga K. Aberrant hippocampal spine morphology and impaired memory formation in neuronal platelet-derived growth factor beta-receptor lacking mice, Hippocampus. 22 (6) (2012) 1371–1378.

529. Thomas R, Morris AWJ, Tai LM. Epidermal growth factor prevents APOE4-induced cognitive and cerebrovascular deficits in female mice. Heliyon 3 (6) (2017) e00319.

530. Enevoldsen MN, Kochoyan A, Jurgenson M, Jaako K, Dmytriyeva O, Walmod PS, Nielsen JD, Nielsen J, Li S, Korshunova I, Klementiev B, Novikova T, Zharkovsky A, Berezin V, Bock E. Neuroprotective and memory enhancing properties of a dual agonist of the FGF receptor and NCAM. Neurobiol. Dis. 48 (3) (2012) 533–545.

531. Scafidi J, Hammond TR, Scafidi S, Ritter J, Jablonska B, Roncal M, Szigeti- Buck K, Coman D, Huang Y, McCarter Jr. RJ, Hyder F, Horvath TL, Gallo V. Intranasal epidermal growth factor treatment rescues neonatal brain injury. Nature 506 (7487) (2014) 230–234.

532. McNaught KSP, Olanow CW, Halliwell B, Isacson O, Jenner P. Failure of the ubiquitin–proteasome system in Parkinson's disease. Nat. Rev. Neurosci. 2 (2001) 589.

533. Sullivan CM, Fisher KC. Temperature selection and the effects of light and tem- perature on movements in fish. Fed. Proc. 6 (1) (1947) 213.

534. Claireaux G, Couturier C, Groison AL. Effect of temperature on maximum swimming speed and cost of transport in juvenile European sea bass (Dicentrarchus labrax). J. Exp. Biol. 209 (17) (2006) 3420–3428.

535. Pang X, Cao ZD, Fu SJ. The effects of temperature on metabolic interaction between digestion and locomotion in juveniles of three cyprinid fish (Carassius auratus, Cyprinus carpio and Spinibarbus sinensis), Comp. Biochem. Physiol. A Mol. Integr. Physiol. 159 (3) (2011) 253–260.

536. Aslam B, Basit M, Nisar MA, Khurshid M and Rasool MH Proteomics: Technologies and Their Applications Journal of Chromatographic Science, 2017, Vol. 55, No. 2, 182–196

SITOGRAPHY

537. https://ncit.nci.nih.gov/ncitbrowser/ConceptReport.jsp?dictionary=NCI_Thesaurus&ns=NCI_Thesaurus&code=C71632

538. www.biologywise.com

539. https://www.zebrafishfilm.org/zebrafish-photos.html

540. www.mechanobio.info